UNIVERSITÉ DE SHERBROOKE

Faculté de génie
Département de génie civil

PERFORMANCE AND STRUT EFFICIENCY FACTOR OF CONCRETE DEEP BEAMS REINFORCED WITH GFRP BARS

Performance et facteur d'efficacité de la bielle de poutres profondes en béton armé avec des barres de PRFV.

Thèse de doctorat
Spécialité : génie civil

Khaled Ahmed AbdelRaheem Mohamed

A dissertation submitted in partial fulfillment
of the requirements for the degree of
Doctor of Philosophy
(Civil Engineering)

Jury: Prof. Brahim BENMOKRANE (directeur de recherche)
Prof. Kenneth W. Neale (co-directeur de recherche)
Prof. Abdeldjelil BELARBI
Prof. Adel EL SAFTY
Prof. Ammar YAHIA

Sherbrooke (Québec) Canada September 2015

ABSTRACT

Deep reinforced concrete beams are commonly used as transfer girders or bridge bents, at which its safety is often crucial for the stability of the whole structure. Such elements are exposed to the aggressive environment in northern climates causing steel-corrosion problems due to the excessive use of de-icing salts. Fiber-reinforced polymers (FRP) emerged as non-corroded reinforcing materials to overcome such problems in RC elements. The present study aims to address the applicability of concrete deep beams totally reinforced with FRP bars. Ten full-scale deep beams with dimensions of 1200 × 300 × 5000 mm were constructed and tested to failure under two-point loading. Test variables were shear-span depth ratio (equal to 1.47, 1.13, and 0.83) and different configurations of web reinforcement (including vertical and/or horizontal web reinforcement). Failure of all specimens was preceded by crushing in the concrete diagonal strut, which is the typical failure of deep beams. The test results indicated that, all web reinforcement configurations employed in the tested specimens yielded insignificant effects on the ultimate strength. However, strength of specimens containing horizontal-only web reinforcement were unexpectedly lower than that of specimens without web reinforcement. The web reinforcement's main contribution was significant crack-width control. The tested specimens exhibited reasonable deflection levels compared to the available steel-reinforced deep beams in the literature. The development of arch action was confirmed through the nearly uniform strain distribution along the length of the longitudinal reinforcement in all specimens. Additionally, the basic assumption of the strut-and-tie model (STM) was adequately used to predict the strain distribution along the longitudinal reinforcement, confirming the applicability of the STM for FRP-reinforced deep beams. Hence, a STM based model was proposed to predict the strength of FRP-reinforced deep beams using the experimental data, in addition to the available experimentally tested FRP-reinforced deep beams in the literature. Assessment of the available STMs in code provisions was conducted identifying the important parameters affecting the strut efficiency factor. The tendency of each parameter (concrete compressive strength, shear span-depth ratio, and strain in longitudinal reinforcement) was individually evaluated against the efficiency factor. Strain energy based calculations were performed to identify the appropriate truss model for detailing

FRP-reinforced deep beams, hence, only four specimens with vertical web reinforcement exhibited the formation of two-panel truss model. The proposed model was capable to predict the ultimate capacity of the tested deep beams. The model was also verified against a compilation of a data-base of 172 steel-reinforced deep beams resulting in acceptable level of adequacy. The ultimate capacity and performance of the tested deep beams were also adequately predicted employing a 2D finite element program (VecTor2), which provide a powerful tool to predict the behavior of FRP-reinforced deep beams. The nonlinear finite element analysis was used to confirm some hypotheses associated with the experimental investigations.

Keywords: Concrete, FRP bars, deep beams, web reinforcement, arch action, strut-and-tie model, efficiency factor, FEM, design, shear strength.

RÉSUMÉ

Les poutres profondes en béton armé (BA) sont couramment utilisées comme poutre de transfert ou coude de pont, comme quoi sa sécurité est souvent cruciale pour la sécurité de l'ensemble de la structure. Ces éléments sont exposés à un environnement agressif dans les climats nordiques causant des problèmes de corrosion de l'acier en raison de l'utilisation excessive de sels de déglaçage. Les polymères renforcés de fibres (PRF) sont apparus comme des matériaux de renforcement non corrodant pour surmonter ces problèmes dans les BA. La présente étude vise à examiner la question de l'applicabilité des poutres profondes en béton complètement renforcées de barres en PRF. Dix poutres profondes à grande échelle avec des dimensions de 1200 × 300 × 5000 mm ont été construites et testées jusqu'à la rupture sous chargement en deux points. Les variables testées comprenaient différents ratios de cisaillement porté/profondeur (égal à 1.47, 1.13 et 0.83) ainsi que différentes configurations d'armature dans l'âme (incluant un renforcement vertical avec ou sans renforcement horizontal). La rupture de tous les spécimens a été précédée par l'écrasement du béton dans le mât diagonal, ce qui est la rupture typique pour les poutres profondes en BA. Les résultats ont révélé que toutes les configurations de renforcement de l'âme employées dans les spécimens d'essais avaient un effet négligeable sur la résistance ultime. Toutefois, la résistance des spécimens contenant uniquement un renforcement horizontal était étonnamment inférieure à celle des spécimens sans renforcement. La contribution principale du renforcement de l'âme était dans le contrôle de la largeur de fissuration. Les spécimens examinés présentaient une déflexion raisonnable par rapport à ce qui est disponible pour les poutres profondes renforcées en acier dans la littérature. Le développement de l'effet d'arche a été confirmé par la distribution quasi uniforme des déformations le long du renforcement longitudinal dans tous les spécimens. En outre, l'hypothèse de base du modèle des bielles et tirants (MBT) a été utilisée adéquatement pour prédire la distribution de déformation le long du renforcement longitudinal, confirmant l'applicabilité du MBT pour les poutres profondes armées de PRF. Par conséquent, un modèle basé sur un MBT a été proposé afin de prédire la résistance des poutres profondes renforcées de PRF en utilisant les données expérimentales en plus de la mise à l'épreuve expérimentalement des poutres profondes renforcées de PRF trouvées dans la littérature. Une

évaluation des MTB disponibles dans les dispositions des codes a été menée afin de déterminer les paramètres importants affectant le facteur d'efficacité de la bielle. La tendance de chaque paramètre (la résistance à la compression du béton, le ratio de cisaillement porté/profondeur, et la déformation dans le renforcement longitudinal) a été évaluée individuellement contre le facteur d'efficacité. Des calculs basés sur l'énergie des déformations ont été effectués pour identifier le modèle de treillis approprié afin de détailler les poutres profondes renforcées de PRF. Par conséquent, seulement quatre spécimens avec un renforcement vertical dans l'âme présentaient la formation de modèles avec deux panneaux de treillis. Le modèle proposé a été capable de prédire la capacité ultime des poutres profondes testées. Le modèle a également été vérifié contre une base de données de 172 poutres profondes renforcées en acier aboutissant en un niveau acceptable de pertinence. La capacité ultime et la performance des poutres profondes testées ont été également adéquatement prédites employant un programme d'éléments finis en 2D (VecTor2), ce qui fournira un puissant outil pour prédire le comportement des poutres profondes renforcées de PRF. L'analyse non linéaire par éléments finis a été utilisée afin de confirmer certaines hypothèses associées à l'étude expérimentale.

Mots-Clés : Béton, barres de PRF, poutre profonde, renforcement de l'âme, effet d'arche, bielle et tirant, facteur d'efficacité, MEF, conception, résistance au cisaillement.

ACKNOWLEDGEMENTS

Thanks to Almighty ALLAH for the gracious kindness in all the endeavors I have taken up in my life.

The author would like to express his gratefulness to the valuable advices and patience of his supervisor, Prof. Brahim Benmokrane, and for giving him the opportunity to conduct such research in Sherbrooke University and providing him support at times when it was most needed. The gratefulness is also extended to the support and assistance of Prof. Kenneth W. Neale who is the co-director of this thesis.

To Dr. Ahmed S. Farghaly, your passion to structural engineering has been an inspiration to me. I cannot thank you enough for the countless sit-downs, late-night conversations and technical brainstorming. This is beside the hand-by-hand work with dedication and devotion in every single step during the whole project. Many thanks also go to my jury Prof. Abdeldjelil Belarbi, Prof. Adel El Safty, and Prof. Ammar Yahia.

A special thanks goes to our group technical staff; Mr. Martin Bernard and Mr. Simon Kelley; who provided valuable assistance during the laboratory work. The author also appreciates the support and encourage of his colleague Dr. Nayera Mohamed. Thanks also go to his entire colleagues in civil engineering department, and the help of Yanis Tighiouart during specimen's preparation.

I am grateful for the scholarship granted to me by the Canada Research Chair in Advanced Composite Materials for Civil Structures and Natural Sciences and Engineering Research Council of Canada (NSERC-Industry Research Chair program).

To my parents, thank you for your commitment to my education and for making me the person that I am today. To my wife Shaimaa and my son Ziad, thank you for your unconditional love and encouragement, your patience and supporting made this possible.

Khaled Ahmed AbdelRaheem Mohamed
September 2015

TABLE OF CONTENTS

LIST OF TABLES

LIST OF FIGURES

CHAPTER 1
INTRODUCTION

1.1 General Background

Infrastructure in northern climate is deteriorating due to the corrosion of steel bars resulted from the large amount of deicing salts used during winter months. The repair and rehabilitation costs consider a constant strain on the available public funds, however, even in hard economic times public infrastructure remains a top spending priority. The fédération international du béton (*fib*, 2006) estimated that the worldwide infrastructure maintenance and repair exceeds 100 billion euros annually. In Canada, the replacement cost of Ontario's bridges and highways is estimated to be approximately 57 billion dollars (MTO, 2009).

That notwithstanding, fiber reinforced polymers (FRP) mitigated the potential durability concern associated with steel reinforcement and propagated as internal reinforcement for concrete structures in aggressive environment. Because of the advantages of FRP bars, they have found their way into numerous construction elements such as beams, one-way and two-way slabs, and, recently, columns and shear walls (Kassem et al. 2011, Bakis et al. 2002, El-Salakawy et al. 2005, Sharbatdar and Saatcioglu 2009, Tobbi et al. 2012, Mohamed et al. 2014). Successful application of FRP-reinforcing bars as concrete reinforcement in a wide variety of construction elements has reached an acceptable level (ACI 440 2007, *fib* Task Group 9.3 2007, ISIS Canada Design Manual No 3 2007). However, only the CSA-S806 (2012) provided guidelines for designing deep beams reinforced with FRP. These guidelines developed based on previous knowledge of steel-reinforced concrete deep beams. That is because there have been very limited research and experimental investigations on FRP-reinforced concrete deep beams, particularly for deep beams without web reinforcement (Farghaly and Benmokrane, 2013, Andermatt and Lubell, 2010).

Reinforced concrete deep beams are considered a major component in the superstructure of bridges. They are used mainly for load distribution such as transfer girders and/or bent caps

(Figure 1.1). Other applications of deep beams are pile caps, folded plates, foundation walls, raft beams, walls of rectangular tanks, hoppers, floor diaphragms and squat walls. Deep beams are characterized as being relatively short and deep with shear spans less than their effective depth. Hence, deep beams mechanism differs from longer beams (slender beams).

Figure 1.1 - Deep beam as transfer girder in bridges

The transition from slender beams behavior to that of deep beams is imprecise. For instance, while the ACI 318 (2014), AASHTO LRFD (2007) and CIRIA Guide (1977) use the span-depth ($l_e/d \leq 4.0$) and the shear span-depth ratio ($a/d \leq 2.14$) limits to define RC deep beams, the Canadian code CSA-S6 (2006) employs only the concept of shear span-depth ratio ($a/d \leq 2.0$). This variation in deep beam definitions among provisions is due to the different definitions of B-region (Bernoulli or Beam) and D-region (distributed or discontinuity) lengths (Schlaich et al. 1987). D-regions are located at approximate distance equal to the member depth; d, from discontinuity points, such as concentrated loads and supports. Beams with only overlapping D-regions are identified as deep beams, while those with D- and B-regions are slender beams.

Several possible modes of failure of deep beams have been identified from physical tests but due to their geometrical dimensions shear strength appears to control their design. Unlike flexural failures, reinforced concrete shear failures are relatively brittle and, particularly for members without stirrups, can occur without warning. Therefore, standards for designing

reinforced concrete structures specify a minimum percentage for web reinforcement, as strength and/or serviceability requirements.

Previous research on steel-reinforced concrete deep beams has indicated that web reinforcement is considered essential for crack control (Tan et al. 1997). Nevertheless, there is disagreement between researchers, as well as in code provisions, about the effect of web reinforcement on the strength of steel-reinforced deep beams. For instance, Mihaylov et al. (2010) reported that web reinforcement improved the strength of the inclined strut and, hence, the shear strength of deep beams. Other experimental observations, however, indicated that web reinforcement had no impact on strength (Birrcher et al. 2013). Moreover, providing the minimum web reinforcement in a steel-reinforced deep beam designed according to ACI 318 (2014) would yield a beam 1.67 times greater than a deep beam without web reinforcement. Canadian codes for steel-RC and FRP-RC (CSA A.23.3-04, and CSA S806-12, respectively), however, require the minimum web reinforcement solely for crack control and consider it has no effect on deep-beam strength. To the authors' knowledge, no investigations have been conducted to examine the effect of web reinforcement on the strength of FRP-reinforced concrete deep beams.

Historically, reinforced concrete deep beams were designed with empirical methods or simple approximations. Within the last decades, strut-and-tie model (STM) has become the preferred method for designing deep beams in codes and standards. A STM idealizes the complex flow of stresses in a structural member as axial elements in a truss member. Struts and ties intersect at nodes. Strut, ties and nodes are the three elements of STM. Concrete struts resist the compressive stress fields, and the reinforcing ties resist the tensile stress. All elements of STM must be proportioned to resist the applied forces.

The current study was aimed to investigate the behavior of FRP-reinforced deep beams, with and without web reinforcement. Experimental and analytical investigations were conducted, and then guidelines for designing of FRP-reinforced deep beams were proposed.

1.2 Objective and Scope

Due to the lack of experimental data for the deep beams reinforced with FRP bars, the current study aims to induce the use of FRP bars as internal reinforcement in reinforced concrete deep beams. Based on this study, recommendations for FRP-reinforced deep beams were given and design guidelines were proposed.

The main objective of the current study was to investigate the behavior of FRP-reinforced concrete deep beams with and without web reinforcement. Moreover, examining the applicability of the strut-and-tie model for FRP-reinforced concrete deep beams, which has been recommended in several RC provisions, was of significant important.

Basically, the objectives of the current study are:

1. Generate more data on the shear behavior of concrete deep beams ($a/d < 2.0$) and reinforced with FRP bars to better understand their performance,

2. Study the effect and role of the web reinforcement on the strength, deformation and serviceability of FRP-reinforced deep beams,

3. Investigate the applicability of the STM for FRP-reinforced deep beams, and

4. Evaluate the parameters affecting the strength of the concrete strut and determine the effect of each parameter, then propose a new strut-and-tie based model for designing FRP-reinforced deep beams.

1.3 Methodology

Based on the objectives of this study, an experimental program was conducted. The results of ten (10) full-scale FRP-reinforced deep beams were analyzed to better understand their performance and behavior. All the deep beams were fabricated and tested at the Structure Laboratory of the University of Sherbrooke. To meet the objectives of the this study and to best identify the behavior and performance of FRP-reinforced deep beams, it was necessary to test specimens that were of comparable size to typical deep beams used in reality. Comparable

to the tested deep beams in the literature, the tested specimens considers among the largest tested FRP- or steel-reinforced deep beams. All the tested specimens in the current study were designed according to the Canadian Code CSA-S806 (2012) and American standards ACI 318 (2014) and ACI 440.1R (2006) to satisfy the design guidelines of deep beams, in addition to the details and anchorage lengths for FRP bars.

The experimental program was divided according to objectives of the current study as follows: three specimens were having three different *a*/*d* ratio (1.47, 1.13, and 0.83); and seven specimens contained different configuration of web reinforcement (horizontal-only, vertical-only, or vertical and horizontal web reinforcement).

The experimental results were analyzed identifying the effect of *a*/*d* ratio and different web reinforcement configurations on the crack pattern and failure mode, the load-deflection response, the ultimate capacity, the crack widths, and the relative displacement measurements of the FRP-reinforced deep beams. The formation of arch action and the development of STM were also investigated. Then, the experimental results were compared to the STMs proposed by CSA S806 (2012), ACI 318 (2014), and other existing STMs for steel-reinforced deep beams. Hence, a new strut-and-tie based model was proposed, yet validated with the experimental results in the current study as well as the test results for FRP- and steel-reinforced deep beams found in the literature.

Finally, numerical simulation of tested deep beams was performed using finite element analysis program (VecTor2; Wong and Vecchio 2002) to predict the deep beam's response. The predictions were then compared to the experimental results. The comparison aims to provide insight to designers about the assumptions and limitations while utilizing FE application to overcome the inherent intricacies of nonlinear finite element analysis and to validate some hypotheses associated with the experimental results.

1.4 Thesis Organization

The thesis consists of seven chapters. The contents of each chapter can be summarized as follows:

Chapter 1 of this thesis presents background information on the research topic, the work objective and the adopted methodology.

Chapter 2 introduces a literature review reporting the past known mechanism of steel-reinforced deep beams. Additionally, the code provisions and the analytical models for steel—reinforced deep beams, in addition to code provision assessment using 470 deep beam tests from the literature are demonstrated. The effect of web reinforcement with different configuration on the behavior of steel-reinforced deep beams is presented. Finally, the background of reinforcing with FRP bars is provided.

Chapter 3 gives the details of the experimental program and the testing procedure. The geometry and reinforcement details of the test specimens, web reinforcement configuration, test setup and procedure, and the instrumentation details are presented. In addition, detailed characteristics of the used materials are provided in Chapter 3.

Chapter 4 addresses the results the experimental investigation conducted in the research program. The general behavior of the tested specimens is described in terms of cracking pattern and mode of failure, ultimate load and failure progression, and load-deflection response. The measured strains in longitudinal reinforcement are discussed to provide evidence on the formation of arching action and the applicability of STM. The effect of each configuration of web reinforcement on strength, deformability and serviceability of the tested specimens is also discussed.

Chapter 5 provides the derivation producer for the strut-and-tie based model. The STMs in ACI and CSA provision were first used to predict the capacity of the tested deep beams, providing inappropriate estimation for the capacity. Additionally, the strut-and-tie based models derived for steel-reinforced deep beams based on theoretical fundamentals were used to predict the ultimate capacity of the tested deep beams. The affected parameters on the strut

efficiency factor were then detailed identifying their tendencies. Then, assessment of the proposed model against FRP- and steel-reinforced deep beams was presented.

Chapter 6 gives details about the finite element simulation for the tested FRP-reinforced deep beams in terms of materials, models and meshing. The results from the FE simulation are compared to the experimental results regarding the load-deflection response, the ultimate capacities, crack pattern, mode of failure, and strain levels in reinforcement and concrete. Analysis based on the FE simulation was discussed to confirm some experiment findings reported in Chapter 4.

Chapter 7 presents a general conclusion of the results obtained from the experiments and analyses with respect to the problems and observations discussed throughout the thesis in addition to recommendations for future work.

It worth mentioning that, Chapter 4, 5, and 6 were corresponding to three submitted technical papers in scientific journals as follows:

- Chapter 4: Mohamed, K., Farghaly, A. S., Benmokrane, B., "Effect of Vertical and Horizontal Web Reinforcement on the Strength and Deformation of Concrete Deep Beams Reinforced with Glass-FRP Bars," *Journal of Structural Engineering*, ASCE, (submitted 30 December 2014).
- Chapter 5: Mohamed, K., Farghaly, A. S., Benmokrane, B., "Strut Efficiency Based Design for Concrete Deep Beams Reinforced with FRP Bars," ACI Structural Journal, (submitted 4 March 2015).
- Chapter 6: Mohamed, K., Farghaly, A. S., Benmokrane, B., Neale K. W., "Nonlinear Finite Element Analysis of Concrete Deep Beams Reinforced with GFRP Bars," *Engineering Structures*, (submitted 13 June 2015).

CHAPTER 2
LITERATURE REVIEW

2.1 Introduction

Numerous test investigations have been devoted to study the behavior of steel-reinforced deep beams. Results of these studies agreed that; strut-and-tie model is a rational method for the design of steel-reinforced deep beams, but with different limitations and exclusions. Strut-and-tie model (STM) has been incorporated in several codes and guidelines for practice, including the Canadian code (CSA S806 2012, CSA A23.3 2014 and CSA S6 2006) and the USA codes (AASHTO LRFD 2007 and ACI 318 2014).

A number of parameters affecting shear behavior have led to understand the shear failure mechanisms and predict the shear strength of deep beams. These parameters include concrete span-depth ratios, amount of longitudinal and web reinforcement, concrete compressive strength, and loading and support conditions. Different researchers have different techniques to identify these parameters. The current chapter will outline some of these researchers' studies on steel- as well as FRP-reinforced deep beams.

2.2 Strength and Behavior of Deep Beams

Deep beam is defined by MacGregor (1997) as a beam in which a significant amount of load is carried to the supports by a compression thrust joining the load and the reaction. This occurs if a concentrated load acts closer than about 2d to the support, or for uniformly loaded beams with a span-depth ratio, l_n/d, less than about 4 to 5; where: d is the depth of the member, l_n is the total span of the member, and a is the distance between a concentrated load and the support.

The basis for this definition is that within a distance of d from a disturbance such as a concentrated load or support, the strain distribution in the member is nonlinear (Schlaich et al., 1987). Plane sections do not remain plane. Regions of nonlinear strain distribution along the

height of the cross-section are called D-regions where 'D' stands for discontinuity or disturbed. Regions of linear strain distribution are called B-regions where 'B' stands for Bernoulli or beam. The B- and D-regions of an asymmetrically loaded beam are shown in Figure 2.1 with the principal strain trajectories. In Figure 2.1, the portion of the beam to the right of the concentrated load is comprised entirely of D-regions and meets the deep beam definition given by MacGregor (1997). While the portion of the beam to the left of the concentrated load contains variety of D- and B-region, and explains the main behavior of slender beams.

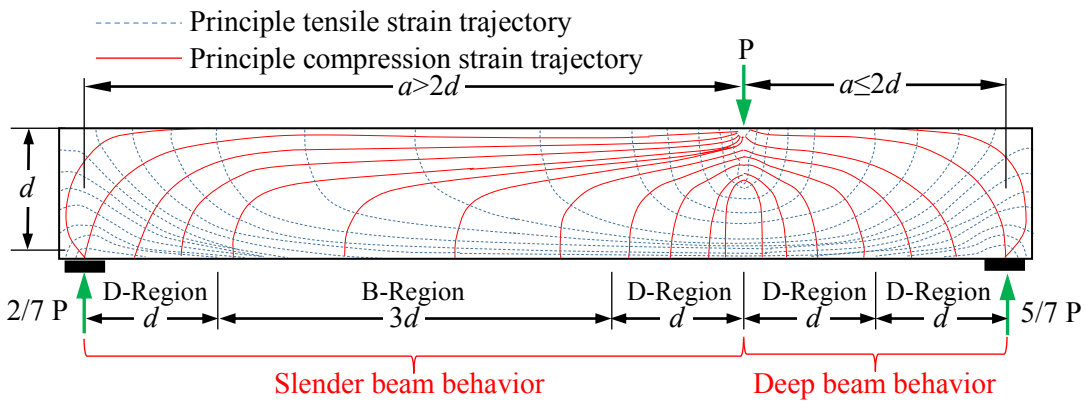

Figure 2.1 - Strain distribution in deep and slender portion of RC beams

Paiva and Siess (1965) were early researchers investigating the shear strength and behavior of moderately (span-depth ratios from 2 to 6) steel-reinforced concrete deep beams. From the results of the tests, they concluded that an increase in the span-depth ratio has no effect on the beam failing in flexure but increases the shear strength of the beam particularly at low span-to-depth ratios. Further researchers found that strength of deep beams controlled by shear rather than flexural strength due to the small value of shear span-to-depth ratio (a/d) (Collins and Kuchma 1999; Oh and Shin 2001; Collins et al. 2008). The same results were reported for deep members with different span-depth ratio (L/d) (Manuel et *al*. 1971) and different load configurations including single point loading, two point loadings and distributed loads (Ramakrishnan and Ananthanarayana 1968, Brown and Bayrak 2007). Unlike flexural failures, reinforced concrete shear failures are relatively brittle and, particularly for members without stirrups, can occur without warning (Collins et al. 2008). An understanding of the

shear strength behavior of deep beams is an essential prerequisite for achieving optimum design and proportioning of such members.

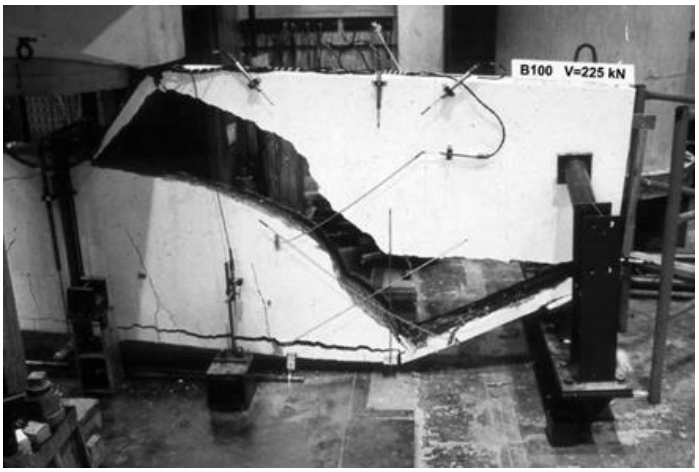

Figure 2.2 - Shear failure of deep beams without stirrups (Collins and Kuchma, 1999)

In general, reinforced concrete beams without web reinforcement resist shear stresses by means of five possible mechanisms: 1) shear resistance of the uncracked concrete compression zone, 2) aggregate interlock, 3) dowel action of the longitudinal reinforcement, 4) residual tensile stresses across cracks, and 5) arch action (ACI-ASCE Committee 1998, Razaqpur and Isgor 2006). The first four mechanisms are principal shear resistance mechanisms in slender beams, which commonly recognized as a truss mechanism (beam action). While the arch action occurs in deep beams in which the load is transferred directly from the load point to the support (ACI-ASCE Committee 1998, Aoyama 1993).

The expected failure mechanisms for beam shown in Figure 2.1 are illustrated in Figure 2.3. The left side of the beam represents the beam action while the right side for the arch action. As shown Figure 2.3(a), the beam action relies on diagonal tensile stresses in the web of the member. The tension in the cracked part of the beam is explained by the ability of the cracks to transfer shear through aggregate interlock. The stresses in the web reduce the tension force T in the bottom chord from its maximum value at mid-span to almost zero near the supports. The member fails when the interlocking of the cracks breaks down and diagonal crack propagates towards the loading point. Deep beams are able to make transition from beam

action to arch action, which consists of direct compression between the loading and support points, and constant tensile stresses in the longitudinal reinforcement (Figure 2.3(b)).

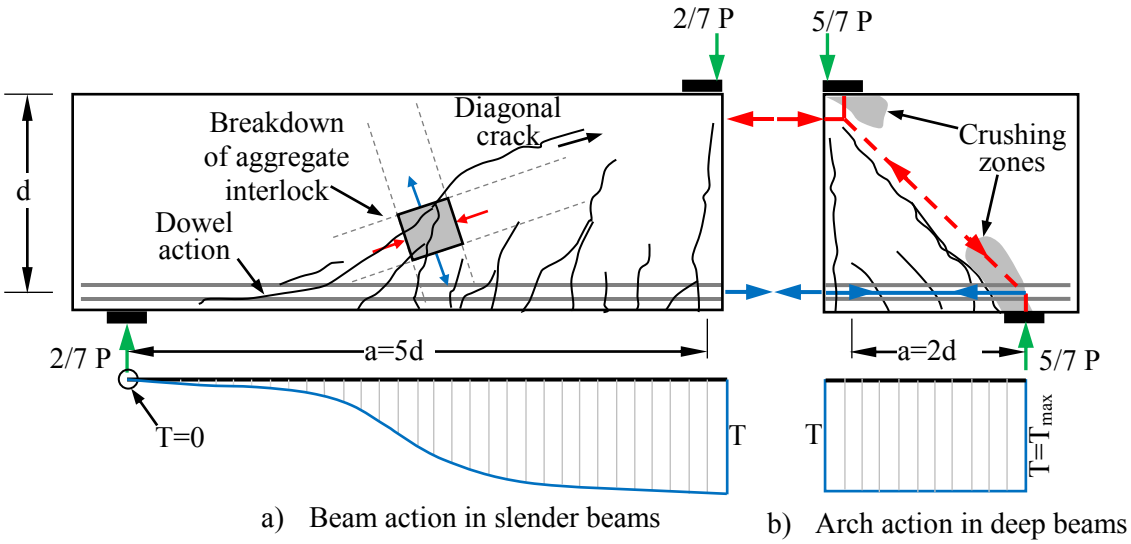

a) Beam action in slender beams b) Arch action in deep beams

Figure 2.3 - Beam action and arch action in RC beams

Fenwick and Paulay (1968) explained that, because of the geometric incompatibility of the two mechanisms, with beam action typically being much stiffer than arch action, nearly all of the shear would be carried by beam action until this mechanism failed. After failure of the beam mechanism, an internal redistribution of stresses could occur and the remaining arch mechanism could then carry even higher shears if the distance between the applied load and the support was sufficiently short (Breña and Roy 2009).

In an attempt to identify the transition point between the beam and arch actions, Kani et al. (1967 and 1979) conducted 362 shear tests on concrete beams without stirrups. Using deep specimens contained a large quantity of longitudinal reinforcement (ρ_w = 2.8%), the study concluded that, when shear span-to-depth ratio (a/d) was less than approximately 2.5, however, a small decrease in shear span caused failure shear to greatly increase. These differences result from longer specimens being controlled by the breakdown of beam action while crushing of a concrete strut controls the shear strength of shorter spans. Figure 2.4 shows the effect of a/d ratio on shear behavior for simple supported beams without web reinforcement and subjected to two concentrated loads at third points as presented by Wight and MacGregor (2009).

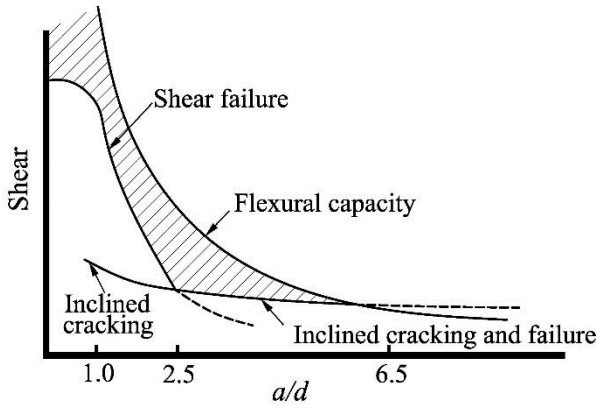

Figure 2.4 - Effect of *a*/*d* ratio on the shear stress (Wight and MacGregor 2009)

Reinforced concrete element subjected to shear stress would develop diagonal cracks at an angle inclined to the steel bars (Hsu, 1988). These cracks would separate the concrete into a series of diagonal concrete struts, which are assumed to resist axial compression. Together with the steel bars, which are assumed to take only axial tension, they form a truss action to resist the applied shear stresses. Hence, a truss model theory was proposed to simplify the forces transition in the truss action. With more investigations and studies for steel reinforced deep beams, the truss model was improved and simplified to be used for design of reinforced concrete deep beams, known later as strut-and-tie model.

2.3 Strut-and-Tie Model

The elastic theory is considered by researchers and practitioners to be the rational and appropriate basis for the design of cracked reinforced concrete beams loaded in bending, shear and torsion (Schlaich et al. 1987). Since all parts of a structure are of similar importance, an acceptable design concept must be valid and consistent for every part of any structure. Furthermore, since the function of the experiment in design should be restricted to verify or dispute a theory but not to derive it, such a concept must be based on physical models which can be easily understood and therefore are unlikely to be misinterpreted. For the design of structural concrete it was, therefore, proposed to generalize the truss analogy in order to apply it in the form of strut-and-tie model to every part of any structure (Schlaich 1987, Hsu, 1988). In the elastic stress distribution of deep members, significant shear is transmitted directly to

the support by diagonal compression. This means that less redistribution is required after cracking, and it seem reasonable to apply strut-and-tie model to deep beams (Schlaich 1987).

The use of strut-and-tie model (STM) allows for easy visualization of the flow of forces. In addition, these truss models represent all internal force effects and do not require separate flexure and shear models, as is the case for slender members analyzed with sectional approaches. STM is based on the lower-bound theory of plasticity and the capacity of the model is always less than the true capacity if the truss is in equilibrium and has sufficient deformation capacity to allow redistribution of forces into the assumed truss elements.

Strut-and-tie model was recommended by design provisions and among researchers to design discontinuity regions (D-region) in reinforced concrete structures. STM reduces complex states of stress within a D-region of a reinforced concrete member into a truss comprised of simple, uniaxial stress paths. Each uniaxial stress path is considered a member of the STM (Figure 2.5). Members of the STM subjected to tensile stresses are called ties; and represent the location where reinforcement should be placed. STM members subjected to compression are called struts. The intersection points of truss member are called nodes. Knowing the forces acting on the boundaries of the STM, the forces in each of the truss members can be determined using basic truss theory.

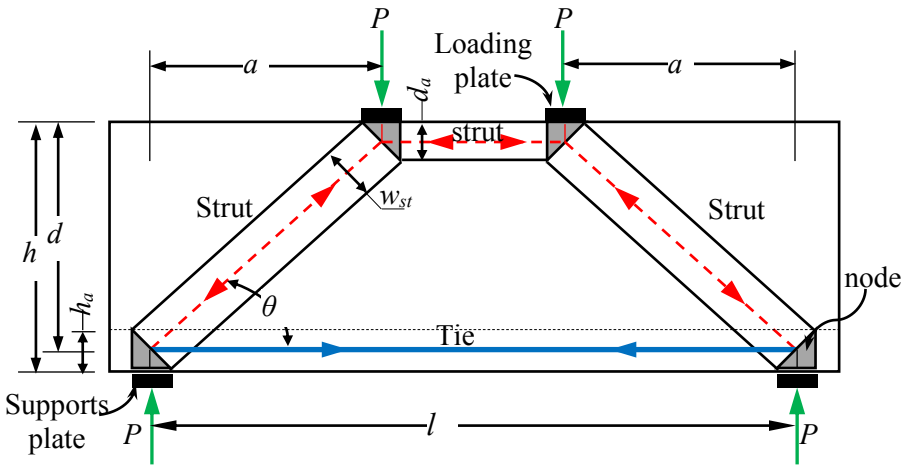

Figure 2.5 - Different components of strut-and-tie

Most design specifications recognize three major node types: CCC, CCT, and CTT nodes. Figure 2.6 illustrates the different types of nodes. A node that connects only compressive forces is called CCC node; while CCT is a node under the action of one tension force and two (or more) compression forces. A CTT node connects one compression force and two (or more) tension forces. Finally, the node under tension forces only is called TTT node. The regions around the nodes are called nodal zones. An extended nodal zone can be used for the analysis of the stresses in the region, including determination of reinforcement anchorage requirements. The ACI 318 (2014) defines a nodal zone as a portion of a member bounded by the intersection of effective strut and tie widths.

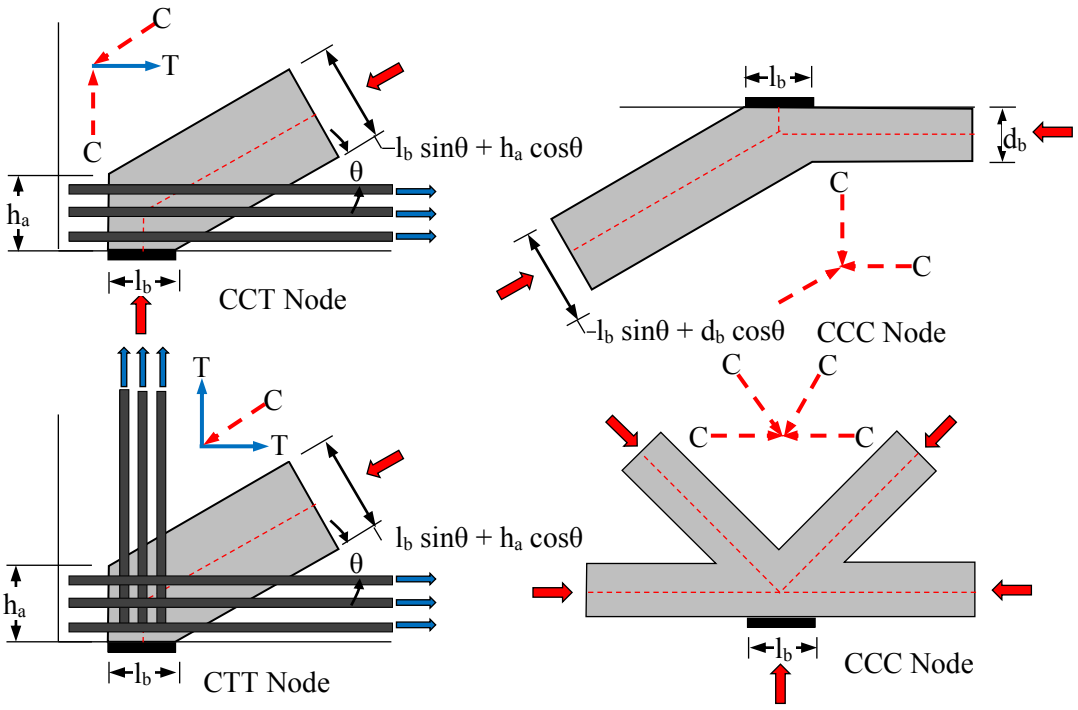

Figure 2.6 - Types of STM node

Two truss models for the right side of the applied load (arch action) for the beam depicted in Figure 2.1 are provided in Figure 2.7. As noted previously, the left side of the beam presents the beam action and would be designed with sectional approach. The first model is a called a single- or one-panel truss model; the second is called a multiple- or two-panel truss model. Either model (or a combination of the two) is acceptable provided that equilibrium condition is met. The choice of the model is left to the designer provision. To avoid compatibility problems and for efficiency, it is good practice for the STM to agree well with the dominant

mechanism of force transfer in the structure. However, the one-panel model was found to be the preferred mechanism for resisting loads in deep beams with limited amount of web reinforcement (Brown and Bayrak 2008).

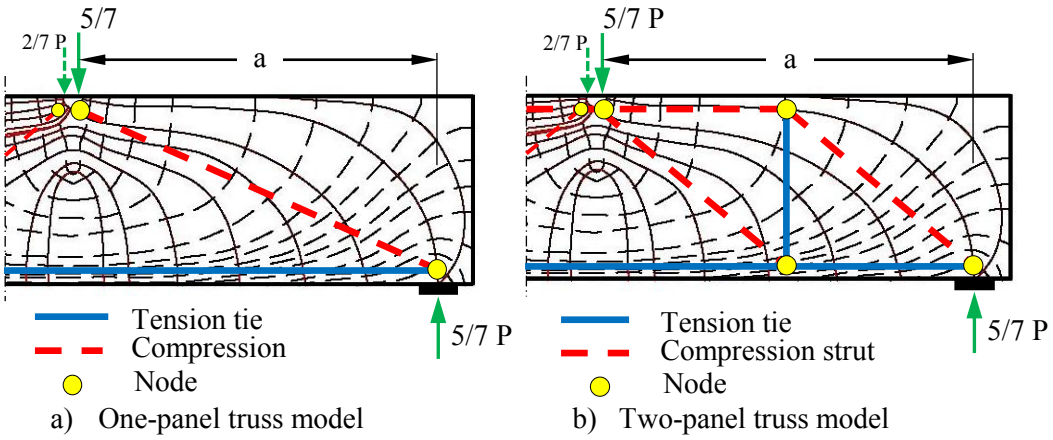

Figure 2.7 - One- and two-panel truss models

Most research and design specifications specify the limiting compressive stress of a strut as the product of the concrete compressive strength, f_c', and an efficiency factor. The efficiency factor is often a function of the geometric shape (or type) of the strut and the type of the node. As discussed by Schlaich and Schäfer (1991), there are three major geometric shape classes for struts: prismatic, bottle-shaped, and compression fan (Figure 2.8). Prismatic and bottle shaped struts are the most basic type of strut, while fan truss are more practical for deep beams with distributed loading. Prismatic struts have uniform cross-sections.

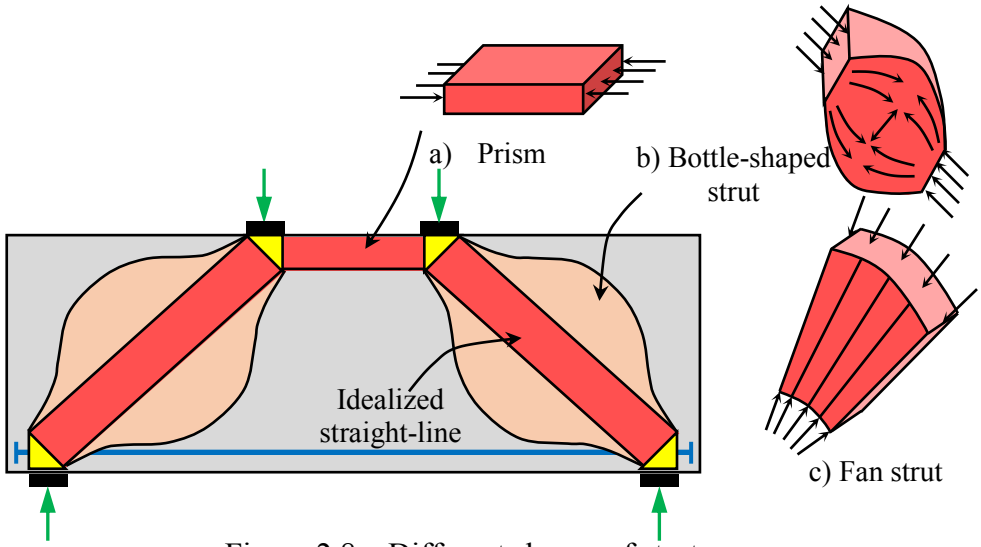

Figure 2.8 – Different shapes of struts

Typically, prismatic struts are used to model the compressive stress block of a beam element as shown in Figure 2.8. Bottle-shaped struts are formed when the geometric conditions at the end of the struts are well defined, but the rest of the strut is not confined to a specific portion of the structural element. The geometric conditions at the ends of bottle-shaped struts are typically determined by the details of bearing pads and/or the reinforcement details of any adjoined steel. The best way to visualize a bottle-shaped strut is to imagine forces dispersing as they move away from the ends of the strut as in Figure 2.8.

One of the primary advantages of STM is its widespread applicability. In theory, any structural concrete member can be represented by a truss model of compression and tension elements and designed with STM principles. However, in cases where flexural theory and sectional approaches are valid, the use of STM is generally too complicated. It is most useful for applications where complicated states of stress exist such as deep beams, corbels, dapped-ends, post-tensioned anchorage zones, or other structural components with loading or geometric discontinuities. Some examples of structures with D-regions are provided in Figure 2.9. Additional background information on STM can be found in several references (Schlaich et al. (1987), Bergmeister et al. (1993), Collins and Mitchell (1997), and *fib*, (1999)).

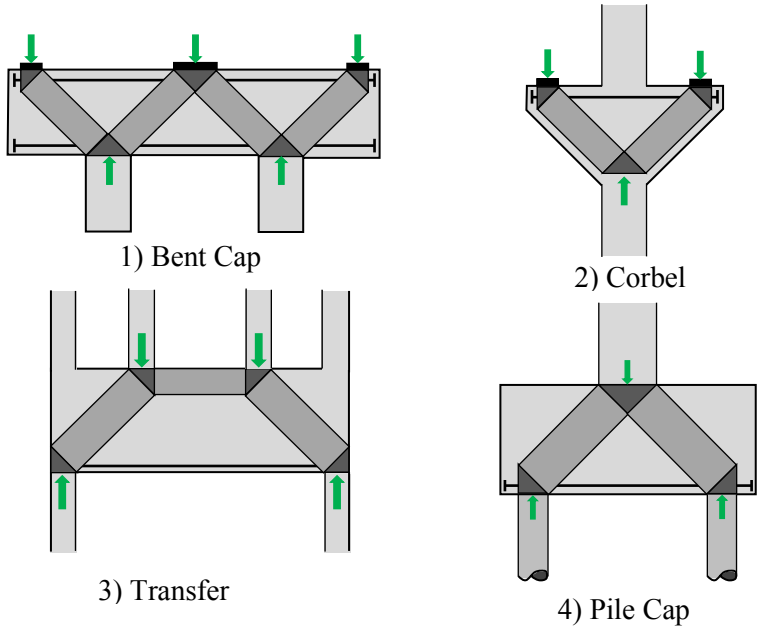

Figure 2.9 - Examples of D-regions in several structures

2.4 Code Provisions for Deep Beam Design

Over the past several decades, new approaches to the shear design of structural concrete have been implemented in codes of practice. The current CSA S806 Code (2012), CSA S6 (2006), CSA A23.3 (2014) and AASHTO LRFD (2007) Bridge Design Specification adopt the use of STM for analysis and design for the shear strength of deep beams. In addition, ACI 318 (2014) depends on the same theory with different applying equations. This section provide a brief description for the STM based procedure used to design of deep beams implemented in each code provison.

2.4.1 Provisions of CSA S806 (2012) and CSA A23.3 (2014)

CSA-S806 (2012) adopted the equations used by CSA-A23.3 (2014) for steel-reinforced deep beams to design FRP-reinforced deep beams. Therefore, equations, limitations and definitions presented in this section are identical in both codes.

CSA-S806 (2012) defines deep beams as a member with a shear span-to-depth ratio of less than 2.0. CSA-S806 (2012) uses the STM to determine internal force effects near supports and the points of application of concentrated loads. Depending on the truss mechanisms, a series of reinforcing steel tensile ties and concrete compressive struts interconnected at nodes was recommended to be idealized to investigate the strength of the concrete structure, components, or region. According to the CSA-S806 (2012), the compressive force of the strut shall not exceed $\phi_c A_c f_c'$, where ϕ_c is the concrete resistance factor (ϕ_c=0.60), A_{cs} is the effective cross-section area of the strut (Figure 2.6) and f_{cu} is the limiting compressive strength of the strut.

The value of f_{cu} based on the modified compression field theory (MCFT) developed by Vecchio and Collins (1986). The MCFT uses equilibrium, compatibility, and stress-strain relationships to predict the shear response of cracked reinforced concrete elements. For members with only longitudinal reinforcement, the theory predicts that failure will occur when the shear stress on the crack faces required for equilibrium reaches the maximum shear stress that can be transmitted by aggregate interlock. The predicted failure shear stress decreases as the predicted width of the inclined crack increases. Thus, failure shear decreases as tensile

strain in the longitudinal reinforcement increases, which is called the strain effect, and as crack spacing near mid-depth increases, the size effect (Collins et al. 2008). The CSA-S806 (2012) equations for STM are presented as follows:

$$f_{cu} = \frac{f_c^{'}}{0.8 + 170\varepsilon_1} \leq 0.85 f_c^{'} \tag{2.1}$$

$$\varepsilon_1 = \varepsilon_F + (\varepsilon_F + 0.002)\cot^2 \alpha_s \tag{2.2}$$

Where α_s is the smallest angle between the compressive strut and the adjoining tie, ε_F is the tensile strain in the concrete in the direction of the tension tie and f_c' is the concrete strength. The stress limits in nodal zones depends on the nodal boundary conditions (Table 2.1).

Table 2.1 - Efficiency factors for CSA-S806 (2012) and AASHTO LRFD (2007)

	Strut and node efficiencies (fc')	Efficiency factor
Struts	Strut with uniform cross section over its length	Eq. (2.1) and (2.2)
	Bottle-shaped struts with minimum web reinforcement	Eq. (2.1) and (2.2)
	Bottle-shaped struts without web reinforcement	Eq. (2.1) and (2.2)
	Struts in tension members	Eq. (2.1) and (2.2)
	All other cases	Eq. (2.1) and (2.2)
Nodes	Nodes bounded by compression or bearing CCC node	0.85
	Nodes anchoring one tie CCT node	0.75
	Nodes anchoring more than one tie CTT and TTT nodes	0.65

According to CSA-S806 (2012), structures, members, or regions (other than slabs or footings) that have been designed in accordance with STM shall contain an orthogonal grid of reinforcing bars near each face. The ratio of reinforcement area to gross concrete area shall be not less than 0.004 for GFRP and AFRP, and 0.003 for CFRP in each direction. The spacing of this reinforcement shall not exceed 200 mm for GFRP and AFRP, and 300 mm for CFRP bars. If located within the tie, the crack control reinforcement may also be considered as tie reinforcement.

It worth mentioning that, the CSA-A23.3 (2014) for the design of steel reinforced deep beams specify lower amount of web reinforcement (minimum ratio of steel web reinforcement shall be more than 0.003 in each direction). The relatively large amount of web reinforcement specified by CSA S806 (2012) is recommended to control the crack width, considering that

FRP-reinforced structures exhibit wider cracks compared to steel-reinforced structures. However, no experimental investigations were conducted to identify the appropriate amount of FRP web reinforcement required for control the crack width within the appropriate limits.

The angle between the strut and any adjoining tie is explicitly considered in the CSA-S806 (2012) STM provisions. Therefore, no limit is placed on that angle. As the angle between the strut and the tie approaches zero, the strength of the strut also approaches zero. Although very small angles are allowed by CSA-S806 (2012), they become impractical due to the diminished efficiency factor of the strut. The diminished efficiency factors and the associated reductions in the allowable strength of struts encourage the design engineer to seek a more refined truss mechanism without such shallow angles.

2.4.2 Provisions of ACI 318 (2014) – Steel Reinforced Deep Beams

According to ACI 318 (2014), deep beams are members loaded on one face and supported on the opposite face so that compression struts can develop between the loads and the supports. In addition, deep beams should have either clear spans equal to or less than four times the overall member depth; or regions with concentrated loads within twice the member depth from the face of the support. Beginning in 2002, the ACI building code stated that deep beams should be designed using either nonlinear analysis or using the STM. Provisions for the use of STM were added as an appendix to the main body of the ACI Building Code in 2002. The ACI 318 (2014) provision, in Chapter 23, provides nominal capacities of the struts of a STM as a fraction of the specified compressive strength of the concrete

$$f_{ce} = 0.85\beta_s f_c' \tag{2.3}$$

where β_s is the strut efficiency factor (Table 2.2), f_c' is the concrete compressive strength, and f_{ce} is the effective compressive strength. For Eq. (A-4) in Section A.3.3 of ACI 318 (2014); (Eq. 2.3); reinforcement that crosses the anticipated crack is included. Struts that meet the minimum reinforcement criterion (Eq. 2.3) make up the second class of struts and those that do not meet the minimum reinforcement criterion make up the third classes of struts

$$\sum \frac{A_{si}}{bs_i} \sin \alpha_i \geq 0.003 \tag{2.4}$$

where A_{si} is the area of surface reinforcement in the i-th layer crossing a strut, s_i is the spacing of reinforcing bars in the i-th layer adjacent to the surface of the member, b is the width of the strut perpendicular to the plane of the reinforcing bars, and α_i is the angle between the axis of the strut and the bars in the i-th layer of reinforcement crossing that strut as in Figure 2.10.

Table 2.2- Efficiency factors for ACI 318 (2014)

	Strut and node efficiencies ($0.85 fc'$)	β_s
Struts	Strut with uniform cross section over its length	1.00
	Bottle-shaped struts with reinforcement satisfying Section A.3.3 (Eq. 2.22)	0.75
	Bottle-shaped struts without reinforcement satisfying Section A.3.3 (Eq. 2.22)	0.60
	Struts in tension members	0.40
	All other cases	0.60
Nodes	Nodes bounded by compression or bearing CCC node	1.00
	Nodes anchoring one tie CCT node	0.80
	Nodes anchoring more than one tie CTT and TTT nodes	0.60

Additionally, ACI 318 (2014) place limits on the allowable stresses at the faces of the nodes (Table 2.2). The nodal efficiency factors are based on the elements that intersect to form the node and are listed in Table 2.2. The strength of a strut must be checked at its minimum cross-sectional area. For a strut, especially a bottle-shaped strut, the minimum area will occur at the ends of the strut where it abuts a node.

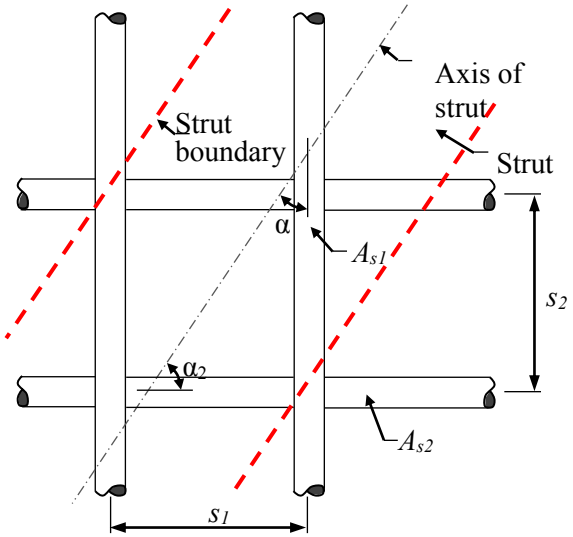

Figure 2.10 - Calculation of reinforcement ratio in ACI 318 (2014)

ACI 318 (2014), Chapter 23, also provides one more restriction on the modeling process. The angle between the axis of any strut and any tie entering a common node may not be less than 25 degrees. This provision stems from the idea that struts will lose capacity as they approach the direction of a tie. Clearly, a strut that is coincident with a tie will have no compressive capacity. The angle of 25 degrees was chosen to eliminate potential problems with struts that form a slight angle with a tie.

2.4.3 Provisions of AASHTO LRFD – Steel Reinforced Deep Beams

In 1994, the first edition of AASHTO LRFD Bridge Design Specifications (1994) referred to using the STM for the design and detailing of certain structural concrete members. The "AASHTO LRFD Bridge Design Specifications 2007" like ACI 318 (2014) places limits on the allowable stress at the faces of the nodes and struts. The AASHTO approach for the allowable stress in a strut, however, is also based on the modified compression field theory (MCFT) developed by Vecchio and Collins (1986) rather than the reinforcement ratios used by ACI 318 (2014). The compressive strength of the strut f_{cu} calculated using the same equation of the CSA-S806 (2012) (Eq. 2.1 and 2.2). For the nodal stress limits, AASHTO LRFD (2007) also specifies factors based on the type of node (Table 2.1).

When AASHTO LRFD (2007) strut-and-tie provisions are used, minimum horizontal and vertical shear reinforcement must be provided. Specifically, AASHTO LRFD (2007) requires that the ratio of reinforcement area to gross concrete area must be no less than 0.003 in each direction (horizontal and vertical).

2.4.4 Literature Assessment for Code Provisions

In the previous three sections, the STM design provisions of CSA A23.3 (2014), ACI 318 (2014), and AASHTO LRFD (2008) were listed. In this section, the implications of using each set of provisions to estimate the capacity of a deep beam are discussed. For the discussion, results obtained from the experimental strength of 470 deep beam tests from the literature were compared to the calculated strength using a single-panel STM with each set of design

provisions. The value of φ was equal to 1.0 in all calculations since the tests were conducted under laboratory conditions.

The assessment of the code provision was performed using the data reported in the following investigations: Clark (1952); De Pavia (1965); Kong et al. (1970); Kani et al. (1979); Fukuhara and Kokusho (1980); Niwa et al. (1981); Smith and Vantsiotis (1982); Kung (1985); Anderson and Ramirez (1989); Walraven and Lehwa (1994); Tan et al. (1995); Tan et al. (1997a); Tan et al. (1997b); Shin et al. (1999); Adebar (2000); Oh and Shin (2001); Aguilar et al. (2002); Lertsrisakulart (2002); Yang et al. (2003); Brown et al. (2006); Quintero-Febres et al. (2006); Zhang and Tan (2007a); Birrcher et al. (2009); and Mihaylov et al. 2010.

Only those references that provided sufficiently complete information on the test setup and material properties were used. This database is considered to be sufficiently large to enable a fair assessment of code provisions. The deep beams that were considered in this assessment include a/d ratios ranging from 0.27 to 2.50, concrete strengths that range from 13.8 to 99.4 MPa, and various combinations of web reinforcements. Beams that were described by the original authors as having a failure mode other than shear (anchorage and flexural failure) were not included in the database. A summary of deep beams is presented in Appendix A.

In the STM, diagonal strut width, w_{st}, was calculated from the geometry of the nodal regions according to the location of the node. The depth of the tie, h_a, was defined by the location of the longitudinal reinforcement and was taking twice the distance between the soffit of the beam to the centroid of the longitudinal reinforcement. To calculate the depth of the top horizontal strut, h_n; and thus the diagonal strut angle, α, an iterative process was done to choose the critical admissible solution and, hence, the maximum predicted shear strength. The iterative process included checking of the stresses at the node.

The results obtained from the steel-reinforced deep beam database are presented in Figure 2.11. The experimental strength was divided by the calculated capacity and plotted in a histogram. A value less than 1.0 implies that the experimental strength was unconservatively estimated. Contrary, a value greater than 1.0 implies a conservative estimate. The mean and coefficient of variation (COV) of the results for CSA A23.3 (2014) and ACI 318 (2014) provisions are presented as well.

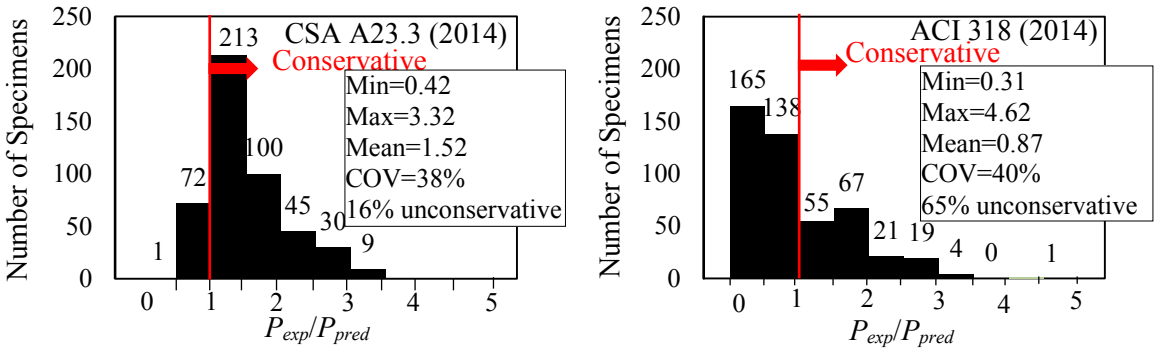

Figure 2.11 - Evaluation of code provisions with steel-reinforced deep beam database

The results indicate that the CSA A23.3 (2014) provisions provided uneconomically conservative estimations of strength; while the ACI 318 (2014) provided unsafe estimation for the strength of the deep beams. The mean experimental/predicted capacity value (P_{exp}/P_{pred}) in CSA A23.3 (2014) provision was 1.52, and the COV was 0.38. While the mean experimental-to-calculated capacity value (P_{exp}/P_{pred}) in ACI 318 (2014) was 0.87, and the COV was 0.40. The unconservative percentage was 16% and 65% for CSA A23.3 (2014) and ACI 318 (2014), respectively. These values indicate that the equations used by both provisions do not catch all the factors affecting the behavior of steel-reinforced deep beams, and led to unsatisfactory estimations of the capacity. The same conclusions were reported by Bahen and Sanders (2009), Brown and Bayrak (2008), and Collins et al. (2008).

The experimental-to-calculated capacity according to the two code provisions were compared by the percentage of the longitudinal reinforcement ratio (ρ%), concrete compressive strength (f_c') and percentage of web reinforcement ($\sum \frac{A_{si}}{bs_i}$) in Figure 2.12(a), (b) and (c), respectively.

As can be notice from Figure 2.12(a), the ACI 318 (2014) gave more scatter estimations for the deep beam capacities associated with the longitudinal reinforcement strains compared to CSA A23.3 (2014) provision. This was mainly attributed to the STM according to ACI 318 (2014), unlike CSA A23.3 (2014), do not accounts for the effect of the longitudinal reinforcement ratio.

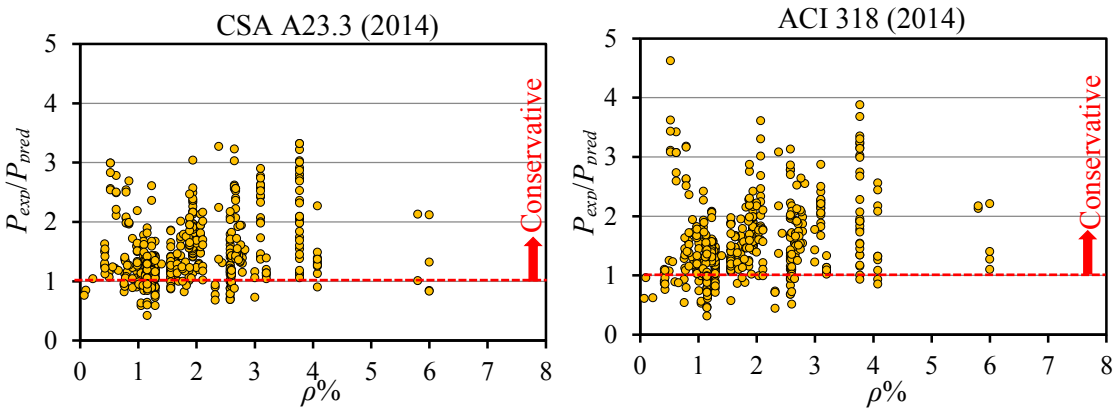

a) Longitudinal reinforcement ratio (ρ%)

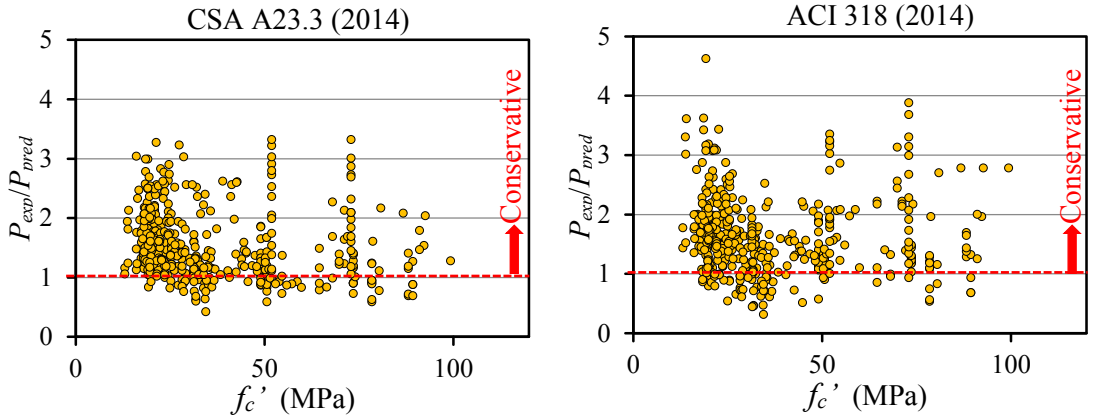

b) concrete compressive strength (f_c')

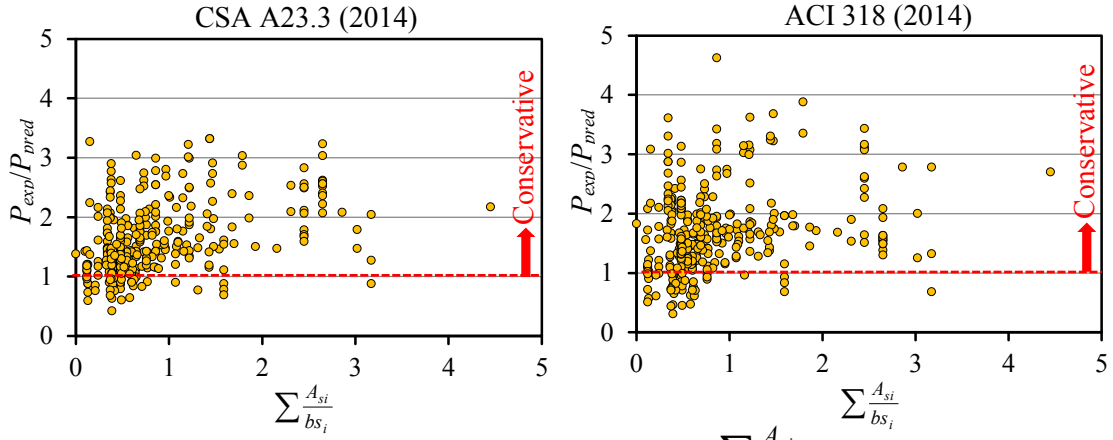

c) Web reinforcement ratio ($\sum \frac{A_{si}}{bs_i}$)

Figure 2.12 - Experimental/calculated capacity for the steel-reinforced deep beams in the database

Figure 2.12(b) shows that the two provisions gave very conservative estimation for deep beams with high strength concrete, for a compressive strength more than approximately 50

MPa. However, the level of conservatism was more pronounced in case ACI 318 (2014). Bahen and Sanders (2009) indicated that the estimations of ACI 318 (2011) and AASHTO LRFD (2008) were very conservative for concrete strengths greater than 48 MPa and 41 MPa, respectively. As mention before, AASHTO LRFD (2007) provision uses the same equations, limitations and exclusions as CSA A23.3 (2014).

In order to assess the adequacy of the two code provisions for the steel-reinforced deep beams with web reinforcement, specimens without web reinforcement were excluded from the database in Figure 2.12(c), resulting in a total number of 319 specimens. Unlike ACI 318 (2014), CSA A23.3 (2014) requires minimum web reinforcement in steel-deep beams for crack control only without any effect on the ultimate strength of the deep beams. On the other hand, ACI 318 (2014) specifies a percentage of minimum web reinforcement to increase the load carrying capacity of the deep beams in addition to the crack control. However, CSA A23.3 (2014) gave more accurate predictions for deep beams' capacity with web reinforcement compared to ACI 318 (2014). Nevertheless, ultimate strength estimations for deep beams with web reinforcement using both codes still very conservative.

Specifications of Canadian codes (CSA S23.3 2014, CSA S806 2012, and CSA S6 2014) calculate the strut strength based on the Modified Compression Field Theory (MCFT) (Vecchio and Collins, 1986). The conducted testing scheme (Vecchio and Collins, 1982) made the compressed concrete – in the direction of the compressive stresses – subjected to tensile strain in the perpendicular direction, which was distributed along the length of the panel edge. During testing, compressive and tensile strains were measured using perpendicular LVDTs attached to the panels along its length to measure the smeared/average strain across the formed cracks.

Accordingly, to accurately predict the ultimate capacity of the deep beams, the average strain along the diagonal strut should be determined through a series of LVDTs attached across the diagonal strut and along its length, which is impractical and could be achieved only through experimental testing.

Therefore, the Canadian specifications assume the tensile strain in the concrete is equal to the tensile strain in the main longitudinal reinforcement (tie). The commentary on CSA S6 (2014) Clause C8.10.3.3 and CSA A23.3 (2014) Clause C11.4.2.3 explained that the tie reinforcement is surrounded by the concrete in the diagonal strut, and if these tensile strains increased, f_{cu} will decreased. This was also observed in FRP-reinforced deep beams (Farghaly and Benmokrane 2013) as increasing the axial stiffness of the tie increased the efficiency of the diagonal strut by increasing the ultimate strength. In addition, the Canadian specifications require a minimum web reinforcement to be placed to act as ties for the diagonal strut and distribute the forces along the strut (Commentary on CSA S6 (2014) Clause C8.10.2 and CSA A23.3 (2014) Clause C11.4.1, and CSA S806 (2012) Clause C8.5.1.

These assumptions over-estimate the average strain, however, it under-estimate the ultimate capacity of the deep beams and lead to conservative, yet safe, predictions. Generally, more investigation is necessary to elaborate over determination of the strain along the diagonal strut length specifically close to the upper node as the deep beams fail mainly due to crushing in the diagonal strut close to the upper loading node.

2.5 Web Reinforcement Effect on Deep Beams' Strength

Researchers are disagreeing regarding the exact effect of web reinforcement on strength of steel-reinforced deep beams. For instant, previous experimental and analytical researches noted that the presence of conventional web reinforcement in the form of vertical stirrups or horizontal bars had little, if any, effect on the strength of the inclined strut. Such reinforcement may delay the cracking process, and this may cause only a small increase in the load carrying capacity of the inclined strut (Mihaylov et al. 2010, Tan et al. 2003, Smith and Vantsiotis 1982). Other researchers reported that web reinforcement is not required for enhancing the efficiency of the concrete strut (Birrcher et al. 2013, Tuchscherer et al. 2010, Brown and Bayrak 2007). This section briefly describes the conducted investigations for the effect of web reinforcement on strength of steel-reinforced deep beams.

Notwithstanding, the use of nominal web reinforcement is considered essential for crack control purposes, because it reduces the likelihood of 'instability' failures due to the out-of-

plane actions related to the heterogeneous nature of concrete (Kotsovos 1988). In addition, web reinforcement resists the tensile stresses transverse to the direction of compression strut as shown in Figure 2.1. Hence, web reinforcement must be placed within the strut to carry the transverse tension.

Web reinforcement in deep beams is most efficient when it is placed perpendicular to the strut axis (Kong et al. 1972, Brown and Bayrak 2006). However, struts are not often aligned with the axes of a deep beam or its reinforcement. As previously mentioned, struts forms between the loadings and reactions points as in Figure 2.5. Alternatively, two layers of reinforcement may be placed orthogonally to provide the necessary transverse reinforcement. If the main diagonal crack is assumed to open without shear slip along the crack, the forces in the reinforcement bars crossing that crack can be calculated as shown in Figure 2.13.

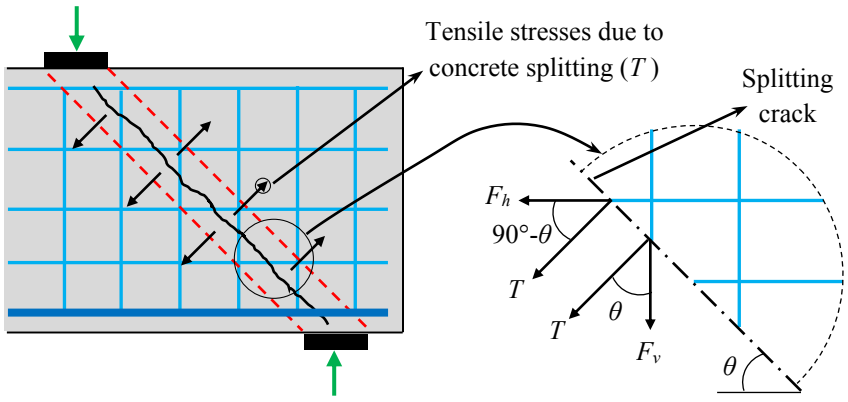

Figure 2.13 – Effect of web reinforcement on strut strength (Brown and Bayrak 2006)

Kong et al. (1970) tested 35 simply supported deep beams of span-to-depth ratios *L/D* ranging from 1 to 3 and clear shear span-to-depth ratios *x/D* from 0.23 to 0.7. The effect of seven different types of web reinforcement on deflections, crack widths, crack patterns, failure modes, and ultimate load in shear were studied. The seven series contains different amount and type of web reinforcement shown in Figure 2.14.

The crack pattern and mode of failure of all the 35 test beams were similar, despite the differences in web reinforcement and in *L/D* and *x/D* ratios. When the load reaches 70 to 90 percent of the ultimate load, cracks were formed near the supports and propagate towards the

loading points. Nevertheless, in series 6 and 7, where web reinforcement were wither presents only near the bottom or else absent, the appearance of this type of diagonal crack was often accompanied by a rather loud noise.

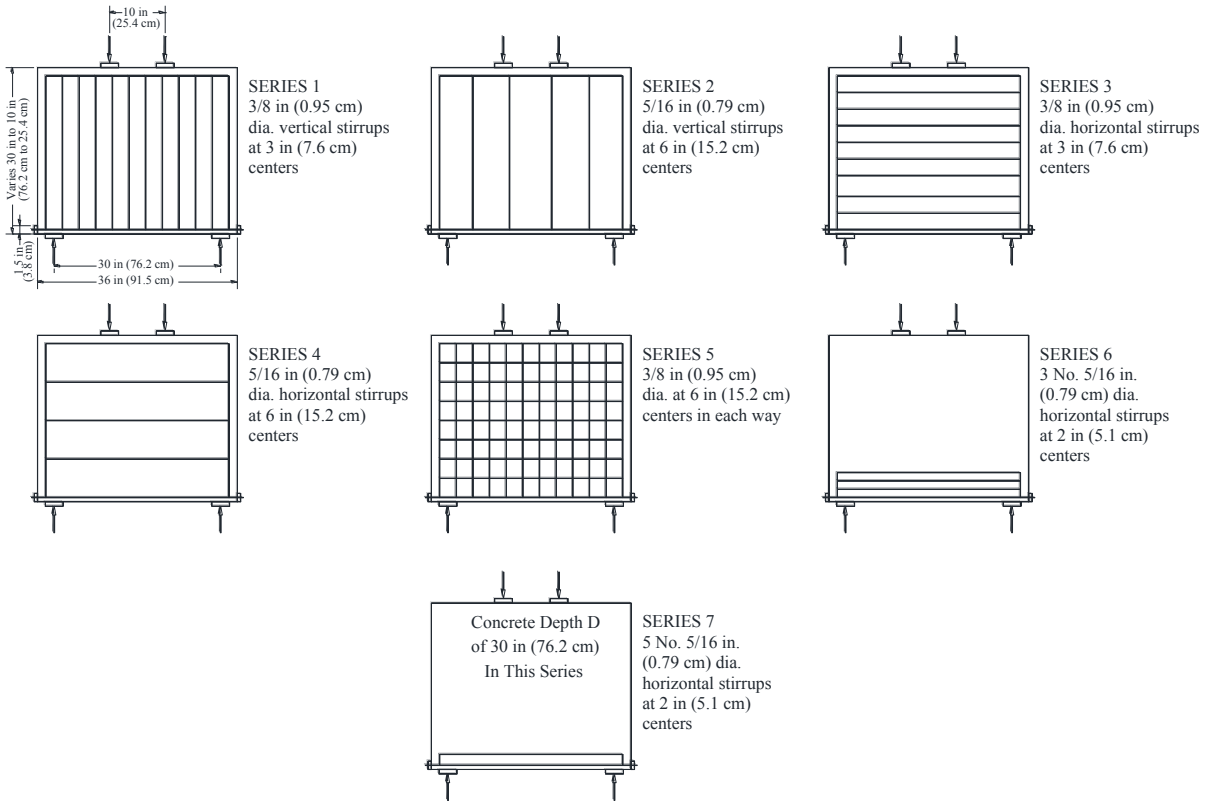

Figure 2.14 - Details for web reinforced tested by Kong et al. (1970)

Kong et al. (1970) concluded that, for control of deflections and crack widths the preferred arrangement of web reinforcement depends very much on the *L/D* and *x/D* ratios. For low *L/D* and *x/D* ratios, only horizontal web reinforcement placed near the bottom at a fairly closed spacing is effective. Where *L/D* is higher than 1.5 and *x/D* higher than 0.35 vertical stirrups can be used and where *L/D* is 3 and *x/D* 0.7, vertical stirrups are preferable to others.

Continuing their study on web reinforcement, Kong et al. (1972) tested another 10 simply supported deep beams incorporating different amount of inclined web reinforcement. They concluded that the inclined web reinforcement is a highly effective type of web reinforcement, comparing with horizontal and vertical web reinforcement, for all the *L/D* and *x/D* ratios studied.

Smith and Vantsiotis (1982) tested 52 concrete deep beams under two equal symmetrically placed point loads. The investigation's objectives were to study the effect of vertical and horizontal web reinforcement and shear span-to-effective depth ratio on inclined cracking shear, ultimate shear strength, mid-span deflection, tension reinforcement strains, and crack width. They concluded the following: i) all 52 beams failed in shear, ii) no significant change in the failure mode was observed between different beams. However, less damage at failure was observed in beams with web reinforcement, iii) a significant decrease in beam stiffness was observed with the major inclined crack formation in the shear span. However, presence of a minimum amount of vertical and horizontal web reinforcement was effective to considerably reduce crack widths and deflections after inclined cracking. Therefore, a minimum percentage of web reinforcement should be used for crack control, iv) inclined cracking loads were considerably lower than ultimate loads for beams with or without web reinforcement, v) presence of vertical and horizontal web reinforcement had no effect on inclined cracking load, vi) in general, web reinforcement increased ultimate shear strength for all beams tested. Addition of up to 1.25 percent and 0.91 percent horizontal web reinforcement increased ultimate shear strength by not more than about 30 percent, vii) presence of vertical web reinforcement increases ultimate shear strength of deep beams. However, vertical stirrups' effectiveness seems to diminish for beams with $a/d < 1.0$, and viii) horizontal web reinforcement appears to have little influence on the ultimate shear strength. Its influence is more noticeable in beams with $a/d < 1.0$.

Rogowsky and MacGregor (1986) tested 7 simply supported deep beams with different amount of horizontal and vertical reinforcement or vertical only web reinforcement. All beams were 2200 mm in length with different heights ranging from 400 to 1000 mm. four a/d ratios were used, 0.75, 1.25, 1.6 and 2. The notice that, the additional amount of horizontal reinforcement had very little effect on the strength. On the other hand, specimens with maximum stirrups specified by ACI 318 (1983), showed a great amount of ductility and failed at much higher shear strength than specimens without web reinforcement.

Tan et al. (1997) investigated the behavior and the ultimate strength of 18 high strength concrete deep beams with concrete cylindrical strength, f_c', ranging from 55 MPa to 86 MPa.

The test specimens are divided into three series based on the shear-span-to-overall-height ratio *a/h*. Each series consists of six beams with different arrangements of horizontal and vertical web reinforcements, i.e., the main variables are the horizontal and the vertical web steel ratios. Observations are made on mid-span deflections, crack widths, failure modes and ultimate strengths. They concluded that the web reinforcement can play an important role for high strength concrete deep beams. For deep beams with $a/d \geq 1.13$, the vertical web steel has greater effect on restraining the diagonal crack width and increasing the ultimate shear resistance of high strength concrete deep beams than the horizontal web steel of the same steel ratio. It is also confirmed that the web steel contribution of high strength deformed bars is significantly greater than that of lower strength plain mild steel bars.

Among 53 deep beams tested by Oh and Shin (2001), different vertical and horizontal shear reinforcement ratios are used. Jung-Keun Oh and Sung-Woo Shin (2001) concluded that the ultimate shear strength of tested beams was increased slightly due to web reinforcement. In deep beams with high strength concrete, ultimate shear strength was increased slightly with addition of vertical shear reinforcement as a/d increased. There was no increase of ultimate shear strength with addition of horizontal shear reinforcement.

Li (2003) tested eight full-scale deep beams under concentrated load to investigate the influence of span-to-depth ratio and the influence of uniformly distributed horizontal and vertical reinforcement. He concluded that, specimens with 0.2% uniformly distributed horizontal reinforcement and 0.2% uniformly distributed vertical reinforcement exhibited totally different responses compared to specimens of the same dimensions without the distributed reinforcement. The former specimens had higher load capacities and more symmetrical cracking patterns. The presence of the uniformly distributed reinforcement resulted in much better crack control at service load levels and hence ail deep beams should contain crack control reinforcement. He also concluded that, the simplified STMs, neglecting the contribution of horizontal and vertical uniformly distributed reinforcement, resulted in conservative predictions provided that bond failure does not occur.

Brown and Bayrak (2006) examined the amount of transverse reinforcement required to resist the tension developed in a bottle-shaped strut and presented an equilibrium-based approach to determining the necessary amount of transverse reinforcement for a bottle-shaped strut. They

concluded that the use of bottle shaped strut without transverse reinforcement should not be permitted regardless of efficiency factor. A minimum amount of reinforcement should be used to compensate for effects of temperature, restrained shrinkage, and other effects that may not be explicitly taken into account. In addition, the amount of transverse reinforcement required to maintain equilibrium in a bottle-shaped strut is a function of the force applied to that strut. Hence, the efficiency factor affects the required reinforcement.

Brown and Bayrak (2007) tested 10 deep beams to examine the impact of load distribution and shear reinforcement on the behavior of the beams. The specimens were 686 mm in depth and 3048 in effective span but with different amount of vertical-only or horizontal-only web reinforcement. They observed that the two specimen with only horizontal web reinforcement carried less shear than the identical specimens with no shear reinforcement of any kind. They explained that this counterintuitive result was likely due to the large amounts of scatter associated with the shear strength of reinforced concrete beams. On the other hand, a small amount of vertical reinforcement increased strength much more effectively than a large amount of horizontal reinforcement. However, additional vertical reinforcement did not seem to produce any additional increase in shear strength.

Birrcher et al. (2009) conducted an experimental study in 37 reinforced concrete deep beam specimens. The specimens are some of the largest deep beams ever tested in the history of shear research. The data from the experimental program and from a database of 179 deep beam tests in the literature were used to address eight tasks associated with the strength and serviceability design and performance of deep beams. One of these eight tasks was to determine an appropriate amount of minimum web reinforcement (stirrups and longitudinal side face reinforcement) considering the strength and serviceability demand of a deep beam.

Birrcher et al. (2009) recommended an appropriate amount of minimum web reinforcement to ensure adequate strength and serviceability performance in deep beams. Numerous tests in the experimental program were used to evaluate the effect of the quantity of web reinforcement on the performance of the member. At an *a/d* ratio of 1.85, tests were conducted on beams with a 21”x23”, 21”x42”, 21”x44”, 21”x75”, and 36”x48” cross-section (533x584, 533.4x1067, 533x1118, 533x1905 mm). At *a/d* ratios of 1.2 and 2.5, two tests were conducted on beams

with a 21”x42” (533x1067 mm) cross-section. Several different distributions of web reinforcement were investigated. The majority of the test specimens had either 0.2% or 0.3% reinforcement in each direction. Stirrups with 2 and 4 legs were used. Two tests were conducted on specimens without web reinforcement.

For beams tested at an *a/d* ratio of 1.2 and 1.85, providing either 0.2% or 0.3% reinforcement did not affect the shear strength of the member. A specimen tested at an *a/d* ratio of 2.5 with 0.3% reinforcement in each direction failed at a substantially higher load than a companion specimen with 0.2% reinforcement.

The specimens tested at an *a/d* ratio less than 2 failed in a manner consistent with a single-panel, direct-strut mechanism. Thus, any reinforcement greater than that which is required to maintain equilibrium in the bottle-shaped strut is unnecessary for strength. The specimens tested at an *a/d* ratio of 2.5 generally failed in a manner that was consistent with a sectional-shear model, or a multiple-panel STM. At this *a/d* ratio, increasing the amount of vertical reinforcement increases the shear strength of the member.

To restrain maximum diagonal crack widths to 0.016 in. (0.406 mm) at first cracking and at estimated service loads, 0.3% reinforcement in each orthogonal direction should be provided and spaced evenly near the side face of the effective strut area. The maximum diagonal crack width of specimens with 0.2% reinforcement in each direction often exceeded 0.016 in. (0.406 mm) at first cracking and at estimated service loads (33% of ultimate), whereas those with 0.3% reinforcement satisfied this limit in general. 0.3% reinforcement is consistent with the current AASHTO LRFD provision (Article 5.6.3.6, 2008) except it is proposed that the amount of reinforcement need not be based on the gross concrete section.

Tuchscherer et al. (2011) fabricated 3 full scale deep beams to evaluate the benefit of distributing stirrups across the web of the deep beams. Two ends of each beam were tested resulting in a total number of 6testes. All specimens were tested with a span-depth ratio (*a/d*) of 1.84. The primary experimental variables were the number of stirrup legs distributed across the web and the amount of web reinforcement. Based on the test results, it can be concluded that distributing stirrup legs across the width of the web of specimens as wide as 36 in. (930 mm) had a small influence on the shear capacity and service-level behavior. Taken in

conjunction with the relative conservatism of the ACI 318 (2008) STM provisions, the influence of stirrups was observed to be considerably less significant. Due to the fact that web reinforcement is relatively ineffective in a deep beam, a limitation of stirrup spacing across the web may be inefficient or unnecessary. Nonetheless, it is generally considered good practice to provide intermediate stirrups across the section of very wide beams. Based on the findings of thier study, they stated that intermediate stirrup legs are not necessary in deep beams as wide as 36 in. (910 mm). Additionally, provided that exterior stirrup legs are transversely spaced no farther than *d* from one another, where *d* is the depth of the beam from the extreme compression fiber to the centroid of the tension reinforcement.

Sahoo et al. (2011) derived an analytical expression for minimum transverse reinforcement required to prevent splitting failure in bottle-shaped struts in terms of the strengths of concrete and steel reinforcement and validated experimentally through isolated strut tests. The isolated strut tests also served to highlight the role of web reinforcement in the load-deformation response of bottle-shaped struts. The proposed expression for minimum reinforcement is comparable with an analogous expression in the literature. According to Sahoo et al. (2011), to prevent splitting failure, it is to be ensured that $\sigma_1 \geq \sigma_2$, then the minimum web reinforcement required to prevent splitting of bottle-shaped struts is given by:

$$\sum \frac{A_{si}}{b_s s_i} \sin^2 \alpha_i \geq 0.28 \frac{\sqrt{f_c'}}{f_y} \tag{2.5}$$

Where σ_1 is the steel stress normal to crack resulting from vertical and horizontal confinements; σ_{1i} is the normal stress across crack due to *i*-th layer (horizontal and vertical) of confining reinforcement; A_{si} area of one layer of surface reinforcement in *i*-th (H is horizontal; V is vertical) orientation crossing strut; b_s is the thickness of bottle-shaped strut or beam or beam-column joint (out-of-plane); s_i is the spacing of surface reinforcement in *i*-th (H is horizontal; V is vertical) orientation; α_i is the angle of inclined struts with strut axis in local STM for bottle-shaped strut for the *i*-th layer.

The left-hand side of this proposed expression (Eq. 2.24) seeks to transform an inclined grid of web reinforcement into its component transverse to the strut axis and the right-hand side gives

the minimum transverse reinforcement required to prevent splitting failure in bottle-shaped struts. The proposed minimum transverse reinforcement requirement compares favorably with an analogous expression given in the literature and has been experimentally validated with the help of isolated strut tests performed by subjecting thin plain and reinforced concrete panels made of three grades of concrete and seven transverse reinforcement ratios to in-plane, displacement-controlled, axial compressive loading. Splitting failure in the isolated bottle-shaped struts has been identified on the basis of a failure criterion proposed in this study. The experimental results for minimum transverse reinforcement were found to be in close agreement with the predictions of the proposed analytical expression.

Sahoo et al. (2011) suggested that, for design practice, the minimum reinforcement requirements from strength and serviceability criteria recommended in the current design codes and the literature may be checked for conformity with the proposed expression to minimize the possibility of catastrophic splitting failures in bottle-shaped struts.

2.6 Fiber Reinforced Polymers

Conventional concrete structures are reinforced with nonprestressed and prestressed steel reinforcement. Corrosion of steel reinforcement in concrete structures induces a serious threat to the integrity and safety of structural concrete members. Costly rehabilitation works represented a challenge to seek technical solutions and alternatives. Traditional corrosion remedies, including the use of stainless steel, epoxy coatings, cathodic protection, chemical inhibitors, and treatment of concrete surfaces, are either expensive or of limited technical value (ACI 440.2R, 2008).

Recently, composite materials made of fibers embedded in a polymeric resin, known as FRPs, have become an alternative to steel reinforcement for concrete structures. FRP reinforcement is one of the most promising new developments for concrete structures. The application of FRP reinforcement is becoming increasingly important in construction industry as well as having great potential in many areas. FRPs offer the designer an outstanding combination of properties not available in other materials. The use of these composites for special applications in construction is highly attractive and cost effective due to improved durability, reduced life

cycle maintenance costs, saving from easier transportation and improved onsite productivity, and low relaxation characteristics. In addition, fatigue strength as well as fatigue damage tolerance of many FRP composites are excellent. Because of their advantages over conventional materials, FRPs have found their way into numerous construction applications (Erki and Rizkalla 1993).

The mechanical behavior of FRP reinforcement differs from the behavior of conventional steel reinforcement. Accordingly, a change in the traditional design philosophy of concrete structures is needed for FRP reinforcement. Therefore, as studying FRP reinforced concrete deep beams, the properties of FRP bars should be discussed.

2.6.1 FRP Reinforcement Type

FRP reinforcing bars can be made from one of three typical fiber materials. These fiber materials include aramid, carbon and glass fibers. Two types were used in the current study, glass fiber reinforcement polymer bars (GFRP) and carbon fiber reinforcement polymer bars (CFRP). Properties of the two FRP bars are presented in the following sections.

i. Glass fiber reinforced polymer (GFRP)

Glass fibers are the most common of all reinforcing fibers for polymeric matrix composites. Glass fibers are classified as fiber drawn from an inorganic product of fusion that has cooled without crystallizing. Among advantages of glass fibers are low cost, high tensile strength, high chemical resistance and excellent insulating properties. Notwithstanding, the disadvantages are relatively low tensile modulus that can be as low as 1/6 of the value of CFRP, sensitivity to abrasion during handling, suffer from alkalinity, and relatively low fatigue resistance in comparison with the CFRP . The types of glass fibers commonly used are E-glass, S-glass and C-glass. E-glass has the lowest cost of all commercially available reinforcing fibers, which is the reason for its widespread use in the FRP industry.

GFRP bars are available in different sizes, ranging from 6 mm in diameter to 32 mm; i.e. from No.2 to No.10 bars. GFRP bars have a sand coated external layer, a mold deformation layer, or a helically wound spiral fiber layer, to create rough surface. The longitudinal strength of

GFRP bars is bar size dependent; due to the material used in deferent bar size and shear lag. The strength of GFRP decreases as the diameter increase. The tensile strength of GFRP bars range between 675–875 MPa. While the modulus of elasticity is 45–60 GPa, and the ultimate strain is in range 1.3–1.9 %.

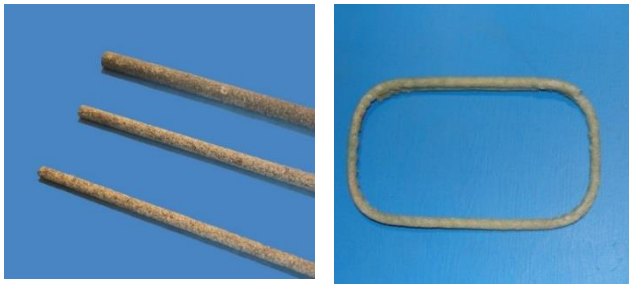

Figure 2.15 - GFRP straight and bent bars

ii. Carbon fiber reinforcement polymer (CFRP)

Carbon fibers are manufactured from one of the three types of precursors (starting materials), namely, polyacrylonitrile (PAN) fibers, rayon fibers or pitch. Among the advantages of CFRP is their exceptional high tensile strength – weight ratio, low tensile modulus – weight ratio, low thermal expiation coefficient, which provides dimensional stability and high fatigue strength. The disadvantages of CFRP bars are their low strain-to-failure, low impact resistance, beside their high cost. These disadvantages, especially due to cost considerations, led to limiting CFRP bars to be used in prestressing tendons and near-surface-mounted (NSM) strengthening more than using it as conventional reinforcing bars.

Carbon fiber reinforced polymer (CFRP) bars are more expensive than GFRP bars. The diameter ranges between 6 mm and 25 mm; i.e. from No.2 to No.8 bars. The tensile strength of CFRP reinforcing bars decreases with the increase of bar diameter.

Figure 2.16 - CFRP straight and bent bars

2.6.2 Properties of FRP Bars

FRP materials are anisotropic and are characterized by high tensile strength with no yielding in the direction of the reinforcing fibers. This anisotropic behavior affects the shear strength and dowel action of FRP bars, as well as their bond performance. Design procedures should account for a lack of deformability in concrete reinforced with FRP bars. A reinforced concrete member reinforced with FRP bars is designed based on its required strength and then checked for serviceability and ultimate state criteria (e.g. crack width, deflection, fatigue and creep rupture endurance). In many instances, serviceability criteria may control the design.

The effects of the differences in the mechanical characteristics of FRP materials and steel had to be considered. These differences include FRP's lack of ductile behavior from the essentially linear elastic stress-strain relationship of the materials until rupture, lower modulus of elasticity, and higher ultimate strength, resulting in significantly different stiffness. Besides, considerations had to be given on using high amount of FRP may lead to brittle failure which is unfavorable in reinforced structures. The main affecting properties investigated to achieve the best FRP bar for longitudinal and web reinforcement of deep beams are; tension strength, shear properties, anchorage properties as well as bond properties as discussed in the following sections.

i. Tensile strength

The tensile strength and stiffness of an FRP bar are dependent on several factors. The most significant factors are fiber volume friction that is defined as the ratio of the volume of fiber to the overall volume of the bar over the unit length. Bar manufacturing process, quality control and rate of resin curing also affect tensile strength (ACI 440.2R, 2008). Moreover, the tensile strength is function of FRP diameter. Due to shear lag, fibers located near the center of cross section are not subject to the same stress as those fibers oriented near the outer surface of FRP (ACI 440.2R, 2008). This phenomenon results in reduced strength and efficiency in larger diameter bars. FRP bars may fail by one of the following failure modes: 1) tensile rupture of fibers; 2) matrix tensile rupture causing separation of the fibers from the matrix; 3)

combination of fiber/matrix interfacial shear failure; and 4) matrix shear failure causing longitudinal splitting (debonding along the fiber/matrix interface).

FRP bars in tension exhibit a linear elastic stress-strain response up to failure as seen in Figure 2.17. Linear elastic response up to failure with low failure strains, a lack in yield plateau with a general lack of ductility, brittle failure, very high tensile strength and relatively low modulus of elasticity, these are the main mechanical properties of FRP bars. Table 2.3 shows typical tensile properties of different FRP bars compared with steel bar properties.

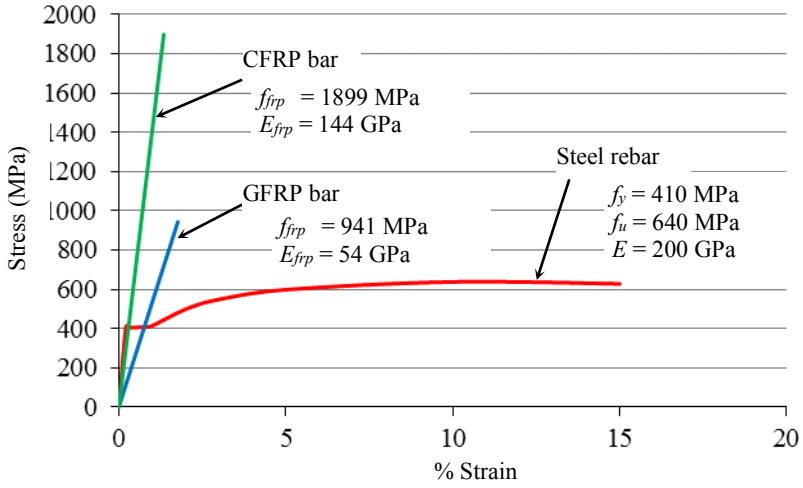

Figure 2.17 - Stress-strain curve for steel bar #4, GFRP bar #4 (V-Rode) and CFRP bar #4

Table 2.3 - Usual tensile properties of reinforcing bars (ACI 440.2R, 2008)

Properties	Steel	GFRP	CFRP	AFRP
Yield Stress MPa	276 to 517	N/A	N/A	N/A
Tensile strength MPa	483 to 690	483 to 1600	600 to 3690	1720 to 2540
Elastic modulus GPa	200	35 to 51	120 to 580	41 to 125
Yield strain %	0.14 to 0.25	N/A	N/A	N/A
Rupture strain %	6.0 to 12.0	1.2 to 3.1	0.5 to 1.7	1.9 to 4.4

ii. Shear properties

Most FRP bar composites are relatively weak in inter-laminar shear where layers of unreinforced resin lie between layers of fibers. Because there is usually no reinforcement across layers, the inter-laminar shear strength is governed by the relatively weak polymer matrix. Orientation of the fibers in an off-axis direction across the layers of fiber will increase the shear resistance, depending upon the degree of offset (ACI 440.2R, 2008).

Due to the low transverse modulus and strength of FRP bars, their dowel resistance for shear stress is insignificant. Additionally, bending of FRP bar into stirrup configuration resulted in significant reduction in the bent bar/stirrup strength at the bend location (El-Sayed et al. 2006). Therefore, FRP shear elements can fail due to either a dowel action rupture or a concentration of stress at a corner in the reinforcement (Hegger et *al*. 2009).

iii. Bend portion strength

As mentioned previously, the unidirectional properties of the FRP materials lower the transverse strength of the FRP bars. This leads to a concentration of stresses at a corner of the bent bars (Hegger et *al*. 2009). Furthermore, bending the FRP bars causes the innermost fibers at the bend to be kinked compared to those at the outermost radius (El-Sayed et al. 2006). The bend capacity of FRP bars is influenced by many factors such as the bending process, the radius of the bend, the type of the reinforcing fibers, and the bar diameter (ACI 440.1R, 2004).

CSA S806 (2012) and ACI 440.2R (2008) recommend the use of B-5 test to measures the ultimate load carrying capacity of a single FRP stirrup subjected to tensile forces in the direction of the straight portion. More information about the test procedure and specimens dimensions can be found in Appendix D of CSA S806 (2012).

iv. Bond characteristics

It is clear that bond properties of FRP reinforcement have a significant effect on the design of any construction. Critical design parameters, such as development and transfer length depend directly on the bond behavior. Also, the design tensile strength, the design modulus, deflection control, crack width calculations, and development length estimations all dependent on bond.

Bond stresses in reinforced concrete members arise from anchorage or development where bars are terminated. In a reinforced concrete flexural member, the tension force is transferred to the reinforcement through the bond between the reinforcement and the surrounding concrete. Bond stresses exist whenever the force in the tensile reinforcement changes. Bond between FRP reinforcement and concrete developed through a mechanism similar to that of

steel reinforcement; and depends on FRP type, elastic modulus, surface deformation, and the shape of the FRP bar (ACI 408 2, 1992).

In the last few years, a large number of tests on several types of FRP bars have been conducted in order to evaluate the interaction phenomenon between FRP bar and concrete. Numerous tests were analyzed to better understand bond mechanism and the influence of types of fibers, the outer surface of FRP bar, bar diameter, bar position in the cast, concrete compression strength, and embedded length. Many factors were investigated to influence the bond between concrete and FRP reinforcement such as, chemical bond, friction due to FRP surface roughness, mechanical interlock of FRP bar against concrete, hydrostatic pressure against the FRP bar due to shrinkage of hardened concrete, and swelling of FRP bars due to temperature change and moisture absorption. Several factors affecting the bond strength of FRP bars such as: 1) types of FRP bars; 2) physical and mechanical properties of FRP bars; 3) surface preparation of FRP bars; 4) concrete compressive strength; 5) method of confinement; 6) type of loading; and 7) embedded length.

2.6.3 Deep Beams Reinforced with FRP Bars

In a considerable number of recent publications, there has been a growing effort to improve design guidelines for concrete structures reinforced with FRP, especially with respect to shear design equations. However, there is a need for more experimental work that systematically studies the effect of some factors, such as the arch action and beam size, on the shear strength of FRP-reinforced concrete members (Razaqpur and Isgor 2006). Likewise, FRP is not being widely specified for RC structures in northern climates, where corrosion of reinforcing steel is a paramount problem, partly due to the scarcity of appropriate design standards for FRP reinforced concrete structures (Razaqpur and Isgor 2006).

Because of the difference in mechanical properties between steel and FRP bars (e.g., lower modulus of elasticity of FRP), the contribution of shear resisting mechanisms in FRP-reinforced deep beams is believed to be different from that in steel-reinforced concrete beams. For instance, FRP reinforced concrete members typically develop wider and deeper cracks than those in concrete members reinforced with steel. Because of such deeper cracks, the

contribution of the uncracked concrete compression zone, dowel action, and aggregate interlock to shear strength is reduced. Moreover, the dowel action for FRP bars is always less than that of steel bars because of its lower transverse strength (El-Sayed et al. 2006). Conversely, the contribution of the arch action mechanism to the shear strength in FRP-reinforced short beams can be improved because of the relatively higher tensile strength of FRP bars (Omeman et al. 2008).

Deep beams reinforced with FRP bars need detailed investigation in view of the relatively lower modulus of elasticity of FRP reinforcement compared with that of steel reinforcement. There have been considerable experimental investigations on FRP-reinforced slender beams but only very limited research on FRP-reinforced concrete deep beams. Most current design guidelines for FRP-reinforced concrete members have developed their recommendations based on previous knowledge of steel-reinforced concrete members. It is, therefore, important to evaluate the performance of deep beams reinforced with FRP compared with that of steel reinforced deep beams to explore any differences in their shear behavior and mode of failure. Moreover, investigating the applicability of the strut-and-tie method for FRP-reinforced concrete deep beams, which has been recommended in several RC design standards to predict the shear strength of steel RC short beams, is of significant importance.

Omeman et al. 2008 was the first who conducted a study to investigate the behavior of CFRP-reinforced concrete short beams subjected to shear forces. The test includes eight concrete short beams reinforced with CFRP and four control concrete beams reinforced with steel. All tested beams were reinforced with only bottom longitudinal reinforcement and no web reinforcement was provided. It was found that CFRP-reinforced beams could achieve shear strength values comparable to or higher than that of similar steel-reinforced beams. This is attributed to the improvement in the arch action mechanism because the tensile strength of CFRP bars is much higher than that of steel, thus leading to a more effective tensile tie.

The second attempt was done by Andermatt and Lubell (2013) by investigate the behavior of concrete deep beams reinforced internally with GFRP. Twelve deep beams with heights ranged from 306 mm to 1005 mm were tested to failure under 4-point bending. The specimens contained longitudinal GFRP reinforcement but no stirrups or distributed web reinforcement.

The primary test variables included the *a*/*d* ratio, which varied from 1.1 to 2.1 and the longitudinal reinforcement ratio. Details of beams tested by Andermatt and Lubell (2013) shown in Figure 2.18.

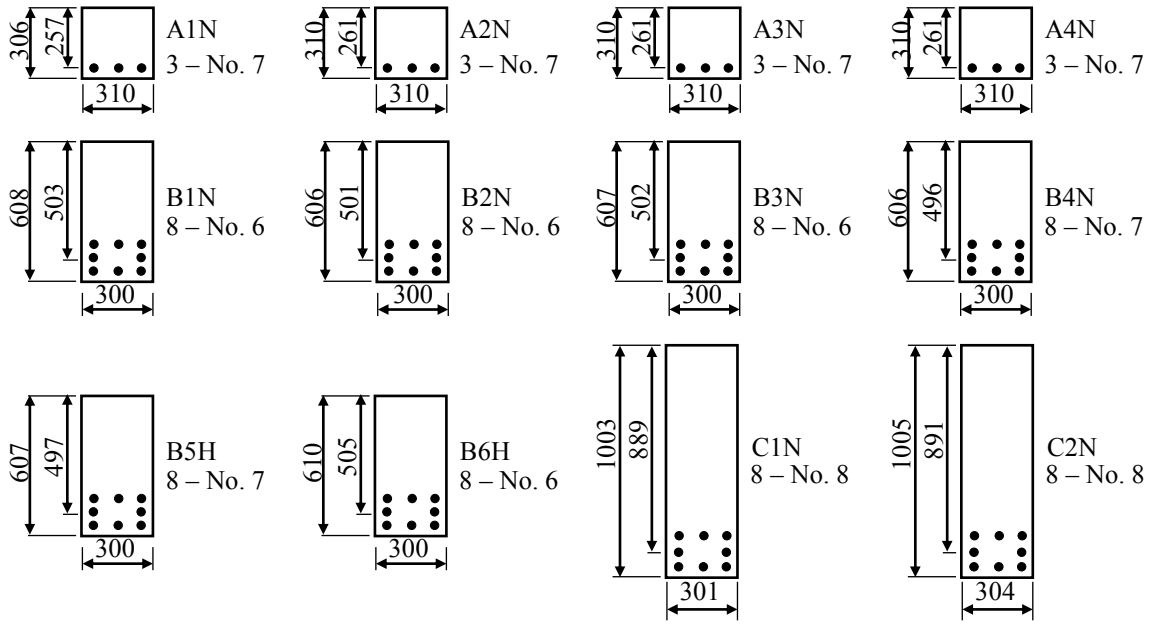

Figure 2.18 - Beam geometry for specimens tested by Andermatt and Lubell 2013(a)

The results indicated that, as shown in Figure 2.19, the load carrying capacity of the specimens decreased as the *a/d* ratio increased. Increasing the reinforcement ratio resulted in a slight increase in capacity. Beam with lower *a/d* ratio showed extremely ductile behavior after concrete crushing in the flexural compression region was detected. This reserve deformation capacity demonstrates the ductility that can be achieved in concrete beams reinforced with GFRP even though the reinforcement remains elastic. Hence, the plasticity required by the selection of certain STMs can possibly be attained through the plastic deformation of the concrete if appropriately detailed. Distributed reinforcement may be required to limit the crack widths.

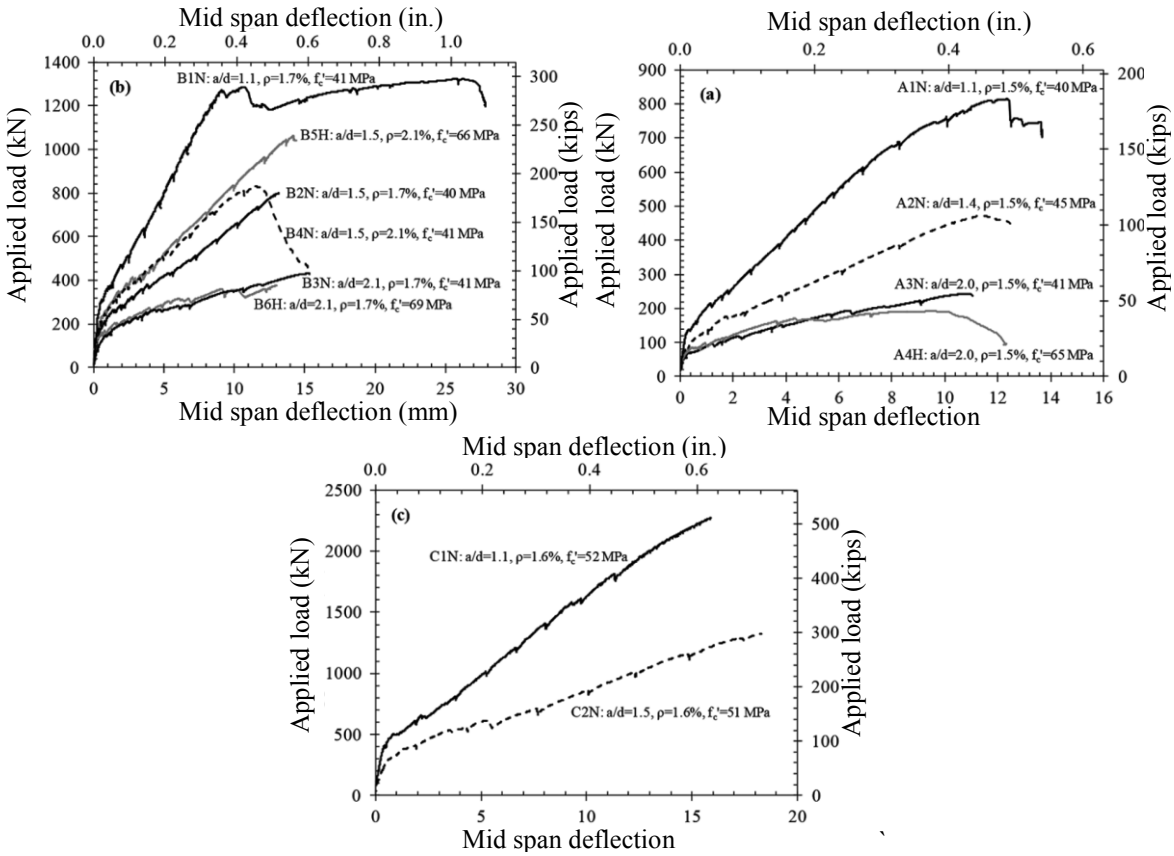

Figure 2.19 - Deflection response of specimens tested by Andermatt and Lubell 2013(a)

The specimens presented in their study were analyzed using the simple truss model and closely followed the internal forces as would be indicated by the theory of elasticity. Limited ductility is required to transmit the loads in the STM. However, the authors advised for conducting more experimental investigations to determine whether the STM approach will accurately predict the behavior in more complex situations.

CHAPTER 3
EXPERIMENTAL PROGRAM

3.1 Introduction

The details of the experimental program for ten full-scale deep beams are presented in this chapter. The design, fabrication and testing of the specimens at the Structural Engineering Laboratory at the University of Sherbrooke are discussed in detail.

3.2 Testing Program

All specimens were in full-scale size with rectangular cross-section, 300 mm width and 1200 mm height. The overall length of all specimens was kept constant (5000 mm), with variable clear spans equal to 3700, 3000, and 2300 mm resulted in different shear span-depth ratio (*a/d*) equal to 1.47, 1.13 and 0.83, respectively. All specimens were tested under two-point loading with constant distance between the two concentrated loads of 500 mm. The applied forces and support reactions were transmitted to the specimens by 203×300 mm and 280×300 mm steel plates, respectively.

The testing program was divided into two series to achieve the objectives of the research project. The purpose of Series I was to optimize the usage of the FRP bars based on the cross-sectional area and the type of the fiber. All specimens of series I contained longitudinal reinforcement with different bar configurations and without web reinforcement. In this series two different types of FRP bars were used, glass-fiber (GFRP) and carbon-fiber (CFRP). The bars diameter in case of glass fibers were #6 (19 mm) and #8 (25 mm) with total number of 8 bars. In case of carbon fibers total number of 12 bars was used with #3 (9.5 mm) and #4 (12.7 mm) bar diameter. Figure 3.1 and Table 3.1 shows series I beams' geometry and details.

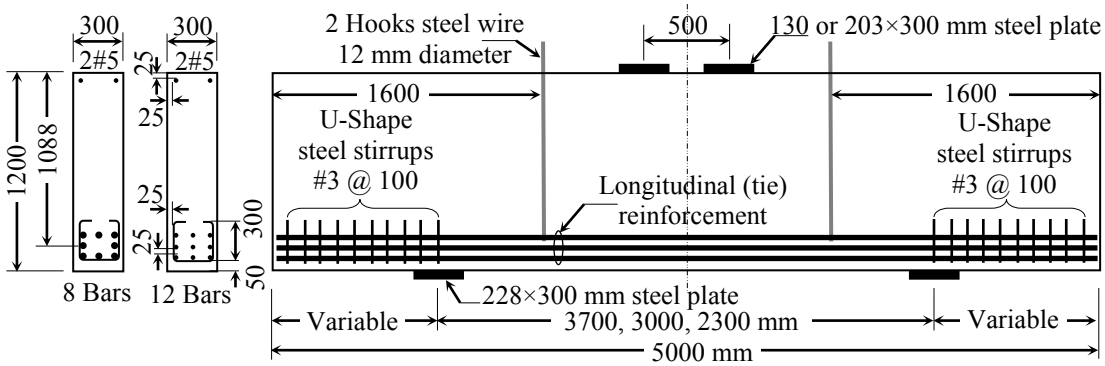

Figure 3.1 - Beam geometry of Series I

Table 3.1 - Series I beams' details

Beam ID	d (mm)	a (mm)	a/d	No of bars	Bar designation	ρ%	l_{b2} (mm)
G8#8†	1087.5	1250	1.13	8	#8	1.21	130×300
G8#6†	1096.5	1250	1.13	8	#6	0.67	130×300
C12#4†	1106	1250	1.13	12	#4	0.44	130×300
C12#3†	1111	1250	1.13	12	#3	0.25	130×300
G1.13	1087.5	1250	1.13	8	#8	1.21	203×300
G0.83	1087.5	900	0.83	8	#8	1.21	203×300
G1.47	1087.5	1600	1.47	8	#8	1.21	203×300

Note: ρ is the ratio of longitudinal tensile reinforcement to effective area (A_s / bd) and l_{b2} is the loading plate width; the support plate size (l_{b1}) for all specimens were 228×300 mm.
Note: † specimens tested by Farghaly and Benmokrane (2013).

The main purpose of Series II was to investigate the effect of web reinforcement on the behavior of FRP-reinforced deep beams on both ultimate load capacity and crack control. Hence, different configurations of FRP web reinforcement including vertical and/or horizontal reinforcement; were used with three different a/d ratios. All specimens had GFRP longitudinal reinforcement of 8 bars #8 (25 mm). The minimum vertical and horizontal web reinforcement are chosen to satisfy the crack control reinforcement specify in CSA S806 (2012) and ACI 318 (2014). Accordingly, when using vertical reinforcement only, #4 (12.7 mm) bars @200 mm were used; and when using horizontal-only web reinforcement, #5 (15.9 mm) bars @195 mm were used. In case of specimen with vertical and horizontal web reinforcement, the same configuration and amount of web reinforcement were used as that in vertical-only and

horizontal-only web reinforcement. As in series I, the three *a*/*d* ratios were equal to 1.43, 1.13 and 0.83. Figure 3.2.(a) to (c) and Table 3.2 shows series II beams' geometry and details.

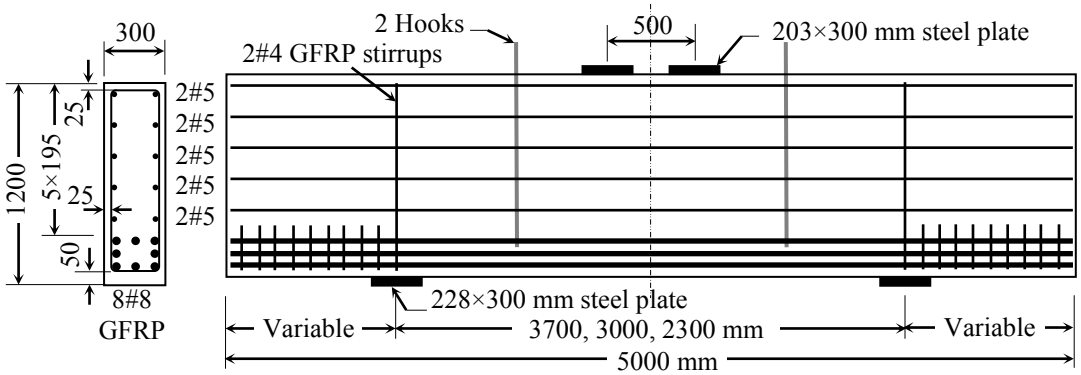

a) Specimens with vertical web reinforcement only

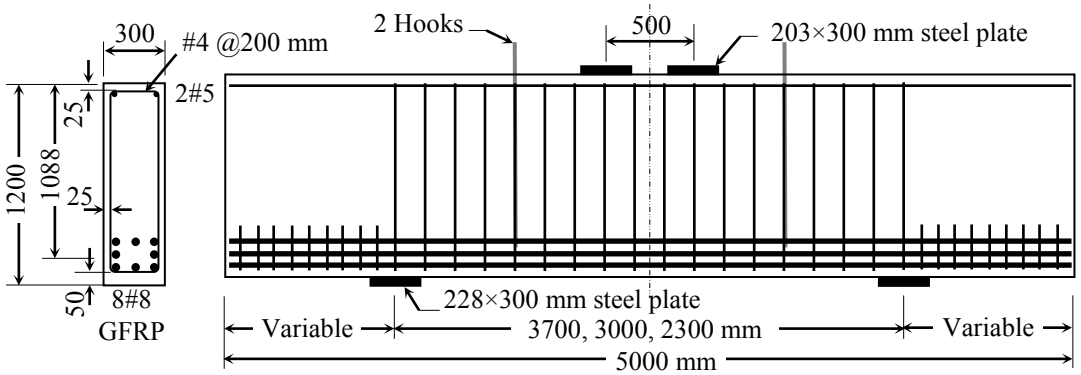

b) Specimens with horizontal web reinforcement only

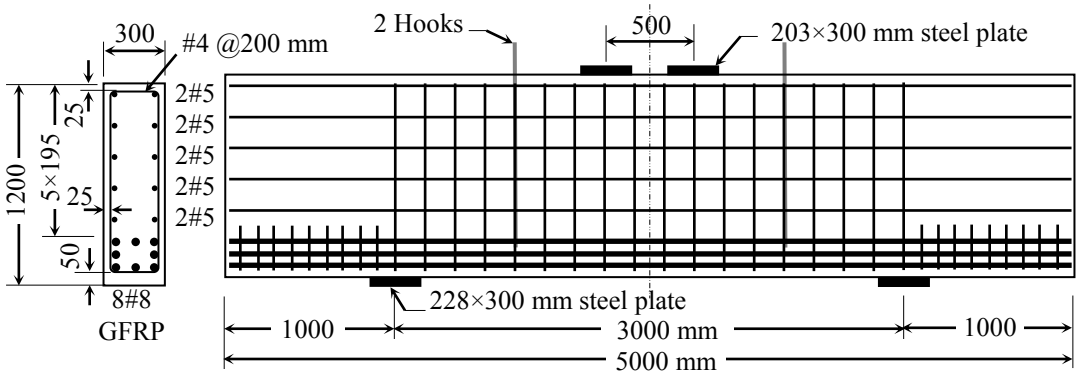

c) Specimen with horizontal and vertical web reinforcement

Figure 3.2 - Beam geometry of series II

Table 3.2 - Series II beams' details

Specimen ID	d (mm)	a (mm)	a/d	No of bars	Bar designation	ρ %	Web reinforcement					
							Vertical			Horizontal		
							s_v (mm)	#	ρ_v %	s_h (mm)	#	ρ_h %
G1.47H	1088	1600	1.47	8	#8	1.21	-	-	-	195	5	0.68
G1.47V	1088	1600	1.47	8	#8	1.21	200	4	0.42	-	-	-
G1.13H	1088	1250	1.13	8	#8	1.21	-	-	-	195	5	0.68
G1.13V	1088	1250	1.13	8	#8	1.21	200	4	0.42	-	-	-
G1.13VH	1088	1250	1.13	8	#8	1.21	200	4	0.42	195	5	0.68
G0.83V	1088	900	0.83	8	#8	1.21	200	4	0.42	-	-	-
G0.83H	1088	900	0.83	8	#8	1.21	-	-	-	195	5	0.68

Note: s_v is distance between vertical reinforcement bars in mm, s_h is distance between horizontal reinforcement bars in mm, ρ_v is the ratio of vertical reinforcement to effective area (A_v / b_w s_v) and ρ_h is the ratio of horizontal reinforcement to effective area (A_h / b_w s_h).

The tested specimens were designed to fail in shear since the objectives of the current study were associated with shear behavior. A minimum longitudinal tension reinforcement ratio of 0.25% was sufficient for the deep beam to fail in shear. Requirements in CSA S806 (2012) and ACI 318 (2014) were satisfied in the design of the test specimens. Spacing requirements between adjacent bars and between layers of bars were met. The bottom cover was set to 50 mm and the sides and top cover was 25 mm. The bars were tied together with a plastic ties; while plastic chairs were placed along the bars to obtain proper clear cover. Sufficient anchorage of the longitudinal reinforcement was provided with straight portions of FRP bars beyond the support. In this straight portion, steel stirrups of #3 (10 mm) diameter every 100 mm were provided to increase the anchorage between FRP bars and concrete. Two steel wires were placed on the third points of the specimens as lifting hocks. The labeling system is shown in Figure 3.3.

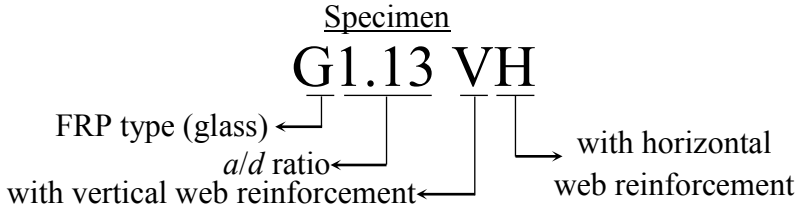

Figure 3.3 - Description of beams' ID naming system

The main purpose of this study is to investigate the behavior of FRP-reinforced deep beams; therefore, efforts were given to eliminate all premature failures. One of the critical issues is the anchorage length beyond the supports. Therefore, sufficient over-hanged length beyond the supports was provided in the current experimental program to ensure the development of arch action (Razaqpur and Isgor 2006) and to eliminate the failure of concrete splitting along the anchorage region (Breña and Roy 2009). The different failure mechanism for each failure mode directly affect strut efficiency factor (β) which would mislead in the interpretation of the factor β. Overall, the provided over-hanged length would be impractical and, therefore, a future study is recommended to investigate different anchorage methods such as bent FRP bars, headed FRP bars, and mechanical anchorage.

3.3 Fabrication of Tested Specimens

All of the test specimens were fabricated at the Structural Engineering Laboratory at University of Sherbrooke. Details of the fabrication process are presented as follow.

3.3.1 Reinforcement

The mechanical properties of the main longitudinal reinforcement; carbon and glass-FRP bars; and the vertical and horizontal web reinforcement are shown in Table 3.3, as reported by the manufacturer (Pultrall Inc., 2012). All bars were delivered in the specified lengths with the appropriate bends. FRP bars employed in this study had a sand-coated surface to enhance bond and force transfer between bars and concrete. The used GFRP bars were made of continuous high-strength E-glass fibers impregnated in a thermosetting vinyl ester resin, additives, and fillers. Straight bars (#5 and #8 bars) implied in this study made of V-Rod high modulus FRP type (Grade III) with a fiber content of 83% by weight, while vertical stirrups made of V-Rod standard modulus FRP type (Grade II) with a fiber content of 73.9% by weight (Pultrall Inc. 2009).

Table 3.3 - Mechanical properties of used FRP bars

Bar type	Bar diameter, φ_f† (mm)	Nominal cross-section area, A_{frp} (mm^2)	Ultimate tensile strength, f_{fu}‡ (MPa)	Modulus of Elasticity, E_{frp} (GPa)
GFRP	13 (#4)	126.7	1312	65.6
	15 (#5)	197.9	1184	62.6
	19 (#6)	285	1105	64.7
	25 (#8)	506.7	1000	66.4
CFRP	9.5 (#3)	71.3	1596	120
	13 (#4)	126.7	1899	144

Note: † number between brackets () are the manufacturer's bar designation; ‡ guaranteed tensile strength equal to the average value - 3×standard deviation (ACI 440.1R, 2006).

3.3.2 Concrete

Ready-mix of normal-weight concrete with a target concrete compressive strength of 40 MPa strength at 28 days was used to cast the test specimens. The compressive strength of concrete was measured using 100 mm in diameter and 200 mm in height standard cylinders in accordance with ASTM C31 and tested in accordance with ASTM C39. A minimum of 6 cylinders of each specimen were prepared. The cylinders were cast at the same time as the test specimen and were cured under the same ambient conditions. A plastic tarp was placed on top of the specimens to limit the loss of water due to evaporation.

A slump test was performed upon the arrival of the mixing truck to the laboratory. The targeted slump was between 100 mm and 150 mm. To increase the workability of the concrete, super-plasticizer was added to the concrete truck mixer after slump test and well mixed with concrete before casting.

3.3.3 Specimens' Construction

After the reinforcing bars arrived from the supplier, the cages were assembled in the laboratory and then moved to the casting area upon completion. Figure 3.4 shows the typical cages of specimen G1.13, G0.83V and G1.13VH. It worth mentioning that, in series I additional 2 FRP bars #5 (15.9 mm) were added as compression reinforcement to prevent compression pre-crack during the lifting of the beams. A wooden formwork was built

specially for this project. The internal face of the formwork was covered by galvanized steel sheets to produce a fair-face surface of the beams. The formwork was assembled to allow casting two beams at a time. Numerous vertical and horizontal steel angles were fabricated and assembled in the outside face of the wood formwork to provide lateral stability to the formwork during concrete dehydration. Maximum distance of 600 mm between vertical or horizontal steel angles was sufficient to bundle the formwork and resist the fresh concrete pressure. Figure 3.5 shows the assembled formwork before casting.

a) G1.13

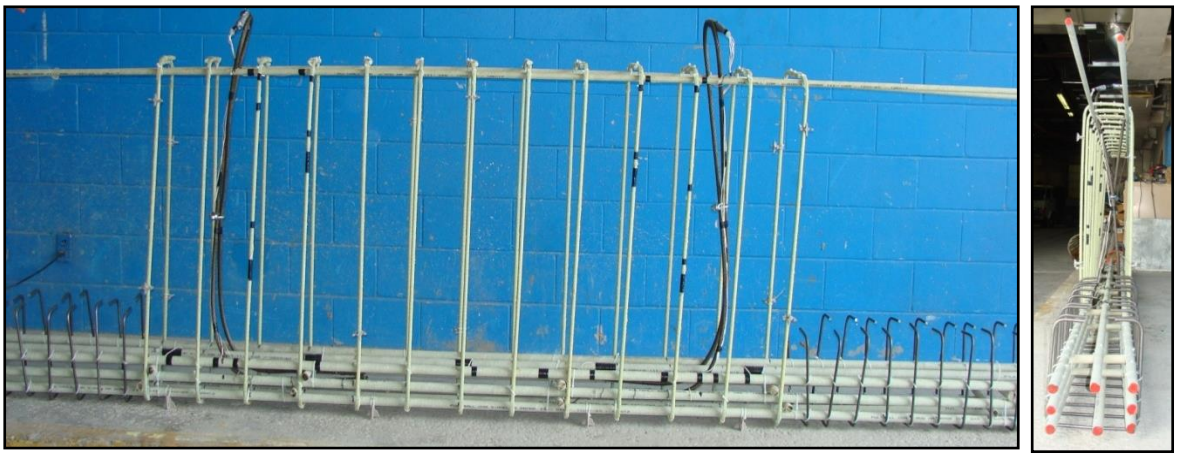

b) GV-0.83.

c) GVH-1.13

Figure 3.4 - Overview of specimens' cages

Figure 3.5 - Formwork in place prior to concrete placement

Figure 3.6 - Placement of concrete

Figure 3.7 - Test specimen after the removal of forms

Figure 3.8 - Curing of concrete

Figure 3.9 - De-molding of specimens using 25-ton crane truck

In the casting day, the ready-mix concrete arrived, a slump test was performed, and super-plasticizer was added. The specimens were cast in the same orientation that they were tested. Internal rod vibrators were used to aid in the consolidation of the concrete. Figure 3.6 shows the placement of the concrete on the formwork. One day after casting, the specimens were de-molded from its formwork (Figure 3.7). Then, the specimens cured under the ambient temperature and covered with clothes and plastic tarps positioned across the beam for seven days (Figure 3.8). Afterwards, specimens were lifted using 25-tons crane truck to prepare the formwork for new casting (Figure 3.9).

The specimens were moved to the testing area using 10-ton capacity truck. Two specimens were transported at a time. The specimen was then lifted and placed in the test setup with an overhead, 10-ton capacity crane.

3.4 Test Setup

To load the specimens to failure, a test setup was designed especially for this project in the Structural Engineering Laboratory at University of Sherbrooke. The load was applied via four hydraulic jack cylinders; each cylinder has a maximum capacity of 980 kN. The cylinders were attached to two transfer beams with four Dywidag bars. Each bar has a diameter of 2.5 inches (50 mm) with maximum capacity of 1400 kN. The ends of the Dywidag bars were attached to 1000 mm thickness rigid floor of the laboratory to transfer the reactions of the hydraulic cylinders. In the current configuration, the test setup can resist a maximum force of approximately 3920 kN.

Two steel transfer beams were designed to transfer the concentrated loads from the cylinders through the Dywidag bars to another spreader steel beam. The steel spreader beam was supported on a two 100 mm diameter rollers to produce the concentrated loads. Two bearing steel plates; 203 mm in width, 300 mm in breadth, and 25 mm in thickness; are placed between the roller and the specimen. A thin layer of high strength grout was applied to the surface of the test specimens at the location of the load bearing plates to provide planar reaction surface.

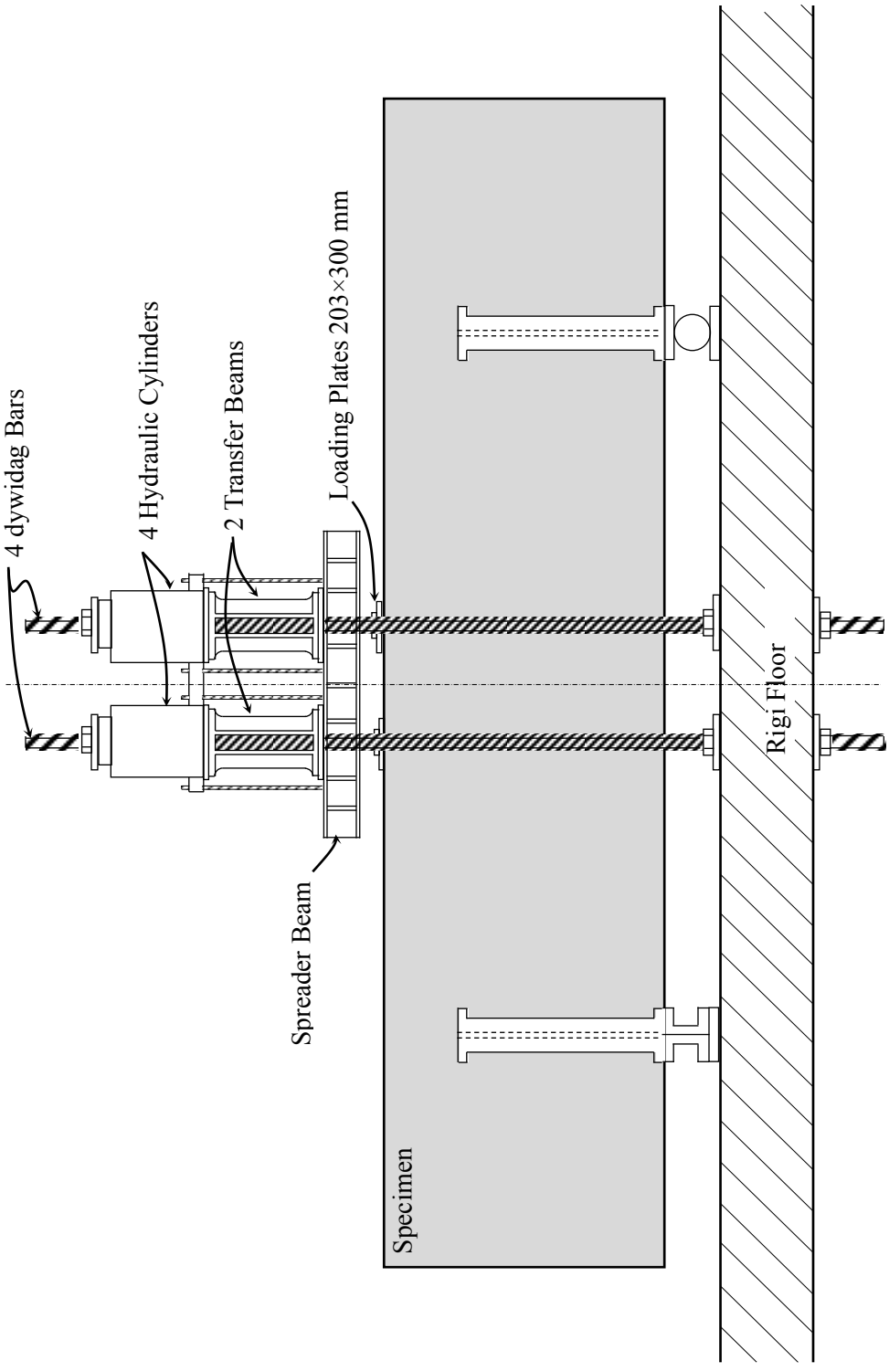

Figure 3.10 - Elevation view of test setup

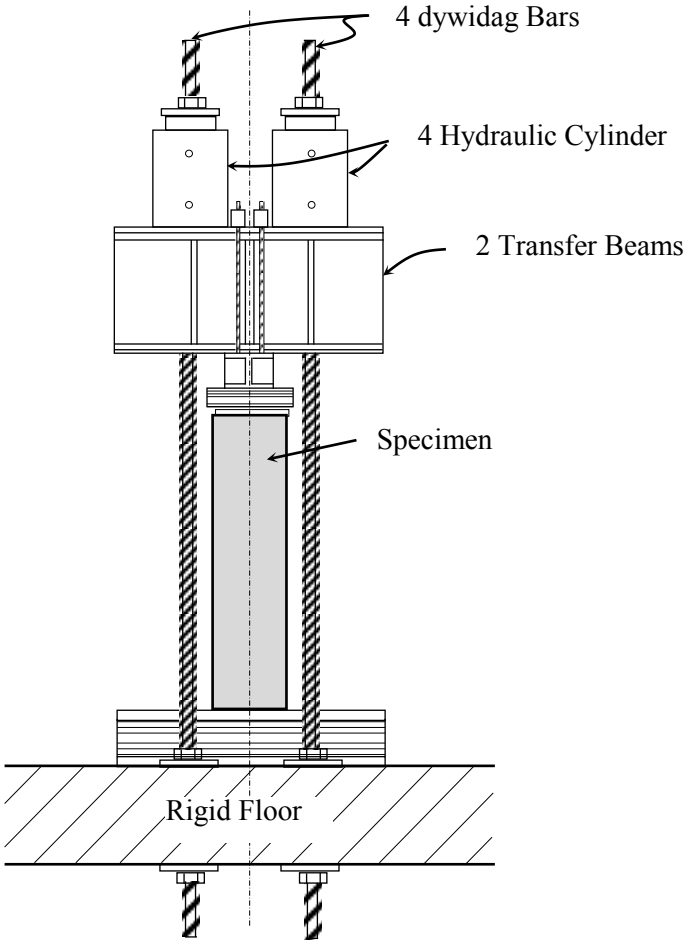

Figure 3.11 - Section view of test setup

All specimens were simply supported with different clear spans. A roller assembly was utilized at one reaction point to create a well-defined roller-supported condition for the specimen. The other support was more rigid support to prevent horizontal deformation described as a hinge-support. Hinge and roller support plates were 230 mm in width, 300 mm in breadth, and 15 mm in thickness. A thin layer of rubber was placed between the supports and specimen surface. Out-of-plan movement of the specimens during test was permitted using two steel I beams attached to the supports. Details of the test setup are depicted in Figure 3.10 to 3.12.

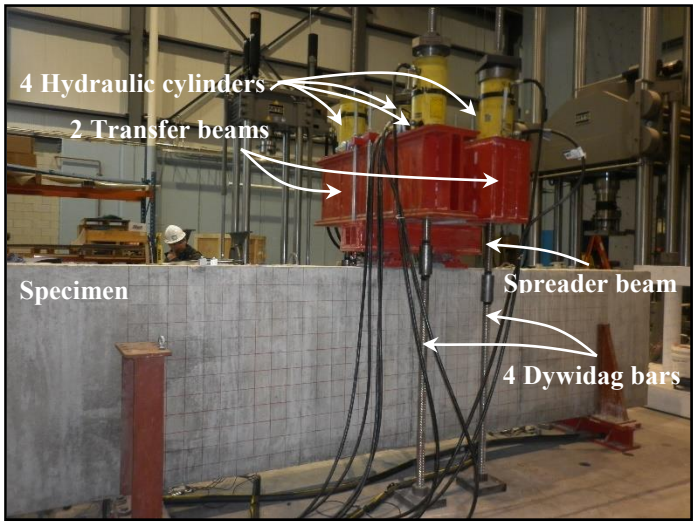

Figure 3.12 - Overview of test setup

3.5 Instrumentation

Different instruments were used to obtain data during the tests in the experimental program. The instrumentations included electrical strain gauges and LVDTs for displacements and crack widths. Details regarding each of these devices are provided in this section.

3.5.1 Strain measurements

Strain gauges were affixed to the longitudinal and web reinforcements in order to measure the change in strain. The gauge type was KFG-6-120-C1-11L3M3R manufactured by Tokyo Kyowa Electronic Instruments Co. These gauges are intended for general-purpose reinforcement applications. The length of the gauges was 6 mm, with a resistance of 120 ohms (± 0.5). The sand coated of the FRP was removed and the FRP bar was polished to provide a relatively smooth surface for the application of the strain gauges. Care was taken not to significantly reduce the cross section of the FRP bars. The gauges were glued to the FRP bars, then a thin layer of water proof rubber was glued over the strain gauge. All strain wires were carefully combined and attached to the hocks to be taken out for the specimens. Typical locations of internal strain gauges for the specimens are illustrated in Figure 3.13 for the cage of specimen G1.13VH and Figure 3.14.

Figure 3.13 - FRP strain gauge for GVH-1.13

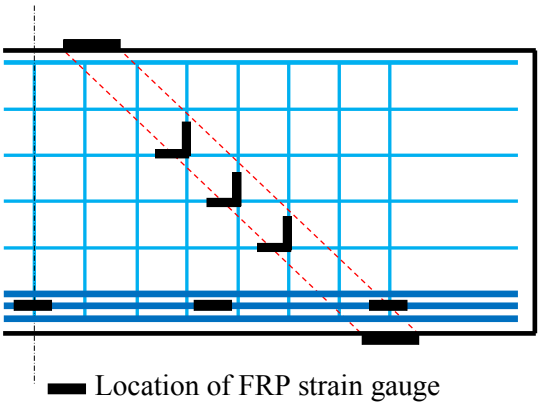

Figure 3.14 - Typical FRP strain gauge location

Strain gauges were attached to legs of stirrups along the assumed centerline of the inclined strut. They were also attached to the horizontal bars on each side of the beams at the intersection with the assumed diagonal strut. The purpose of locating a gauge along the strut centerline was to measure FRP strains at or close to the primary diagonal crack.

The strain in the primary tension reinforcement was also monitored in each specimen. Five strain gauges were glued along the longitudinal reinforcement. The purpose of these gauges was to monitor the strain in the primary tension tie throughout the shear span. Other researchers have monitored strain in a similar fashion to compare the behavior of the test specimen to an assumed STM (Rogowsky et al., 1986; Quintero-Febres et al., 2006; and Tan et al., 2007).

Concrete strain gauges were utilized to better understand the flow of forces from the load point to the near support. Ten concrete strain gauges were applied for each specimen. Four strain gages were placed, for each side of the specimen, at the third points of the direct strut, along a line perpendicular to the centerline of the strut. In this orientation, the dispersion of the compression across a strut was measured. Another strain gauge was placed in the horizontal strut between the two applied loads. The length of the concrete gauges was 60 mm, with a resistance of 120 ohms (± 1.0).The concrete strain gage location is shown in Figure 3.15.

Readings of surface concrete strain gauges were very low, and, in most cases, the concrete gauge corrupted immediately after the formation of the main diagonal crack. In addition, the concrete strain gauge read a local strain values, which might not be an accurate way to measure such values. Therefore, a long base length LVDTs were used to measure the concrete strains instead of concrete strain gauges. Nevertheless, in some cases, concrete strain gauges were used along with the concrete strain LVDTs, to confirm their accuracy.

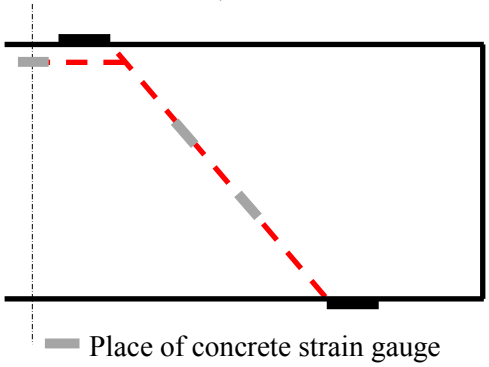

Figure 3.15 - Concrete strain gauge locations for Series I

A total number of 7 LVDTs were used in Series II to measure the concrete strain. A horizontal LVDT with base length of 300 mm was used at the horizontal strut, between the two loading points. In the two diagonal struts, three LVDTs were used per strut to measure the strain at the diagonal strut, one at horizontal, vertical and diagonal direction. The horizontal and vertical LVDTs had a base length of 300 mm while the base length for diagonal LVDT was 400 mm. LVDTs at strut region were placed after the formation of the main diagonal crack, in order to identify its direction and location. After the formation of the main diagonal crack the test stopped, the main diagonal crack width measured and kept monitored during test then the LVDTs were glued to the specimen. The value of the main diagonal crack width was excluded from the LVDTs readings. Figure 3.16 shows the typical locations of concrete strain LVDTs.

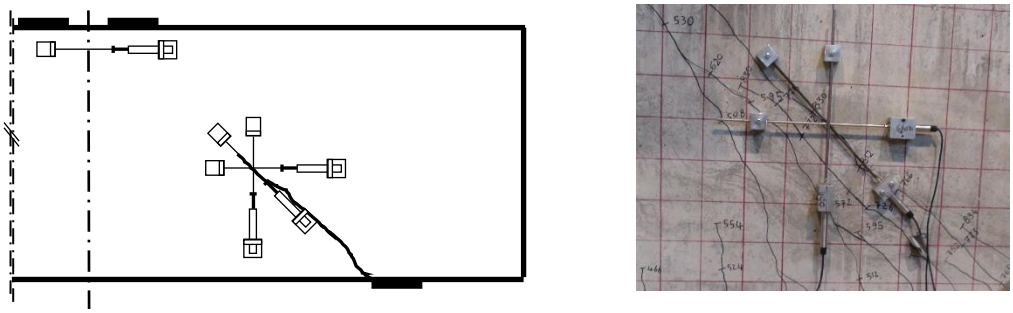

Figure 3.16 - Typical location for concrete strain LVDTs in Series II

3.5.2 Displacement and cracks measurements

The displacement of the specimens during testing was measured using four 50 mm LVDTs located under the load points, and the mid-span of the beam. LVDTs were calibrated and assembled before testing. In some cases, a wide crack opening in the compression zone between the two loading points appeared, hence, the mid-span upper LVDT was removed. Positions of displacement LVDTs is depicted in Figure 3.17.

Diagonal crack width measurements were monitored for the test specimens as part of the experimental program. The width of the diagonal cracks was recorded using two 20 mm LVDTs, one on each shear span for specimen under investigation at a distance 200 mm from the soffit of the deep beam. These LVDTs' were attached to the beams during test to measure the main crack width that causes failure. This crack was identified by the crack formulated between the load points and the supports. However, another diagonal crack was formed parallel to the first one at specimens with web reinforcement (horizontal and/or vertical). Hence, another two 20 mm LVDTs were attached, one in each side, to measure their widths. The position of the LVDTs crack measurements are depicted in Figure 3.18.

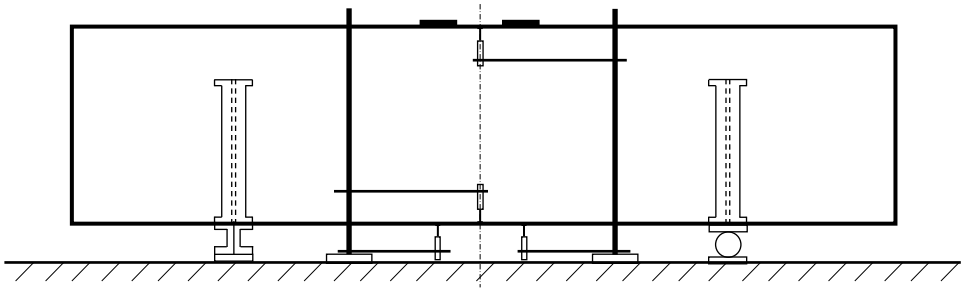

Figure 3.17 - Location of displacement LVDTs

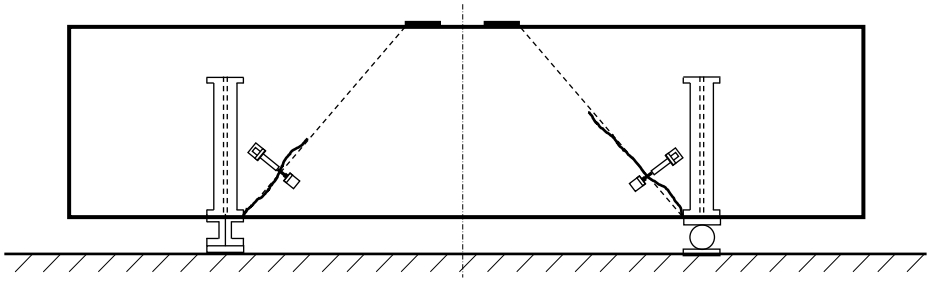

Figure 3.18 - Location of crack measurements LVDTs

3.6 Test Procedure

Beams were loaded with two concentrated loads to the failure. An initial load of 10% of the maximum expected load carrying capacity of the beam applied to the specimen before testing. The reason of applying an initial load is to insure that all the test setup parts are in rest before testing. Loading was then applied to the beam with 5 kN intervals until failure.

During test, the tested beam was inspected for any new or extended cracks. Cracks were marked and the load that cracks formulated or extended at was written. Some notes were taken during test such as the first crack load and main crack widths at the beginning of formulation. For safety precaution, the upper part of the test setup (hydraulic cylinders and spreader steel beams) was attached to a 10-ton crane to carry it in case of sudden failure of the beam occurred. Figure 3.19 shows specimen G1.47 while testing.

Figure 3.19 – Specimen G1.47 during testing

CHAPTER 4
EXPERIMENTAL RESULTS AND ANALYSIS

Foreword

Authors and Affiliation

- Khaled Mohamed: PhD candidate, Department of Civil Engineering, University of Sherbrooke.
- Ahmed Sabry Farghaly: Postdoctoral Fellow, Department of Civil Engineering, University of Sherbrooke, and Associate Professor, Assiut University, Egypt.
- Brahim Benmokrane: Department of Civil Engineering, University of Sherbrooke, Sherbrooke.

Journal: *Journal of Structural Engineering*, ASCE

Acceptation state: submitted December 30, 2014.

Reference: Mohamed, K., Farghaly, A. S., and Benmokrane, B., "Effect of Vertical and Horizontal Web Reinforcement on the Strength and Deformation of Concrete Deep Beams Reinforced with Glass-FRP Bars," *ASCE Journal of Structural Engineering*.

Abstract

Ten full-scale concrete deep beams reinforced with glass-fiber-reinforced polymer (GFRP) with a cross section of 1200 × 300 mm were tested to failure under two-point loading. The test variables were the configuration of web reinforcement (horizontal and/or vertical) and shear span-to-depth ratio (a/d = 1.47, 1.13, and 0.83). All specimens exhibited sufficient deformation required to develop arch action, which was confirmed by crack propagation and an almost linear strain profile in the main longitudinal reinforcement, in addition to the typical failure mode of crushing in the concrete diagonal strut. The results show that the vertical web reinforcement had no clear impact on ultimate capacity, while the configuration with horizontal-only web reinforcement unexpectedly resulted in a lower ultimate capacity compared to the specimens without web reinforcement. The web reinforcement's main contribution was significant crack-width control.

Keywords: deep beams; fiber-reinforcement polymer; web reinforcement; arch action

4.1 Introduction

A reinforced-concrete deep beam is a structural member with a relatively small ratio of shear span to depth (a/d) such that the behavior is shear dominated. Deep beams have various structural applications such as transfer girders, pile caps, and foundation walls. In deep beams, the strain distribution is nonlinear and the load is transferred to the support by a compression strut joining the loading point and the support (Smith and Vantsiotis 1982, Mau and Hsu 1989, MacGregor 1997, Collins et al. 2008, Tuchscherer et al. 2011).

The climatic conditions in some areas, however, call for alternative types of reinforcement to overcome corrosion issues due to the large amounts of deicing salts used during winter months. Salt application hastens the corrosion of steel bars, causing deterioration in reinforced-concrete structures, especially bridges. Fiber-reinforced-polymer (FRP) bars are emerging as a realistic and cost-effective alternative reinforcing material to prevent costly corrosion issues related to steel reinforcement and now deliver an acceptable level of performance (ACI 440, 2007, *fib* Task Group 9.3, 2007). Because of their advantages, FRP bars have found their way into numerous construction elements such as beams, slabs, columns, and, recently, walls (Kassem et al. 2011, Bakis et al. 2002, El-Salakawy et al. 2005, Tobbi et al. 2012, Mohamed et al. 2014). Proper design of FRP-reinforced deep beams serving as the main girders in bridges calls for investigation into the arch action developed by deep beams totally reinforced with FRPs.

The procedure of the strut-and-tie model for designing of steel-reinforced concrete deep beams is based on the lower-bound theorem, which posits that no failure occurs in any of the strut-and-tie elements (strut, node, or tie) until the main steel longitudinal reinforcement has yielded (Quintero-Febres et al. 2006, Tuchscherer et al. 2011). FRPs, however, are elastic materials and, therefore, the capacity estimation is consistent with the lower-bound theorem since the stress field satisfies the requirement of internal equilibrium with no failure of the strut-and-tie elements. Andermatt and Lubell (2013) confirmed the formation of arch action in FRP-reinforced concrete deep beams using crack orientation, measured strain in the longitudinal reinforcement, and reserve capacity after formation of the diagonal crack. Similarly, Farghaly and Benmokrane (2013) confirmed the development of arch action using the strain profile of

the longitudinal reinforcement in concrete deep beams reinforced with different FRP types and ratios. All these studies involved, however, deep beams without web reinforcement.

Previous research on steel-reinforced concrete deep beams has indicated that web reinforcement is considered essential for crack control (Tan et al. 1997). Nevertheless, there is disagreement between researchers, as well as in code provisions, about the effect of web reinforcement on the strength of steel-reinforced deep beams. For instance, Mihaylov et al. (2010) reported that web reinforcement improved the strength of the inclined strut and, hence, the shear strength of deep beams. Other experimental observations, however, indicated that web reinforcement had no impact on strength (Birrcher et al. 2013). Moreover, providing the minimum web reinforcement in a steel-reinforced deep beam designed according to ACI 318 (2014) would result in increasing the capacity by 1.67 over the capacity of a deep beam without web reinforcement. CSA A.23.3 (2014), and CSA S806 (2012) for steel-RC and FRP-RC, respectively, however, require the minimum web reinforcement solely for crack control with no effect on deep-beam strength. To the authors' knowledge, no investigations have been conducted to examine the effect of web reinforcement on the strength of FRP-reinforced deep beams.

The main objective of this study was to demonstrate that entirely GFRP-reinforced concrete deep beams (main longitudinal and web reinforcements) could achieve reasonable strength and deformation. It also experimentally assessed the web-reinforcement effect.

4.2 Crack Pattern and Mode of Failure

Figures 4.1 to 4.5 show the crack patterns for all the specimens at different load stages. The first crack to appear was flexural within the range of 11% to 18% of the ultimate load (Stage 1). The flexural crack was formed at the soffit of the deep beam between the loading points and propagated vertically up to approximately 80% of the deep-beam depth. Subsequently, additional flexural cracks formed at the constant-moment region. The flexural cracks in the specimens without web reinforcement were wider than those in the specimens with web reinforcement. Within the range of 19% to 35% of the ultimate load, the first shear crack

appeared independently from the flexural cracks, followed by adjacent shear cracks. The number and width of these adjacent shear cracks increased with *a*/*d* ratio.

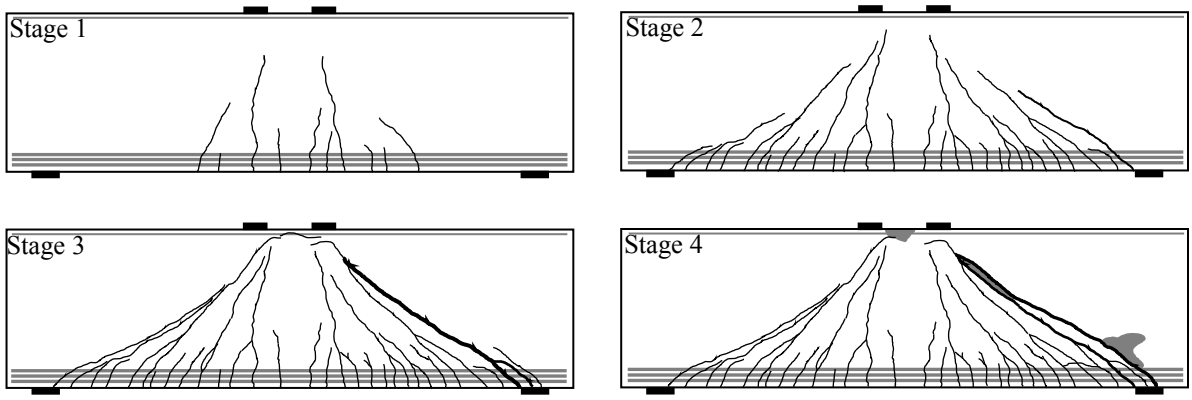

(a) G1.47

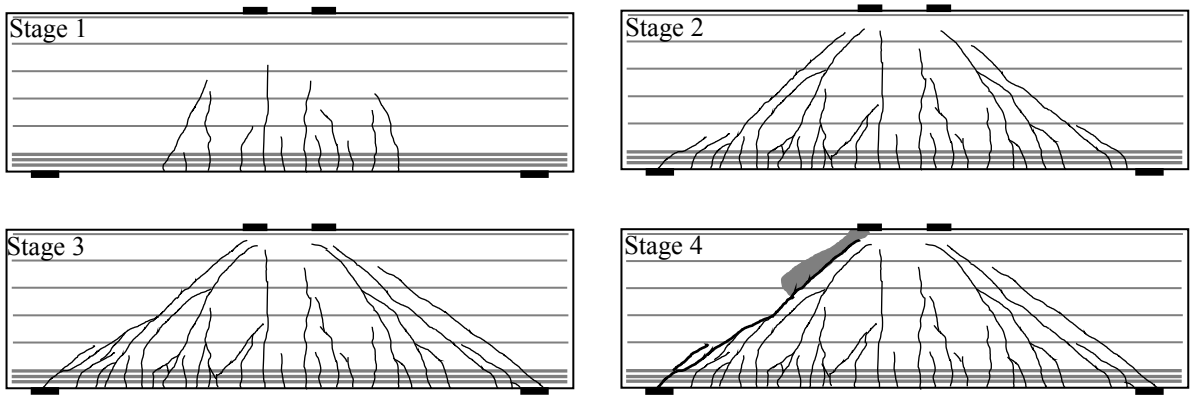

(b) G1.47H

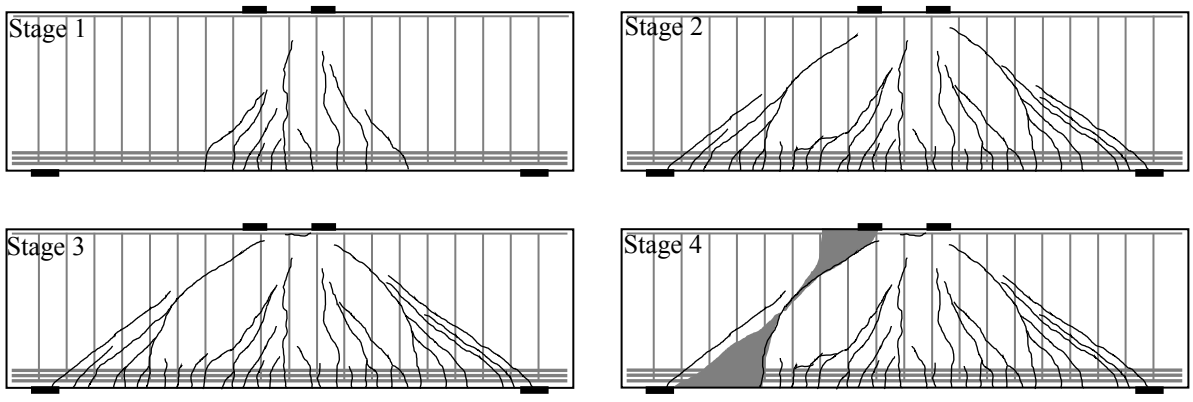

(c) G1.47V

Figure 4.1 - Crack pattern of deep beams with *a*/*d* ratio of 1.47

The main diagonal crack was formed between the loading and support plates through the expected diagonal strut at 27% and 44% of the ultimate load (Stage 2). With incremental load application, the main diagonal crack extended toward the inner edge of the support plate and the outer edge of the loading point until the specimens failed. Once the main diagonal crack appeared, all other shear cracks stopped widening and propagating. While the specimens without web reinforcement experienced only one main diagonal crack, the specimens with web reinforcement had parallel cracks adjacent to the first main diagonal crack. These cracks defined the direction of the concrete diagonal strut. Afterwards, at approximately 75% to 85% of the ultimate load, a new horizontal crack was formed between the loading points in the specimens with *a*/*d* values of 1.47 and 1.13 only, which defined the direction of the horizontal strut (Stage 3).

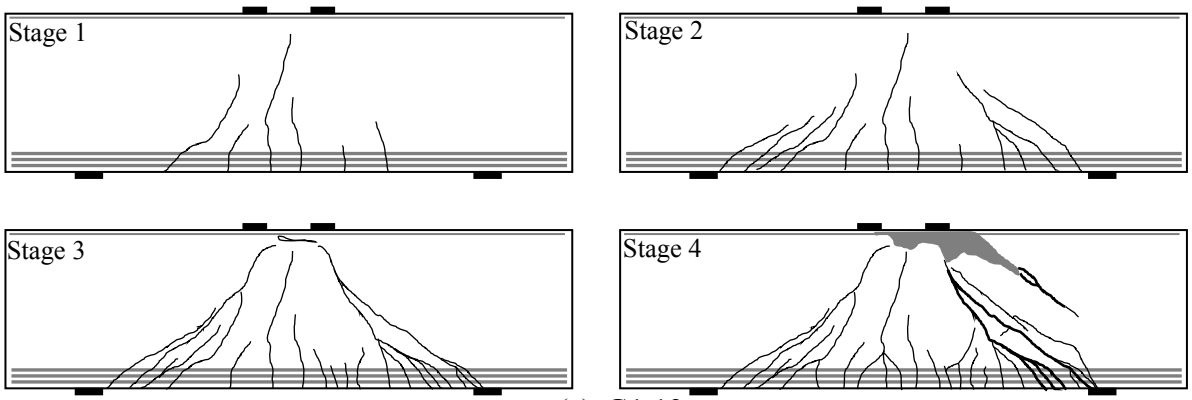

(a) G1.13

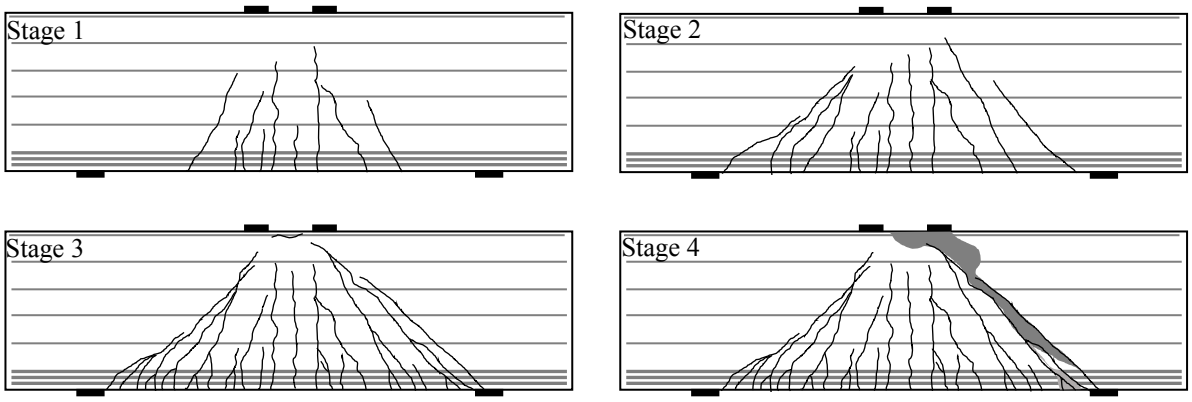

(b) G1.13H

Figure 4.2 - Crack pattern of deep beams with *a*/*d* ratio of 1.13

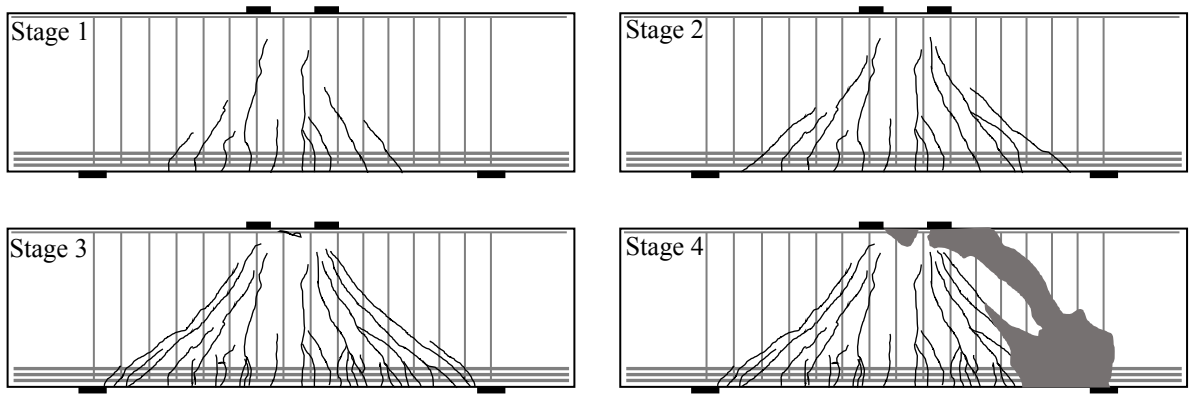

(c) G1.13V

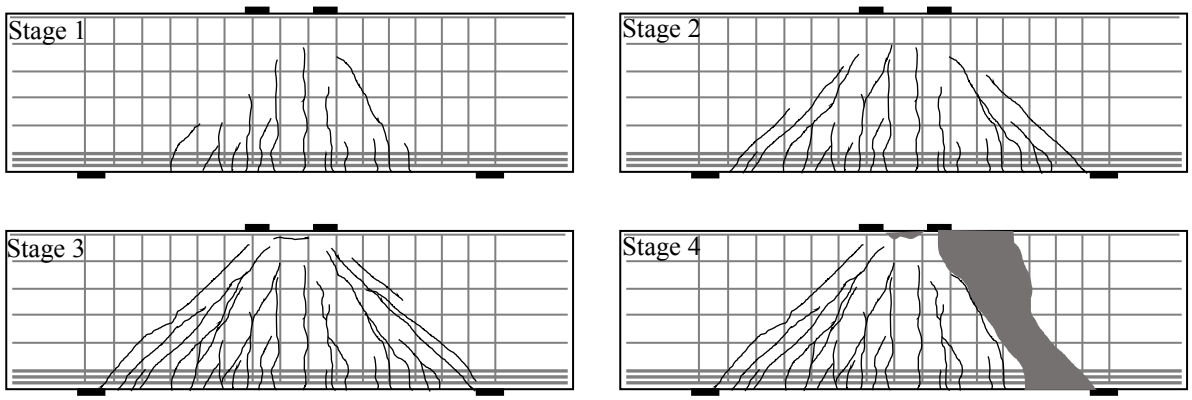

(d) G1.13VH

Figure 4.2 – Crack pattern of deep beams with *a*/*d* ratio of 1.13 (continued)

All the specimens experienced brittle failure, with relatively less brittle failure for the specimens with horizontal-only web reinforcement compared to the other specimens. No premature failure due to anchorage failure of the tension reinforcement was observed. The failure mode for all specimens was identified as complete or partial crushing of the concrete diagonal strut. In the specimens with *a*/*d* values of 1.13 and 1.47, the failure was associated with the crushing of the horizontal strut (Figure 4.4). Furthermore, the main longitudinal bars spalled the concrete cover next to the support plates (Figure 4.5-a).

In the deep beams with horizontal-only web reinforcement, the doweling of the horizontal bars, as shown in Figure 4.5-b, softened the surrounding concrete, causing localized crushing of the concrete diagonal strut. On the other hand, the vertical web reinforcement confined the concrete in the strut area, which distributed the failure along the height of the concrete

diagonal strut. Failure of all the specimens with vertical web reinforcement was associated with rupture in the bent portion of the vertical bars (Figure 4.5-c).

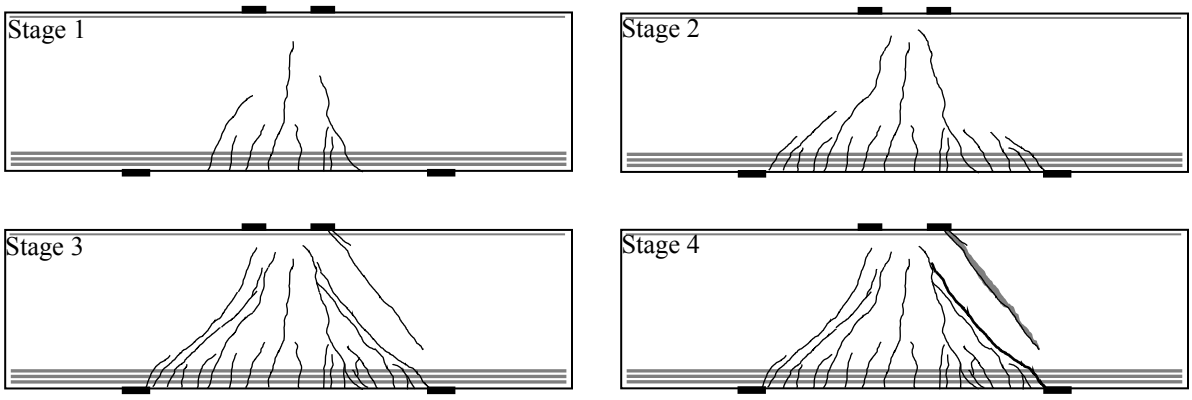

a) G0.83

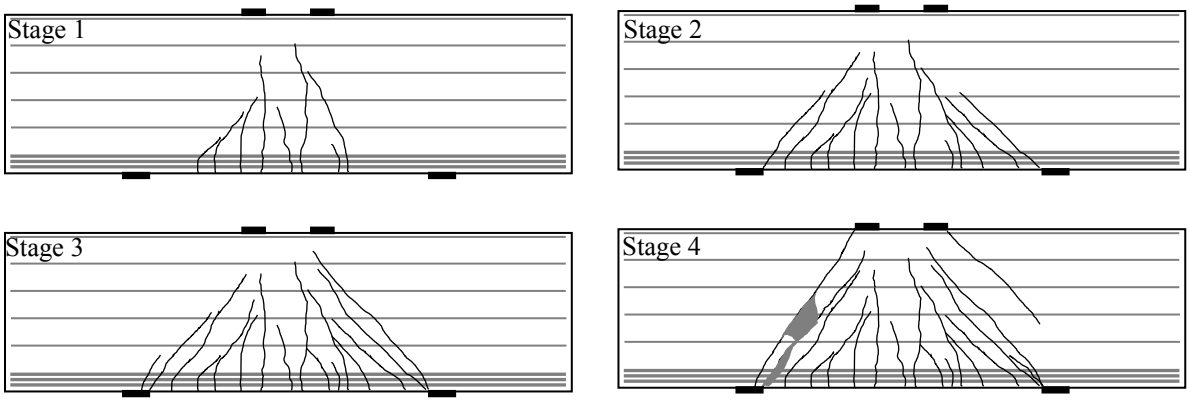

b) G0.83H

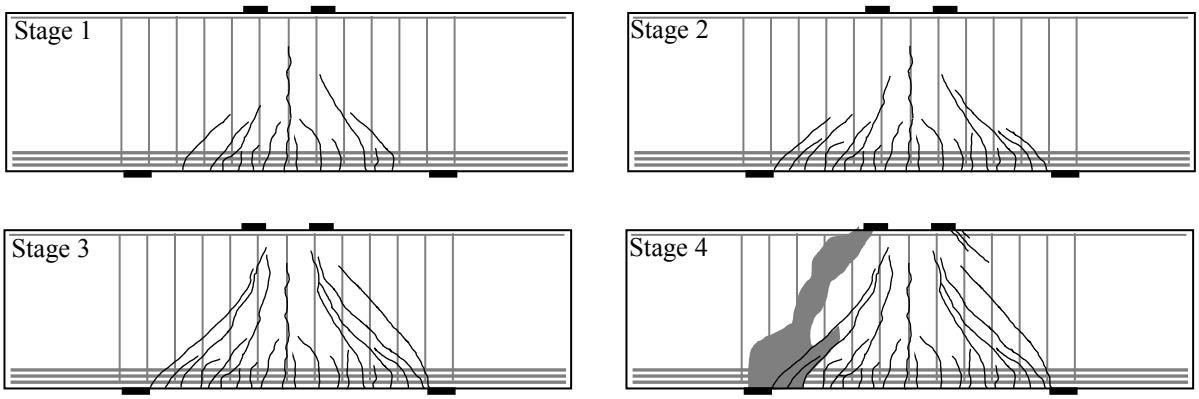

c) G0.83V

Figure 4.3 - Crack pattern of deep beams with *a*/*d* ratio of 0.83

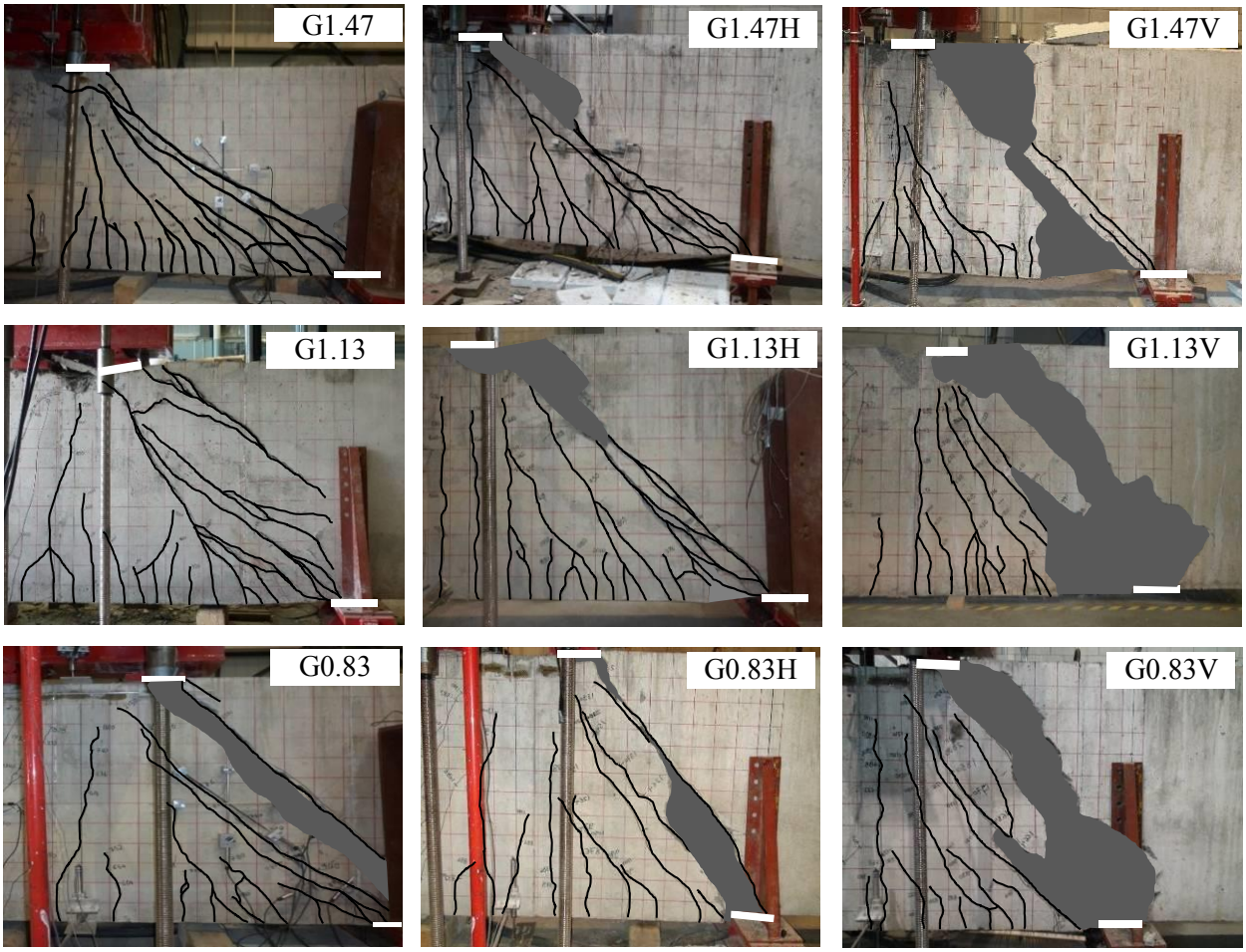

Figure 4.4 – Mode of failure of all tested specimens (Shaded area indicates crushed concrete)

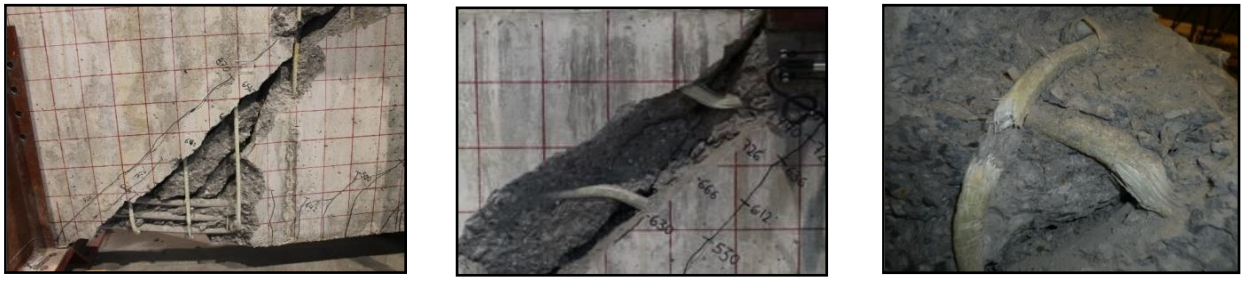

(a) Concrete spalling beside support (G1.47V)

(b) Dowelling of horizontal bars (G1.47H)

(c) Rupture of vertical bars at bent portion (G1.13V)

Figure 4.5 – Failure-associated degradation

4.3 Ultimate Loads and Failure Progression

Table 4.1 presents the experimental results of the failure progression for all the tested specimens at different loading stages. In addition to the absolute load values, normalized loads to concrete compressive strength (f_c') were also presented as $P/f_c'bd$ to eliminate the differences in f_c'. The loads were normalized to f_c' rather than $\sqrt{f_c'}$, as the failure of the tested deep beams was typically preceded by the crushing of the concrete diagonal strut. For this behavior, the capacity of the deep beam is primarily dependent on the compressive strength of the concrete in the direct strut (MacGergor 1997, Razaqpur et al. 2004, Collins et al. 2008, Tuchscherer et al. 2011). Therefore, codes and provisions calculate the strength of strut as a function of f_c', indicating a linear scaling of f_c' (ACI 318, 2014, AASHTO 2007, CSA S806 2012, CSA A23.3 2014, *fib* 1999).

Web reinforcement, whether vertical or horizontal, had almost no effect on either the first flexural cracking load, the first shear cracking load, or the main diagonal cracking load for each group of specimens with the same *a*/*d*. Vertical and horizontal web reinforcement in G1.13VH significantly increased the main diagonal cracking load in comparison to the other specimens with the same *a*/*d*. Meanwhile, the increase in *a*/*d* slightly increased the first flexural cracking load and significantly increased the first diagonal and main diagonal cracking loads. To demonstrate the effect of web reinforcement and *a*/*d* on the load-carrying capacity of FRP-reinforced deep beams, Figure 4.6 plots the normalized ultimate loads against *a*/*d* for the tested specimens according to their web-reinforcement configurations.

The *a*/*d* had a significant effect on the normalized ultimate load, as the normalized ultimate load increased as the *a*/*d* decreased. Moreover, providing vertical-only web reinforcement had almost no significant effect on the normalized ultimate load—except for G1.47V, which had the highest *a/d*—and for which the ultimate load capacity was 18% higher than the specimen without reinforcement (G1.47). A similar trend was observed with the normalized ultimate load of the specimens with vertical and horizontal web reinforcement (G1.13VH), with an increase of almost 9% compared to G1.13. Generally, vertical web reinforcement (with or without horizontal bars) had no significant effect on the normalized ultimate load of GFRP-

reinforced deep beams. This is consistent with the results for steel-reinforced deep beams (Tuchscherer et al. 2011, and Birrcher et al. 2013).

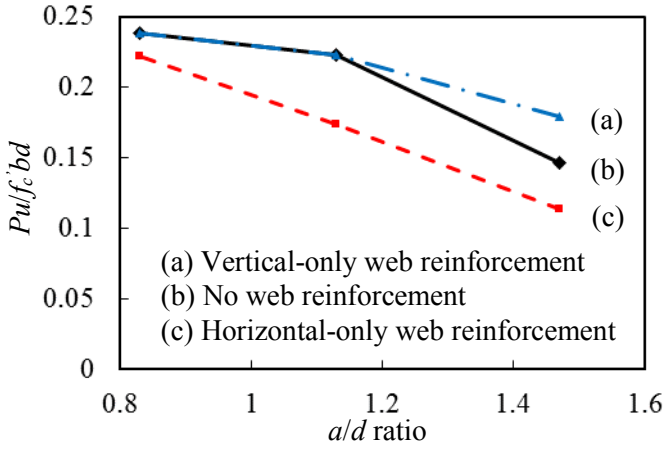

Figure 4.6 – Effect of a/d on normalized ultimate load capacity

On the other hand, the horizontal-only web reinforcement had a negative effect on the ultimate load capacity of the tested deep beams for all a/d values (the normalized ultimate load of specimens G1.47H, G1.13H, and G0.83H decreased by 23%, 21%, and 7% compared to specimens G1.47, G1.13, and G0.83, respectively). Brown and Bayrak (2007) reported this phenomenon of decreased ultimate load for steel-reinforced deep beams with horizontal-only web reinforcement, attributing it to experimental scatter. Since the failure of the tested specimens was preceded by the crushing of the concrete in the diagonal strut, this drop could be attributed to degradation of the compressive strength in the concrete strut. Clarification for such unexpected behavior is discussed in the following section.

The variables used in Table 4.1 can be defined as follows: d is the distance from the extreme compression fiber to the centroid of the FRP tension reinforcement; f_c', and E_c are the concrete compressive strength and modulus of elasticity, respectively, measured using at least three concrete cylinders for every concrete batch and tested at the time of testing the specimens; f_{sp} is the concrete tensile strength obtained from at least three spilt-cylinder test for every concrete batch and tested at the time of testing the specimens P_f is the initial flexural crack load; P_s is the first diagonal shear crack load; P_{cr} is the main diagonal crack load; P_u is the ultimate load at failure; and Δ_{max} is the maximum deflection at mid-span.

Table 4.1 – Summary of experimental results

Specimen ID	f_c' (MPa)	f_{sp} (MPa)	E_c (GPa)	Initial flexure crack		First shear crack		Main diagonal crack		Ultimate		Δ_{max} (mm)
				P_f (kN)	$P_f/f_c'bd$	P_s (kN)	$P_s/f_c'bd$	P_{cr} (kN)	$P_{cr}/f_c'bd$	P_u (kN)	$P_u/f_c'bd$	
G8-6†	49.3	4.6	33.0	420	0.026	520	0.032	728	0.045	1447	0.089	12.3
G8-8†	49.3	4.6	33.0	440	0.027	540	0.034	749	0.047	1906	0.119	12.2
C12-3†	38.7	3.8	29.2	365	0.028	470	0.036	680	0.053	1191	0.092	9.9
C12-4†	38.7	3.8	29.2	375	0.029	480	0.037	699	0.054	1601	0.125	10.1
G1.13	37	3.4	28.6	328	0.028	550	0.046	740	0.061	2687	0.223	22.0
G1.13H	44.6	3.7	31.4	457	0.031	746	0.051	861	0.059	2533	0.174	17.7
G1.13V	44.6	3.7	31.4	457	0.031	680	0.047	980	0.067	3236	0.223	19.0
G1.13VH	37	3.4	28.6	372	0.031	681	0.057	1100	0.091	2904	0.241	16.5
G1.47	38.7	3.5	29.2	320	0.025	380	0.030	570	0.045	1849	0.146	29.1
G1.47H	45.4	3.8	31.7	292	0.020	494	0.033	740	0.050	1695	0.114	18.3
G1.47V	45.4	3.8	31.7	280	0.019	494	0.033	725	0.049	2650	0.179	29.0
G0.83	38.7	3.5	29.2	376	0.030	950	0.075	1175	0.093	3000	0.238	10.7
G0.83H	43.6	4.4	31.0	375	0.026	1100	0.077	1264	0.089	3166	0.222	8.30
G0.83V	43.6	4.4	31.0	440	0.031	1170	0.082	1350	0.095	3387	0.238	12.0

Note: † tested by Farghaly and Benmokrane (2013)

4.4 Load–Deflection Response

Figure 4.7 categorizes the specimens according to *a*/*d* values to illustrate the response of the normalized load–deflection relationship. The mid-span deflection was measured with two LVDTs (at the top and bottom of the deep beam). The LVDTs produced identical readings until a horizontal crack formed through the horizontal strut between the two loading points (at 70% to 80% of the ultimate load), which affected the readings of the top LVDT. Therefore, the deflection in Figure 4.7 was plotted based only of readings from the lower LVDT.

All of the specimens exhibited bilinear response up to failure. Prior to the first flexural crack, the specimens with horizontal web reinforcement (with or without vertical web reinforcement) exhibited higher stiffness than the specimens without, representing the higher gross cross-sectional inertia due to the horizontal bars. After the formation of the first flexural crack, all of the specimens exhibited a slight reduction in stiffness, representing a cracked specimen with reduced moment of inertia, but with different tendencies, depending on web-reinforcement

configuration and *a*/*d*. This behavior is similar to that reported by Tan and Lu (1999), and Mihaylov et al. (2010) for steel-reinforced deep beams in which the main longitudinal steel bars did not yield but the stiffness was reduced due to cracking.

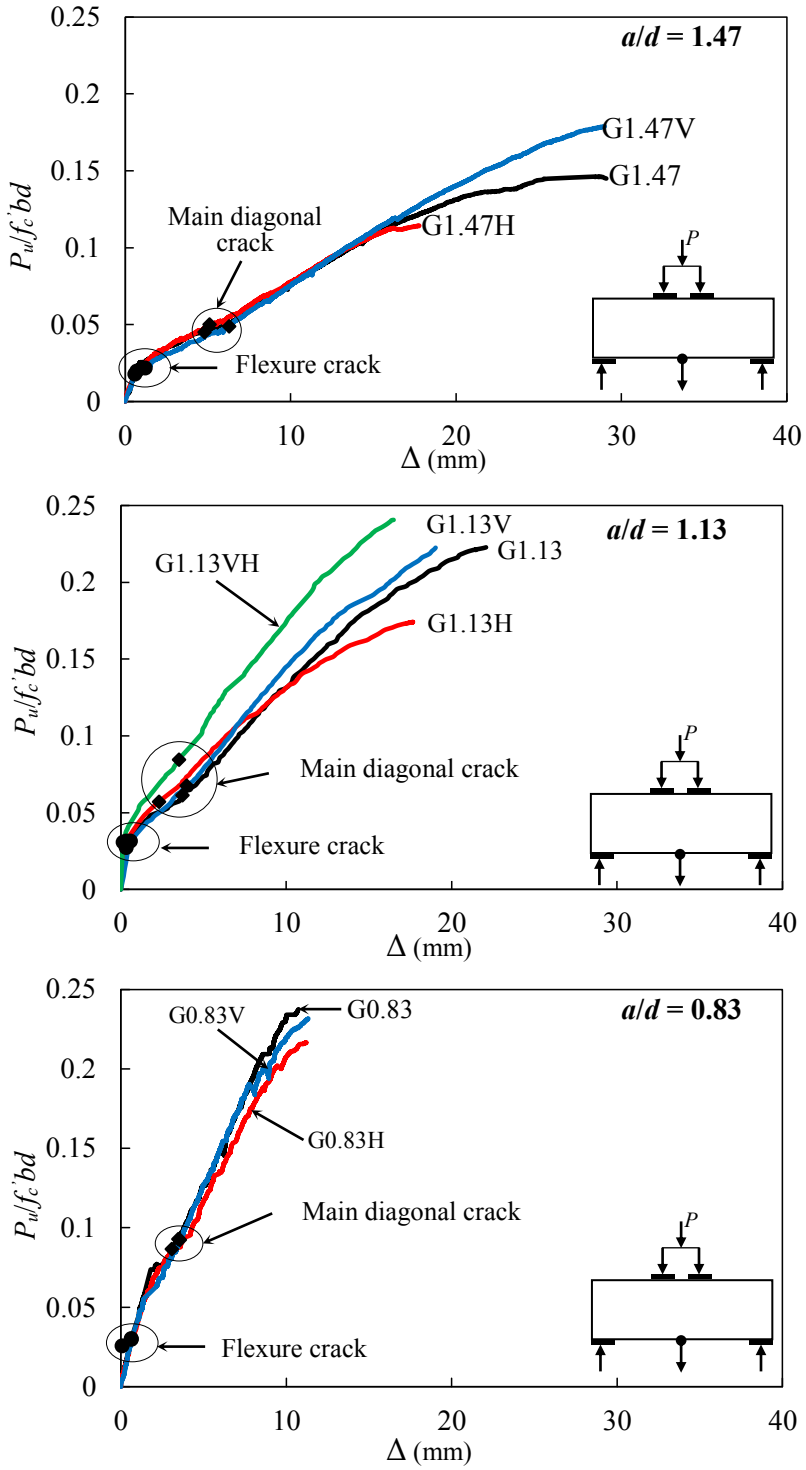

Figure 4.7 - Normalized ultimate load–deflection response

As the load increased, shear cracks propagated in the shear span of the specimens, followed by the formation of the main diagonal crack. The main diagonal crack was associated with a slight increase in specimen stiffness, illustrating the redistribution of internal stresses through the formation of an arch action, which enhanced specimen stiffness by reserving the capacity. Therefore, the deformation of the tested deep beams may have occurred as the result of flexural and shear cracks, leading to the development of an arch action. Similarly to steel-reinforced deep beams, arch action in beams with FRP reinforcement depends on adequate deformation capacity for distributing the forces and on the stresses applied to the elements not exceeding their failure criteria: yield for steel bars (corresponding to tensile strength for FRP bars) and plastic capacity of concrete (Tuchscherer et al. 2014).

4.4.1 Specimens with Horizontal-Only Web Reinforcement

The stiffness of the horizontal-only web reinforced specimens was slightly higher than that of the other specimens once the first flexural crack had formed (Figure 4.7). That notwithstanding, a drop in stiffness was observed at 64%, 70%, and 44% of the ultimate load in G1.47H, G1.13H, and G0.83H, respectively. This resulted in specimen failure at lower normalized loads and deflections (Δ_{max}) compared to the other specimens (Table 4.1).

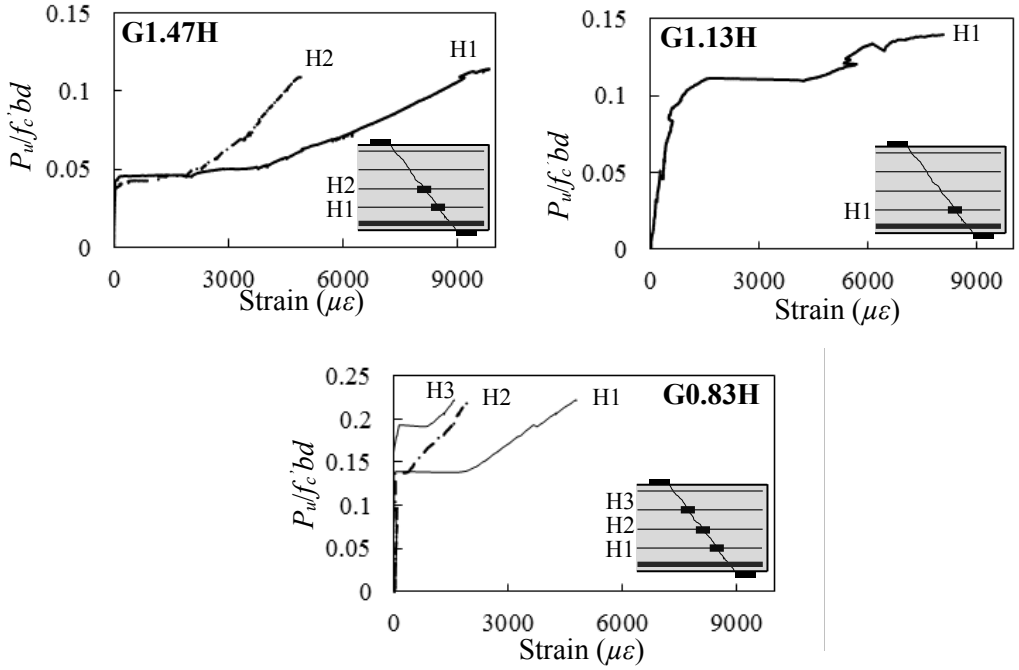

Figure 4.8 – Measured strain in horizontal bars for the deep beams with horizontal-only web reinforcement

This unexpected behavior might be attributed to high tensile strain in the horizontal bars affecting the strength and stiffness of the concrete diagonal strut. Figure 4.8 shows the measured strains in the horizontal bars for the specimens with horizontal-only web reinforcement. These high strains generated radial tensile forces around the bars, which, in turn, weakened the compression capacity of the concrete diagonal strut (Figure 4.9). The principal compressive stress in the concrete diagonal strut has been found to be a function not only of the principal compressive strain (ε_2) but also of the existing principal tensile strain (ε_1) in the perpendicular bars (Vecchio and Collins 1993, Zhang and Hsu 1998). Therefore, the presence of large transverse tensile strains in the horizontal reinforcement in our study resulted in substantial reductions in the strength and stiffness of the concrete diagonal strut, compared to the specimens without web reinforcement. Therefore, the failure of the specimens with horizontal-only reinforcement was relatively softer and at lower ultimate load capacity.

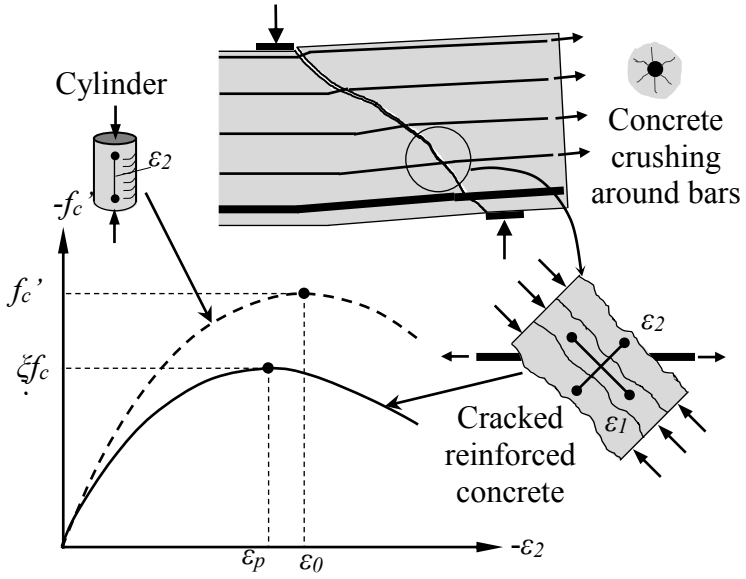

Figure 4.9 – Softening of compressive strut due to transverse tensile strains

Further clarification could be yielded by the measured strain of the concrete diagonal strut (Figure 4.10). This figure clearly illustrates that the strains measured in the horizontal-only web reinforced specimens were significantly higher than that of the other specimens at the same load level. That would indicate possible excessive strength degradation due to transverse strain. This significantly decreased the strength of concrete diagonal strut and the ultimate load capacity in the specimens with horizontal-only web reinforcement, compared to those with no web reinforcement.

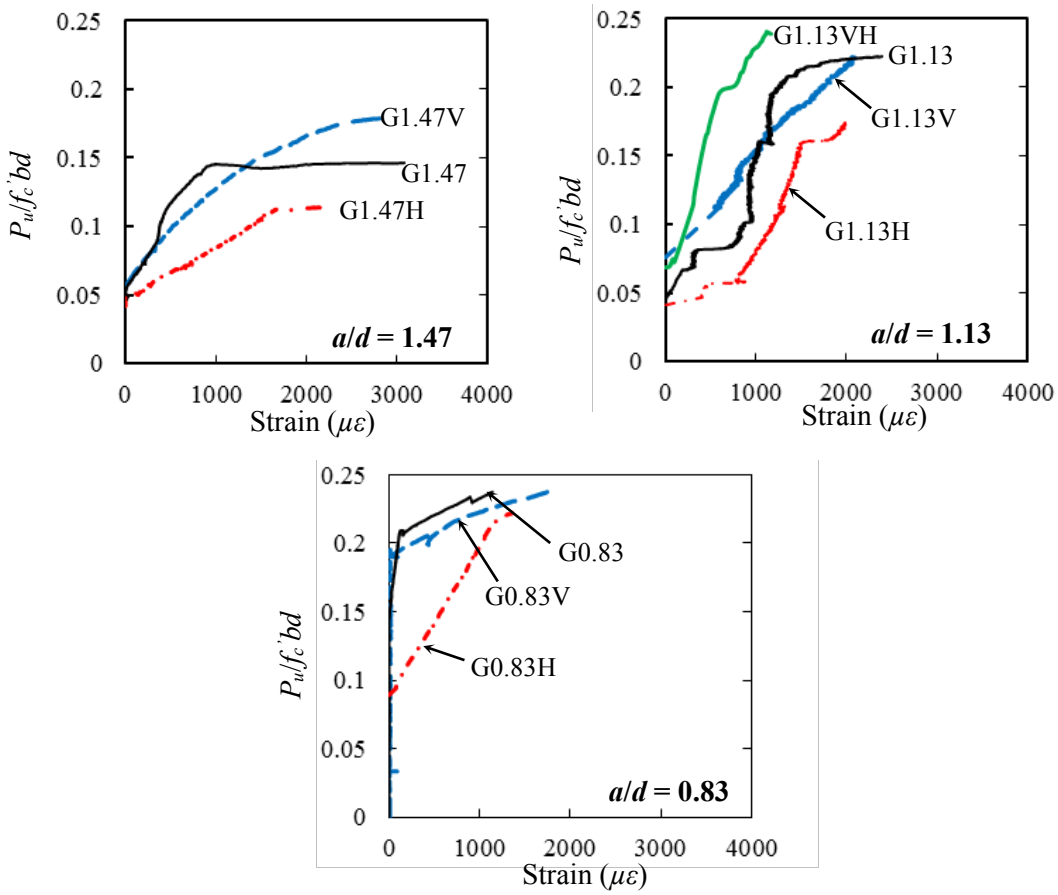

Figure 4.10 – Concrete strain at the concrete diagonal strut

4.4.2 Specimens with Vertical-Only Web Reinforcement

The deep beams with vertical-only web reinforcement exhibited nearly similar or slightly higher stiffness than the deep beams without web reinforcement (Figure 4.7), causing the specimens to fail at almost similar normalized ultimate loads as the deep beams with no web reinforcement.

Figure 4.11 shows the strains measured in the vertical bars on the failure side of G1.47V, G1.13V, and G0.83V. In most cases, compression forces in the concrete diagonal strut area exposed the vertical bars to compressive strains. Unlike in the specimens with horizontal-only web reinforcement, the concrete in the diagonal strut was not softened due to the low strains in the vertical web reinforcement. Consequently, no degradation in the concrete diagonal strut occurred, as can also be observed in the concrete strain measurements at the concrete diagonal strut (Figure 4.10).

The relatively low strains in the vertical web reinforcement at the area of the concrete diagonal strut might be explained by the tensile stresses transferred through the vertical bars from the applied loads being compensated by the confined compression stresses of the diagonal strut acting upon the vertical reinforcement. The portions of the vertical bars outside the diagonal strut, however, were carrying high tensile strains since the vertical bars ruptured at failure (Figure 4.5-c). Therefore, the vertical web reinforcement did not increase the strength of the concrete diagonal strut, causing the specimens to fail at normalized ultimate load capacities similar to those of the specimens without web reinforcement (Table 4.1).

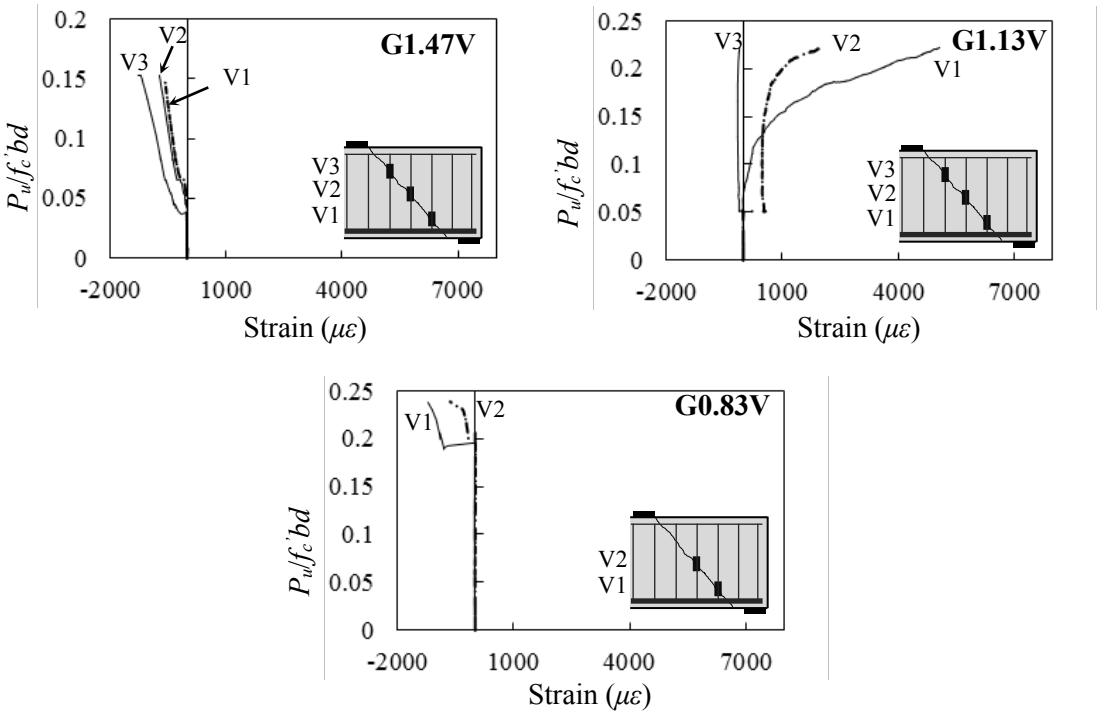

Figure 4.11 – Measured strain in the vertical bars for the deep beams with vertical-only web reinforcement

4.4.3 Specimens with Horizontal and Vertical Web Reinforcement

Providing vertical and horizontal web reinforcement significantly increased the stiffness of G1.13VH compared to G1.13. Yet a slight increase in specimen capacity was noticed, resulting in decreased corresponding deflection (Table 1 and Figure 4.7).

Figure 4.12 illustrates the strains measured in the vertical and horizontal web reinforcement. Given the horizontal bars in the flexural direction, the strains in the horizontal bars were higher than in the vertical bars. The horizontal-bar strain was, however, lower than in the specimen with horizontal-only web reinforcement (G1.13H). Nevertheless, behavior of vertical bars was similar to that in the specimen with vertical-only web reinforcement (G1.13V) in terms of relatively small measured strains in the vertical bars and rupture of bent portion of the vertical bars.

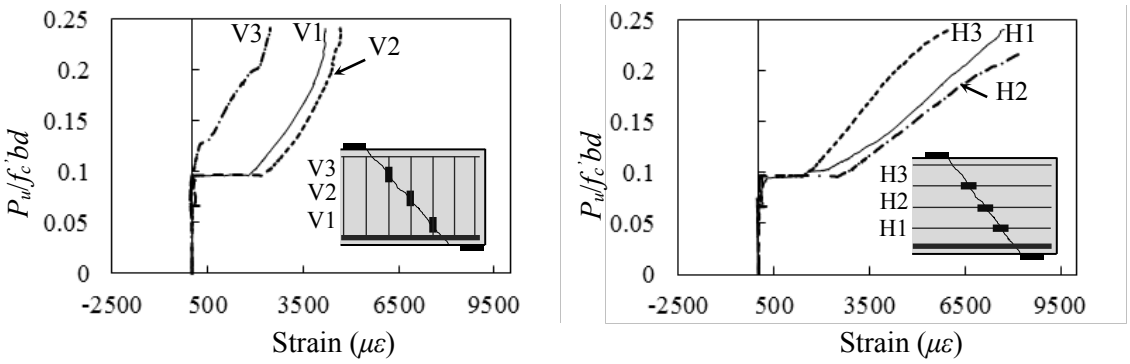

a) Vertical reinforcement b) Horizontal reinforcement

Figure 4.12 – Measured strains in the web reinforcement in G1.13VH

4.5 Development of Arch Action in the Tested Specimens

The predominant mechanism of shear transfer in a deep-beam region is attributed to the diagonal strut's arch action. Although the formation of arch action in FRP-reinforced deep beams without web reinforcement has been confirmed (Andermatt and Lubell, 2013(a); Farghaly and Benmokrane, 2013), it was important to examine its formation in the tested specimens. Arch action develops through sufficient deformation in a deep beam produced by the formation of a truss model that is in equilibrium and the stresses in all its elements should not exceed their capacities. In our study, the tested specimens exhibited reasonable deflection levels compared to the available steel-reinforced deep beams of similar dimensions and reinforcement found in the literature (Mihaylov et al. 2010).

Moreover, the main longitudinal reinforcement serves as a tie for the arch and should carry approximately constant tensile strains along its length. Figure 4.13 presents the data for the five strain gauges in the main longitudinal reinforcement at different stages. At the ultimate load, the strain distribution for all of the tested specimens was almost linear, confirming the formation of arch action once the main diagonal crack occurred at almost 50% of the ultimate load capacity.

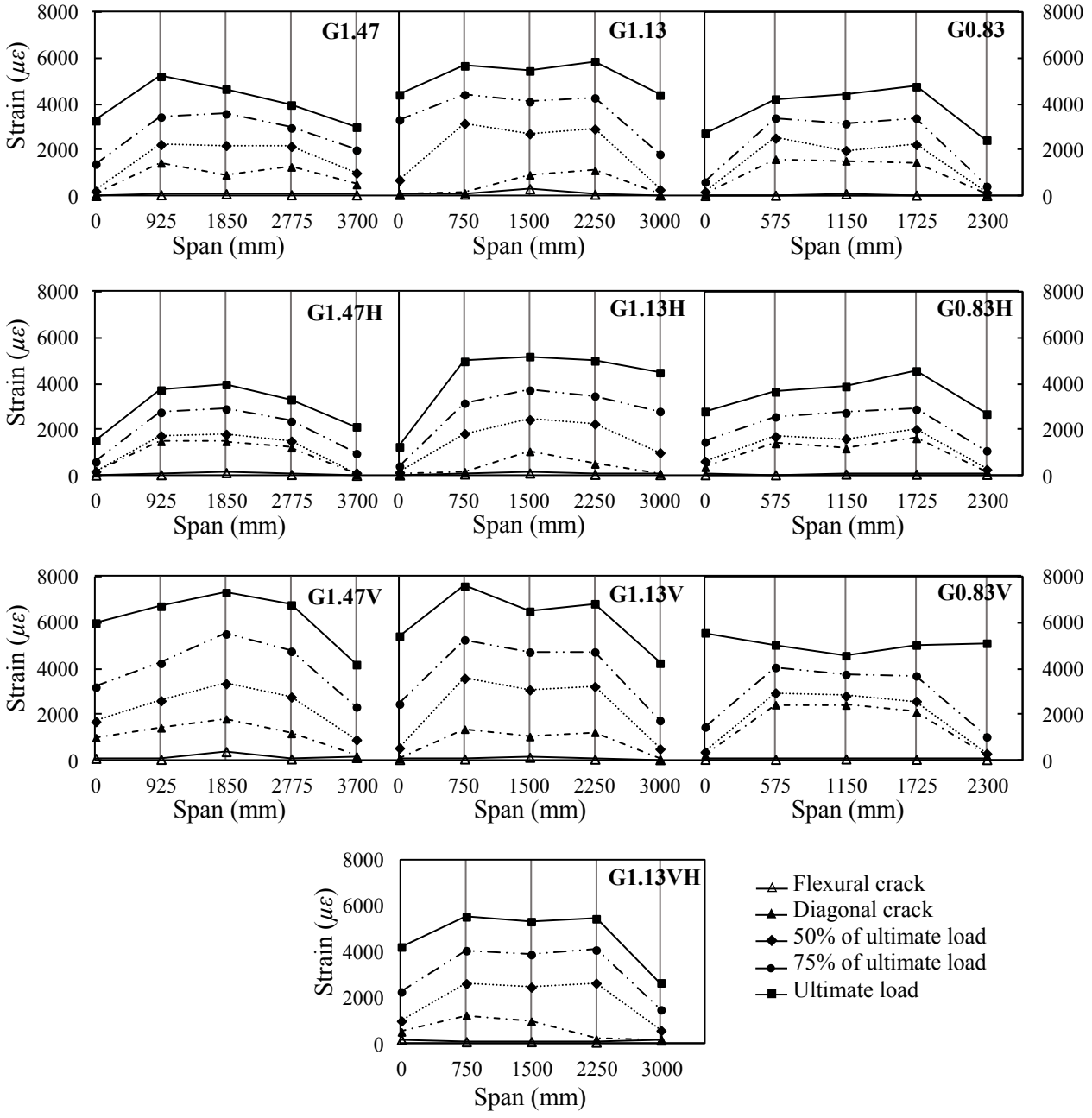

Figure 4.13 – Strain distribution in the main longitudinal reinforcement

In another way to confirm the development of the arch action, the STM was assumed to be appropriate for the tested deep beams rather than the traditional sectional-shear analysis method in order to follow the theory of elasticity (Andermatt and Lubell, 2013(b)). Accordingly, the STM in CSA S806 (2012) (Figure 4.14) was used to calculate the predicted strains (ε_{pre}). The width of the upper horizontal strut (h_n) was calculated with the measured concrete strains in the horizontal strut at ultimate load (ε_c) as follows:

$$h_n = \frac{P_u/2\cot\alpha}{b\varepsilon_c E_c} \le \frac{P_u/2\cot\alpha}{bf_c'} \tag{4.1}$$

where b is the deep-beam width and E_c is the concrete modulus of elasticity calculated from the concrete cylinders. An iteration process was required in order to calculate the angle between the strut and tie (α) and h_n. Using the axial stiffness of the GFRP longitudinal bars ($A_{frp}.E_{frp}$) — with A_{frp} and E_{frp} being the cross-sectional area and the modulus of elasticity of the GFRP bars, respectively - and the experimental ultimate capacity of a specimen, P_u, the predicted strain in the tie at ultimate load can be calculated as follows:

$$\varepsilon_{pre} = \frac{P_u/2\cot\alpha}{A_{frp}E_{frp}} \tag{4.2}$$

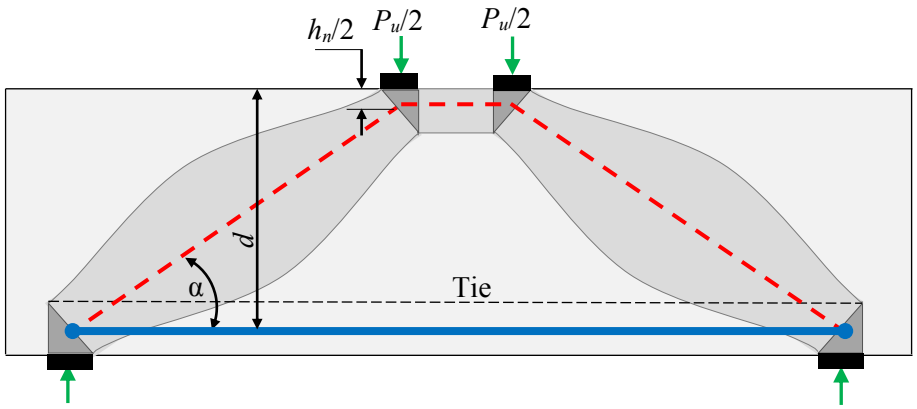

Figure 4.14 – Strut-and-tie model

Table 4.2 presents the percentage average of the five measured readings of strain gauges to the predicted tie strain ($\varepsilon_{exp}/\varepsilon_{pre}$), which ranged from 77% to 98% (with a mean value of 90% and coefficient of variation (CoV) of 7%), demonstrating the applicability of the STM for the tested deep beams. The lowest $\varepsilon_{exp}/\varepsilon_{pre}$ was for the specimens with horizontal web

reinforcement (with or without vertical web reinforcement), in which the horizontal web reinforcement served, along with the main longitudinal reinforcement, as ties and reduced the experimental strains in the main longitudinal reinforcement. The aforementioned discussion examined all the criteria for the development of the arch action in the FRP-reinforced deep beams.

Table 4.2 – Measured and predicted tie strain at ultimate

Specimen ID	f_c' (MPa)	E_c (MPa)	h_n (mm)	ε_{exp} ($\mu\varepsilon$)	ε_{pre} ($\mu\varepsilon$)	$\varepsilon_{exp}/\varepsilon_{pre}$ (%)
G8-6†	49.3	33000	92	5310	5103	96
G8-8†	49.3	33000	70	7774	7230	93
C12-3†	38.7	29238	102	4050	4181	97
C12-4†	38.7	29238	70	6742	6203	92
G1.13	38.7	29670	66	4617	5211	89
G1.13H	45.4	31950	61	3676	4765	77
G1.13V	45.4	31920	80	6988	7517	93
G1.13VH	37	29100	77	5664	5947	95
G1.47	44.6	31700	88	5035	5635	89
G1.47H	44.6	31680	117	7126	7301	98
G1.47V	38.7	29600	99	4498	4831	93
G0.83	43.6	31350	84	4037	5062	80
G0.83H	43.6	31300	76	4999	5396	93

Note: † tested by Farghaly and Benmokrane (2013)

It is worth mentioning that, specimen G1.47 was built in comparable size to Specimen S0M tested by Mihaylov et al. (2010) with steel-reinforcement. The behavior of both specimens is similar in terms of failure progression, failure mode (crushing in the diagonal strut), and uniform strain distribution in longitudinal reinforcement. Nevertheless, specimen G1.47 exhibited a higher deflection at ultimate load than that in S0M, hence, GFRP-reinforced deep beam had achieved a sufficient deformation capacity required to form the arch action as in the steel-reinforced deep beams.

4.6 Relative Displacement-Induced Deformation

In an effort to understand the effect of the horizontal and vertical web reinforcement on the behavior of the deep beams, the failure mechanism of the tested specimens was developed

through the deformation process. In general, the diagonal shear crack divided the specimens into three segments: the middle part under the loading points and the two parts above the supports. The applied loads pushed the middle part downwards. While the two supports prevented the other two parts from moving downward, the supported parts rotated around the support plates to follow the middle loaded part (Figure 4.15). This describes the basic principle of deep beams, since the plane section does not remain plane. This rotation was represented by two relative displacements: horizontal relative displacement (Δ_h) and vertical relative displacement (Δ_v).

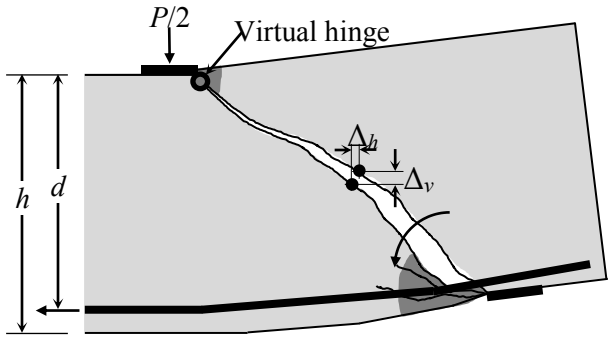

Figure 4.15 – Relative displacement in the deep beams

The horizontal and vertical relative displacements between the middle and supported parts were measured with two perpendicular LVDTs (horizontal and vertical) attached at mid-depth of the deep beam and across the main diagonal crack once it was formed (Figure 3.16). Figure 4.16 provides the values of Δ_h and Δ_v for all of the tested specimens. A positive sign for displacements indicates the opening of the diagonal crack. The deformation pattern described in Figure 4.15 was also fully described for steel-reinforced deep beams with Zurich targets (Mihaylov et al. 2013).

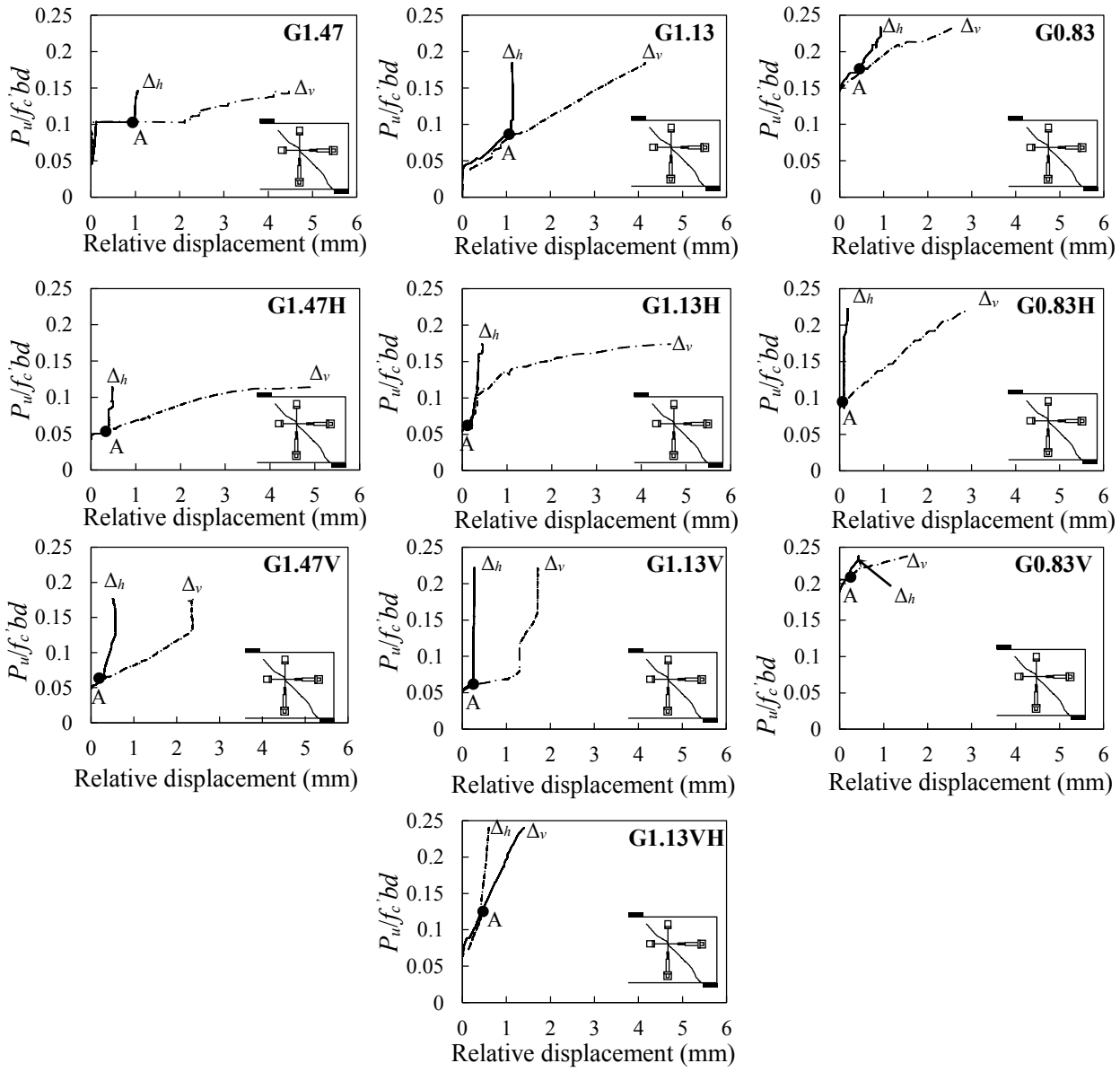

Figure 4.16 – Horizontal and vertical relative displacement

According to Figure 4.16, the horizontal and vertical relative displacements in all specimens increased simultaneously with increased load up until a certain point A. After point A, Δ_h remained constant, while Δ_v continued to increase with load until failure.

Since the deep-beam failure was dominated by shear rather than flexure, the diagonal shear cracks initiated and rapidly propagated upward to the compression zone and simultaneously downward to the support plates (Figure 4.17-a). The compressive stresses in the concrete in the compression zone close to the loading point prevented the diagonal shear crack from

progressing upward, which formed a virtual hinge at the tip of the diagonal shear crack. This virtual hinge caused the supported part to rotate around the compression zone, which further opened the diagonal shear crack as the load increased (Figure 4.17-b). Therefore, Δ_h and Δ_v increased simultaneously after the formation of the shear diagonal crack, up to point A, as shown in Figure 4.16.

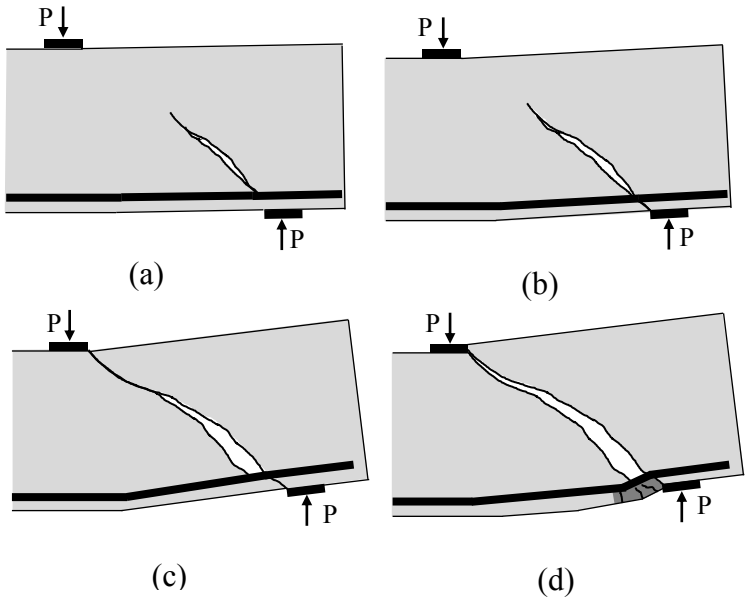

Figure 4.17 – Failure progression

At the same time, before reaching point A, the concrete strain in the horizontal strut increased nearly linearly (Figure 4.18). As the load reached the level corresponding to point A, the concrete strain in the horizontal strut promptly increased with increased load, as shown in Figure 4.18. This could be attributed to the excess compression stresses on the virtual hinge zone. This deteriorated the compressed concrete and led to the diagonal crack passing through the virtual hinge (Figure 4.17-c). Therefore, the supported part did not follow the deformation of the middle part at point A (Figure 4.17-d), causing Δ_h to be constant with load, while Δ_v increased until failure.

Figure 4.16 clearly shows a more obvious increase in Δ_h and Δ_v in the specimens with higher a/d values under increasing load than in the specimens with lower a/d values. This was attributed to the higher deformation that occurred in deep beams with higher a/d values compared to those with lower a/d values.

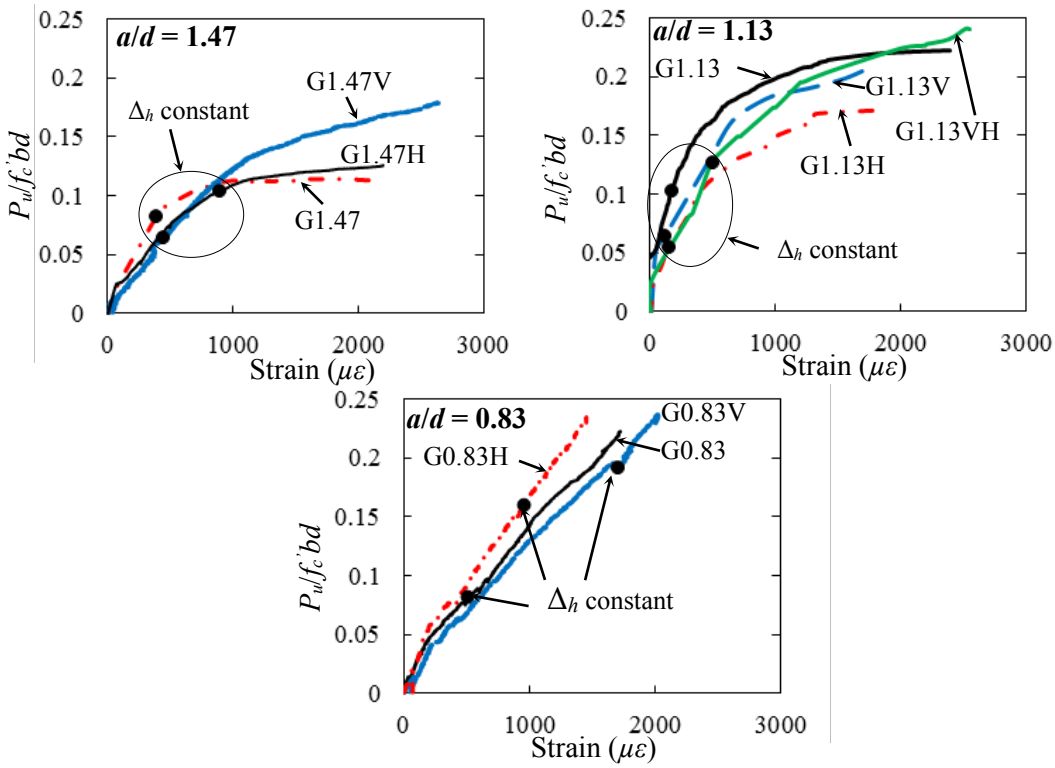

Figure 4.18 – Concrete strain at the horizontal strut

4.6.1 Effect of Horizontal Bars on Relative Displacement

Figure 4.16 also brings out that the web reinforcement configuration significantly affected Δ_h and Δ_v. The presence of horizontal bars in the deep beams with horizontal-only web reinforcement significantly decreased the rotation of the supported parts around the virtual hinge, causing Δ_h to decrease in comparison to the specimens without web reinforcement (Δ_h decreased by 52%, 60%, and 81% for G1.47H, G1.13H, and G0.83H compared to G1.47, G1.13, and G0.83, respectively). Therefore, the flexural stiffness of the deep beams with horizontal-only web reinforcement was higher than those without web reinforcement (see Figure 4.7). After the failure of the virtual hinge, Δ_v increased with load even more than in the specimens without web reinforcement (Δ_v increased by 13% in G1.47H, G1.13H, and G0.83H compared to G1.47, G1.13, and G0.83, respectively). The horizontal web reinforcement resisted the horizontal movement between the two parts. When the two parts separated, however, releasing energy, it would be expected that the Δ_v in these specimens would be higher than the corresponding specimens without web reinforcement, especially since FRP

bars have a low dowel force resistance. This increase in Δ_v indicates that the deep beams with horizontal-only web reinforcement exhibited a greater downward movement of the loaded part, resulting in high transverse shear stress (dowel force) on the horizontal bars, as shown in Figure 4.5-b.

4.6.2 Effect of Vertical Bars on Relative Displacement

As shown in Figure 4.16, Δ_h was smaller in the specimens with vertical-only reinforcement than in those without web reinforcement (Δ_h decreased by 35%, 60%, and 9% in specimens G1.47V, G1.13V, and G0.83V compared to G1.47, G1.13, and G0.83, respectively), since the presence of vertical web reinforcement restrained the rotation of the supported parts, causing a decrease in Δ_h. In addition, the vertical bars anchored the separated parts of the deep beams, thereby reducing Δ_v in comparison to the specimens without web reinforcement (Δ_v decreased by 45%, 59%, and 41% in specimens G1.47V, G1.13V, and G0.83V compared to G1.47, G1.13, and G0.83, respectively).

4.6.3 Effect of Horizontal and Vertical Bars on Relative Displacement

The horizontal and vertical web reinforcement decreased the horizontal and vertical relative displacement at ultimate load by 48% and 66%, respectively, compared to the specimens without web reinforcement (G1.13). This decrease in both types of relative displacement caused the specimen stiffness to increase in comparison to the other specimens with the same a/d (Figure 4.7).

4.7 Crack Width

Crack width was studied to further examine the behavior of the tested deep beams. The flexural cracks propagated first from the deep beam soffit with a width range of 0.05 to 0.08 mm. The openings of the flexural cracks were much narrower than those of the diagonal shear cracks and did not exceed for the maximum crack width of 0.5 mm specified by JSCE (1997), CSA S806 (2012), and CSA S6 (2014). Once the main diagonal crack was formed, a high accuracy LVDT was placed at the bottom one-third of the deep-beam depth where the crack

was propagated to monitor its width. Some specimens exhibited the formation of more than one diagonal crack. In such cases, the new diagonal cracks were also monitored with other LVDTs. Figure 4.19 shows the monitored crack width at the main diagonal crack. The width of the main diagonal crack developed more rapidly in the longer specimens than in the shorter ones. The increase in the deep-beam *a*/*d* significantly increased the main-crack width at ultimate load (the maximum crack width at ultimate load for specimens G1.47, G1.13, and G0.83 was 8.5 mm, 6 mm, and 2.4 mm, respectively). At the ultimate load level of G1.47 (1849 kN), the crack width in specimens G1.47, G1.13 and G0.83 was 8.5 mm, 3.2 mm, and 1.2 mm, respectively.

The presence of web reinforcement—horizontal or vertical—significantly decreased the crack width at ultimate load compared to the deep beams with no web reinforcement with the same *a*/*d*. At the same loading level, the vertical-only web reinforcement provided more significant crack-width control than the horizontal-only web reinforcement. For instance, at the same load level, the horizontal-only web reinforcement decreased the crack width by 42% to 51% compared to no web reinforcement. On the other hand, the vertical-only web reinforcement decreased the crack width by 67% to 88% compared to no-web reinforcement at the same load level. From this, it can be deduced that web reinforcement played a significant role in controlling the crack width in the GFRP-reinforced deep beams.

The ability of web reinforcement to control the crack width was in consistent with the findings in relative displacement measurements, as the web reinforcement significantly decreased the relative displacement across the main diagonal crack (Figure 16) through decreasing the rotation of the supported parts around the virtual hinge. The decrease in relative displacement for specimens with vertical-only web reinforcement was more pronounced than that in specimens with horizontal-only web reinforcement, clarifying the higher effectiveness of vertical bars to control crack widths. As discussed earlier, the horizontal bars to restrain the opening of the crack width alone resulted in high transverse shear stress (dowel forces) on the horizontal bars reducing their capability to restrain crack width; while the vertical bars anchored the two separated parts reducing the crack width in comparison to specimens without web reinforcement. Similarly, controlling the crack width by adding web reinforcement has been reported for steel-reinforced deep beams (Tan et al. 1997, Mihaylov et al. 2010, Birrcher

et al. 2013). This was attributed to the capability of web reinforcement to resist the transverse tensile stresses existing between cracks; which controls the crack width.

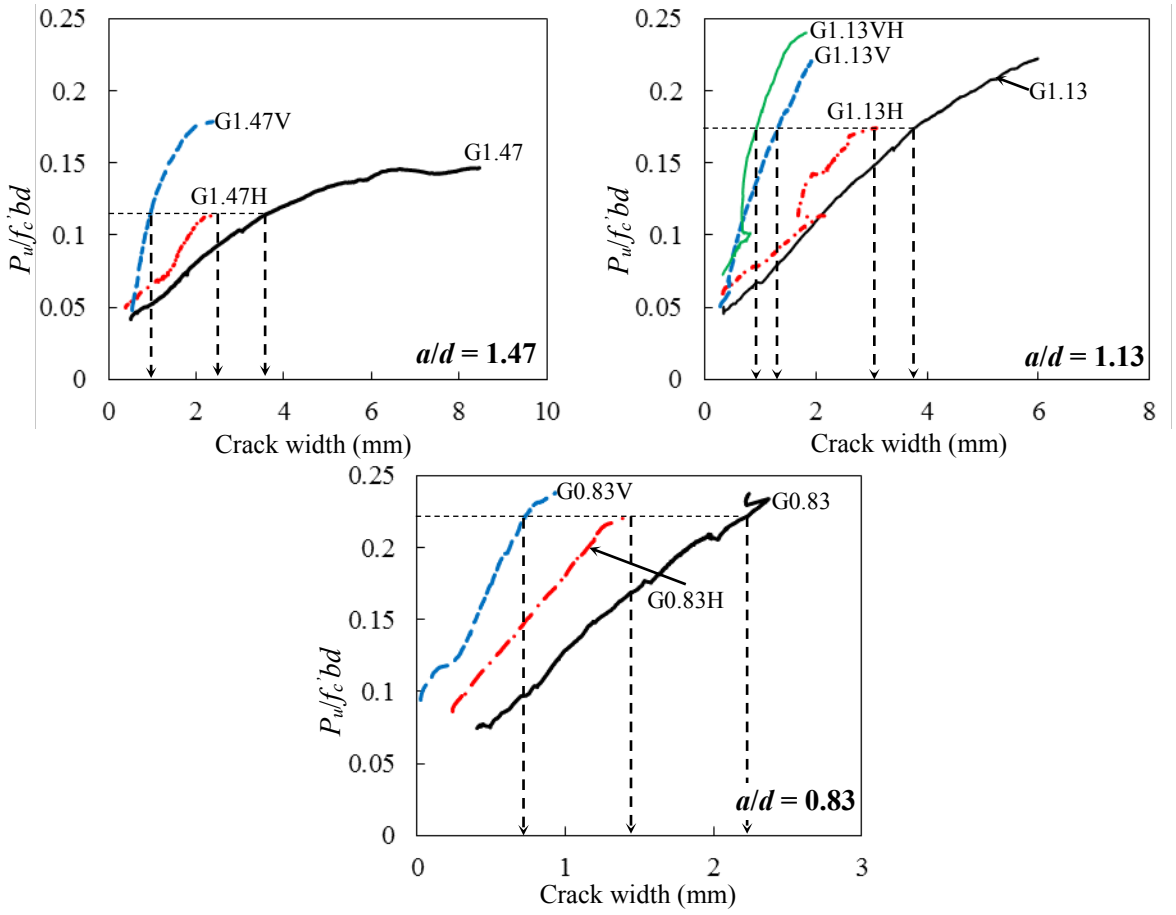

Figure 4.19 - Crack width

Design engineers are usually concerned with crack width at service load rather than that at ultimate load in the case of structural elements. To investigate the serviceability performance of the tested specimens, the relationship between the percentage of the maximum applied load and the diagonal crack width was plotted (Figure 4.20). In a study by Birrcher et al. (2013), the serviceability load for deep beams was calculated using the ASSHTO LRFD (2007) strength equation and found to be one-third of the experimental capacity. Accordingly, using the same calculations as Birrcher et al. (2013), the serviceability load was calculated according to CSA S806 (2012) and ACI 440.1R (2006) and was found to be equal to 30% of the ultimate experimental capacity of the deep beam. This was calculated assuming that nominal capacity

is 2/3 of experimental capacity, 75% of the service load is dead load, and 25% of the service load is live load.

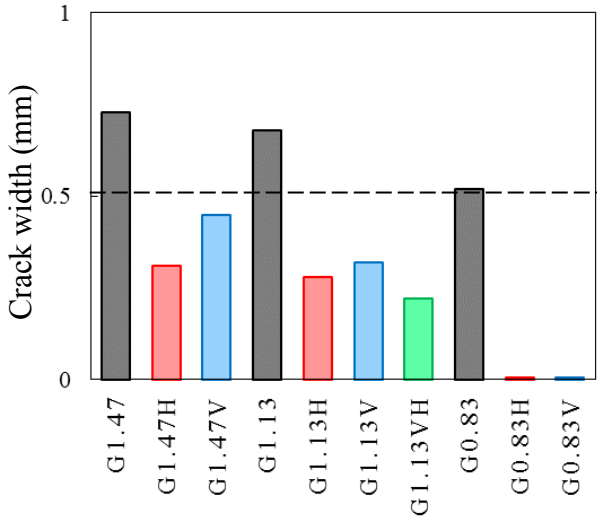

Figure 4.20 - Crack width at 33% of the ultimate load

In G0.83H and G0.83V, the main diagonal crack initiated at a load higher than the assumed service load. Consequently, no data were recorded at the assumed service load. As can be seen in Figure 20, all of the specimens without web reinforcement had cracks exceeding the maximum width of 0.5 mm specified in JSCE (1997), CSA S806 (2012), and CSA S6 (2014). The other specimens with vertical-only or horizontal-only web reinforcement satisfied this limit. Moreover, it can be seen that the crack width at the assumed service load for the deep beams with horizontal-only web reinforcement was less than that in the deep beams with vertical-only web reinforcement. It can therefore be concluded that the horizontal-only web reinforcement provided greater crack-width control at service loads.

4.8 Conclusion

The objective of the current study was to investigate the behavior of GFRP-reinforced deep beams, emphasizing the effect of web reinforcement for such structural elements. Ten full-scale GFRP-reinforced deep beams with *a*/*d* ratios equal to 1.47, 1.13, and 0.83, and with different web reinforcement configurations were tested and investigated to achieve this objective. On the basis of the current results and analysis, the following conclusions can be drawn:

- The tested GFRP-reinforced deep beams failed in a brittle manner due to the crushing in the diagonal compression strut, which is consistent with the failure mode of steel-reinforced deep beams. In addition, the uniform strain profile of the longitudinal reinforcement proves the development of arch action.
- The tested specimens exhibited the deformability required to satisfy equilibrium without violating the failure criteria at any point. This was confirmed by thorough investigation of the failure mechanism progression through the induced relative displacement.
- The applicability of the strut-and-tie model for the tested GFRP-reinforced deep beams was confirmed by employing the model to predict the strain profile in the main longitudinal reinforcement, which was consistent with the experimental results with a mean value of 90% and CoV of 7%.
- The vertical-only web reinforcement was insignificant in enhancing the ultimate strength of the GFRP-reinforced deep beams. The normalized ultimate capacity increased by less than 18% when vertical-only web reinforcement was provided in comparison to specimens without web reinforcement.
- Horizontal-only web reinforcement is not recommended, as this configuration resulted in lower shear capacity due to the induced concrete softening in the diagonal concrete strut because of the high strain in the horizontal bars, which deteriorated the concrete at the diagonal strut.
- The insignificant effect of all web reinforcement configuration on the shear-strength capacity is in contradiction with the recommendation in ACI 318 (2014) of increasing the deep-beam strength when minimum web reinforcement is used. More experimental investigation is required to clarify this critical point.
- The web reinforcement provided significant crack control in the GFRP-reinforced deep beams, as the presence of the web reinforcement reduced the crack width by 77% compared to the deep beam without reinforcement. This is in agreement with the findings for experimental studies of steel-reinforced deep beams, as well as the existing code for steel and FRP-reinforced deep beams (ACI 318, 2014 and CSA S806, 2012, respectively).
- The minimum amount of web reinforcement specified by ACI 318 (2014) and CSA S806 (2012) was sufficient to control the crack width at the assumed service load of 30% of the

ultimate load. The amount of web reinforcement used in the tested specimens satisfied the crack-width limit of 0.5 mm specified in JSCE (1997), CSA S806 (2012), and CSA S6 (2014), while all the specimens without web reinforcement exceeded this limit.

Although the web reinforcement in GFRP-reinforced deep beams did not prove to be essential for strength, minimum web reinforcement should be provided in structures in which the response is dominated by shear, even when serviceability concerns are not crucial. This is prudent to attenuate unforeseen actions during the design process, such as the effect of temperature and shrinkage. The amount of web reinforcement specified in ACI 318 (2014) and CSA S806 (2012) should be used as a guide, until further research on the appropriate amount of FRP web reinforcement is conducted.

CHAPTER 5
STRUT EFFICIENCY BASED DESIGN

Foreword

Authors and Affiliation

- Khaled Mohamed: PhD candidate, Department of Civil Engineering, University of Sherbrooke.
- Ahmed Sabry Farghaly: Postdoctoral Fellow, Department of Civil Engineering, University of Sherbrooke, and Associate Professor, Assiut University, Egypt.
- Brahim Benmokrane: Department of Civil Engineering, University of Sherbrooke, Sherbrooke.

Journal: *ACI Structural Journal*, ACI

Acceptation state: submitted March 4, 2015.

Reference: Mohamed, K., Farghaly, A. S., and Benmokrane, B., 2015, "Strut Efficiency-Based Design for Concrete Deep Beams Reinforced with Glass-FRP Bars," *ACI Structural Journal*.

Abstract

In this paper, a strut-and-tie-based model is proposed to predict the shear strength of FRP-reinforced deep beams. An assessment of the available strut-and-tie methods (STMs) in ACI and CSA provisions was conducted, identifying the important parameters affecting the strut efficiency factor. The tendency of each parameter (concrete compressive strength, shear span-depth ratio, strain in longitudinal reinforcement) was assessed against the efficiency factor. The data from the 28 specimens with and without web reinforcement, including 12 tested FRP-reinforced concrete deep beams in our study and 16 FRP-reinforced deep beams taken from the literature, were used to assess the proposed model. The model was capable of capturing the failure mode and predicting the ultimate capacity of the tested FRP-reinforced deep beams. The proposed model was verified against a compilation of databases on 172 steel-reinforced deep beams, resulting in an acceptable level of adequacy.

Keywords: strut-and-tie model; efficiency factor; deep beams; FRP bars; shear strength

5.1 Introduction

Deep beams have relatively small span-to-depth ratios (a/d), so that shear strain becomes dominant. Hence, traditional sectional-design approaches based on plane sectional theory are not applicable for the design of deep beams in which the plane section does not remain plane, thereby requiring a different approach. In deep beams, externally applied loads are transferred directly to the supports by strut action (MacGregor 1997). As a result, provisions—such as in ACI and CSA—recommend the use of strut-and-tie model for designing reinforced-concrete deep beams.

The strut-and-tie model (STM) idealizes the complex flow of stresses using a pin-jointed truss consisting of compression struts and tension ties, which allows for easier monitoring of the force flow (Schlaich et al. 1987). The STM can only be applied to an element, however, if the truss model follows the lower-bound theorem, under which the capacity of an STM is always lower than the structure's actual capacity. If the truss model is in equilibrium, the truss will exhibit the deformation capacity required to redistribute the internal stresses and the stresses applied to the STM elements within their limit capacity.

In practice, deep beams are commonly used when designing transfer girders or bridge bents. These elements are exposed to aggressive environments in northern climates, which causes the steel bars to corrode. So, researchers have examined the use of fiber-reinforced polymer (FRP) instead of steel as internal reinforcement in deep beams (Andermatt and Lubell 2013-a and b, Farghaly and Benmokrane 2013). The tested FRP-reinforced deep beams demonstrated sufficient deformability to distribute the stresses according to the STM. CSA S806 (2012) introduced the STM for FRP-reinforced deep beams, which is the same model specified in CSA A23.3 (2014) for steel-reinforced deep beams, although the STM was not used in ACI 440.1R (2006). Therefore, our study aimed at assessing the factors affecting the efficiency of the concrete strut and at developing a new STM based on the tested FRP-reinforced deep beams.

5.2 Strut-and-Tie Model

The strut-and-tie model (STM) is an approach used to design discontinuity regions (D-regions) in reinforced-concrete structures to reduce the complex states of stress into a truss comprised of simple, uniaxial stress paths (Figure 5.1). The members of the STM subjected to tensile stresses are called ties and represent the location where reinforcement should be placed, while the members subjected to compression are called struts. The points where truss members intersect are called nodes. Most design specifications recognize three major node types: CCC nodes (bounded by struts only), CCT nodes (bounded by one tie and two or more struts), and CTT nodes (bounded by one strut and two or more ties). If the forces acting on STM boundaries are known, the forces in each of the truss members can be determined using basic truss theory.

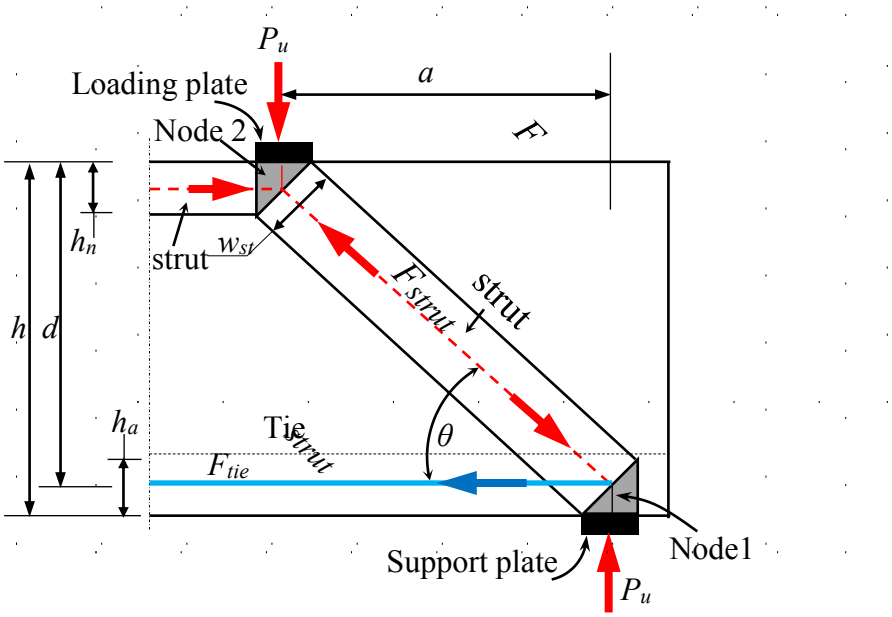

Figure 5.1 –Strut-and-tie model (one-panel)

The ACI and CSA STMs design provisions allow the use of any truss configuration according to designer provisions. In general, the one-panel STM shown in Figure 5.1 was found to be the preferred mechanism in steel-reinforced deep beams with a limited amount of web reinforcement (Brown and Bayrak 2006) and was therefore applied to the tested FRP-reinforced deep beams.

Defining the geometry of the nodal regions involves calculating stresses on struts and nodal faces as follows (Figure 5.2). An iterative procedure would be used to calculate the capacity based on the condition of limiting the stresses acting on the truss components (struts, ties, and nodes) to their permitted allowable stress levels in order to satisfy the lower-bound theorem. The allowable design stress on struts and nodal faces (f_{ce}) varied according to the design provisions, as discussed in the following section.

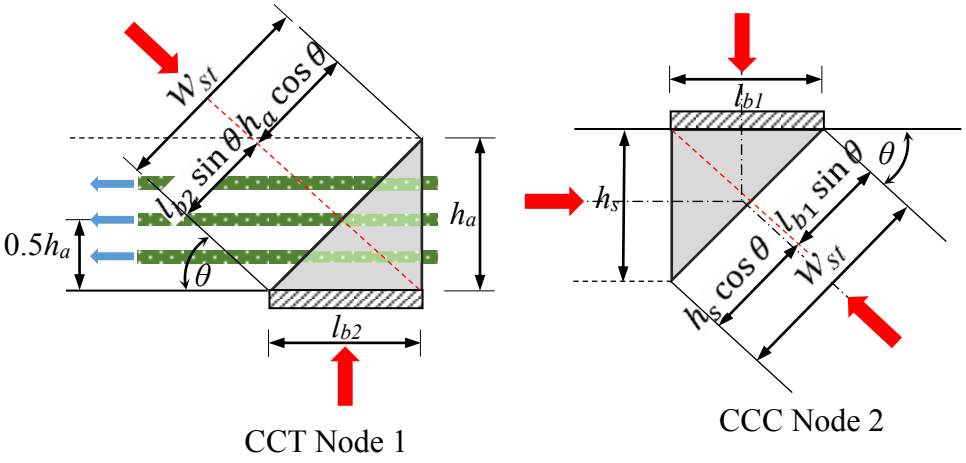

Figure 5.2 – STM nodal geometry

5.2.1 Provision of ACI 318 (2014)

ACI 318 (2014) in Chapter 23 provides the STM-based design for deep beams. The nominal force carried by the strut is calculated as $F_{ns} = f_{ce} A_{cs}$; where A_{cs} is the smaller cross-sectional area at either end of the strut and f_{ce} is calculated as follows:

$$f_{ce} = 0.85\beta_s f_c' \tag{5.1}$$

where f_c' is the concrete compressive strength.

The strut efficiency factor (β_s) depends on strut geometry, the reinforcement provided, and stress conditions in the member. For a strut of uniform cross-sectional area over its length, $\beta_s = 1.0$, while, for a bottle-shaped strut, $\beta_s = 0.6$ when no web reinforcement is provided and $\beta_s = 0.75$ with reinforcement in order to satisfy the minimum web reinforcement specified as follows:

$$\sum \frac{A_{si}}{bs_i} \sin \alpha_i \geq 0.003 \tag{5.2}$$

where A_{si} is the reinforcement cross-sectional area crossing the strut in the i-th layer of reinforcement at spacing s_i and angle α_i to the strut axis, and b is the strut width perpendicular to the plane of the reinforcing bars.

Additionally, ACI 318 (2014) places limits on the allowable stresses at the node faces. The nominal force carried by the nodal zone is calculated as $F_{nn} = f_{ce} A_{nz}$; where A_{nz} is the area of the nodal face and f_{ce} is calculated as follows:

$$f_{ce}=0.85\beta_n f_c' \tag{5.3}$$

The value of the nodal efficiency factor (β_n) in ACI 318 (2014) depends on the node boundary condition, taken as equal to 1.0 for CCC nodal zones and 0.80 for CCT nodal zones.

5.2.2 Provision of CSA S806 (2012)

CSA S806 (2012) uses the STM to determine the internal forces in deep beams reinforced with FRP bars. The strut compressive force shall not exceed $f_{ce} A_{cs}$; where A_{cs} is the effective cross-sectional area of the strut and f_{ce} is calculated based on the modified compression field theory (Vecchio and Collins 1986) as follows:

$$f_{cu} = \frac{f_c'}{0.8 + 170\varepsilon_1} \leq 0.85 f_c' \tag{5.4}$$

$$\varepsilon_1 = \varepsilon_F + \left(\varepsilon_f + 0.002\right)\cot^2 \alpha_s \tag{5.5}$$

where ε_{frp} is the tensile strain in the tie bar located closest to the tension face in the deep beam and inclined at angle θ to the strut axis.

CSA S806 (2012) specifies that the stress limits in nodal zones shall not exceed $0.65\alpha f_c'$, where α depends on the nodal boundary conditions 0.85 in CCC nodes and 0.75 in CCT nodes. Moreover, the provision specifies minimum web reinforcement ratio of 0.003 in each direction with a maximum spacing of 200 mm (7.87 in) for crack control.

5.2.3 Assessment of the Design Provisions

The STM design provisions provided in ACI 318 (2014) and CAS S806 (2012) were used to calculate the capacity of the deep beams tested in our study as well as that of FRP-reinforced deep beams taken from the literature (Farghaly and Benmokrane 2013; Andermatt and Lubell 2013-a). Specimens that were relatively small in scale and/or flexurally dominated were omitted, as they do not represent the real case of deep beams in practice. Figure 5.3 shows the comparison between the experimental and predicted load capacity using both provisions. The calculated capacities according to both provisions were scattered with different levels of deficiency due to the inherent shortcomings in each provision.

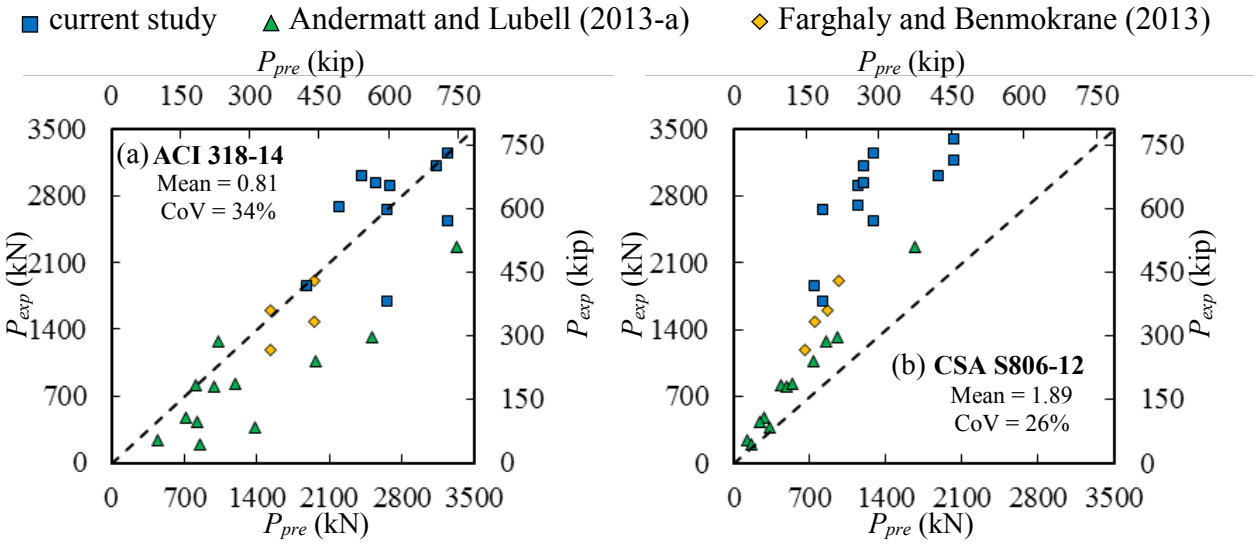

Figure 5.3 – Predicted/experimental capacity using STM in; (a) ACI and (b) CSA provisions

The STM in ACI provisions predicted the failure of either the upper or the lower node of the inclined strut for all specimens, which is consistent with the experimental results. The capacity prediction using the STM in ACI 318 (2014) was overestimated and arbitrary, with a mean experimental-to-predicted value of 0.81 and coefficient of variation (CoV) of 34% (Figure 5.3-a). An overestimation was also observed for the steel-reinforced deep beams (Reineck and Todisco 2014, Tuchscherer et al. 2014, Hong and Ha 2012). The overestimated capacities produced by the STM in ACI 318 (2014) for FRP-reinforced deep beams could be explained by the fact that it neglects the effect of concrete softening in the diagonal strut resulting from the presence of high strains in the longitudinal reinforcement (Eq. 5.5). Moreover, as shown in

Table 5.1, , the prediction for the capacity of deep beams with web reinforcement based on ACI 318 (2014) would exceed the capacity of deep beams without web reinforcement by 20%, which is inconsistent with the experimental results in our study (Table 5.1).

Table 5.1 – Capacity prediction of tested FRP-reinforced deep beams

Specimen ID		b (mm)	d (mm)	l_{b1} (mm)	l_{b2} (mm)	f_c' (MPa)	A_{frp} (mm^2)	E_{frp} (GPa)	P_{exp} (kN)	ACI 318 P_{exp}/P_{pred}	CSA S806 P_{exp}/P_{pred}	Proposed Model P_{exp}/P_{prop}
Authors	G1.47	300	1088	232	203	38.7	4054	66.4	1849	0.98	2.48	1.08
	G1.47H	300	1088	232	203	45.4	4054	66.4	1695	0.64	2.05	1.10
	G1.47V	300	1088	232	203	45.4	4054	66.4	2650	1.00[a]	1.15[a]	1.04[a]
	G1.13	300	1088	232	203	37	4054	66.4	2687	1.22	2.35	1.05
	G1.13H	300	1088	232	203	44.6	4054	66.4	2533	0.78	1.97	0.98
	G1.13V	300	1088	232	203	44.6	4054	66.4	3236	1.23[a]	1.45[a]	1.15[a]
	G1.13VH	300	1088	232	203	37	4054	66.4	2904	0.94[a]	1.45[a]	1.00[a]
	G0.83	300	1088	232	203	38.7	4054	66.4	3000	1.24	1.59	1.44
	G0.83H	300	1088	232	203	43.6	4054	66.4	3166	0.78	1.56	1.05
	G0.83V	300	1088	232	203	43.6	4054	66.4	3387	0.83	1.67	1.08
	SG1.13	300	1088	232	203	43.1	3928	66.0	2928	1.15	2.44	1.15
	SG1.13VH	300	1088	232	203	43.1	3928	66.0	3110	1.11[a]	1.41[a]	1.10[a]
Farghaly and Benmokrane (2013)	G6#8	300	1097	232	130	49.3	2280	47.6	1477	0.75	1.96	0.98
	G8#8	300	1088	232	130	49.3	4054	51.9	1906	0.97	1.97	1.15
	C12#3	300	1111	232	130	38.7	856	120	1191	0.77	1.83	1.08
	C12#4	300	1106	232	130	38.7	1520	144	1601	1.04	1.85	1.16
Andermatt and Lubell (2013-a)	A1N	310	257	100	100	40.2	1188	41.1	814	1.00	1.86	1.23
	A2N	310	261	100	100	45.4	1188	41.1	472	0.66	1.68	1.31
	A3N	310	261	100	100	41.3	1188	41.1	244	0.55	1.89	1.65
	A4N	310	261	100	100	64.6	1188	41.1	192	0.22	1.13	1.14
	B1N	300	503	200	200	40.5	2576	37.9	1274	1.23	1.50	1.00
	B2N	300	501	200	200	39.9	2576	37.9	800	0.81	1.66	1.26
	B3N	300	502	200	200	41.2	2576	37.9	432	0.53	1.82	1.61
	B4N	300	496	200	200	40.7	3168	41.1	830	0.69	1.53	1.19
	B5N	300	497	200	200	66.4	3168	41.1	1062	0.54	1.44	1.32
	B6N	300	505	200	200	68.5	2576	37.9	376	0.27	1.14	1.18
	C1N	301	889	330	330	51.6	4224	42.3	2270	0.68	1.36	0.99
	C2N	304	891	330	330	50.7	4224	42.3	1324	0.53	1.38	1.15
Mean value										0.83	1.77	1.17
CoV										34%	25%	15%

[a] Based on two-panel truss model. P_{exp}: Ultimate load at failure recorded during testing, P_{pred}: Predicted load from ACI or CSA provisions, P_{prop}: Predicted load from the proposed model, l_{b1}: loading plate width, l_{b2}: support plate width.
All deep beams reinforced entirely with glass-FRP bars except C12#3 and C12#4 reinforced with carbon-FRP bars.
Note: 1 mm = 0.0394 in.; 1 MPa = 145 psi; 1 kN = 0.225 kips.

Figure 5.3-b shows the conservative prediction based on CSA S806 (2012) for the FRP-reinforced concrete deep beams tested by Andermatt and Lubell (2013-a) and Farghaly and Benmokrane (2013). The level of conservatism was increased for the specimens tested in our study. This level of conservatism was expected as the method exaggerates the negative effect of concrete softening in the diagonal strut due to the longitudinal reinforcement strain through the calculation of ε_1 (Eq. 5.5). It is worth mentioning that the maximum strain in the longitudinal reinforcement is limited to 0.002 in the case of steel-reinforced deep beams, but it could reach 0.01 in the case of FRP-reinforced deep beams, which increases ε_1 and, in return, underestimates the efficiency of the diagonal strut. Therefore, it was expected to yield to significantly lower predictions than that of the experiments on deep-beam specimens. The value of the mean ratio of 1.89 indicated the conservative uneconomical prediction with a CoV of 26%. Therefore, it can be deduced that the STMs adopted by ACI and CSA do not adequately reflect the capacity of FRP-reinforced deep beams and, consequently, the model must be modified.

5.2.4 Other Existing ST-Based Models

This section examine the ability of the existing STM based models built for steel-reinforced deep beams to predict the ultimate capacity of the tested GFRP-reinforced deep beams. The predicted capacities are presented in Figure 5.4, employing ST-based models developed by Matamoros and Wong (2003), Russo et al. (2005), Park and Kuchma (2007), and Mihaylov et al. (2013).

i. *Matamoros and Wong Model (2003)*

The total shear strength is calculated as follows:

$$V = \frac{0.3}{a/d} f_c' b w_{st} + A_{tv} f_{yv} + 3(1 - a/d) A_{th} f_{yh} \tag{5.6}$$

where A_{tv} and A_{th} is the vertical and horizontal reinforcement area within the shear span, a, respectively. The term $0.3/(a/d)$ has an upper limit of $0.85\sin\theta$, where $\tan\theta \approx 1/(a/d)$, and the term $(1 - a/d)$ has a lower limit of 0. The diagonal strut has a uniform width, w_{st}, depending on

the node geometry at the support. The yield stress of vertical (f_{yv}) and horizontal (f_{yh}) web reinforcement was assumed to be equal to the ultimate strength of the vertical and horizontal web reinforcement, respectively.

The model was not following the lower-bound theorem by neglecting the effect of the nodal geometry at loading point, which in most cases governed the width of the diagonal strut. In addition, the model accounted for the effect of vertical and/or horizontal web reinforcement on the capacity of the GFRP-reinforced deep beams, which contradict with the experimental results of the current study. Therefore, the predicted capacities according to the proposed model was scattered, with mean experimental to predicted values of 0.69, and coefficient of variation (CoV) of 48%.

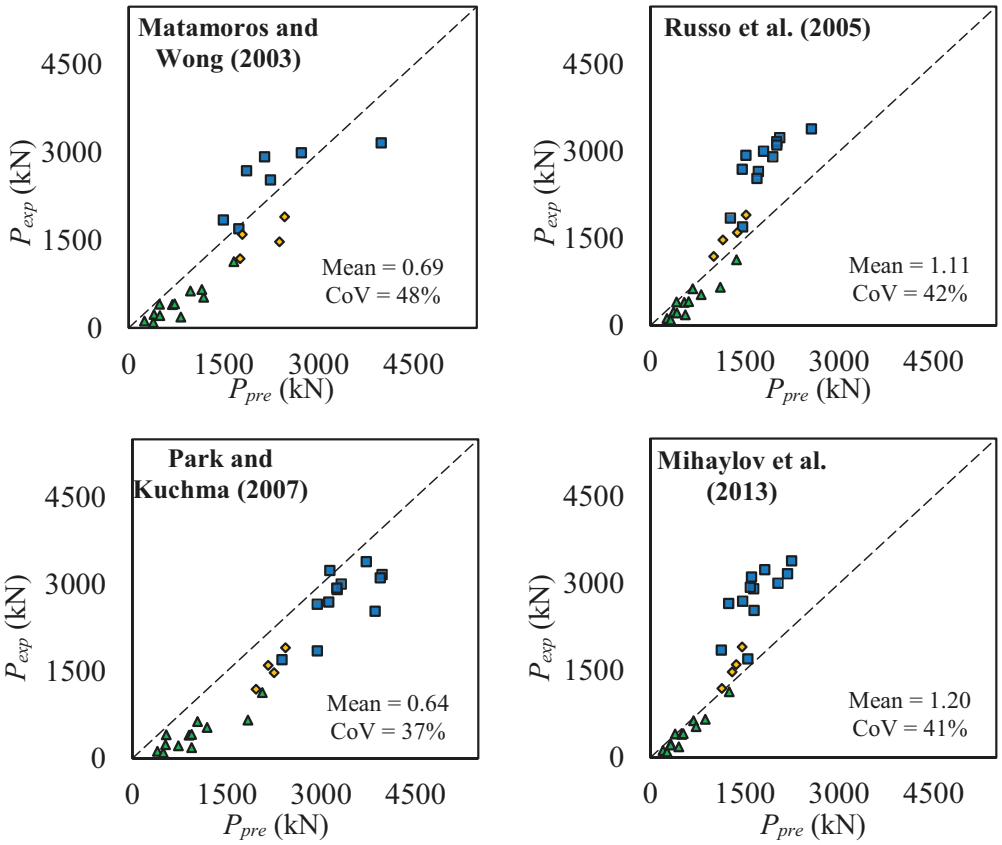

Figure 5.4 – Predicted vs experimental capacity using ST-based models

ii. *Russo et al. Model (2005)*

The suggested expression for the shear strength considered the effect of normal- and high-strength concrete, and was given as follows

$$V = 0.545\left(k\chi f_c^{'}\cos\theta + 0.25\rho_h f_{yh}\cot\theta + 0.35(a/d)\rho_v f_{yv}\right)bd \quad (5.7.a)$$

$$k = \sqrt{(n\rho_f)^2 + 2n\rho_f} - n\rho_f \quad (5.7.b)$$

$$\chi = \left[0.74\left(f_c^{'}/105\right)^3 - 1.28\left(f_c^{'}/105\right)^2 + 0.22\left(f_c^{'}/105\right) + 0.87\right] \quad (5.7.c)$$

where n is the ratio of steel to concrete elastic modulus (in the current study $n = E_{frp}/E_c$), ρ_f, ρ_h, and ρ_v are the steel ratios of the longitudinal reinforcement, and horizontal and vertical web reinforcement, respectively. The model accounted for the width of the loading plate only, w_l, with no consideration to the support plate width. The model led to uneconomically conservative and scattered estimation for the capacity of GFRP-reinforced deep beams, as it also considered for the effect of vertical and horizontal web reinforcement (with mean experimental to predicted value of 1.11 and CoV of 42%).

iii. *Park and Kuchma Model (2007)*

The STM-based model requires an iterative procedure to calculate the capacity of the deep beam. The procedure begins with selecting the value of the applied load, then the forces and strains in concrete strut and reinforced ties are calculated. The tensile strain in the direction perpendicular to the concrete strut, ε_r, can be calculated from $\varepsilon_r = \varepsilon_v + \varepsilon_h - \varepsilon_d$, where ε_v and ε_v are the tensile strains in the horizontal and vertical web reinforcement (equal to 0.0025 for not defined web reinforcement), ε_d is the compressive strain in the concrete. Using the state of strains in each member, the stresses are determined as follow

$$\sigma_d = \xi f_c^{'}\left[2\left(\frac{\varepsilon_d}{\xi\varepsilon_0}\right) - \left(\frac{\varepsilon_d}{\xi\varepsilon_0}\right)^2\right] \quad \text{for } \frac{\varepsilon_d}{\xi\varepsilon_0} \le 1.0 \quad (5.8.a)$$

$$\sigma_d = \xi f_c^{'}\left[1 - \left(\frac{\varepsilon_d/(\xi\varepsilon_0) - 1}{2/(\xi - 1)}\right)^2\right] \quad \text{for } \frac{\varepsilon_d}{\xi\varepsilon_0} > 1.0 \quad (5.8.b)$$

$$\varepsilon_0 = 0.002 + 0.001\,\frac{f_c^{'} - 20}{80} \text{ for } 20 \le fc' \le 100 \text{ MPa} \quad (5.8.c)$$

$$\xi = \frac{5.8}{\sqrt{f_c^{'}}} * \frac{1}{\sqrt{1 + 400\varepsilon_r}} \le \frac{0.9}{\sqrt{1 + 400\varepsilon_r}} \quad (5.8.d)$$

where ε_0 is a concrete cylinder strain corresponding to the cylinder strength fc', and the softening coefficient, ξ, depends on the model proposed by Hsu and Zhang (1997), which based on the conditions of equilibrium and compatibility to calculate the effect of the tensile strains in the perpendicular direction to the compressive strains. The secant moduli for each member can be determined from the softening coefficient, and then compared to that calculated from the assumed applied load. The first assumption for the secant moduli could be the elastic moduli. If the differences between the secant moduli are larger than 0.1%, then the steps are repeated until convergence. The procedure is completed when the stress in either the horizontal or diagonal concrete strut reach their capacity.

The model overestimated the capacity with mean experimental/predicted value of 0.64 and CoV of 37%. The overestimation of specimens' capacity could be attributed to limiting the transverse strains to 0.0025 for specimens with no web reinforcement. This value could be much higher for FRP-reinforced deep beams, at which the FRP bars exhibit higher strains when compared to steel bars, leading to softening of the concrete struts.

iv. *Mihaylov et al. Model (2013)*

The kinematic theory was combined with equilibrium equations and stress-strain relationships to predict the shear strength and deformations of deep beams. In calculating the maximum shear strength resisted by the deep beam, V, the model followed the format of conventional design as the sum of the contribution of the shear resisted by the critical loading zone, V_{CLZ}, by aggregate interlock, V_{ci}, by vertical web reinforcement, V_s, and by dowel action, V_d. as follows

$$V = V_{CLZ} + V_{ci} + V_s + V_d \tag{5.9}$$

$$V_{CLZ} = f_{avg} b l_{b1e} \sin^2 \alpha \tag{5.10}$$

where the average compressive stress is given as $f_{avg} = f_c'^{0.8}$ (MPa), and the effective width of the loading plate, l_{b1e}, equals to $(V/P)l_{b1}$. l_{b1} and l_{b2} are the loading and support plate size, respectively. The model depends in calculating the shear resisted by the aggregate interlock on the simplified modified compression field theory (Bentz et al. 2006) as follows

$$V_{ci} = \frac{0.18\sqrt{f_c'}}{0.31 + \frac{24w}{a_g + 16}} \tag{5.11}$$

where w is the crack width, and a_g is the maximum size of coarse aggregate. The shear resisted by the vertical stirrups is calculated as follows

$$V_s = \rho_v b\left(d\cot\alpha_1 - l_0 - 1.5l_{b1e}\right)f_v \geq 0 \tag{5.12}$$

where f_v is the stress in the vertical web reinforcement ($f_v = [0.0175\ l_{b1e}\ \cot\theta/d].E_{frp}$). The angle of the critical crack, α_1, shall not be taken smaller than the angle θ of the cracks that developed in a uniform stress field. The angle θ can be calculated from the simplified modified compression field theory (Bentz et al. 2006), or can be taken equal to 35°.

When applying the model proposed by Mihaylov et al. (2013) for the tested deep beams, V_d for longitudinal GFRP reinforcement was neglected as specified by ACI 440.1R (2004). This could led to the underestimated capacity for the tested specimens as presented in Figure 5.4 (with mean experimental/predicted value of 1.20 and CoV of 41%). From the previous discussion, other existing ST-based models for steel-reinforced deep beams are inadequate to predict the capacity of FRP-reinforced deep beams, which rises the necessity of proposing new ST-based model for FRP-reinforced deep beams.

5.3 Strut Efficiency Factor

An adequate detailing of truss elements is necessary to ensure the safety of deep beams. This requires that none of the stresses in the STM elements exceed the allowable capacities: yield in steel or rupture in FRP longitudinal reinforcement of the tie or the strut's concrete effective compressive strength. Tie failure — either rupture of the FRP or yielding of the steel bars— can be eliminated by providing an adequate amount of longitudinal reinforcement so as to induce the failure in the struts or nodes (ACI 318, 2011; CSA S806, 2012).

Various studies have been conducted to assess the parameters affecting the strut's concrete strength in steel-reinforced deep beams (Reineck and Todisco 2014, Brown and Bayrak 2008).

Generally, the design procedure of struts or nodes in the STM has been to combine the effect of strut stress and strain conditions, reinforcement details, and concrete strength (or concrete softening) into one factor, namely the efficiency factor (β_s). Thus, the efficiency factor can be defined as the ratio of stress in the strut (f_{ce}) to the compressive strength of the concrete (f_c'); it is calculated as follows:

$$\beta_s = \frac{f_{ce}}{0.85 f_c'} = \frac{F_{strut}}{0.85 A_{strut\ (\min)}\ f_c'} \tag{5.13}$$

The diagonal strut force (F_{strut}) can be calculated from the truss equilibrium as shown in Figure 5.1 and divided by the minimum cross-sectional area of the strut ($A_{strut(min)}$) to determine the maximum stress (f_{ce}). The minimum cross-sectional area of the strut can be determined by multiplying the width of the diagonal strut (w_{st}) by the deep beam's breadth (b) at both ends of the strut. w_{st} can be easily determined from node geometry, as shown in Figure 5.2. The individual effect of each parameter influencing β_s for the FRP-reinforced deep beams is discussed in the following section.

5.3.1 Parameters Affecting Strut Efficiency Factor

Figure 5.5 shows the tendency of the efficiency factor (β_s) with changing parameter values: concrete compressive strength (f_c'), shear span-depth ratio (a/d), and strain of longitudinal reinforcement (ε_1) with insignificant web reinforcement effect.

ACI 318 (2014) provisions do not take into account these parameters in calculating β_s. Moreover, the constant values of β_s equal to 0.6 and 0.75—assigned for specimens without and with minimum web reinforcement, respectively—places the prediction in the upper limit of the data cloud, as shown in Figure 5.4, and leads to an unsafe estimation of the deep beam's capacity. On the other hand, the efficiency factor in CSA S806 (2012) explicitly accounts for ε_1, implicitly considers the effect of the a/d ratio through the term $cot^2\theta$, and does not account for the effect of f_c'. Nevertheless, the efficiency factor provided by CSA provision lies on the lower limit of the data cloud in Figure 5.5, leading to a conservative but uneconomic estimation of the deep beam's capacity.

Figure 5.5-a shows a relatively clear trend of the negative effect of f_c' on β_s, although the FRP-reinforced deep beams tested had a limited variety of f_c'. This was observed by Andermatt and Lubell (2013-a), who attributed that to the limited deformation due to the more brittle nature of the higher strength concrete, which reduced the efficiency of the diagonal concrete strut. The correlation between the shear strength of deep beams and a/d shown in Figure 5.5-b is predictable (the increased a/d decreased the deep beam's strength), as reported in many studies and most notably in the shear tests conducted by Kani et al. (1979).

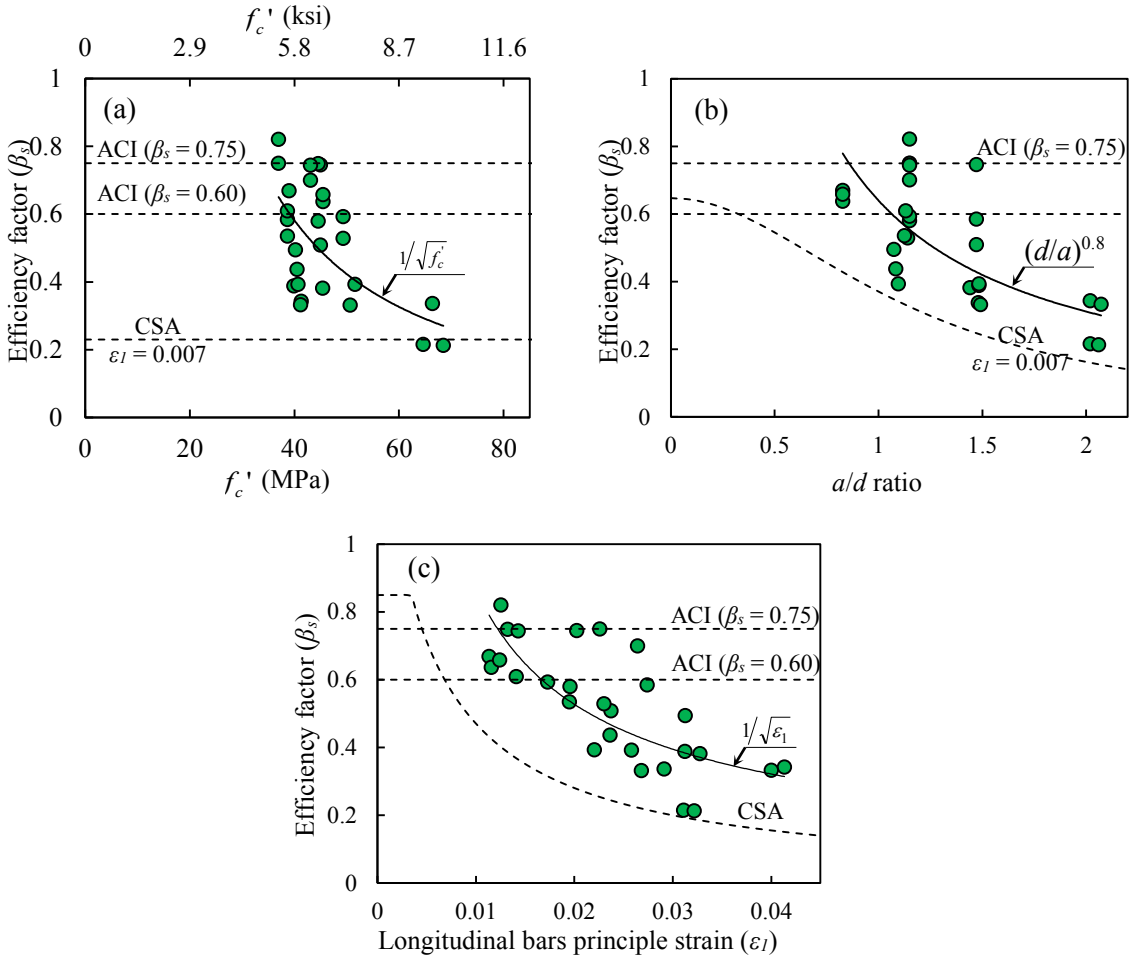

Figure 5.5 – Factors affect the measured efficiency factor

In the steel-reinforced deep beams, the concrete softening in the diagonal strut was relatively insignificant, since steel-reinforced ties should not reach their yield capacity in order to satisfy the lower-bound theory. Therefore, the tensile strains in the steel reinforcement were relatively low (less than 0.002). The relatively low elastic modulus of FRP bars, however, induced

relatively high strains in the FRP longitudinal reinforcement (compared to the steel), which significantly affected the strength of the diagonal strut and, therefore, the efficiency factor.

It should be mentioned that the strain of the longitudinal reinforcement cannot be used directly since the softening of concrete in compression is a function of the principal tensile and compressive strains (ε_1 and ε_2, respectively), while ε_2 is set to 0.002 for crushed concrete in the diagonal strut (Vecchio and Collins 1986). Therefore, the efficiency factor was related to ε_1 rather than the strain of the longitudinal bars, as shown in Figure 5.4(c). Farghaly and Benmokrane (2013) reported the ultimate capacity of the tested FRP-reinforced deep beams could be increased solely by increasing the axial stiffness of the longitudinal reinforcement, thereby reducing its strain and enhancing the efficiency of the diagonal strut strength.

5.3.2 Proposed Development of β_s

Based on the aforementioned discussion, β_s is a function of (f_c', a/d, ε_1) and can be set in a form as follows:

$$\beta_s = z \,.\, (f_c')^a \,.\, (a/d)^b \,.\, (\varepsilon_1)^c \tag{5.14}$$

where z is constant and a, b, and c are the constants representing the correlation between each parameter and β_s.

Figure 5.5 shows the results of the least-squares regression performed to identify the correlation of each parameter as -0.5, -0.8, and -0.5 for a, b, and c, respectively. The constant z was set to 0.5 to have the estimation in the lower limit of the data. Therefore, the efficiency factor β_s can be calculated as follows:

$$\beta_s = 0.5 \frac{1}{\sqrt{f_c'}} \frac{1}{(a/d)^{0.8}} \frac{1}{\sqrt{\varepsilon_1}} \qquad \text{(SI unit)} \tag{5.15}$$

where ε_1 is given by Eq. 5.5 and a/d is limited to unity for specimens having a a/d of less than 1.0, to prevent overstressing the strut.

5.4 Assessment of Proposed Model

Figure 5.6 shows the comparison of the predicted ultimate capacity based on the proposed model (Eq. 5.15) versus the experimental results of the current and previous studies of a total of 28 FRP-reinforced deep beams. The predicted capacity was governed by the failure of the diagonal concrete struts in all specimens, which is consistent with the experimental results. The proposed model safely estimated the ultimate capacity with a mean value of 1.22 and CoV of 19%.

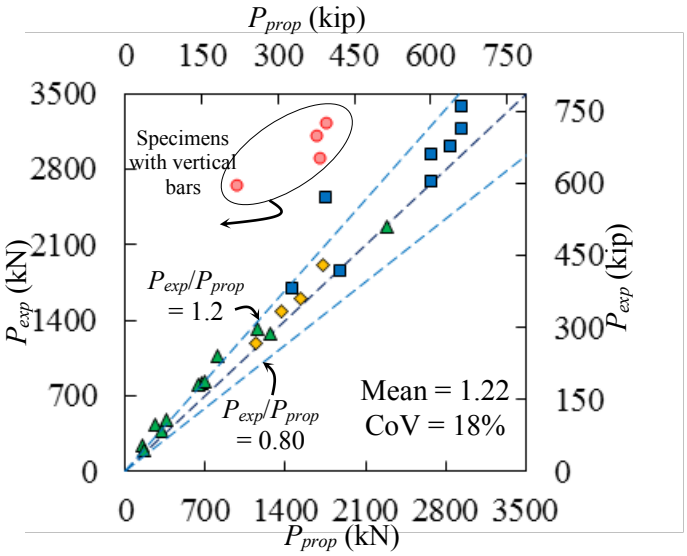

Figure 5.6 – Evaluation of the proposed model (one-panel)

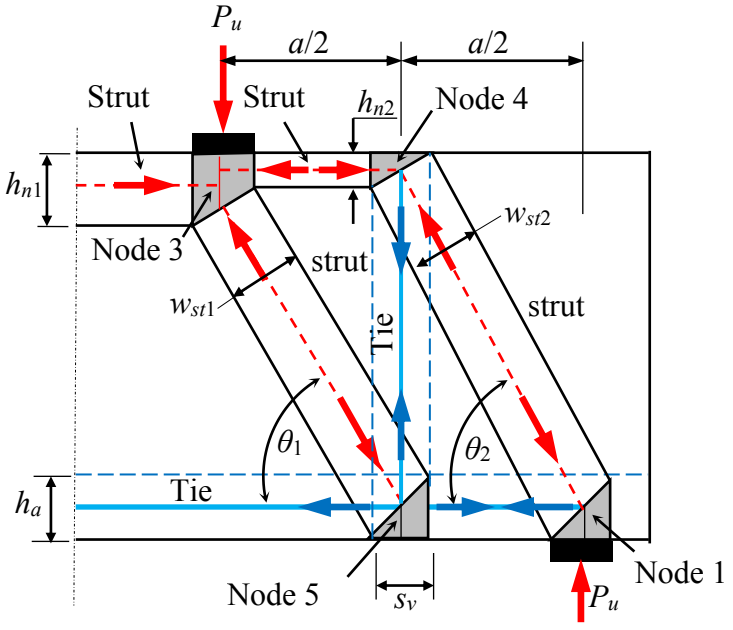

Figure 5.7 – Two-panel truss model

As illustrated in Figure 5.6, however, the model underestimated the experimental capacity of four specimens. Those four specimens had vertical web reinforcement, which would allow for the formation of the two-panel truss model (Figure 5.7) instead of the one-panel truss model shown in Figure 5.1. Figure 5.8 shows the geometry of the nodal regions and the stresses acting on struts and nodal faces. The typical failure mode of specimens with vertical web reinforcement, given in Figure 5.9, could support this suggestion. Therefore, it was essential to examine the two-panel truss model for the tested beams.

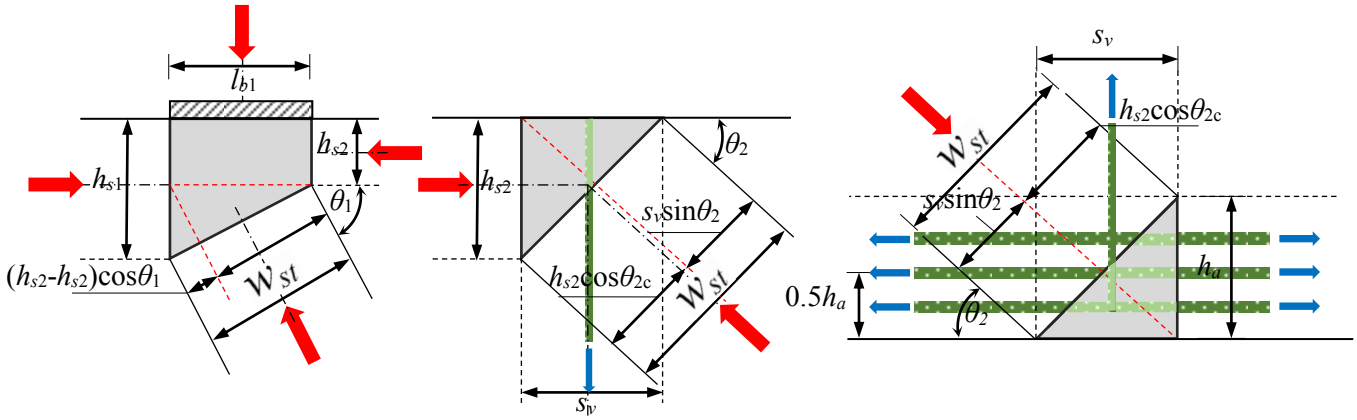

Figure 5.8 – Nodal geometry of two-panel truss model

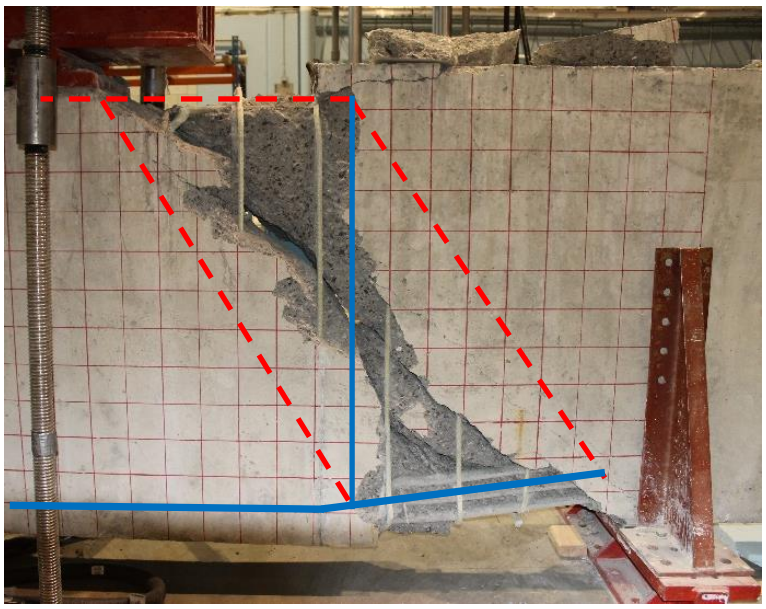

Figure 5.9 – Formation of two-panel STM in tested deep beams with vertical stirrups

5.4.1 Strain-Energy Concept

According to Schlaich et al. (1987), the truss model—either the one-panel or the two-panel model shown in Figures 5.1 and 5.7, respectively—that contains the least strain energy is likely to be comparable to the experimental results. The strain energy for a truss model is equal to the sum of the strain energy of each member in the STM (struts and ties). To calculate the strain energy for each member, the area under the stress–strain curve such an element is multiplied by its volume. The strain energy for one- and two-panel truss models was calculated from the collected data of FRP-reinforced deep beams to examine the appropriate truss model.

The stress–strain relationship for concrete and FRP reinforcement was based on the actual material properties for the deep beams tested in the current study. For the deep beams in previous studies, however, the model developed by Popovics (1973) and modified by Collins and Mitchell (1997) to account for HSC was used to predict the concrete stress–strain curve. FRP reinforcement behaves linearly, so the maximum stresses and strains for the longitudinal reinforcement was calculated from the force acting on the tie and the bar's elastic modulus (E_{frp}). The maximum strains in the vertical and horizontal web reinforcement were taken as the measured strains during testing. Based on the geometry of the strut-and-tie model (see Figures 5.1 and 5.7 for details) and the experimental ultimate capacity, the force in each truss member and its stress and strain in either the one- or two-panel truss model were determined.

All struts were assumed prismatic-shaped to calculate their volumes, considering that the dispersion of compression in a bottle-shaped strut produce less stresses at the middle of the strut than that at the ends of the strut. These lower stresses compensate the greater cross-sectional area at the middle of the strut; hence, the assumption of using prismatic-shaped strut was convenient. The area of the diagonal struts at both ends calculated as multiplying the width of the strut (as in Figures 5.1 and 5.7) by the width of the deep beam (b), then, the strut volumes were calculated multiplying the area by the length of the strut. The total area of the longitudinal reinforcement was considered to calculate the ties' volumes. For the two-panel truss model, all the vertical and horizontal reinforcement within the deep beam shear-span were included in determining the volume of the web reinforcement.

Basically, the strain energy can also be represented as the area under the load-deflection curve, which was used to verify the strain energy calculation. Figure 5.10 shows the relationship between the least strain energy from the one- and two-panel truss models and that from the area under load-deflection curve. It clearly shows that the calculation procedure defined by Schlaich et al. (1987) resulted in an acceptable prediction of the strain energy, with mean value of 1.12 and CoV of 15%.

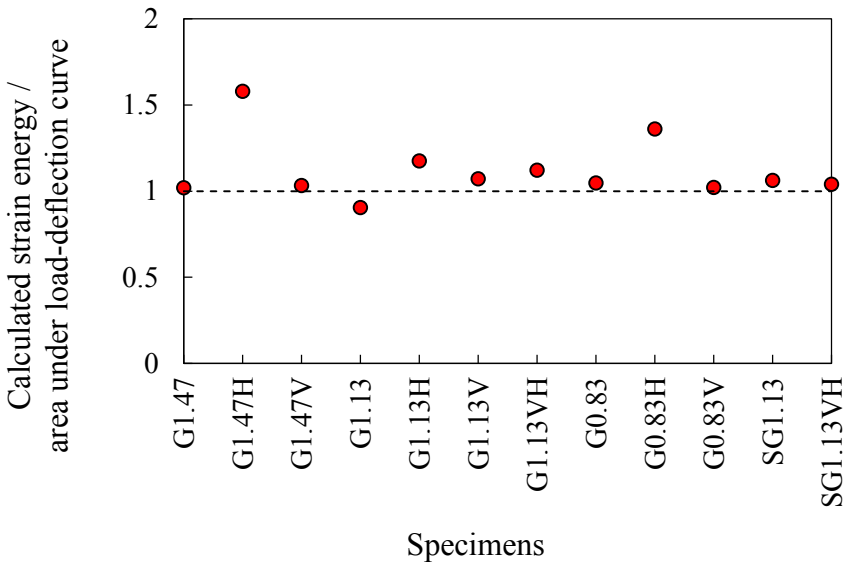

Figure 5.10 – Calculated strain energy verses area under load-deflection curve

Figure 5.11 shows the data for the strain-energy ratio (ratio of one-panel to two-panel strain energies). Accordingly, one-panel truss model would be used if the strain energy ratio is less than one. Figure 5.11 depicts that the strain energy ratio for all tested FRP-reinforced deep beams resulted in the use of the one-panel truss model, except for the four specimens with vertical web reinforcement, which acted as a vertical tie between the two struts and led to using the two-panel truss model.

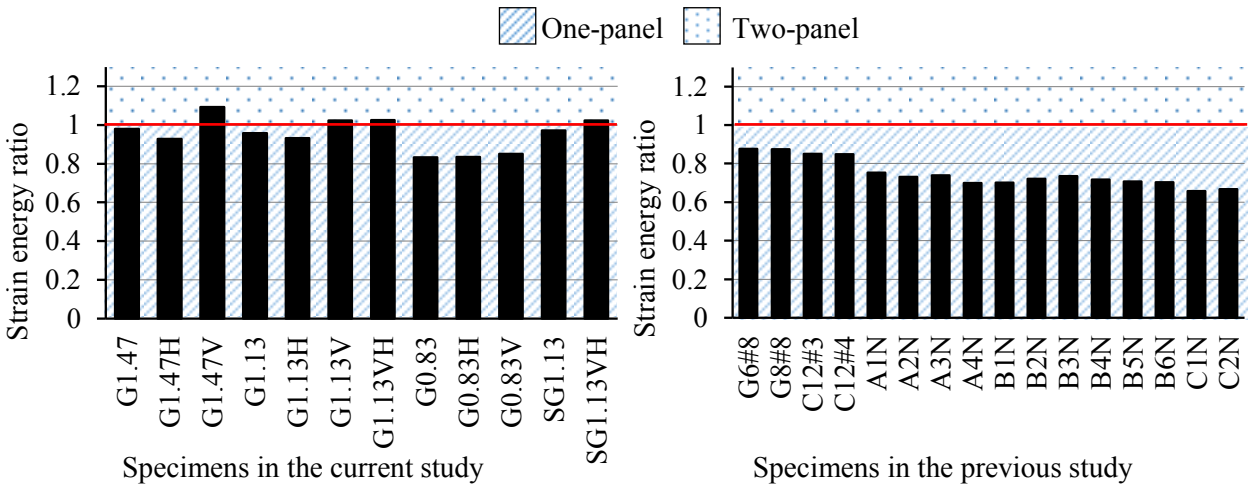

Figure 5.11 - Strain energy ratio for tested FRP-reinforced deep beams

Applying the two-panel solution for specimens with vertical web reinforcement using the proposed truss model resulted in more accurate estimation of the specimen's capacity, as shown in Figure 5.12. The mean value and CoV for the experimental-to-proposed capacity were 1.17 and 15%, respectively. The two-panel solution was also applied to predict the capacity according to the STM in ACI 318 (2014) and CSA S806 (2012), but it insignificantly improved the predicted values (see Table 5.1).

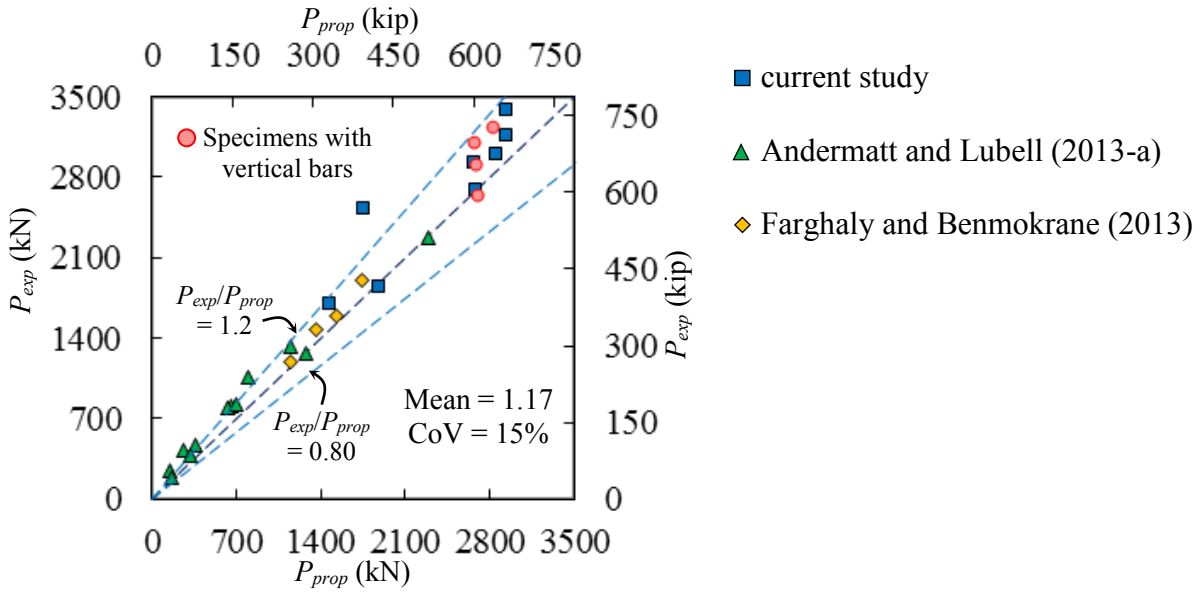

Figure 5.12 – Evaluation of the proposed model based on one- and two-panel truss models

Further verification for the proposed model was conducted by comparison to the steel-reinforced deep beams, showing its applicability. As long as the steel bars were properly anchored, no yield in the longitudinal steel reinforcement occurred, and the failure was induced by concrete crushing at the struts. Therefore, the proposed model was used to calculate the capacity of 172 steel-reinforced deep beams gathered from the literature (Clark 1951, Foster and Gilbert 1998, Oh and Shin 2001, Aguilar et al. 2002, Zhang and Tan 2007b, Alcocer and Uribe 2008, Mihaylov et al. 2010, Tuchscherer et al. 2011, and Birrcher et al. 2014). The beams were of comparable size to the deep beams currently used in practice, therefore small-scale specimens with a total height of less than 500 mm (19.7 in.) were not considered. The deep beams included in the assessment had a/d values ranging from 0.27 to 2.20, concrete strengths ranging from 13.8 to 120 MPa (2.0 to 17.4 ksi), and various combinations of web reinforcement. Beams that were described as having a failure mode other than shear (anchorage and/or flexural failure) were not included in the assessment. More details of deep beam databased used in the evaluation depicted in Appendix A.

Figure 5.13-a shows calculated capacities using the proposed model versus the reported experimental capacity. The proposed model was capable of predicting the ultimate capacity of steel-reinforced deep beams with a mean experimental-to-predicted value of 1.09 and CoV of 22%. Figures 5.12-b and -c show the predicted capacity using the STMs in ACI 318 (2014) and CSA A23.3 (2014), respectively. Consistent with the predicted results for the FRP-reinforced deep beams, ACI 318 (2014) overestimated the capacity of the specimens and CSA A23.3 (2014) produced conservative but uneconomic estimations of capacity.

In designing the steel-reinforced deep beams, the strain of the main longitudinal steel bars are not allowed to reach the yielding strain and only the elastic part of the stress–strain curve is used (Quintero-Febres et al. 2006, Tuchscherer et al. 2011). This procedure is exactly as using FRP bars as a main longitudinal reinforcement of deep beams, as the FRP bars are already an elastic material. Therefore, the proposed model was assessed against the steel- and FRP-reinforced deep beams showing its applicability in both cases.

This could be explained as the strain in the main longitudinal reinforcement was lower in case of steel reinforcement than that of FRP bars. Therefore, the effect of the main longitudinal reinforcement strain should be incorporated to the strut efficiency factor (β) counting for the

different level of the strains (Farghaly and Benmokrane 2013). Therefore, the main longitudinal reinforcement strain was counted in the proposal of the modified β, and produced good estimations for steel- and FRP-reinforced deep beams.

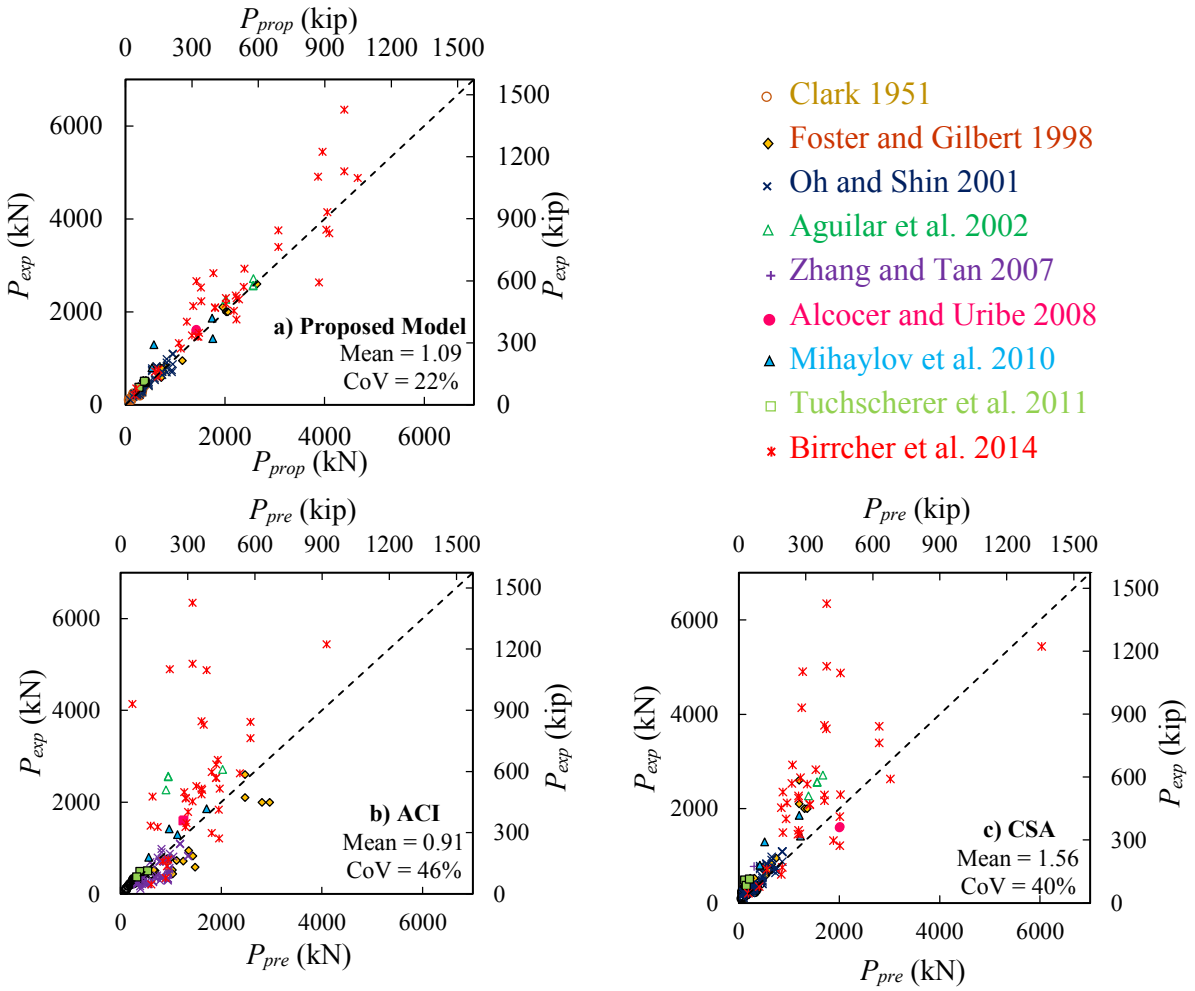

Figure 5.13 - Predicted verses experimental capacity for steel-reinforced deep beams

5.5 Conclusions

The main purpose of this research was to assess the accuracy of the strut-and-tie models in design provisions (ACI and CSA) and to quantify the efficiency factor with the affecting parameters. The efficiency factor in ACI 318 (2014) overestimated the ultimate capacity. The efficiency factor in CSA S806 (2012), however, underestimated the ultimate capacity, which could lead to uneconomic designs. These results reveal the importance of having a more

rational model for estimating the efficiency factor. Therefore, a new model for the strut efficiency factor—accounting for the concrete compressive strength, shear span-depth ratio, and strain in the longitudinal reinforcement—was proposed. The strain-energy concept was used to identify the development of either a one- or two-panel truss model. The procedure for strain-energy calculation was verified by comparing the results to the area under the load–deflection curves for the tested deep beams. The two-panel truss model was found to be appropriate for the specimens with vertical web reinforcement. Nevertheless, the authors recommend the use of the one-panel truss model, since it yields an acceptable level of conservatism. The proposed model was compared against the available FRP-reinforced deep beams and to steel-reinforced deep beams. The proposed model produced safe estimations for capacity predictions with an acceptable level of conservatism.

CHAPTER 6
NONLINEAR ANALYSIS OF TESTED DEEP BEAMS

Foreword

Authors and Affiliation

- Khaled Mohamed: PhD candidate, Department of Civil Engineering, University of Sherbrooke.
- Ahmed Sabry Farghaly: Postdoctoral Fellow, Department of Civil Engineering, University of Sherbrooke, and Associate Professor, Assiut University, Egypt.
- Brahim Benmokrane: Department of Civil Engineering, University of Sherbrooke, Sherbrooke.
- Kenneth W. Neale: Professor Emeritus, Department of Civil Engineering, University of Sherbrooke, Sherbrooke.

Journal: *Engineering Structures Journal*

Acceptation state: submitted June 13, 2015.

Reference: Mohamed, K., Farghaly, A. S., Benmokrane, B., Neal, K. W., "Nonlinear Finite Element Analysis of Concrete Deep Beams Reinforced with GFRP Bars," *Engineering Structures Journal*.

Abstract

Ten full-scale deep beams reinforced entirely with glass-fiber reinforced-polymer (GFRP) bars were tested to failure under two-point loading. The specimens were configured with three different shear span-depth ratios (a/d = 1.47, 1.13, and 0.83) and different web reinforcement configurations (vertical and/or horizontal). Finite element (FE) simulations for the ten deep beams were conducted to perform an in-depth investigation regarding the failure mechanisms. The FE model was verified capturing the crack patterns, failure modes, strains in the reinforcement and concrete and load-deflection response, resulting in good agreement with the experimental results. The results show that the simulation procedures employed were stable and compliant, and that they provided reasonably accurate simulations of the behavior. The FE analysis was used to confirm some hypotheses associated with the experimental investigations.

Keywords: Concrete, GFRP bars, failure mechanisms, deep beams, FEM.

6.1 Introduction

Reinforced concrete deep beams are used mainly for load transfer, such as transfer girders, bent-caps, and pile caps. These structural elements are subjected to deterioration in northern climate due to the corrosion of steel bars resulting from the large amount of deicing salts used during winter months. Substituting steel bars with non-corrodible fiber-reinforced polymer (FRP) in the reinforced concrete elements has become an acceptable solution to overcome steel-corrosion problems. However, experimental investigations on FRP-reinforced deep beams have been very limited, particularly for those lacking web reinforcement (Andermatt and Lubell (2013-a), Farghaly and Benmokrane (2013), Kim et al. (2014)).

Codes and provisions have adopted the use of the strut-and-tie model (STM) for the design of steel-reinforced deep beams (ACI 318, 2014; CSA A23.3, 2014; *fib*, 1999) and FRP-reinforced deep beams (CSA S806 2012). The STM is applicable for deep beams as plane sections do not remain plane and nonlinear shearing strains dominate the behavior. Many researchers have developed simplified expressions to predict the capacity of deep beams based on STM (Matamoros and Wong 2003, Russo et al. 2005, Park and Kuchma 2007, Mihaylov et al. 2013). The STM provides a simple design methodology based on the lower-bound theorem; however, its implementation requires an iterative process and graphical assumption for the truss model. The developed expressions are governed by the variables affecting the behavior of deep beams; such as the concrete compressive strength, the a/d ratio, and the reinforcement ratio and modulus of elasticity of the longitudinal and web reinforcements. However, the accuracy of the developed expressions is affected by the estimated factor for each aforementioned variable. It is worth mentioning that, the factor of each variable is estimated based on the available experimental results, which could be limited in number, or insufficient analytical results that cannot be obtained from experiments.

The finite element method (FEM) is considered as other means for in-depth analysis. The FEM currently represents the most complex and advanced approach for predicting the response of reinforced concrete structures. In the current study, an experimental investigation for GFRP-reinforced deep beams was conducted to assess the capability of FEM to predict the mechanism of such structural element.

6.2 FEM Numerical Simulation

The inelastic 2D continuum analysis tool VecTor2 (Wong and Vecchio, 2012) was used to predict the behavior of the tested GFRP-reinforced deep beams. This program employs the rotating-angle smeared crack modeling approach and implements both the Modified Compression Field Theory (MCFT) (Vecchio and Collins, 1986) and the Distributed Stress Field Model (DSFM) (Vecchio, 2000a). The MCFT was based on the assumption that the average direction of the principal compressive stresses coincides with the average direction of the principal compressive strains and the critical cracks are parallel to this direction. In contrast, the DSFM explicitly accounts for the slip deformations at the critical cracks, which resulted in a delayed rotation of the stress field with respect to the strain field. The critical cracks in the DSFM were kept perpendicular to the direction of the principle tensile stresses.

6.2.1 Applied FE Models

A fine meshing, with 48 elements over the specimen's height, was used through the analysis, as shown in Fig. 6.1. To improve the analysis speed and reduce bandwidth consumption, only half the beam span was modeled by providing horizontal restraints along the edge nodes representing the mid-span. To discretize the specimens, the model was built with different numbers of plane-stress rectangular elements with two translational degree of freedom at each node and without smeared reinforcement. The longitudinal FRP reinforcement, vertical and horizontal FRP web reinforcement, and steel anchorage stirrups beyond the supports were represented explicitly by truss elements, and perfectly bonded to the concrete elements.

In terms of concrete constitutive modeling, DSFM was used for compression post-peak response of the concrete (modified Park-Kent, 1982, shown in Figure 6.2), pre-peak compression response (Popovic HSC model, 1973), compression softening (Vecchio, 1992), tension stiffening (modified Bentz, 1999), tension softening (linear), confinement (Kupfer/Richart model, 1969), concrete dilation (variable Kupfer, 1969), cracking criterion (Mohr-coulomb).

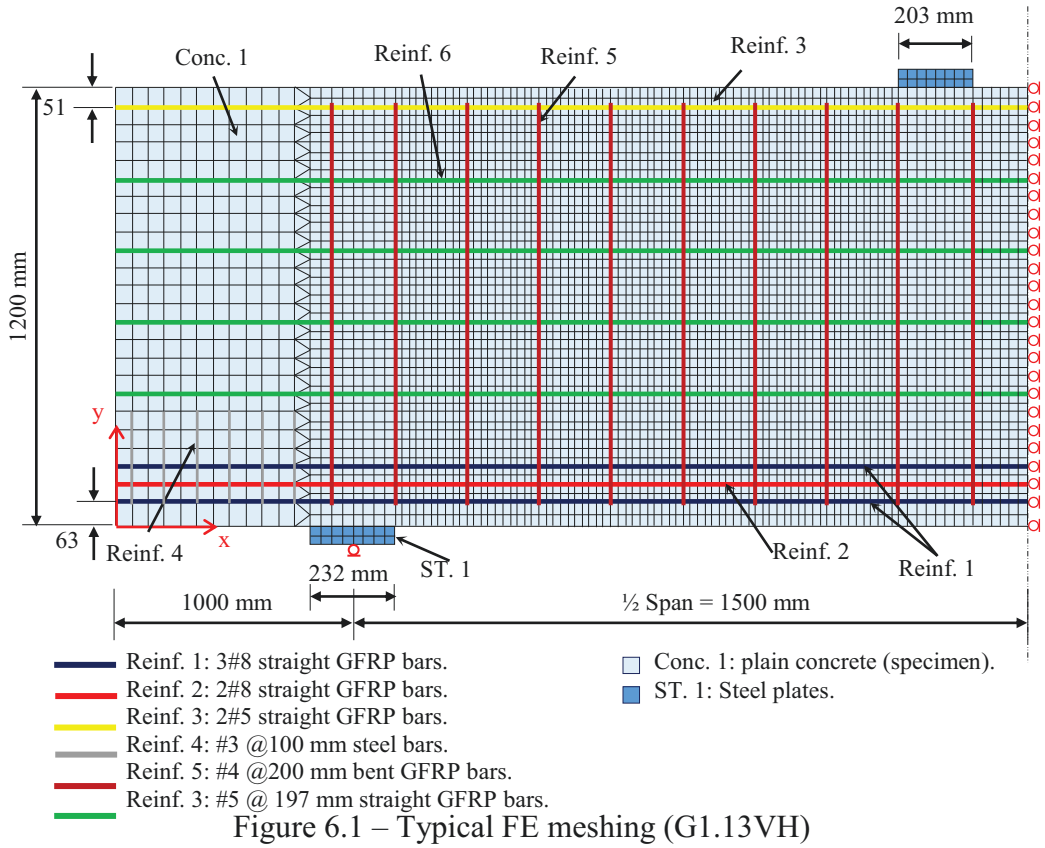

Figure 6.1 – Typical FE meshing (G1.13VH)

The dowel action of the GFRP bars was not considered as recommended by ACI 440.1R (2004), and the refined model by Dhakal-Maekawa (2002) was used for the rebar buckling of the GFRP bars. The GFRP-reinforcement hysteretic response was modeled using the linear hysteretic response proposed by Seckin (1981) as GFRP reinforcement is well known as a linear elastic stress-strain response material.

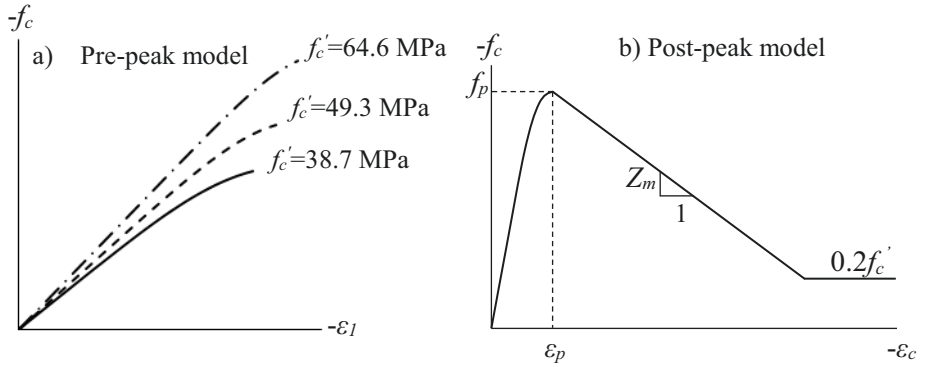

Figure 6.2 - Concrete pre- and post-peak response

6.2.2 Crack Pattern and Failure Mode

Figure 6.3 shows the comparison between the crack patterns observed during tests and predicted by the FE analysis. Similar to the experimental results, the first cracks determined by FE were flexure, followed by shear cracks, then the main diagonal crack formed above the longitudinal reinforcement, then extended to the support and loading plates. Vertical cracks at the top surface of the specimens above the reaction points were also noted in both FE prediction and during testing. These cracks were formed due to the length of the over-hanging parts beyond the supports in addition to the low compression reinforcement ratio, especially in specimens without web reinforcement. However, the width of these cracks during the tested was insignificant comparing to the results from FE.

Failure modes according to FE results were in consistent with the experimental observations, which were failure in the compression concrete strut for all simulated deep beams except for G1.13 and G1.47 where the failure mode was identified as shear failure in the FE analysis.

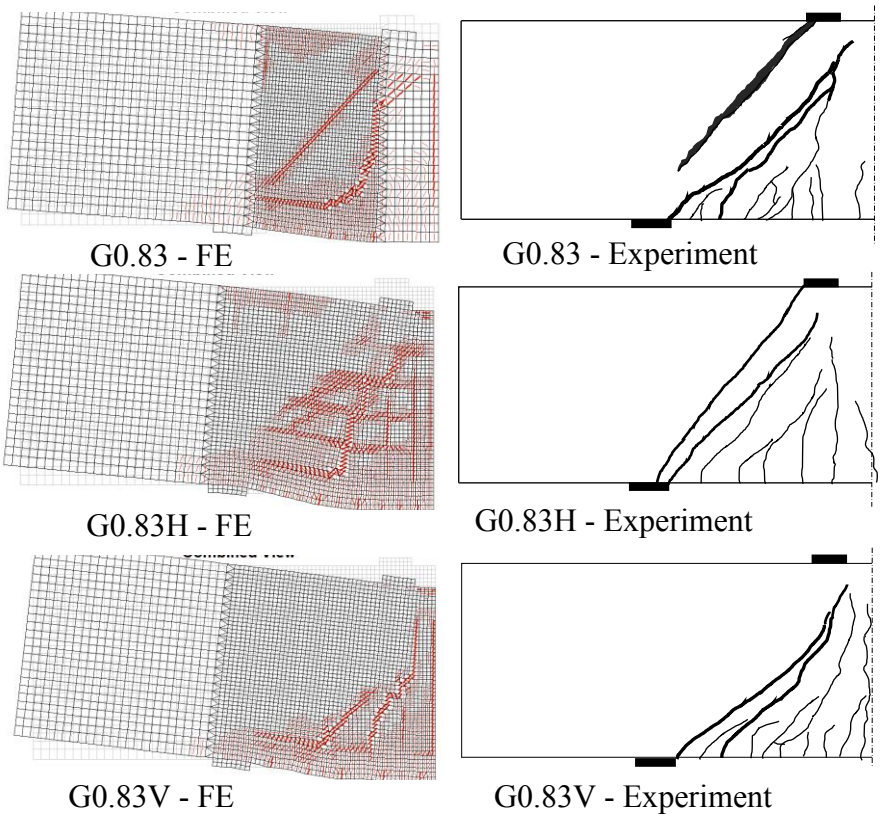

Figure 6.3 – Crack pattern and failure mode from experimental observation and FE

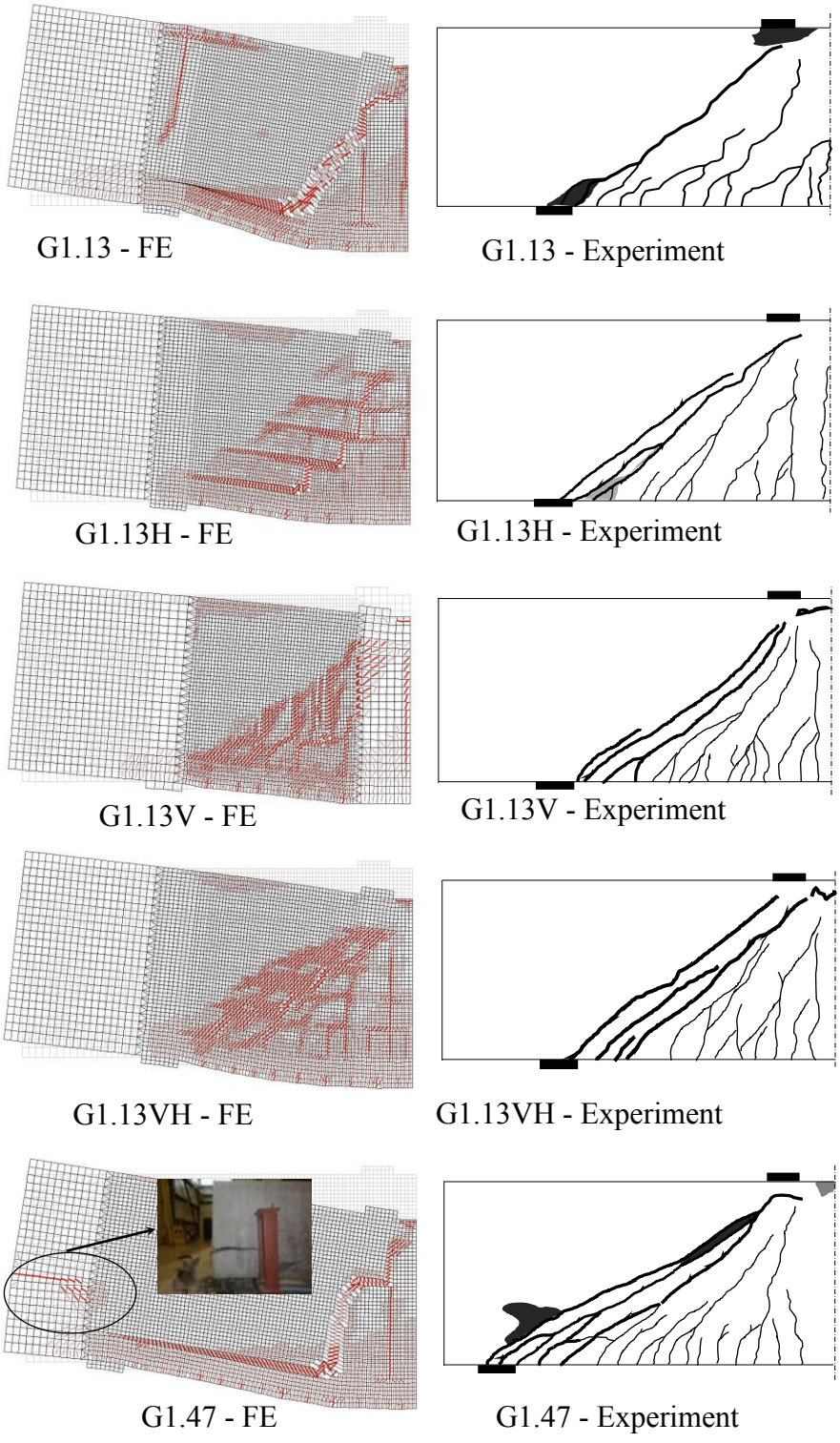

Figure 6.3 – Crack pattern and failure mode from experimental observation and FE (continued)

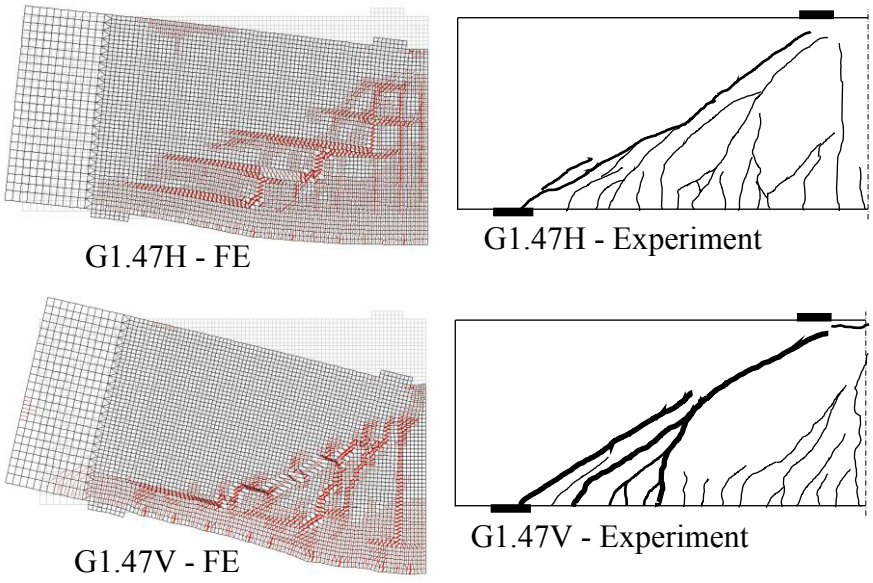

Figure 6.3 – Crack pattern and failure mode from experimental observation and FE (continued)

6.2.3 Load-Deflection Response

Figure 6.4 presents the comparison between the experimental normalized load (P_u/bdf_c')-deflection response to the FE simulation ones. Deep beams initial stiffness predicted by FE was approximately the same as that from the experimental results up to the formation of the first flexural crack. The FE was able to capture the experimental first flexure-cracking load with less than 3% difference. Afterwards, in both the experimental and FE results, stiffness of the specimens decreased with the same tendency until the formation of the main diagonal crack. At this point, the experimental results showed a small increase in deep beam stiffness due to the formation of the arch action. Although the formation of arch action was captured by the FE simulation, as will be discussed later, its formation did not show the same effect presented in the experimental results. Over all, the FE analysis could simulate the normalized load-deflection response to a certain degree of satisfaction.

The FE simulations slightly overestimated the deflection corresponding to the ultimate load and yielded conservative, but did produce acceptable predictions of ultimate load capacities

(Table 6.1) with a mean value for all simulated specimens of 1.09 with a coefficient of variation of 9%. The most accurate predictions were for specimens without web reinforcement, while specimens with web reinforcement led to more conservative predictions. These results are consistent with the findings for deep beams containing little or no web reinforcement reported by Vecchio (2000b), clarifying that the rotating crack models such as the MCFT can provide a viable and accurate method for the analysis of reinforced beams without web reinforcement that fail in shear.

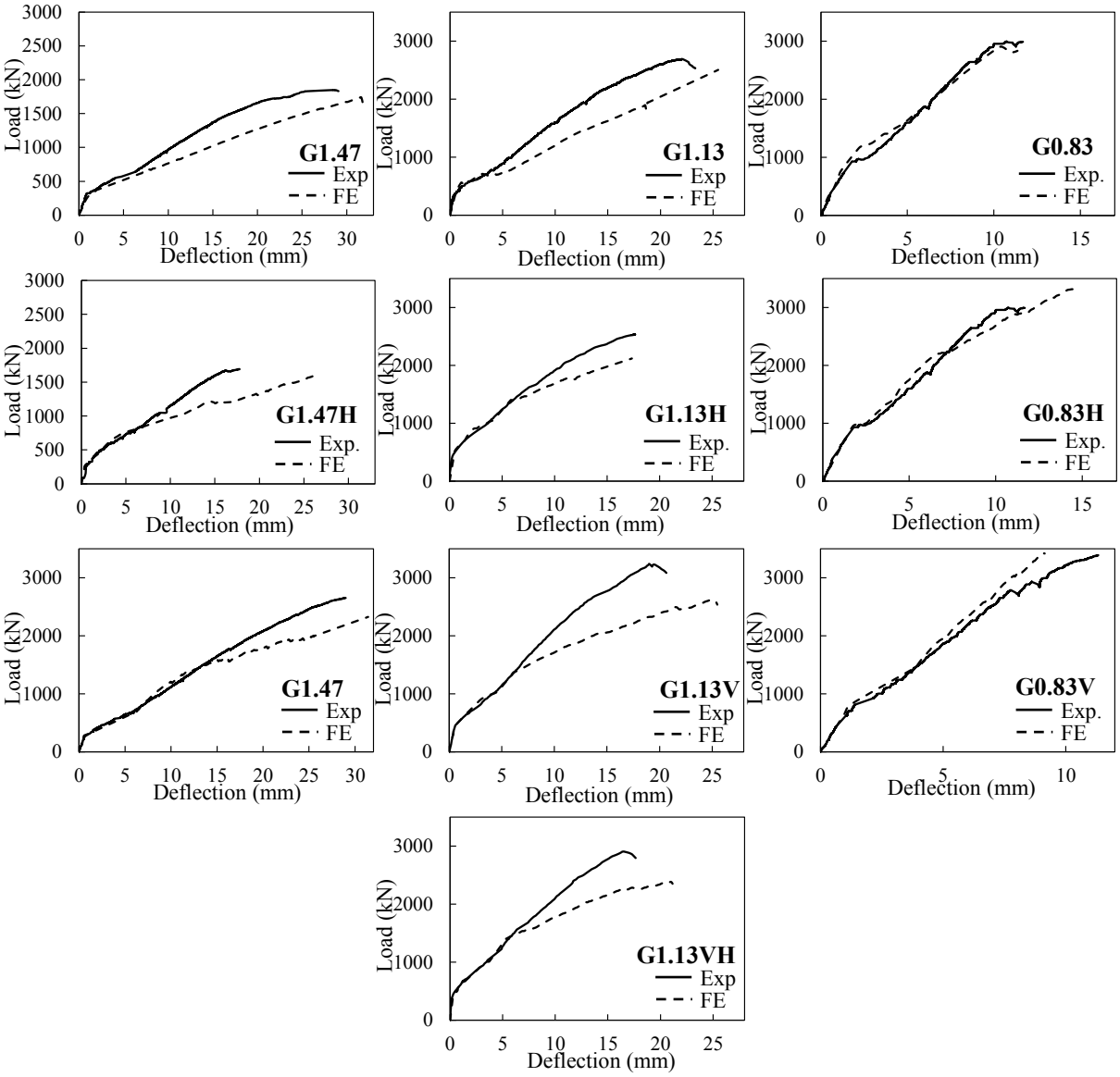

Figure 6.4 – Experimental versus FE normalized load-deflection response

It is worth mentioning that, in the experiments the closed form of the vertical bars confined the concrete zone under the loading points. This confinement effect cannot be simulated by the used 2D simulation tool (VecTor2). Therefore, the ultimate load prediction of the FE simulation for specimens with vertical web reinforcement was lower than that of the experimental results.

Table 6.1 – Capacity Prediction from FE simulation

Deep Beam ID	f_c' (MPa)	Exp.		FEM		
		P_{exp} (kN)	$P_{exp}/f_c'bd$	P_{pred} (kN)	$P_{pred}/f_c'bd$	P_{exp}/P_{pred}
G1.47	38.7	1849	0.146	1761	0.139	1.05
G1.47H	45.4	1695	0.114	1591	0.107	1.07
G1.47V	45.4	2650	0.179	2325	0.157	1.14
G1.13	37	2687	0.223	2488	0.206	1.08
G1.13H	44.6	2533	0.174	2140	0.147	1.18
G1.13V	44.6	3236	0.222	2610	0.179	1.24
G1.13VH	37	2904	0.241	2400	0.199	1.21
G0.83	38.7	3000	0.238	3125	0.247	0.96
G0.83H	43.6	3166	0.223	3314	0.233	0.96
G0.83V	43.6	3387	0.238	3456	0.242	0.98

6.2.4 Strain Levels

The reinforcement strains captured from the FE simulations were compared to the ones measured through the experimental tests for the longitudinal and web reinforcements in Figures 6.5 and 6.6, respectively. The strain distribution through the length of the longitudinal reinforcement was almost linear either for those measured from tests or captured by FE, which evidenced the formation of arch action in the numerically simulated deep beams and confirms the good agreement between the experimental and FE strain distribution (Figure 6.5). The strains in the web reinforcements (horizontal and/or vertical) were measured experimentally at the web reinforcements intersecting with the virtual diagonal line connecting the loading and support points. The stains depicted from FE analysis were taken at approximately the same locations. Figure 6.6 shows the good correlation between the experimentally measured web reinforcement strains and those predicted by the FE analysis.

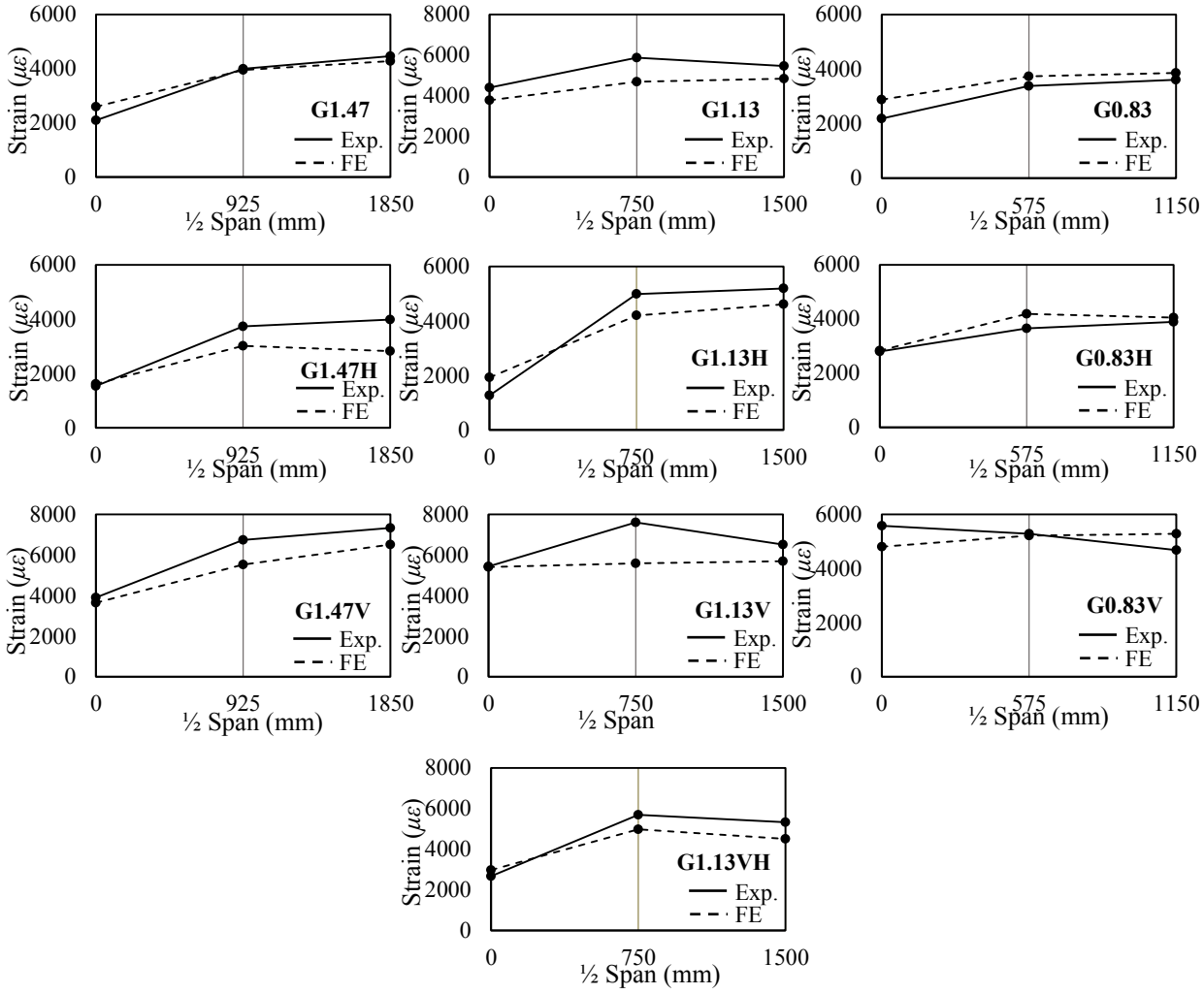

Figure 6.5 – Experimental versus FE longitudinal GFRP-reinforcement strain at ultimate

Similarly, the simulated concrete strains at the diagonal and horizontal struts were compared to the experimental ones as shown in Figures 6.7 and 6.8, respectively. The simulated strains of the diagonal strut for most cases were slightly lower than those measured experimentally due to the small diversity in location of the main diagonal crack from the experiment to the simulation (Figure 6.7). On the other hand, the simulation results of the strains of the horizontal strut showed perfect correlation with the experimental measurements as shown in Figure 6.8.

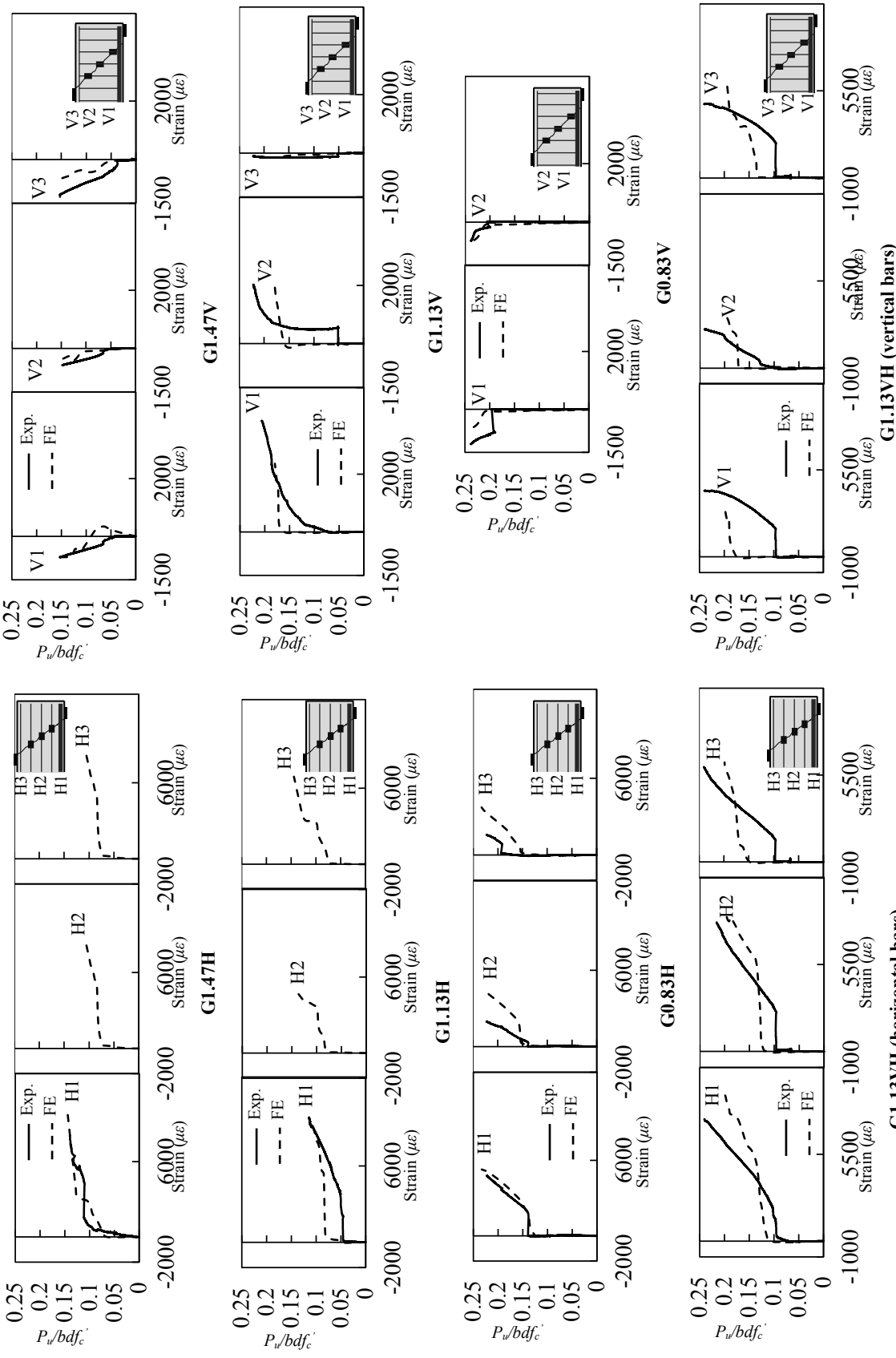

Figure 6.6 – Experimental versus FE strains at web reinforcement

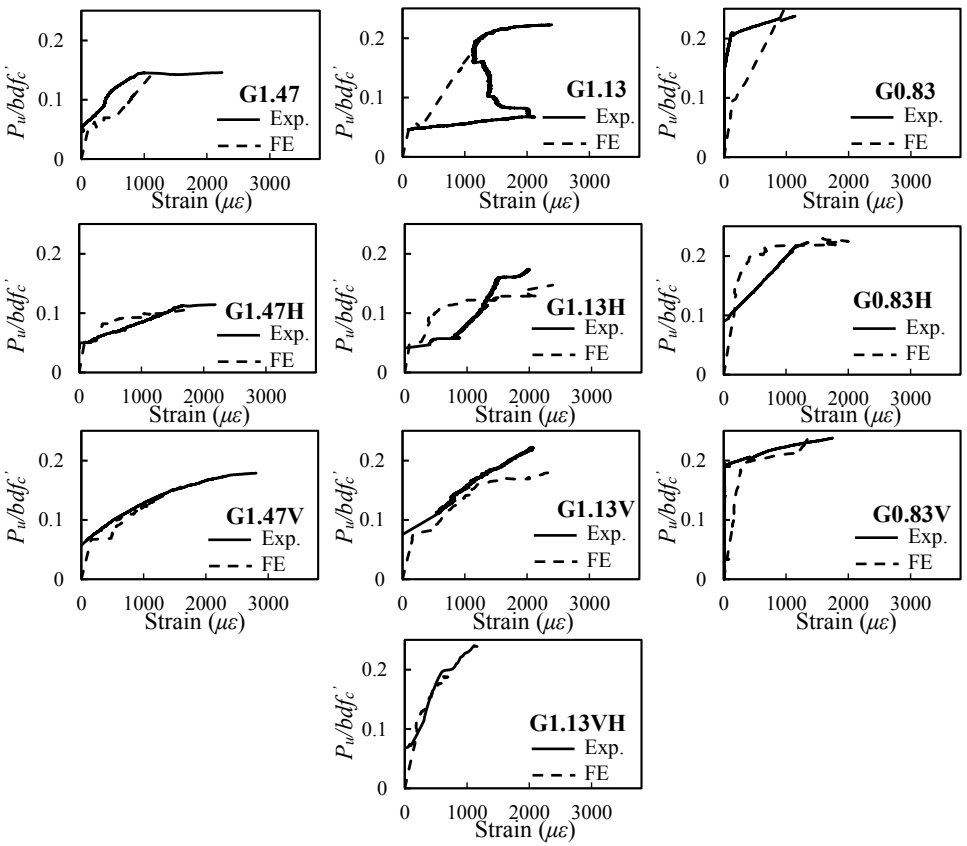

Figure 6.7 – Experimental versus FE concrete strain at the diagonal strut

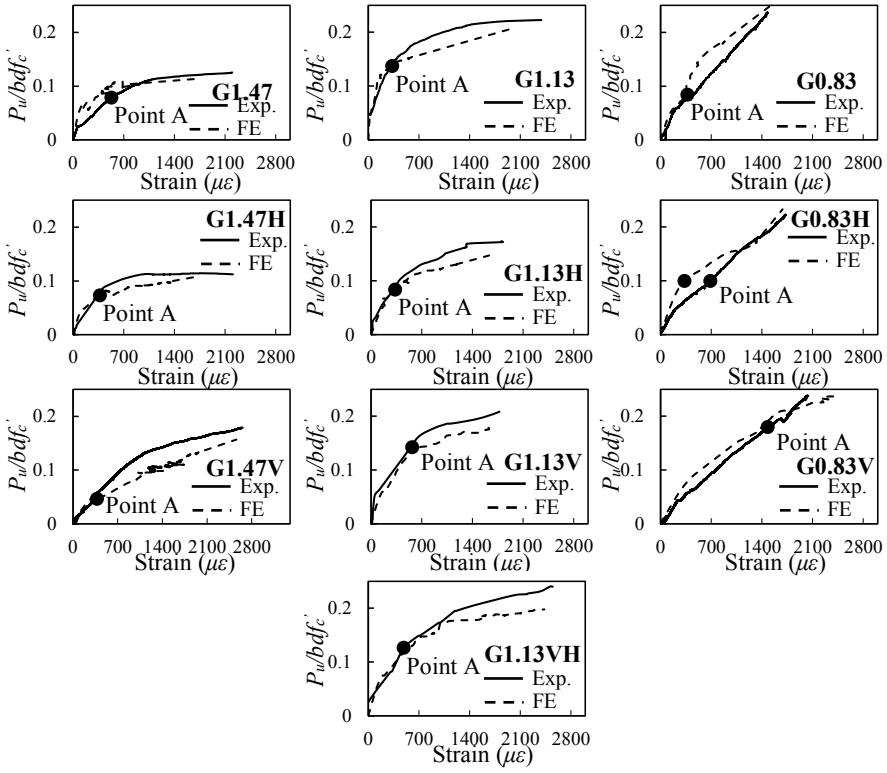

Figure 6.8 – Experimental versus FE concrete strain at the horizontal strut

6.3 Analysis Based on FE Simulation

6.3.1 Deformation Behavior of Deep Beams

Deformation of specimens was measured using two perpendicular LVDTs (horizontal and vertical) attached across the main diagonal crack to measure the horizontal and vertical relative displacements. Readings of the LVDTs are shown in Figure 6.9, in addition to the predicted relative displacements from FE modeling.

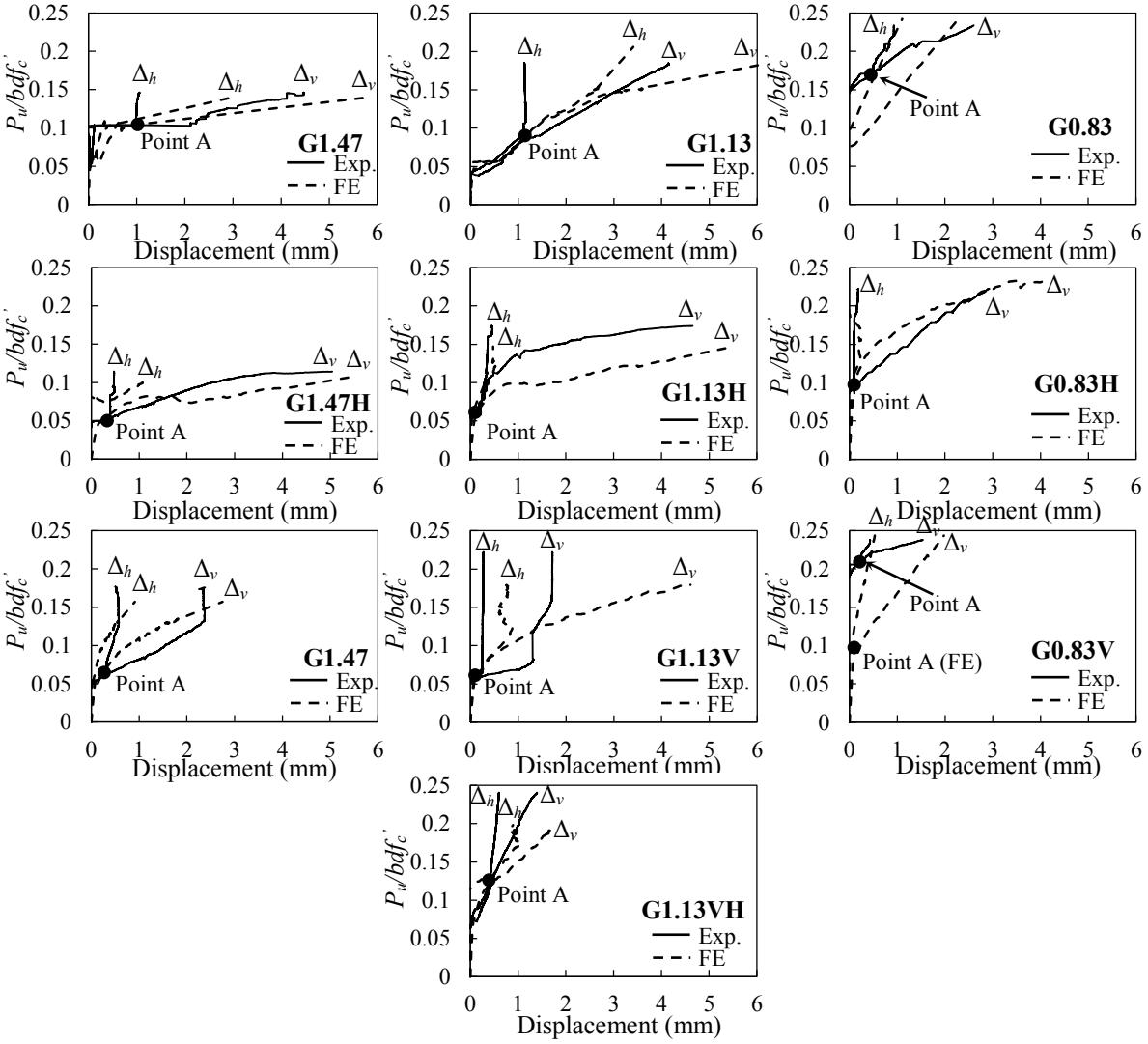

Figure 6.9 – Experimental and FE relative displacement

To discuss the observations in Figure 6.9, the failure progression of deep beams should first be discussed, as illustrated in Figure 6.10. It was observed during the testing that the main diagonal crack divided the specimens into three parts, the middle part below the loading points, and the two parts above the supports. The loading was pushing the middle part downward, while the supports were preventing the other parts from moving. Hence, two perpendicular LVDTs (horizontal and vertical) were attached across the main diagonal crack to measure the deformation of the specimens.

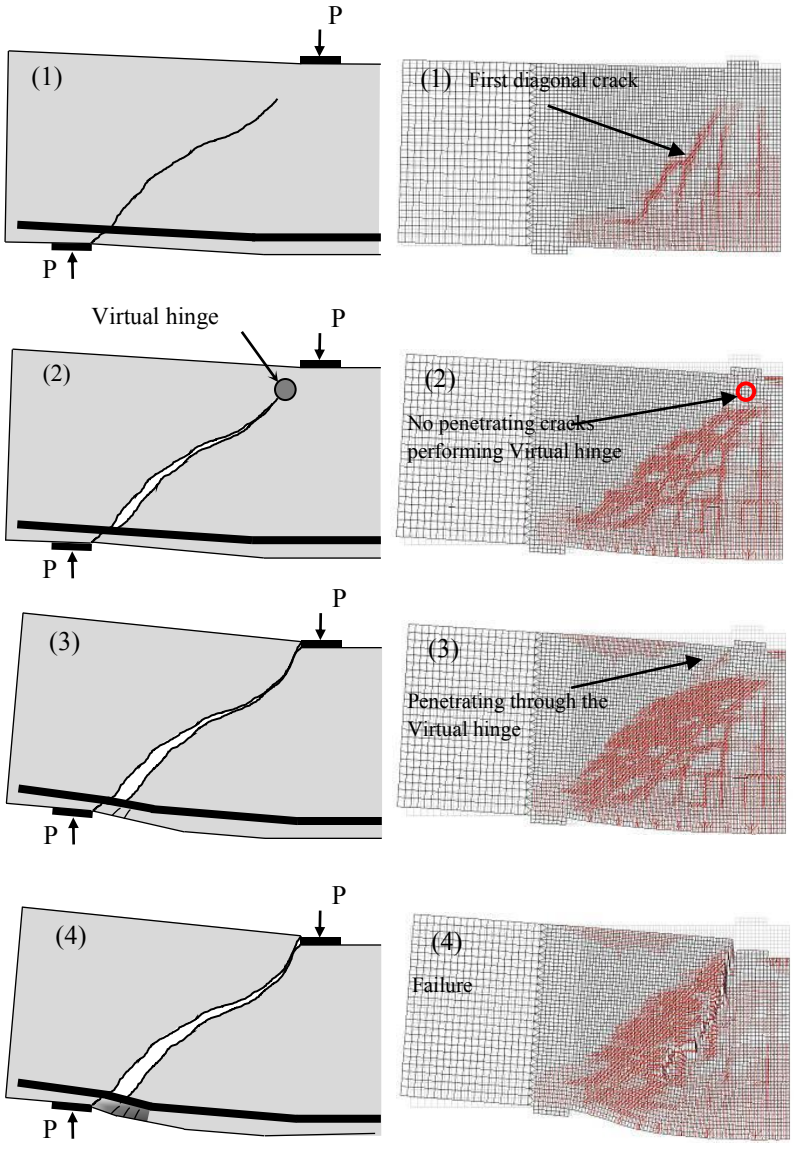

Figure 6.10 – Failure progression

As shown in Figure 6.10-a1, the main diagonal crack formed above the longitudinal reinforcement and propagated to the loading and support plates. This was observed during testing, and confirmed by the FE modeling (Figure 6.10-b1). The compressed concrete at the horizontal strut prevented the main diagonal crack from further propagating up to the loading points, which may have formed a virtual hinge above the crack (Figure 6.10-a2 and b2); this resulted in approximately the same values of horizontal and vertical relative displacements (prior to point A in Figure 6.9). Thus, it was suggested that the over-support parts were rotating around the formed virtual hinge.

With an increase the load, the main diagonal crack penetrated through the horizontal strut (Figure 6.10-a3 and b3), and damaged the virtual hinge (point A in Figure 6.9). After point A, the over-support parts stopped rotating and the loading was pushing the middle part up to failure (Figure 6.10-a4 and b4), which illustrates the constant value of the horizontal relative displacement after point A.

The formation of the virtual hinge was confirmed analytically through the strain distribution along the width of the diagonal and horizontal struts close to the loading point at load levels corresponding to; formation of the main diagonal crack, point A (crack penetrated through the virtual hinge), and ultimate load as shown in Figure 6.11. The strain distributions were determined at diagonal distances of 75, 150, 225, 300, and 375 mm from the loading point for the diagonal strut at locations 1 to 5, and at location 6 for the horizontal strut (Figure 6.11).

Figure 6.11 shows that the concrete strain at the formation of the main diagonal crack in the concrete under the loading point was less than 800 $\mu\varepsilon$ up to diagonal distance of 225mm from the loading point. This proved the uncracking of this concrete zone and the formation of a virtual hinge before reaching point A, which confirms the findings discussed in Figure 6.10-a2 and 6.10-b2. With further load increase, relative horizontal and vertical displacements were generated due to the load-induced deformations as the over-support part rotated around the formed virtual hinge. It is essential to mention that, the strain level of the diagonal strut at load level corresponding to formation of the first diagonal crack was reaching more than 1400 $\mu\varepsilon$ with the increasing of the diagonal distance from the loading point of more than 300 mm. This indicates a cracked concrete at this distance as shown in Figure 6.10-a2 and 6.10-b2.

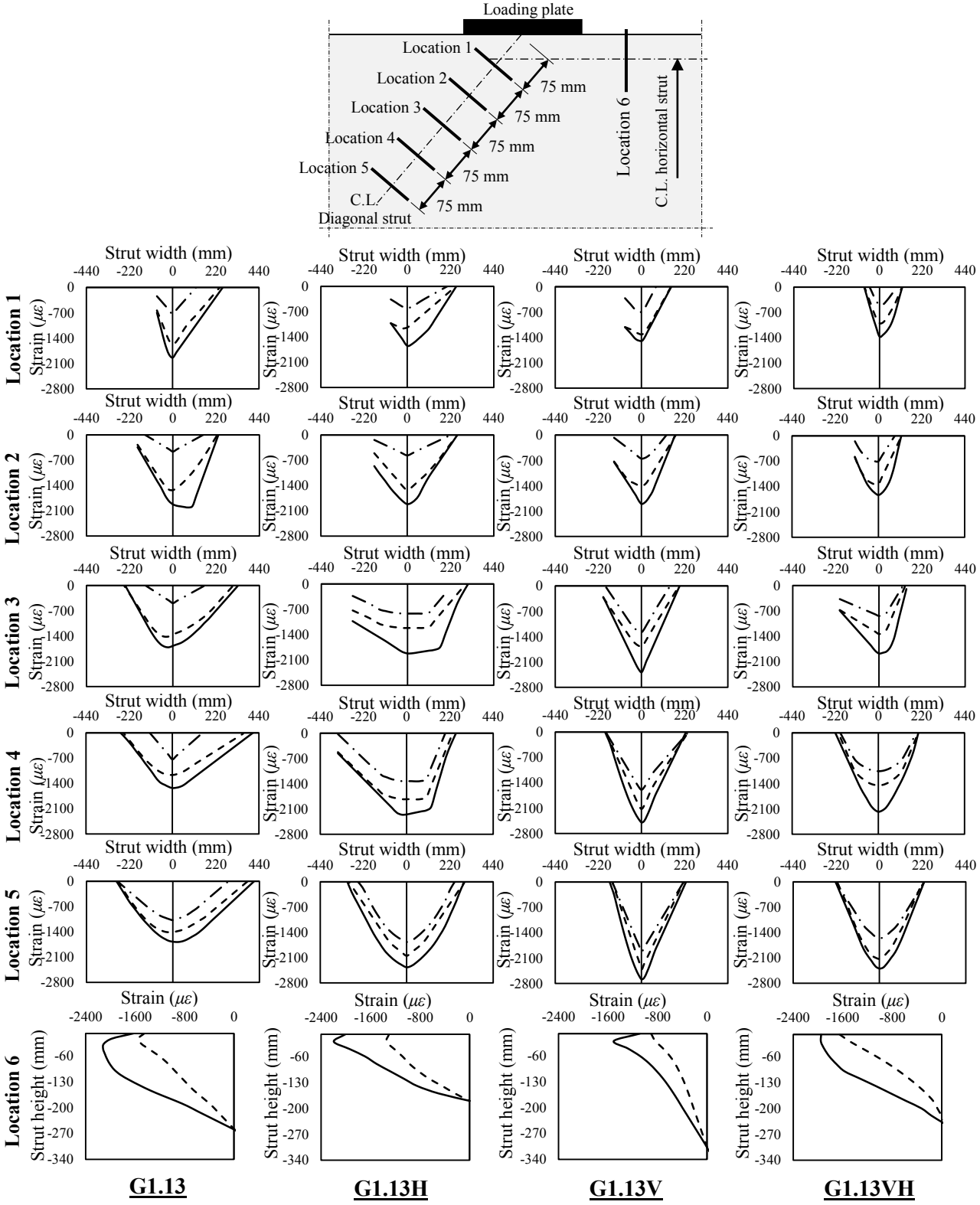

Figure 6.11 – Concrete strain distribution around the virtual hinge

The concrete strain at point A reached more than 70% of the concrete strain of the ultimate load (Figure 6.11), indicating deteriorated concrete at this load level, which confirms the findings discussed in Figure 6.10-a3 and b3. The penetration through the virtual hinge (concrete deterioration) promptly increased not only the concrete strain in the diagonal strut but also in the horizontal strut as well. Additionally, the strain distribution width (can reflect the strut width) increased after the formation of the main diagonal crack, and became constant after point A. It is worth mentioning that, the presence of horizontal and/or vertical web reinforcement did not affect the strain values either at different load levels or at different distance from the loading point. However, it clearly reduced the width of the inclined and horizontal struts.

6.3.2 Effect of Web Reinforcement on Ultimate Capacity

Table 6.1 shows that the presence of vertical web reinforcement did not increase significantly the normalized ultimate load over no-web reinforced deep beams either in the experimental or FE simulation results. Moreover, the FE simulation resulted in the same experimental findings that the deep beams with horizontal-only web reinforcement had their normalized ultimate load decreased compared to the deep beams without web reinforcement. This unexpected behavior was observed also for the steel-reinforced deep beams with horizontal-only web reinforcement tested by Brown and Bayrak (2007), illustrating this to the experimental scatter. The FE simulation was used to further understand this behavior.

Experimental results indicated that the normalized ultimate load of specimens with horizontal-only web reinforcement for G1.47H, G1.13H, and G0.83H decreased by 22%, 21%, and 6%, when compared to G1.47, G1.13, and G0.83, respectively. This reduce in the normalized load was also captured by the FE simulation. Since failure of specimens was due to crushing in the concrete diagonal strut, this reduction could be attributed to the concrete softening.

Concrete softening was explained by Vecchio and Collins (1986), as the principal compressive stress in the concrete diagonal strut is a function of the principal compressive strains in addition to the existing principal tensile strain in the perpendicular bars. Therefore, the high strains in the horizontal bars (Figure 6.7) perpendicular to the direction of the concrete strut softened the concrete around the bars and reduced the concrete strain at the diagonal strut

(Figure 6.6). As a result, concrete surrounding the horizontal web reinforcement exhibited excessive cracks when compared to other specimens, as noticed in the crack pattern predicted by FE simulation (Figure 6.3).

The measured the vertical bars strains in Figure 6.6 was localized at the center of the strut; hence, the compression forces in the diagonal strut exposed the vertical bars to compressive strains. However, failure of all specimens with vertical bars was associated with rupture of the bent portion of the vertical bar, indicating high tensile stresses in portions outside the diagonal strut. This observation was confirmed through the FE simulation, as the captured strains in the vertical bars above the diagonal strut were indicating high tensile strains as shown in Figure 6.12 compared to those captured at the center of the diagonal strut (Figure 6.6) causing the softening of the concrete at this zone.

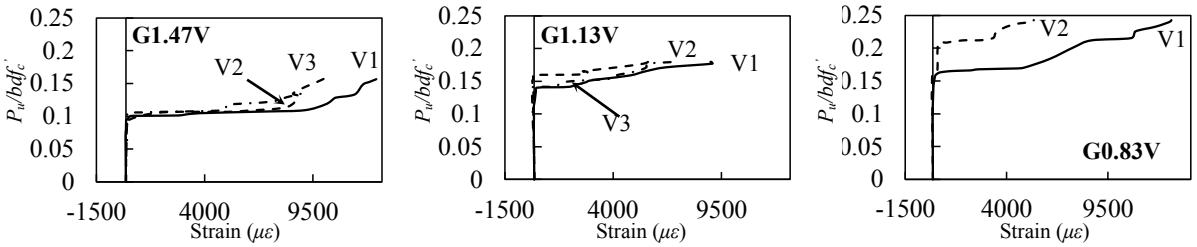

Figure 6.12 – Strains at vertical web reinforcement outside diagonal strut (from FE modeling)

6.4 Conclusions

A finite element investigation was conducted to simulate the behavior of ten full-scale deep beams reinforced with GFRP bars. On the basis of the analytical study, the following conclusion can be drawn:

1. The FE simulation adequately predicted the response of the tested GFRP-reinforced deep beams regarding the crack progression, failure mode, strains in the reinforcement and concrete, and load-deflection response.

2. The FE simulation was not be able to capture the confinement effect of the closed stirrups of the vertical web reinforcement due to the limitation of the 2D simulation program

(VecTor2). However, the simulation still resulted in an acceptable level of accuracy comparing to the experimental results.

3. The experimental hypothesis of the formation of virtual hinge was confirmed through the FE conducted investigation. This was observed for all specimens regardless of the web reinforcement configuration.

4. High values of concrete strains surrounding the horizontal bars captured from the FE analysis showed the concrete deterioration behavior resulted in the negative effect of the horizontal-only web reinforced on the strength of the GFRP-reinforced deep beams.

5. Using the FE simulation tool enabled capturing strain values at certain locations that would not have been able to be examined based on the experimental results; this confirms the uncertainties regarding the failure mechanism hypotheses of FRP-reinforced deep beams.

CHAPTER 7
CONCLUSIONS AND RECOMMENDATIONS

7.1 General Conclusion

The main objective of the current research was to induce constructing concrete deep beams entirely reinforced with FRP bars, to overcome steel-corrosion problems, and to examine the use of the STM for predicting the capacity of FRP-reinforced deep beams. Ten full-scale FRP-reinforced deep beams were tested to failure under two-point loading to achieve the objective of this study. The test variables were chosen to examine the effect of the a/d ratio, and different configurations of web reinforcement. Strength, deformation and serviceability of the tested specimens were investigated. The development of arch action was confirmed by the crack propagation and an almost linear strain distribution in the main longitudinal reinforcement, in addition to the typical failure mode of crushing in the concrete diagonal strut. A strut-and-tie-based model was presented to calculate the efficiency factor of the strut identifying the parameters affecting the strength of the deep beam. The proposed model was evaluated against the tested deep beams as well as the available test results in the literature. Based on the current results and analysis, the following conclusions can be drawn:

- Failure of all tested specimens was preceded by crushing in the diagonal compression strut, which is the typical failure of deep beams. Failure of specimens with horizontal-only web reinforcement was relatively less brittle than other specimens, and of specimens with vertical web reinforcement was associated with rupture at the bent portion of the vertical bar crossing the strut.
- Vertical web reinforcement, whether with or without horizontal web reinforcement, is not required for strength purposes, as it had no significant effect on the initial flexure load, first shear cracking load, diagonal cracking load, and ultimate load (the highest effect was the increase of the normalized ultimate capacity of G1.47V by less than 18% compared to G1.47).

- Horizontal-only web reinforcement was found to be undesirable to be used in FRP-reinforced deep beams, as it had negative effect on the ultimate capacity of the tested deep beams. This unexpected capacity reduction was investigated, leading to the assumption that the concrete softening due to the high strain in the horizontal bars deteriorated the concrete at the diagonal strut.
- Combining horizontal web reinforcement with vertical bars in G1.13VH can mitigate the negative effect of using horizontal-only web reinforcement on the ultimate capacity, however, with insignificant increase in the normalized ultimate capacity compared to specimens without web reinforcement (the increase in strength was less than 9%).
- The development of arch action coincided with the formation of the main diagonal crack, indicting the redistribution of the internal stresses. The development of the arch action was confirmed by measuring similar strains at different locations on the main longitudinal reinforcement (tie reinforcement)
- The strut-and-tie model (STM) can be used to predict the strain of the main longitudinal reinforcement with an experimental-to-predicted mean value for the tested specimens of 0.90 and CoV of 9%. This indicates that the tested specimens exhibited the deformation capacity required to satisfy equilibrium without violating the failure criteria at any point, which provides the lower-bound estimated capacity, and confirming the applicability of STM.
- It is recommended to use web reinforcement (vertical-only or vertical and horizontal) to control the crack width (serviceability requirement) of the GFRP-reinforced deep beams. The vertical web reinforcement is more effective in resisting the crack width than the horizontal web reinforcement at ultimate load.
- At assumed service load of 30% of the ultimate load, all configurations of web reinforcement satisfied a crack width limit of 0.5 mm specified by ACI 440.1R (2006) and CSA S806 (2012), while all specimens without web reinforcement exceeded this limit.
- The horizontal-only web reinforcement provided greater crack-width control than the vertical-only web reinforcement at service load. Another benefit of using horizontal web reinforcement that the horizontal bars contributed, along with the longitudinal reinforcement, in resisting the tensile strains in arch action.

- Although the web reinforcement in GFRP-reinforced deep beams was found to be not required for strength, it is recommended to include minimum web reinforcement in structures at which the response is dominated by shear, even in cases where serviceability concerns are not crucial. This is prudent to restrain unaccounted actions during the design process, such as the effect of temperature and shrinkage. It is recommended to provide the amount of web reinforcement specified by ACI 318 (2014) and CSA S806 (2012) as a guide, until further research for the appropriate amount of FRP web reinforcement is conducted.
- Applying the STM in accordance to ACI 318 (2014) gives overestimated and arbitrary predictions of the ultimate capacity of the FRP-reinforced deep beams with mean value of 0.81 and CoV of 34%. Furthermore, the STM provided by CSA S806 (2012) could lead to uneconomically conservative estimations for the ultimate capacity with mean value of 1.89 and CoV of 26%.
- Other employed strut-and-tie-based models for steel-reinforced deep beams are not recommended to estimate the capacity of the FRP-reinforced deep beams with different level of safety and conservatism depending on the applied model.
- The strut efficiency factor is a function of the concrete compressive strength (f_c'), shear span-depth ratio (a/d), and strain of longitudinal reinforcement (ε_1), with insignificant web reinforcement effect. However, ACI 318 (2014) does not account for any of these parameters except for the web reinforcement; and CSA S806 (2012) overestimate the effect of f_c' and ε_1.
- It is recommended to use the one-panel truss model solution for FRP-reinforced deep beams as it can produce acceptable levels of conservatism. The one-panel solution was the appropriate model for all specimens except for four specimens with vertical web reinforcement. This was confirmed applying strain energy concept to identify the development of either one-panel or two-panel truss model.
- A new model for the strut efficiency factor was proposed based on the parameters affecting the strength of the strut. The model was compared against the available FRP-reinforced deep beams (28 specimens) in addition to the steel-reinforced deep beams (172

specimens). The proposed model produced safe estimation for the capacity prediction, with acceptable level of conservatism.

- Finite element (FE) investigation was conducted to simulate the behavior of the tested deep beams and adequately predicted their response in terms of crack progression, failure mode, strains in the reinforcement and concrete, and load-deflection response.
- Using the FE simulation tool enabled capturing strain values at certain location that would not been able to be examined based on the experimental results, which confirms uncertainty regarding the failure mechanism hypothesis of FRP-reinforced deep beams.
- The experimental hypothesis of the forming of virtual hinge was confirmed through the FE conducted simulation. This was accomplished by determining the concrete strains near the loading zone corresponding to the formation of the main diagonal crack, which proved the uncracked concrete at this zone. The presence of web reinforcement had no effect on the formation of the virtual hinge.
- The FE simulation was used also to confirm the high strains in the vertical web reinforcement outside the diagonal strut, which resulted in the rupture of the bent portion of the vertical bars noticed during tests. The FE analysis showed the concrete deterioration behavior resulted in the negative effect of the horizontal-only web reinforced on the strength of the GFRP-reinforced deep beams.

7.2 Recommendations for Future Work

Results of the current study consider a promising step toward implementing FRP bars as only reinforcement in deep beams, and applying strut-and-tie model for analyzing FRP-reinforced elements. Additional research is recommended based on the findings of the current study to cover the following points:

- Web reinforcement amounts used in this study were chosen based on the recommendation of CSA S806 (2012). However, there is no experimental evidence to support the relatively large amount of web reinforcement specified by CSA S806 (2012), except the fact that FRP-reinforced slender-beams exhibit more and wider cracks that that in steel-reinforced slender-beams. Moreover, the excessive amounts of web reinforcement are not required to increase the strength of the diagonal strut.

Therefore, the amount of web reinforcement needs to be assessed, in order to estimate the optimum amount of web reinforcement required in FRP-reinforced deep beams to control the crack width.

- The use of STM was implemented to predict the capacity of FRP-reinforced deep beams. One of the primary advantages of STM is its widespread applicability in cases where the flexure theory and section-based design approaches are not valid. It is not known, however, whether the STM is applicable for more complex disturbed regions that containing FRP reinforcement. Therefore, it is recommended to examine the applicability of STM for other FRP-reinforced elements, such as coupling beams, squat-wall, beam-column connections and pile caps.

- To apply the STM to a structure, sufficient deformation is required to redistribute the internal forces and form the arch action. The STM was applied to steel-reinforced structures; presuming that the structures sustained sufficient deformations required to apply the lower-bound theorem. The term "sufficient deformation" was widely used among researchers, yet, has not been quantified. The use of other reinforcing materials rather than steel reinforcement rises the importance of quantifying the sufficient deformation, to identify the limitation of employing STM to a structure. Hence, additional research is required to determine the deformation capacity required by the lower-bound theorem to apply a STM.

- Numerous research studies have been conducted on relatively small-sized deep beams (less than 500 mm in depth), presuming that testing small-sized specimens would possess the same mechanism as the real deep beams in practice. However, maintaining dimensional accuracy in concrete geometry, reinforcing bars' details, and loading conditions in highly scaled tests should be considered. In addition, relatively small-sized specimens would not allow for the redistribution of the internal forces and the formation of the arch action due to the size limitations. The transition from small-sized deep beams to larger ones needs further investigation. Therefore, it is of interest to elaborate over this issue by studying the size effect on the behavior and mechanism of reinforced concrete deep beams.

- One further step is to examine the resisting mechanism of FRP-reinforced deep beams subjected to reversed cyclic loads. This issue is relevant to ensure adequate design of FRP-reinforced deep beams located in seismic zones, especially if the similarity between the load-bearing mechanisms under reversed cyclic loads in deep beams and those in other slender-beams is recognized. Finally, the experimental testing for continuous FRP-reinforced deep beams is of significant importance.

7.3 Conclusion

L'objectif principal de la présente recherche était d'induire la construction de poutres profondes en béton entièrement renforcées de barres en PRF, pour surmonter les problèmes de corrosion de l'acier, et d'examiner l'utilisation de MBT pour prédire la capacité des poutres profondes renforcées de PRF. Dix poutres profondes à grande échelle renforcée de PRF ont été testées jusqu'à la rupture sous un chargement en deux points pour atteindre l'objectif de cette étude. Les variables d'essais ont été choisies afin d'examiner l'effet du ratio *(a/d*), et différentes configurations de renforcement de l'âme. La résistance et la déformation des spécimens testés ont été étudiées. Le développement de l'effet d'arche a été confirmé par la propagation de fissures et de la distribution quasi linéaire des déformations dans le renforcement longitudinal principal, en plus du mode de rupture typique de l'écrasement du béton dans le mât diagonal. Un modèle par bielles et tirants a été présenté pour calculer le facteur d'efficacité de la bielle identifiant les paramètres affectant la solidité de la poutre profonde. Le modèle proposé a été évalué par rapport à l'essai des poutres profondes ainsi que des résultats de tests disponibles dans la littérature. Basées sur les résultats actuels et l'analyse, les conclusions suivantes peuvent être tirées :

- La rupture de tous les spécimens testés a été précédée par écrasement dans la bielle oblique de compression, ce qui est typique pour les poutres profondes. La rupture des spécimens avec un renforcement uniquement horizontal dans l'âme a été relativement moins fragile que d'autres spécimens, et des spécimens avec renforcement vertical dans l'âme ont été associés à la rupture dans la partie courbe de la barre verticale traversant la bielle.

- Le renforcement vertical dans l'âme, avec ou sans renforcement horizontal, n'est pas requis pour augmenter la résistance, car il n'a eu aucun effet significatif sur la charge en flexion initiale, la charge pour la première fissure en cisaillement, la charge de fissuration diagonale, et de la charge ultime (la plus forte incidence a été l'augmentation de la capacité ultime normalisée de G1.47V par moins de 18 % par rapport à G1.47).
- Les renforcements uniquement horizontaux dans l'âme ont été jugés peu souhaitables pour être utilisés dans des poutres profondes renforcées de PRF, comme elles avaient un effet négatif sur la capacité ultime des poutres profondes testées. Cette réduction de capacités imprévue a été étudiée, conduisant à l'hypothèse que l'adoucissement du béton en raison de la déformation élevée dans les barres horizontales détériorait le béton à la bielle oblique.
- Une combinaison du renforcement horizontal dans l'âme avec des barres verticales dans G1.13 VH peut atténuer l'effet négatif, de l'utilisation seule des barres horizontales, sur la capacité ultime, cependant, avec une augmentation insignifiante dans la capacité ultime normalisée par rapport aux spécimens sans renforcement dans l'âme (l'augmentation de la résistance était inférieure à 9 %).
- Le développement de l'effet d'arche coïncide avec la formation de la fissure en diagonale principale, indiquant la redistribution des contraintes internes. Le développement de l'effet d'arche a été confirmé par la mesure de déformations analogues à différents endroits sur le renforcement longitudinal principal (renforcement dans le tirant).
- Un modèle par bielles et tirant (MBT) peut être utilisé pour prédire les déformations du renforcement longitudinal principal avec des données expérimentales/prédites pour les spécimens examinés avec une moyenne de 0,90 et un coefficient de variation (CV) de 9 %. Ceci indique que les spécimens d'essais ont exhibé une capacité de déformation nécessaire pour satisfaire l'équilibre sans violer les critères de défaillance en tout point, ce qui fournit une capacité estimée de limite inférieure, et confirmant l'applicabilité d'un MBT.

- Il est recommandé d'utiliser un renforcement dans l'âme (uniquement vertical ou horizontal et vertical) pour contrôler la largeur de fissuration (exigence d'utilisation) pour les poutres profondes renforcées de polymère renforcé de fibres de verre (PRFV). Le renforcement vertical de l'âme est plus efficace pour résister à l'augmentation de la largeur de fissuration que le renforcement horizontal de l'âme lorsque la charge ultime est appliquée.
- À une charge d'utilisation supposée équivalant à 30 % de la charge ultime, toute configuration de renforcement de l'âme satisfait une limite de largeurs de fissuration de 0,5 mm spécifié par l'ACI 440.1R (2006) et la norme CSA S806 (2012), alors que tous les spécimens sans renforcement de l'âme dépassaient cette limite.
- Le renforcement uniquement horizontal de l'âme fournit un contrôle plus grand de la largeur de fissuration que le renforcement uniquement vertical de l'âme pour la charge d'utilisation. Un autre avantage de l'utilisation de renforcement horizontal de l'âme est que les barres horizontales contribuent, avec le renforcement longitudinal, à la résistance aux contraintes de traction dans l'effet arche.
- Bien que le renforcement de l'âme dans les poutres profondes renforcées de PRFV soit jugé non nécessaire pour la résistance, il est recommandé d'inclure un minimum de renforcement de l'âme dans les structures auxquelles la réponse est dominée par le cisaillement, même dans les cas où les préoccupations d'utilisation ne sont pas essentielles. Il est prudent de limiter les actions non comptabilisées au cours du processus de conception, telles que l'effet de la température et le rétrécissement. Il est recommandé de fournir la quantité de renforcement de l'âme spécifiée par l'ACI 318 (2014) et la norme CSA S806 (2012) comme un guide, jusqu'à ce que davantage de recherche pour la quantité appropriée de renforcement de l'âme avec des PRF soit menée.
- L'application d'un MBT conformément à l'ACI 318 (2014) donne une prédiction surestimée et arbitraire de la capacité ultime des poutres profondes renforcées en PRF avec une valeur moyenne de 0,81 et un CV de 34 %. En outre, le MBT fourni par la norme CSA S806 (2012) pourrait conduire à une estimation prudente et conservatrice pour la capacité ultime avec valeur moyenne de 1.26 et un CV de 26 %.

- D'autres modèles de bielles et tirant pour les poutres profondes renforcées d'acier ne sont pas recommandés pour l'estimation de la capacité de poutres profondes renforcées de PRF avec différents niveaux de sécurité et de conservatisme selon le modèle appliqué.
- Le facteur d'efficacité de la bielle est fonction de la résistance en compression du béton (fc'), le ratio de cisaillement portée-profondeur (a/d), et la déformation de l'armature longitudinale (ε_l), avec un effet insignifiant dû au renforcement de l'âme. Toutefois, l'ACI 318 (2014) ne tient compte d'aucun de ces paramètres sauf pour le renforcement de l'âme et la norme CSA S806 (2012) surestime l'effet de fc' et ε_l.
- Il est recommandé d'utiliser comme solution le modèle de treillis avec un panneau pour les poutres profondes renforcées en PRF comme il peut produire un niveau acceptable de conservatisme. Cette solution était le modèle approprié pour tous les échantillons, à l'exception de quatre spécimens avec un renforcement vertical de l'âme. Cela a été confirmé en appliquant le concept de l'énergie de déformation pour identifier le développement d'un modèle de treillis avec un ou deux panneaux.
- Un nouveau modèle pour facteur d'efficacité de la bielle a été proposé en se basant sur les paramètres affectant la solidité de la bielle. Le modèle a été comparé aux poutres profondes renforcées en PRF (28 spécimens) disponible en plus des poutres profondes renforcées en acier (172 spécimens). Le modèle proposé produit une estimation sécuritaire pour la prédiction de la capacité avec un niveau acceptable de conservatisme.
- Une étude par éléments finis (EF) a été menée pour simuler le comportement de poutres profondes testées et prédire adéquatement leur réponse en termes de fissuration, le mode de rupture, la progression des déformations dans le renforcement et le béton, et la réponse de la flèche en fonction de la charge.
- L'utilisation de l'outil de simulation par EF a permis l'étude des valeurs de déformations à certains endroits qu'y n'aurait pas pu être examinée sur la base des résultats expérimentaux, ce qui a confirmé certaine incertitude concernant l'hypothèse sur le mécanisme de rupture des poutres profondes renforcées de PRF.

- L'hypothèse expérimentale de la formation de charnière virtuelle a été confirmée par les simulations par EF. Cela a été accompli par la détermination de la déformation du béton près de la zone de chargement correspondant à la formation de la fissure diagonale principale, ce qui a prouvé le béton non fissuré à cette zone. La présence de renforcement dans l'âme n'a eu aucun effet sur la formation de la charnière virtuel.

Les simulations par EF ont été utilisées également pour confirmer les déformations élevées dans le renforcement vertical de l'âme à l'extérieur de la bielle oblique, ce qui s'est traduit par la rupture de la partie courbe des barres verticales remarquée pendant les tests. L'analyse des simulations par EF a montré que le comportement de la détérioration du béton a entraîné l'effet négatif, du renforcement uniquement horizontal de l'âme, sur la résistance des poutres profondes renforcées en PRF.

7.4 Recommandations pour des travaux futurs

Les résultats de l'étude actuelle envisagent une étape prometteuse vers la mise en œuvre de barres en PRF comme armature unique dans les poutres profondes, et l'application de modèle par bielles et tirants pour analyser les éléments renforcés de PRF. Des recherches supplémentaires sont recommandées en se basant sur les conclusions de l'étude en cours pour couvrir les points suivants :

- Les quantités de renforcement dans l'âme utilisées dans cette étude ont été choisies en fonction de la recommandation de la norme CSA S806 (2012). Toutefois, il n'y a aucune preuve expérimentale à l'appui pour les quantités relativement grandes spécifiées par la norme CSA S806 (2012), sauf le fait que les poutres minces renforcées en PRF montrent plus de fissures et des fissures plus larges pour les poutres minces renforcées en acier. En outre, les quantités excessives de renforcement dans l'âme ne sont pas nécessaires pour augmenter la résistance de la bielle oblique. Par conséquent, la quantité de renforcement dans l'âme doit être évaluée, afin d'estimer la quantité optimale de renforcement dans l'âme requise dans les poutres profondes renforcées en PRF pour contrôler la largeur des fissurations.

- L'utilisation d'un MBT a été mise en œuvre afin de prédire la capacité des poutres profondes renforcées en PRF. L'un des principaux avantages des MBT est sa grande applicabilité dans les cas où la théorie de flexion et l'approche par conception basée sur les sections ne sont pas valides. On ne sait toutefois pas si le MBT est applicable pour les régions plus complexes perturbées qui contiennent des barres d'armature en PRF. Par conséquent, il est recommandé d'examiner l'applicabilité des MBT pour d'autres éléments renforcés de PRF, tels que les poutres de couplage, les murs de faible hauteur, les connexions poutre-colonne et les chapeaux de pieux.
- Pour appliquer les MBT à une structure, une déformation suffisante est nécessaire afin de redistribuer les forces internes et former l'effet d'arche. Le MBT a été appliqué à des structures renforcées en acier ; présumant que ces structures soutiennent des déformations suffisantes nécessaires pour appliquer le théorème des limites inférieures. Le terme <<déformation suffisante>> était largement utilisé entre les chercheurs, mais n'a pas été quantifié. L'utilisation d'autres matériaux de renforcement plutôt que le renforcement en acier augmente l'importance de quantifier la déformation suffisante, afin d'identifier la limitation de l'emploi de MBT pour une structure. Par conséquent, des recherches supplémentaires sont nécessaires pour déterminer la capacité de déformation requise par le théorème des limites inférieures pour appliquer un MBT.

Une autre étape serait d'examiner le mécanisme résistant des poutres profondes renforcées de PRF soumis à des charges cycliques inversées. Cette question est pertinente pour assurer une conception adéquate des poutres profondes renforcées de PRF situées dans les zones sismiques, surtout si la similitude est reconnue entre les mécanismes de support de charge sous des charges cycliques inversées pour les poutres profondes et ceux pour d'autres poutres mince. Enfin, des essais expérimentaux pour des poutres profondes continues renforcées de PRF sont d'une importance significative.

REFERENCES

AASHTO, "AASHTO LRFD Bridge Design Specifications," 1st Edition, American Association of State Highway and Transportation Officials (*AASHTO*), Washington, 2007.

AASHTO, "AASHTO LRFD Bridge Design Specifications," 2nd Edition, American Association of State Highway and Transportation Officials (*AASHTO*), Washington, 1998.

AASHTO, "AASHTO LRFD Bridge Design Specifications," 1st Edition, American Association of State Highway and Transportation Officials (*AASHTO*), Washington, 1994.

ACI Committee 318 (2014). "Building Code Requirements for Structural Concrete and Commentary (ACI 318-14)." *ACI*, Farmington Hills, MI, 520 pp.

ACI Committee 318 (2011). "Building Code Requirements for Structural Concrete and Commentary (ACI 318-11)." *ACI*, Farmington Hills, MI, 503 pp.

ACI Committee 318 (2008). "Building Code Requirements for Structural Concrete and Commentary (ACI 318-08)." *ACI*, Farmington Hills, MI, 473 pp.

ACI Committee 440 (2007). "Report on Fiber-Reinforced Polymer (FRP) Reinforcement Concrete Structures (ACI 440R-07)." *ACI*, Farmington Hills, MI, 100 pp.

ACI Committee 440 (2006). "Guide for the Design and Construction of Concrete Reinforced with FRP Bars (ACI 440.1R-06)." *ACI*, Farmington Hills, MI, 44 pp.

ACI Committee 440 (2004). "Guide Test Methods for Fiber-Reinforced Polymers (FRPs) for Reinforcing or Strengthening Concrete Structures (ACI 440.3R-04)." *ACI*, Farmington Hills, MI, 40 pp.

Adebar, P., (2000) "One way shear strength of large footings," Canadian Journal of Civil Engineering, 27 (3), pp. 553-562.

Aguilar, G., Matamoros, A. B., Parra-Montesinos, G., Ramirez, J. A., Wight, J. K. (2002). "Experimental Evaluation of Design Procedures for Shear Strength of Deep Reinforced Concrete Beams," *ACI Structural Journal*, 99 (4), pp. 539-548.

Alcocer, S.M., and Uribe, C.M., "Monolithic and Cyclic Behavior of Deep Beams Designed Using Strut-and-Tie Models," *ACI Structural Journal*, 105 (3), 2008, pp. 327-337.

Andermatt M. F., Lubell, A. L. (2010) "Behavior of Concrete Deep Beams with Internal GFRP Reinforcement," Proceedings of 8th International Conference on Short and Medium Span Bridges, Niagara Falls, 10 pp.

Andermatt, M. F., Lubell A. S. (2013a). "Behavior of Concrete Deep Beams Reinforced with Internal Fiber-Reinforced Polymer—Experimental Study." *ACI Structural Journal*, 110 (4), 585-594.

Andermatt, M. F., Lubell A. S. (2013b). "Strength Modeling of Concrete Deep Beams Reinforced With Internal Fiber-Reinforced Polymer." *ACI Structural Journal*, 110 (4), 595-605.

Anderson, N. S., Ramirez, J. A. (1989). "Detailing of Stirrup Reinforcement." *ACI Structural Journal*, 86(5), pp. 507-515.

Aoyama, H. (1993). "Design Philosophy for Shear in Earthquake Resistance in Japan." Earthquake Resistance of Reinforced Concrete Structures—A Volume Honoring Hiroyuki Aoyama, University of Tokyo Press, Tokyo, Japan, pp. 407-418.

ASCE (2008). "Minimum design loads for buildings and other structures." *ASCE 7*, Reston, VA.

ASTM D7205 / D7205M – 06 (2011). Standard Test Method for Tensile Properties of Fiber Reinforced Polymer Matrix Composite Bars.

Bahen, N., Sanders, D. H. (2009) "Investigation of Strut Strength Using a Deep-Beam Database," *ACI Structural Journal*, SP-265(18), pp. 385-404.

Bakis, C. E., Bank, L. C., Brown, V. L., Cosenza, E., Davalos, J. F., Lesko, J. J.,Machida, A., Rizkalla, S. H., and T. C. Triantafillou, T. C. (2002). "Fiber-Reinforced Polymer Composites for Construction—State-of-the-Art Review." *J. Compos. Constr.*, 6(2), 73-87.

Bentz, E. C., (1999). "Sectional analysis of reinforced concrete members." PhD thesis, Department of Civil Engineering, University of Toronto, Toronto, ON, Canada, pp. 310.

Bentz, E. C., Vecchio, F. J., and Collins, M. P., (2006). "Simplified Modified Compression Field Theory for Calculating Shear Strength of Reinforced Concrete Members." *ACI Structural Journal*, 103(4), pp. 614-624.

Bergmeister, K., Breen, J. E., Jirsa, J. O., and Kreger, M. E., (1993). "Detailing for Structural Concrete, *Report No. 1127-3F*, Center for Transportation Research, University of Texas at Austin, Austin, Texas.

Birrcher, D., Tuchscherer, R., Huizinga, M., Bayrak, O., Wood, S., and Jirsa, J., (2009). "Strength and Serviceability Design of Reinforced Concrete Deep Beams," *Report No. 0-5253-1*, Center for Transportation Research, University of Texas at Austin, Austin, TX, 400 pp.

Birrcher, D. B., Tuchscherer, R. G., Huizinga, M., Bayrak, O. (2013). "Minimum Web Reinforcement in Deep Beams." *ACI Structural Journal*, 110 (2), 297-306..

Birrcher, D. B., Tuchscherer, R. G., Huizinga, M., Bayrak, O. (2014). "Depth Effect in Deep Beams." *ACI Structural Journal*, 111 (4), 731-740.

Breña, S. F., Roy, N. C. (2009). "Evaluation of Load Transfer and Strut Strength of Deep Beams with Short Longitudinal Bar Anchorages." *ACI Structural Journal*, 106(5), pp. 679-689.

Brown, M. D., Sankovich, C. L., Bayrak, O., Jirsa, J. O., Breen, J. E., and Wood, S. L., (2006). "Design for Shear in Reinforced Concrete Using Strut-and-Tie Models, *Report No.*

0-4371-2, Center for Transportation Research, University of Texas at Austin, Austin, Texas.

Brown, M. D., Bayrak, O. (2006). "Minimum Transverse Reinforcement for Bottle-Shaped Struts," ACI Structural Journal, V. 103, No. 6, November 2006, pp. 813-822.

Brown, M. D., Bayrak, O. (2007). "Investigation of Deep Beams with Various Load Configurations," *ACI Structural Journal*, V. 104, No. 5, pp. 611-620.

Brown, M. D., Bayrak, O. (2008). "Design of Deep Beams Using Strut-and-Tie Models-Part I: Evaluating U.S. Provisions," *ACI Structural Journal*, 105 (4), pp. 395-404.

CEB-FIP, (2008). "Practitioners' Guide to Finite Element Modeling of Reinforced Concrete Structures," Bulletin 45. pp. 337.

CIRIA Guide No. 2, (1977) "The Design of Deep Beams in Reinforced Concrete," Ove Arup & Partners/Construction Industry Research and Information Association, London, pp. 131.

Clark, A. P., (1951). "Diagonal Tension in Reinforced Concrete Beams," *ACI Journal*, 48(10), pp. 145-156.

Collins, M. P., Bentz, E. C., Sherwood, E. G. (2008). "Where is Shear Reinforcement Required? Review of Research Results and Design Procedures." *ACI Structural Journal*, 105(5), pp. 590-600

Collins, M. P., Kuchma, D. (1999). "How Safe Are Our Large, Lightly-Reinforced Concrete Beams, Slabs and Footings?" *ACI Structural Journal*, 96(4), pp. 482-490.

Collins, M.P., Mitchell, D. (1997). "Prestressed Concrete Structures." Response Publications, Canada, 766 p.

CSA A23.3 (2014). "Design of Concrete Structures Standard." Canadian Standards Association, Mississauga, Ontario, Canada, 295 pp.

CSA A23.3 (2004). "Design of Concrete Structures Standard." Canadian Standards Association, Mississauga, Ontario, Canada, 240 pp.

CSA S6 (2014). "Canadian Highway Bridge Design Code." Canadian Standards Association, Mississauga, Ontario, Canada, 894 pp.

CSA S6 (2006). "Canadian Highway Bridge Design Code." Canadian Standards Association, Mississauga, Ontario, Canada, 1078 pp.

CSA S806 (2012). "Design and construction of building components with fiber-reinforced polymers." Canadian Standards Association, Mississauga, Ontario, Canada, 208 pp.

CSA S807 (2010). "Specification for Fibre Reinforced Polymers." Canadian Standards Association, Mississauga, Ontario, Canada, 44 pp.

De Pavia, H. A. R., Siess, C. P., (1965). "Strength and Behavior of Deep Beams," *ASCE Structural Journal*, 91(ST5), pp. 19-41.

El-Salakawy, E., Benmokrane, B., El-Ragaby, A., and Nadeau, D. (2005). "Field Investigation on the First Bridge Deck Slab Reinforced with Glass FRP Bars Constructed in Canada." *J. Compos. Constr.*, 9(6), pp. 470-479.

El-Sayed, A. K. (2006). "Concrete Contribution to the Shear Resistance of FRP-Reinforced Concrete Beams," PhD dissertation, Université de Sherbrooke, Sherbrooke, QC, Canada, 252 pp.

El-Sayed, A. K., El-Salakawy, E. F., Benmokrane, B. (2006). "Shear Strength of FRP-Reinforced Concrete Beams without Transverse Reinforcement," *ACI Structure Journal*, 103, (2), pp. 235-243.

Erki, M. A., Rizkalla, S. (1993). "FRP Reinforcements for Concrete Structures: A Sample of International Production." *Concrete International*, 15(6), 48-53.

Eurocode 2, (1992). "Design of Concrete Structures, Part 1, General Rules and Regulations for Buildings," English Edition, British Standards Institution, London.

Farghaly, A. S., Benmokrane, B. (2013). “Shear Behavior of FRP-Reinforced Concrete Deep Beams without Web Reinforcement.” *J. Compos. Constr*, 17 (6), 04013015.1-10.

Fédération Internationale du Béton, *fib* (2007). “FRP reinforcement in RC structures.” Task Group 9.3, Lausanne, Switzerland.

Fédération Internationale du Béton, *fib*, Structural Concrete, (1999). “Textbook on Behaviour, Design, and Performance.” Volume 1 (bulletin 1), International Federation for Structural Concrete, Lausanne, Switzerland, 224 pp.

Fenwick, R. C., and Paulay, T., (1968). “Mechanisms of Shear Resistance of Concrete Beams,” Journal of the Structural Division, *ASCE Journal*, 94(ST10) pp. 2235-2350.

Fukuhara, M., Kokusho, S., (1980). "Ultimate shear strength of reinforced concrete beams with high tension shear reinforcement," Transactions of the Japan Concrete Institute, Vol. 2, pp. 255-262.

Hegger, J., Niewels, J., and Kurth, M., (2009). “Shear Analysis of Concrete Members with Fiber Reinforced Polymers (FRP) As Internal Reinforcement,” FRPRCS-9 Sydney, Australia.

Hong, S., Ha, T. (2012). “Effective Capacity of Diagonal Strut for Shear Strength of Reinforced Concrete Beams without Shear Reinforcement.” *ACI Structural Journal*, 109 (2), 139-148.

Hsu, T. C. (1988) “Softened Truss Model Theory for Shear and Torsion,” *ACI Structure Journal*, 85(6), pp. 424-635.

Hsu, T. T. C., Zhang, L. X. B., (1997). “Nonlinear Analysis of Membrane Elements by Fixed-Angle Softened-Truss Model.” *ACI Structural Journal*, 94 (5), pp. 483-492.

ISIS Canada (2007). “Reinforcing concrete structures with fiber-reinforced polymers – Design Manual No. 3.” ISIS Canada Corporation, Manitoba, Canada.

Japan Society of Civil Engineers (JSCE), (1997). "Recommendations for Design and Construction of Concrete Structures Using Continuous Fiber Reinforced Materials," Research Committee on Continuous Fibre Reinforced Materials, A. Machida, ed., Tokyo, Japan, 325 pp.

Joint ACI-ASCE Committee 445, (1998). "Recent Approaches to Shear Design of Structural Concrete," *Journal of Structural Engineering, ASCE*, 24(12), pp. 1375-1417.

Kani, G. N. J. (1967). "How Safe Are Our Large Concrete Beams?" *ACI Structure Journal*, 64 (3), pp. 128-141.

Kani, M. W., Huggins, M. W., Wittkopp, R. R. (1979). "Kani on Shear in Reinforced Concrete," University of Toronto Press, Toronto, Canada, 225pp.

Kassem, C., Farghaly, A. S., and Benmokrane, B. (2011). "Evaluation of Flexural Behavior and Serviceability Performance of Concrete Beams Reinforced with FRP Bars." *J. Compos. Constr.*, 15(5), 682–695.

Kim, D., Lee, J., Lee, Y-H. (2014). "Effectiveness Factor of Strut-and-Tie Models for Concrete Deep Beams Reinforced with FRP Rebars." Composites Engineering: Part B, 56(2014), 117-125.

Kong, F.-K., Robins, P. J., Cole, D. F. (1970). "Web Reinforcement Effects on Deep Beams," *ACI Structure Journal*, 69(3), pp. 172-187.

Kong, F.-K., Robins, P. J., Cole, D. F. (1972). "Deep beams with inclined web reinforcement," *ACI Strucutre Journal*, 69(16), 1972, pp. 172-176.

Kotsovos, M. D. (1988). "Design of Reinforced Concrete Deep Beams," *The Structural Engineer*, 66 (2), pp. 28-32.

Küng, R., (1985) "Ein Beitrag zur Schubsicherung im Stahlbetonbau", Betonstahl in Entwicklung, Heft 33, Tor-Esteg Steel Corporation, Luxemborg (in German).

Kupfer, H., Hilsdorf, H.K.and Rusch, H., 1969. "Behavior of Concrete under Biaxial Stress", *ACI Journal*, 87 (2), pp. 656-666.

Lu, W.-Y. (2006). "Shear Strength Prediction for Steel Reinforced Concrete Deep Beams," *Journal of Engineering Structures*, 62(10), pp. 933-942.

MacGregor, J. G. (1997). "Reinforced Concrete, Mechanics and Design," 3rd Edition, Prentice Hall, New Jersey, 939 pp.

Manuel, R. F., Slight, B. W., Suter, G. T. (1971). "Deep Beam Behavior Affected by Length and Shear Span Variations," *ACI Structure Journal*, 68(12), pp. 954-958.

Matamoros, A. B., Wong, K. H. (2003). "Design of Simply Supported Deep Beams Using Strut-and-Tie Models," *ACI Structure Journal*, 100 (6), pp. 704-712.

Mau, S. T., Hsu, T. T. C. (1989). "Formula for the Shear Strength of Deep Beams," *ACI Structure Journal*, 86(5), pp. 516-523.

Mihaylov, B. I., Bentz, E. C., Collins, M. P. (2010). "Behavior of Large Deep Beams Subjected to Monotonic and Reversed Cyclic Shear." *ACI Structural Journal*, 107(6), 726-734.

Mihaylov, B. I., Bentz, E. C., Collins, M. P. (2013). "Tow-Parameter Kinematic Theory for Shear Behavior of Deep Beams." *ACI Structural Journal*, 110 (3), 447-456.

Ministry of Transportation of Ontario (MTO), (2009), "Quick Facts." Obtained from http://www.mto.gov.on.ca/english/about/quickfacts.shtml.

Mohamed, N., Farghaly, A. S., Benmokrane, B., and Neale, K. W., (2014), "Experimental Investigation of Concrete Shear Walls Reinforced with Glass Fiber–Reinforced Bars under Lateral Cyclic Loading." *J. Compos. Constr.*, 10.1061/(ASCE)CC.1943-5614.0000393.

Mohamed, N., Farghaly, A. S., Benmokrane, B., Neale, K. W. (2014), "Numerical Simulation of Mid-Rise Concrete Shear Walls Reinforced with GFRP Bars Subjected to Lateral Displacement Reversals," *Engineering Structures, Elsevier*, 73 (2014), pp. 61-72.

Niwa, J., Maekawa, K, Okamura, H., (1981). "Non-linear Finite Element Analysis of Deep Beams," advanced Mechanics of Reinforced Concrete, IABSE Colloqium Delft Netherlands, pp. 625-638

Oh J.-K., Shin, S.-W. (2001). “Shear Strength of Reinforced High-Strength Concrete Deep Beams,” *ACI Structural Journal*, 98(2), pp. 164-173.

Omeman, Z., Nehdi, M., El-Chabib, H. (2008). “Experimental study on shear behavior of carbonfiber- reinforced polymer reinforced concrete short beams without web reinforcement,” *Canadian Journal of Civil Engineering*, 35, pp. 1-10

Park, J.-W., Kuchma, K. (2007). “Strut-and-Tie Model Analysis for Strength Prediction of Deep Beams,” *ACI Structural Journal*, 104 (6), pp. 657-666.

Popovics, S. (1973). "A Numerical Approach to the Complete Stress-Strain Curve of Concrete", *Cement and Concrete Research*, 3(5), pp. 583-599.

Quintero-Febres, C. G., Parra-Montesinos, G., Wight, J. K., (2006). “Strength of Struts in Deep Concrete Members Designed Using Strut-and-Tie Method,” *ACI Structural Journal*, 103(4), pp.577-586.

Ramakrishnan, V., Ananthanarayana, Y. (1968). “Ultimate Strength of Deep Beams in Shear,” *ACI Structural Journal*, 65(2), pp. 87-98.

Razaqpur, G., Isgor, O. B. (2006). “Proposed Shear Design Method for FRP-Reinforced Concrete Members without Stirrups,” ACI Structure Journal, 103(1), pp. 93-102.

Reineck, K., Todisco, L. (2014). “Database of Shear Tests for Non-Slender Reinforced Concrete Beams without Stirrups.” *ACI Structural Journal*, 111 (6), 1363-1372.

Rogowsky, D. M., MacGregor, J. G. (1986). “Design of Reinforced Concrete Deep Beams.” *Concrete International*, 8(8), 49-58.

Rogowsky, D. M., MacGregor, J. G., Ong, S. Y. (1986). “Test of Reinforced Concrete Deep Beams,” *ACI Structure Journal*, 83(4), pp. 614-623.

Russo, G., Venir, R., Pauletta, M. (2005). “Reinforced Concrete Deep Beams—Shear Strength Model and Design Formula,” *ACI Structure Journal*, 102(3), pp. 429-437.

Sahoo, D. K., Singh, B., and Pradeep Bhargava, (2011). “Minimum Reinforcement for Preventing Splitting Failure in Bottle-Shaped Struts.” *ACI Structure Journal*, 108(2), pp. 206-216.

Schlaich, J., Schäfer, K. (1991). “Design and Detailing of Structural Concrete Using Strut-and-Tie Models,” *Journal of Structural Engineer*, 69(6), pp. 113-125.

Schlaich, J., Schäfer, K., Jennewein, M. (1987). "Toward a Consistent Design of Structural Concrete," *J. Prestressed Concrete Inst.*, 32(3), pp. 74-150.

Scott, B. D., Park, R., Priestley, M. J. N. (1982). "Stress-Strain Behavior of Concrete Confined by Overlapping Hoops at Low and High Strain Rates", *ACI Journal*, 79(1), pp.13-27.

Seckin, M. (1981). "Hysteretic Behaviour of Cast-in-Place Exterior Beam-Column-Slab Subassemblies", Ph.D. Thesis, Department of Civil Engineering, University of Toronto, 266 pp.

Sharbatdar, M. K., Saatcioglu, M. (2009). “Seismic Design of FRP Reinforced Concrete Structures.” *Asian J. Applied Sci.*, 2(3), 211-222.

Smith K. N., Vantsiotis, A. S. (1982) “Shear Strength of Deep Beams,” *ACI Structure Journal*, 79(3), pp. 201-213.

Structural Use of Concrete, (1985). “Part 1: Code of Practice for Design and Construction.” BS 8110: 1985, British Standards Institution, London.

Tan, K.H., Cheng, G. H., Zhang, N. (2007). “Experiment to mitigate size effect on deep beams,” *Magazine of Concrete Research*, Online, 15 pp.

Tan, K. H., Kong, F. K., Teng, S., Guan, L., (1995). "High-Strength Concrete Deep Beams with Effective Span and Shear Span Variations," *ACI Structural Journal*, 92(4), pp. 395-405.

Tan, K. H., Kong, F. K., Teng, S., Weng, L. W. (1997a). "Effect of Web Reinforcement on High-Strength Concrete Deep Beams," *ACI Structural Journal*, 94(5), pp. 572-582.

Tan K. H., Tang C. Y. Tong K., (2003). "A Direct Method for Deep Beams with Web Reinforcement," *Magazine of Concrete Research*, 55(1), pp.53–63.

Tan, K. H., Teng, S., Kong, F. K., Lu, H. Y. (1997b). "Main Tension Steel in High Strength Concrete Deep and Short Beams," *ACI Structural Journal*, 94(6), pp. 752-768.

Tobbi, H., Farghaly, A. S., and Benmokrane, B. (2012). "Concrete Columns Reinforced Longitudinally and Transversally with Glass Fiber-Reinforced Polymer Bars." *ACI Structural Journal*, 109(4), 551-558.

Tuchscherer, R., Birrcher, D., Huizinga, M., Bayrak, O. (2010). "Confinement of Deep Beam Nodal Regions," *ACI Structure Journal*, 107(6), pp. 709-717.

Tuchscherer, R., Birrcher, D., Huizinga, M., Bayrak, O. (2011). "Distribution of Stirrups across Web of Deep Beams," *ACI Structure Journal*, 108(1), pp. 108-115.

Tuchscherer, R. G., Birrcher, D. B., Williams, C. S., Deschenes, D. J., Bayrak, O. (2014). "Evaluation of Existing Strut-and-Tie Methods and Recommended Improvements." *ACI Structural Journal*, 111 (6), 1451-1460.

Vecchio, F. J., (1992). "Finite Element Modeling of Concrete Expansion and Confinement", *ASCE Journal of Structural Engineering*, 118(9), pp. 2390-2406.

Vecchio, F. J. (2000a). "Analysis of Shear-Critical Reinforced Concrete Beams," *ACI Structural Journal*, 97(1), pp. 102-110.

Vecchio, F. J. (2000b) "Disturbed Stress Field Model for Reinforced Concrete: Formulation," *Journal of Structural Engineering*, 126(9), pp. 1070-1077.

Vecchio, F. J., Collins, M. P. (1986). "Modified Compression Field Theory for Reinforced Concrete Elements Subjected to Shear," *ACI Structural Journal*, 83(2), pp. 219-231.

Vecchio, F. J., and Collins, M. P. (1993). "Compression Response of Cracked Reinforced Concrete," *ASCE Journal of Structural Engineering*, 119(12), pp. 3590-3610.

Walraven, J., Lehwalter, N., (1994). "Size Effects in Short Beams Loaded in Shear," *ACI Structural Journal*, 91(5), pp. 585-593.

Wong, P. S., Vecchio, F. J. (2002). "VecTor2 & Formworks User's Manuals." Department of Civil Engineering, University of Toronto, Toronto, ON, Canada, 213 pp.

Wight, J. K. and MacGregor, J. G. (2009). "Reinforced Concrete: Mechanics and Design." (5th edition), Pearson Prentice Hall, Upper Saddle River, New Jersey.

Yang, K.-H., Chung, H.-S., Lee, E.-T., Eun, H.-C., (2003). "Shear characteristics of high-strength concrete deep beams without shear reinforcements," *Journal of Engineering Structures*, 25(10), pp. 1343-1352.

Zhang, N., Tan, K.-H. (2007a) "Direct Strut-And-Tie Model for Single Span and Continuous Deep Beams," *Journal of Engineering Structures*, 29(11), pp. 2987-3001.

Zhang, N., Tan, K.-H. (2007b) "Size effect in RC Deep Beams: Experimental Investigation and STM Verification," *Journal of Engineering Structures*, 29(12), pp. 3241-3254.

Zhang, L. X., Hsu, T. T. C., (1998). "Behavior and Analysis of 100 MPa Concrete Membrane Elements," *Journal of Structural Engineering*, 124(1), pp. 24-34.

APPENDIX A

Evaluation Data-Base for Steel-Reinforcement Deep Beams

The following details are presented in Table A.1 for 470 specimens in the evaluation database: f_c' = concrete compressive strength, MPa; b = beam width, mm; d = distance from extreme compression fiber to centroid of tensile reinforcement, mm; a = shear span, mm; a/d = shear span-to-depth ratio; $\rho = A_s/bd$ = ratio of longitudinal reinforcement to effective cross-section area, %; $\rho_h = A_h/bs_h$ = ratio of horizontal reinforcement to effective cross-section area, %; s_h = spacing of horizontal bars across the beam web, mm; $\rho_v = A_v/bs_v$ = ratio of vertical reinforcement to effective cross-section area, %; s_v = spacing of vertical stirrups, mm; P_{exp} = experimental ultimate shear capacity of the deep beam, kN; P_{pred} = calculated ultimate shear capacity of the deep beam according to CSA A23.3 (2014), ACI 318 (2014), and the proposed model in kN.

It worth mentioning that relatively small size specimens with total height less than 500 mm was not considered when applying the proposed model in Chapter 5, as they do not represent the real case of deep beams in practice.

Table A.1 - Evaluation steel-reinforced deep beam database.

Beam ID	f_c' (MPa)	b (mm)	d (mm)	a (mm)	a/d	ρ (%)	ρ_h (%)	ρ_v (%)	P_{exp} (kN)	P_{exp}/P_{pred}		
										CSA-A23.3-14	ACI 318-14	Proposed Model
Clark (1952)												
A1-1	24.65	203	387	914	2.36	3.1	0.00	0.38	224.2	3.42	1.06	1.45
A1-2	23.65	203	387	914	2.36	3.1	0.00	0.38	210.9	3.34	1.04	1.37
A1-3	23.39	203	387	914	2.36	3.1	0.00	0.38	224.2	3.59	1.11	1.46
A1-4	24.75	203	387	914	2.36	3.1	0.00	0.38	246.4	3.74	1.16	1.59
B1-1	23.36	203	387	762	1.97	3.1	0.00	0.37	280.7	2.54	1.18	0.91
B1-2	25.37	203	387	762	1.97	3.1	0.00	0.37	258.4	2.17	1.00	0.83
B1-3	23.68	203	387	762	1.97	3.1	0.00	0.37	286.4	2.56	1.19	0.93
B1-4	23.3	203	387	762	1.97	3.1	0.00	0.37	270.0	2.45	1.14	0.88
B1-5	24.61	203	387	762	1.97	3.1	0.00	0.37	243.3	2.10	0.97	0.78
B2-1	23.24	203	387	762	1.97	3.1	0.00	0.73	302.9	2.75	1.28	0.99
B2-2	26.34	203	387	762	1.97	3.1	0.00	0.73	323.8	2.63	1.21	1.03
B2-3	24.92	203	387	762	1.97	3.1	0.00	0.73	336.7	2.87	1.33	1.08
B6-1	42.13	203	387	762	1.97	3.1	0.00	0.37	381.2	2.06	0.89	1.09
C1-1	25.65	203	387	610	1.58	2.07	0.00	0.34	279.3	1.36	0.84	0.89
C1-2	26.34	203	387	610	1.58	2.07	0.00	0.34	312.7	1.49	0.92	1.00
C1-3	23.96	203	387	610	1.58	2.07	0.00	0.34	247.7	1.28	0.80	0.80
C1-4	29.03	203	387	610	1.58	2.07	0.00	0.34	287.8	1.27	0.76	0.90
C2-1	23.65	203	387	610	1.58	2.07	0.00	0.69	291.8	1.52	0.94	0.94
C2-2	24.99	203	387	610	1.58	2.07	0.00	0.69	302.9	1.51	0.92	0.97
C2-3	24.13	203	387	610	1.58	2.07	0.00	0.69	325.6	1.67	1.03	1.05
C2-4	26.96	203	387	610	1.58	2.07	0.00	0.69	290.0	1.36	0.82	0.92
C3-1	14.07	203	387	610	1.58	2.07	0.00	0.34	225.0	1.82	1.22	0.76
C3-2	13.79	203	387	610	1.58	2.07	0.00	0.34	201.9	1.66	1.11	0.68
C3-3	13.93	203	387	610	1.58	2.07	0.00	0.34	189.9	1.54	1.04	0.64
C4-1	24.48	203	387	610	1.58	3.1	0.00	0.34	310.9	1.47	0.97	0.92
C6-2	45.23	203	387	610	1.58	3.1	0.00	0.34	425.7	1.21	0.72	1.14
C6-3	44.68	203	387	610	1.58	3.1	0.00	0.34	436.8	1.26	0.74	1.17
C6-4	47.57	203	387	610	1.58	3.1	0.00	0.34	430.1	1.18	0.69	1.14
D1-1	26.2	203	394	457	1.16	1.63	0.00	0.46	302.9	0.81	0.72	0.88
D1-2	26.13	203	394	457	1.16	1.63	0.00	0.46	358.5	0.96	0.85	1.04
D1-3	24.55	203	394	457	1.16	1.63	0.00	0.46	258.4	0.73	0.65	0.75
D2-1	23.99	203	394	457	1.16	1.63	0.00	0.61	291.8	0.83	0.75	0.85
D2-2	25.89	203	394	457	1.16	1.63	0.00	0.61	314.0	0.85	0.75	0.91
D2-3	24.79	203	394	457	1.16	1.63	0.00	0.61	336.2	0.94	0.84	0.98
D2-4	24.48	203	394	457	1.16	1.63	0.00	0.61	336.7	0.95	0.85	0.98
D3-1	28.2	203	394	457	1.16	2.44	0.00	0.92	396.8	0.91	0.87	1.00
D4-1	23.1	203	394	457	1.16	1.63	0.00	1.22	314	0.92	0.84	0.92
A0-1	21.51	203	387	914	2.36	0.98	0.00	0.00	88.2	1.74	0.91	1.33
A0-2	25.99	203	387	914	2.36	0.98	0.00	0.00	106.9	1.80	0.91	1.53
A0-3	23.68	203	387	914	2.36	0.98	0.00	0.00	118	2.14	1.10	1.73
B0-1	23.58	203	387	762	1.97	0.98	0.00	0.00	119.8	1.29	1.01	0.94
B0-2	23.91	203	387	762	1.97	0.98	0.00	0.00	93.4	0.99	0.77	0.73

Table A.1 - Evaluation steel-reinforced deep beam database.

Beam ID	f_c' (MPa)	b (mm)	d (mm)	a (mm)	a/d	ρ (%)	ρ_h (%)	ρ_v (%)	P_{exp} (kN)	P_{exp}/P_{pred}		
										CSA-A23.3-14	ACI 318-14	Proposed Model
Clark (1952), *Continue…*												
B0-3	23.51	203	387	762	1.97	0.98	0.00	0.00	127	1.37	1.07	1.00
C0-1	24.68	203	387	610	1.58	0.98	0.00	0.00	172.6	1.02	1.09	1.34
C0-2	23.48	203	387	610	1.58	0.98	0.00	0.00	176	1.08	1.17	1.38
C0-3	23.58	203	387	610	1.58	0.98	0.00	0.00	165.4	1.01	1.09	1.29
D0-1	25.86	203	394	457	1.16	0.98	0.00	0.00	223.6	0.69	0.87	0.77
D0-2	26.2	203	394	457	1.16	0.98	0.00	0.00	262.4	0.80	1.01	0.90
D0-3	25.96	203	394	457	1.16	0.98	0.00	0.00	225	0.69	0.87	0.64
De Pavia (1965)												
G23S-11	24.6	51	305	203	0.67	0.83	0.00	0.00	89.8	1.23	1.58	-
G33S-11	23.3	76	203	203	1.00	1.67	0.00	0.00	85.3	1.29	1.38	-
G33S-31	19.9	76	203	203	1.00	2.58	0.00	0.00	106.9	1.71	2.02	-
G34S-11	35.2	76	203	203	1.00	1.67	0.00	0.00	109.8	1.20	1.18	-
G43S11	24.2	102	152	203	1.33	1.67	0.00	0.00	76.9	1.46	1.21	-
G44S-11	37.0	102	152	203	1.33	1.67	0.00	0.00	83.6	1.14	0.86	-
Kong et al. (1970)												
A1-1	24.6	203	390	914	2.34	3.10	0.00	0.38	222.5	2.63	2.05	-
A1-2	23.6	203	390	914	2.34	3.10	0.00	0.38	209.1	2.57	2.02	-
A1-3	23.4	203	390	914	2.34	3.10	0.00	0.38	222.5	2.77	2.18	-
A1-4	24.8	203	390	914	2.34	3.10	0.00	0.38	244.7	2.90	2.27	-
B1-1	23.4	203	390	762	1.95	3.10	0.00	0.37	278.8	2.42	2.22	-
B1-2	25.4	203	390	762	1.95	3.10	0.00	0.37	256	2.07	1.88	-
B1-3	23.7	203	390	762	1.95	3.10	0.00	0.37	284.8	2.44	2.24	-
B1-4	23.3	203	390	762	1.95	3.10	0.00	0.37	268.1	2.33	2.14	-
B1-5	24.6	203	390	762	1.95	3.10	0.00	0.37	241.5	2.00	1.82	-
B2-1	23.2	203	390	762	1.95	3.10	0.00	0.73	301.1	2.62	2.41	-
B2-2	26.3	203	390	762	1.95	3.10	0.00	0.73	322.2	2.52	2.28	-
B2-3	24.9	203	390	762	1.95	3.10	0.00	0.73	334.9	2.74	2.50	-
B6-1	42.1	203	390	762	1.95	3.10	0.00	0.37	379.3	1.98	1.67	-
C1-1	25.6	203	390	610	1.56	2.07	0.00	0.34	277.7	1.59	2.46	-
C1-2	26.3	203	390	610	1.56	2.07	0.00	0.34	311.1	1.73	2.68	-
C1-3	24.0	203	390	610	1.56	2.07	0.00	0.34	245.9	1.48	2.33	-
C1-4	29.0	203	390	610	1.56	2.07	0.00	0.34	285.9	1.47	2.24	-
C2-1	23.6	203	390	610	1.56	2.07	0.00	0.69	290.0	1.77	1.83	-
C2-2	25.0	203	390	610	1.56	2.07	0.00	0.69	301.1	1.75	1.80	
C2-3	24.1	203	390	610	1.56	2.07	0.00	0.69	323.7	1.94	2.01	-
C2-4	27.01	203	390	610	1.56	2.07	0.00	0.69	288.2	1.58	1.60	-
C3-1	14.1	203	390	610	1.56	2.07	0.00	0.34	223.7	2.13	3.61	-
C3-2	13.8	203	390	610	1.56	2.07	0.00	0.34	200.3	1.94	3.30	-
C3-3	13.9	203	390	610	1.56	2.07	0.00	0.34	188.1	1.81	3.01	-
C4-1	24.5	203	390	610	1.56	3.10	0.00	0.34	309.3	1.73	2.87	-
C6-2	45.2	203	390	610	1.56	3.10	0.00	0.34	423.8	1.41	2.13	-
C6-3	44.7	203	390	610	1.56	3.10	0.00	0.34	434.9	1.46	2.21	-
C6-4	47.6	203	390	610	1.56	3.10	0.00	0.34	428.6	1.37	2.05	-

Table A.1 - Evaluation steel-reinforced deep beam database.

Beam ID	f_c' (MPa)	b (mm)	d (mm)	a (mm)	a/d	ρ (%)	ρ_h (%)	ρ_v (%)	P_{exp} (kN)	P_{exp}/P_{pred}		
										CSA-A23.3-14	ACI 318-14	Proposed Model
Kong et al. (1970), *Continue…*												
D1-1	26.2	203	390	457	1.17	1.63	0.00	0.46	301.1	1.14	1.40	-
D1-2	26.1	203	390	457	1.17	1.63	0.00	0.46	356.7	1.36	1.67	-
D1-3	24.5	203	390	457	1.17	1.63	0.00	0.46	256.6	1.03	1.28	-
D2-1	24.0	203	390	457	1.17	1.63	0.00	0.61	290.0	1.18	1.47	-
D2-2	25.9	203	390	457	1.17	1.63	0.00	0.61	312.2	1.20	1.47	-
D2-3	24.8	203	390	457	1.17	1.63	0.00	0.61	334.4	1.33	1.65	-
D2-4	24.5	203	390	457	1.17	1.63	0.00	0.61	334.9	1.34	1.67	-
D3-1	28.2	203	390	457	1.17	2.44	0.00	0.92	394.9	1.31	1.71	-
D4-1	23.1	203	390	457	1.17	1.63	0.00	1.22	312.2	1.31	1.65	
Kani et al. (1979)												
24	27.9	152	271	407	1.50	1.87	0.00	0.00	182	1.56	1.25	-
25	24.6	152	271	543	2.00	1.87	0.00	0.00	104.1	1.71	2.28	-
26	27.1	152	271	543	2.00	1.87	0.00	0.00	78.1	1.18	1.65	-
27	29.8	152	271	678	2.50	1.87	0.00	0.00	51.4	1.01	1.15	-
28	29.2	152	271	678	2.50	1.87	0.00	0.00	54.3	1.07	1.23	-
45	25.5	151	133	272	2.05	2.83	0.00	0.00	64.6	1.53	2.55	-
46	25.5	151	136	272	2.00	2.76	0.00	0.00	69.1	1.61	2.64	-
67	30.3	157	528	543	1.03	2.75	0.00	0.00	548	1.32	1.44	-
69	27.4	155	542	543	1.00	2.67	0.00	0.00	585.6	1.38	1.70	-
71	24.8	152	549	1087	1.98	2.71	0.00	0.00	196.9	1.92	1.87	-
85	25.5	154	274	272	0.99	2.69	0.00	0.00	233.6	1.48	1.91	-
87	27.2	154	269	272	1.01	2.72	0.00	0.00	239.6	1.40	1.74	-
94	25.3	154	273	543	1.99	2.77	0.00	0.00	110.6	1.94	2.07	-
95	25.3	153	275	678	2.47	2.75	0.00	0.00	72.8	1.34	1.54	-
99	26.2	153	272	679	2.50	2.73	0.00	0.00	77.2	1.43	1.66	-
100	27.2	153	270	544	2.02	2.75	0.00	0.00	111.9	1.94	2.10	-
102	25.3	153	269	543	2.02	0.76	0.00	0.00	48.8	0.94	1.28	-
105	26.2	152	272	679	2.50	0.77	0.00	0.00	41.5	1.12	1.12	-
109	25.0	153	271	407	1.50	0.76	0.00	0.00	71.9	0.82	0.54	-
129	17.6	155	275	407	1.48	1.78	0.00	0.00	143.3	1.79	1.56	-
134	17.4	154	273	544	1.99	1.81	0.00	0.00	59.9	1.32	1.46	-
135	17.4	149	274	544	1.98	1.86	0.00	0.00	76.8	1.74	1.91	-
141	19.3	151	270	544	2.01	0.81	0.00	0.00	48.7	1.16	1.44	-
142	19.3	156	276	544	1.97	0.77	0.00	0.00	58.3	1.37	1.63	-
148	19.9	152	274	408	1.49	0.79	0.00	0.00	79.9	1.08	0.79	-
149	18.0	153	272	678	1.50	0.78	0.00	0.00	43.7	1.33	1.39	-
150	18.0	153	273	678	2.48	0.77	0.00	0.00	46.2	1.40	1.45	-
151	19.3	154	273	679	2.49	0.78	0.00	0.00	35.6	1.05	1.08	-
162	34.3	153	272	543	1.99	0.77	0.00	0.00	59.0	0.91	1.34	-
163	35.4	156	273	678	2.49	0.76	0.00	0.00	40.5	0.96	0.93	-
181	33.9	154	272	543	2.00	1.79	0.00	0.00	65.2	0.82	1.27	-
184	35.1	154	271	407	1.50	1.80	0.00	0.00	163.3	1.17	0.88	-

Table A.1 - Evaluation steel-reinforced deep beam database.

Beam ID	f_c' (MPa)	b (mm)	d (mm)	a (mm)	a/d	ρ (%)	ρ_h (%)	ρ_v (%)	P_{exp} (kN)	P_{exp}/P_{pred}		
										CSA-A23.3-14	ACI 318-14	Proposed Model
Kani et al. (1979); *Continue…*												
188	33.1	153	277	543	1.96	1.76	0.00	0.00	92.6	1.21	1.79	-
199	36.0	152	273	544	1.99	1.83	0.00	0.00	76.8	0.93	1.46	-
201	35.2	155	274	272	0.99	2.65	0.00	0.00	253.7	0.88	0.94	-
204	34.8	152	275	543	1.97	2.69	0.00	0.00	147.1	1.72	2.52	-
205	35.2	153	275	544	1.98	2.69	0.00	0.00	125.5	1.45	2.12	-
215	36.0	154	274	679	2.48	2.67	0.00	0.00	88.1	1.43	1.66	-
266	18.1	153	272	673	2.48	0.50	0.00	0.00	32.5	1.15	1.07	-
270	20.1	152	273	542	1.99	0.50	0.00	0.00	41.4	1.07	1.25	-
3041	26.9	152	1097	2195	2.00	2.72	0.00	0.00	326.2	1.36	1.51	1.13
3042	26.4	154	1095	2737	2.50	2.70	0.00	0.00	237.0	1.55	1.25	1.08
Fukuhara and Kokusho (1980)												
(1)-1	23.6	180	340	1200	1.76	3.20	0.00	0.00	97.5	1.20	1.13	-
(2)-1	31.8	180	340	1200	1.76	3.20	0.00	0.00	104.6	1.14	1.06	-
(2)-2	31.8	180	340	1200	1.76	3.20	0.00	0.00	101.0	1.10	1.02	-
(3)-1	23.6	180	340	1600	2.35	3.20	0.00	0.00	81.1	1.04	1.13	-
(4)-1	19.5	180	340	1200	1.76	3.20	0.00	0.00	85.7	1.14	1.09	-
(4)-2	19.5	180	340	1200	1.76	3.20	0.00	0.00	104.6	1.39	1.33	-
Niwa et al. (1981)												
T1	35.8	100	228	200	0.88	6.00	0.00	0.00	314.5	2.12	1.27	-
T2	54.7	100	507	200	0.39	3.00	0.00	0.00	514.0	0.73	1.22	-
T3	13.1	100	228	200	0.88	3.00	0.00	0.00	114.0	1.16	1.43	-
T4	13.1	100	507	150	0.30	3.00	0.00	0.00	212.5	1.06	1.77	-
T5	66.6	100	507	200	0.39	6.00	0.00	0.00	881.5	0.84	1.40	-
T6	35.8	100	507	150	0.30	6.00	0.00	0.00	577.5	1.32	2.21	-
T7	59.9	100	228	150	0.66	6.00	0.00	0.00	446.0	0.83	1.10	-
Smith and Vantsiotis (1982)												
0A0-44	20.5	102	305	305	1.0	1.94	0.00	0.00	139.5	1.19	1.90	-
0A0-48	20.9	102	305	305	1.0	1.94	0.00	0.00	136.1	1.14	1.81	-
1A1-10	18.7	102	305	305	1.0	1.94	0.23	0.28	161.2	1.49	1.72	-
1A3-11	18.0	102	305	305	1.0	1.94	0.45	0.28	148.3	1.41	1.64	-
1A4-12	16.1	102	305	305	1.0	1.94	0.68	0.28	141.2	1.48	1.75	-
1A4-51	20.5	102	305	305	1.0	1.94	0.68	0.28	170.9	1.45	1.66	-
1A6-37	21.1	102	305	305	1.0	1.94	0.91	0.28	184.1	1.53	1.74	-
2A1-38	21.7	102	305	305	1.0	1.94	0.23	0.63	174.5	1.42	1.61	-
2A3-39	19.8	102	305	305	1.0	1.94	0.45	0.63	170.6	1.50	1.72	-
2A4-40	20.3	102	305	305	1.0	1.94	0.68	0.63	171.9	1.48	1.69	-
2A6-41	19.1	102	305	305	1.0	1.94	0.91	0.63	161.9	1.46	1.69	-
3A1-42	18.4	102	305	305	1.0	1.94	0.23	1.25	161.0	1.5	1.74	-
3A3-43	19.2	102	305	305	1.0	1.94	0.45	1.25	172.7	1.55	1.79	-
3A4-45	20.8	102	305	305	1.0	1.94	0.68	1.25	178.6	1.5	1.71	-
3A6-46	19.9	102	305	305	1.0	1.94	0.91	1.25	168.1	1.47	1.68	-
0B0-49	21.7	102	305	368	1.21	1.94	0.00	0.00	149.0	1.57	2.20	-
1B1-01	22.1	102	305	368	1.21	1.94	0.23	0.24	147.5	1.53	1.49	-

Table A.1 - Evaluation steel-reinforced deep beam database.

Beam ID	f_c' (MPa)	b (mm)	d (mm)	a (mm)	a/d	ρ (%)	ρ_h (%)	ρ_v (%)	P_{exp} (kN)	P_{exp}/P_{pred}		
										CSA-A23.3-14	ACI 318-14	Proposed Model
Smith and Vantsiotis (1982), *Continue…*												
1B3-29	20.1	102	305	368	1.21	1.94	0.45	0.24	143.6	1.61	1.59	-
1B4-30	20.8	102	305	368	1.21	1.94	0.68	0.24	140.3	1.53	1.50	-
1B6-31	19.5	102	305	368	1.21	1.94	0.91	0.24	153.4	1.76	1.75	-
2B1-05	19.2	102	305	368	1.21	1.94	0.23	0.42	129.0	1.51	1.50	-
2B3-06	19.0	102	305	368	1.21	1.94	0.45	0.42	131.2	1.54	1.54	-
2B4-07	17.5	102	305	368	1.21	1.94	0.68	0.42	126.1	1.59	1.61	-
2B4-52	21.8	102	305	368	1.21	1.94	0.68	0.42	149.9	1.57	1.53	-
2B6-32	19.8	102	305	368	1.21	1.94	0.91	0.42	145.2	1.65	1.64	-
3B1-08	16.2	102	305	368	1.21	1.94	0.23	0.63	130.8	1.76	1.79	-
3B1-36	20.4	102	305	368	1.21	1.94	0.23	0.77	159	1.76	1.73	-
3B3-33	19.0	102	305	368	1.21	1.94	0.45	0.77	158.4	1.87	1.86	-
3B4-34	19.2	102	305	368	1.21	1.94	0.68	0.77	155.0	1.80	1.80	-
3B6-35	20.6	102	305	368	1.21	1.94	0.91	0.77	166.1	1.83	1.79	-
4B1-09	17.1	102	305	368	1.21	1.94	0.23	1.25	153.5	1.97	2.00	-
0C0-50	20.7	102	305	457	1.5	1.94	0.00	0.00	115.7	1.78	2.19	-
1C1-14	19.2	102	305	457	1.5	1.94	0.23	0.18	119.0	1.95	2.42	-
1C3-02	21.9	102	305	457	1.5	1.94	0.45	0.18	123.4	1.81	1.48	-
1C4-15	22.7	102	305	457	1.5	1.94	0.68	0.18	131.0	1.86	1.52	-
1C6-16	21.8	102	305	457	1.5	1.94	0.91	0.18	122.3	1.80	1.48	-
2C1-17	19.4	102	305	457	1.5	1.94	0.23	0.31	124.1	1.97	1.64	-
2C3-03	19.2	102	305	457	1.5	1.94	0.45	0.31	103.6	1.69	1.42	-
2C3-27	19.3	102	305	457	1.5	1.94	0.45	0.31	115.3	1.87	1.57	-
2C4-18	20.4	102	305	457	1.5	1.94	0.68	0.31	124.6	1.93	1.60	-
2C6-19	20.8	102	305	457	1.5	1.94	0.91	0.31	124.1	1.91	1.57	-
3C1-20	21.0	102	305	457	1.5	1.94	0.23	0.56	140.8	2.13	1.76	-
3C3-21	16.5	102	305	457	1.5	1.94	0.45	0.56	125.0	2.33	1.99	-
3C4-22	18.3	102	305	457	1.5	1.94	0.68	0.56	127.7	2.18	1.84	-
3C6-23	19.0	102	305	457	1.5	1.94	0.91	0.56	137.2	2.26	1.90	-
4C1-24	19.6	102	305	457	1.5	1.94	0.23	0.77	146.6	2.36	1.97	-
4C3-04	18.5	102	305	457	1.5	1.94	0.45	0.63	128.6	2.16	1.82	-
4C3-04	19.2	102	305	457	1.5	1.94	0.45	0.77	152.4	2.49	2.08	-
4C4-25	18.5	102	305	457	1.5	1.94	0.68	0.77	152.6	2.57	2.17	-
4C6-26	21.2	102	305	457	1.5	1.94	0.91	0.77	159.5	2.39	1.98	-
0D0-47	19.5	102	305	635	2.08	1.94	0.00	0.00	73.4	2.16	2.16	-
4D1-12	16.1	102	305	635	2.08	1.94	0.23	0.42	87.4	3.04	1.99	-
Küng (1985)												
C	19.8	140	200	500	2.50	0.56	0.00	0.00	26.5	1.24	1.23	
D	18.9	140	200	500	2.50	0.81	0.00	0.00	30.5	1.27	1.40	-
E	18.9	140	200	500	2.50	1.10	0.00	0.00	43.0	1.62	1.89	-
F	18.9	140	200	500	2.50	1.82	0.00	0.00	54.0	1.75	2.15	-
E-1	20.1	140	200	500	2.50	1.10	0.00	0.00	40.4	1.49	1.73	-

Table A.1 - Evaluation steel-reinforced deep beam database.

Beam ID	f_c' (MPa)	b (mm)	d (mm)	a (mm)	a/d	ρ (%)	ρ_h (%)	ρ_v (%)	P_{exp} (kN)	P_{exp}/P_{pred}		
										CSA-A23.3-14	ACI 318-14	Proposed Model
Anderson and Ramirez (1989)												
1	39.0	203	425	914	2.15	2.65	0.00	2.65	478.6	2.62	1.59	-
2	41.4	203	425	914	2.15	2.65	0.00	2.65	489.7	2.56	1.54	-
3	42.7	203	425	914	2.15	2.65	0.00	2.65	511.1	2.60	1.55	-
4	27.5	203	425	914	2.15	2.65	0.00	2.65	439.9	3.23	2.08	-
5	28.7	203	425	914	2.15	2.65	0.00	2.65	426.6	3.03	1.93	-
6	29.4	203	425	914	2.15	2.67	0.00	2.65	368.8	2.56	1.63	-
7	32.1	203	425	914	2.15	2.67	0.00	2.65	391	2.52	1.58	-
8	33.9	203	425	914	2.15	2.67	0.00	2.65	359.9	2.22	1.38	-
9	34.4	203	425	914	2.15	2.67	0.00	2.65	395.4	2.40	1.49	-
10	31.0	203	425	914	2.15	2.67	0.00	2.65	386.6	2.56	1.63	-
11	32.3	203	425	914	2.15	2.67	0.00	2.65	368.8	2.36	1.49	-
12	33.2	203	425	914	2.15	2.67	0.00	2.65	330.9	2.07	1.30	-
Walraven and Lehwa (1994)												
V011	16.1	200	360	360	1.00	1.13	0.00	0.00	226.0	1.13	1.35	-
V012	21.8	200	360	360	1.00	1.13	0.00	0.00	322.0	1.25	1.42	-
V013	22.1	200	360	360	1.00	1.13	0.00	0.00	344.0	1.33	1.50	-
V021	13.9	200	360	360	1.00	1.13	0.00	0.00	220.0	1.24	1.52	-
V023	20.1	200	360	360	1.00	1.13	0.00	0.00	347.0	1.44	1.66	-
V024	25.2	200	360	360	1.00	1.13	0.00	0.00	396.0	1.38	1.51	-
V031	20.0	200	360	360	1.00	1.13	0.00	0.00	323.0	1.35	1.55	-
V032	18.2	200	360	360	1.00	1.13	0.00	0.00	318.0	1.43	1.68	-
V033	19.8	200	360	360	1.00	1.13	0.00	0.00	246.0	1.03	1.20	-
V022	19.2	200	360	360	1.00	1.13	0.00	0.00	270.0	1.13	1.31	-
V511	19.8	200	560	560	1.00	1.12	0.00	0.00	350.0	1.09	1.31	0.98
V411	19.4	200	740	740	1.00	1.10	0.00	0.00	365.0	0.84	1.01	1.11
V211	20.0	200	930	930	1.00	1.08	0.00	0.00	505.0	0.93	1.11	1.00
Tan et al. (1995)												
A-0.27	58.8	110	463	125	0.27	1.23	0.00	0.48	675	0.93	2.08	-
A-0.27	51.6	110	463	125	0.27	1.23	0.00	0.48	630	0.99	2.07	-
A-0.27	53.9	110	463	125	0.27	1.23	0.00	0.48	640	0.96	2.06	-
A-0.27	57.3	110	463	125	0.27	1.23	0.00	0.48	630	0.89	1.97	-
B-0.54	56.0	110	463	250	0.54	1.23	0.00	0.48	468	0.87	1.48	-
B-0.54	45.7	110	463	250	0.54	1.23	0.00	0.48	445	0.93	1.56	-
B-0.54	53.9	110	463	250	0.54	1.23	0.00	0.48	500	0.93	1.61	-
B-0.54	53.0	110	463	250	0.54	1.23	0.00	0.48	480	0.89	1.56	-
C-0.81-2.15	51.2	110	463	375	0.81	1.23	0.00	0.48	403	1.14	1.33	-
C-0.81-3.23	44.0	110	463	375	0.81	1.23	0.00	0.48	400	1.31	1.46	-
D-1.08-2.15	48.2	110	463	500	1.08	1.23	0.00	0.48	270	1.10	1.21	-
D-1.08-3.23	44.1	110	463	500	1.08	1.23	0.00	0.48	280	1.21	1.37	-
D-1.08-4.30	46.8	110	463	500	1.08	1.23	0.00	0.48	290	1.20	1.33	-
D-1.08-5.38	48.0	110	463	500	1.08	1.23	0.00	0.48	290	1.18	1.30	-
E-1.62-3.23	50.6	110	463	750	1.62	1.23	0.00	0.48	220	1.67	1.41	-
E-1.62-4.30	44.6	110	463	750	1.62	1.23	0.00	0.48	190	1.59	1.38	-

Table A.1 - Evaluation steel-reinforced deep beam database.

Beam ID	f_c' (MPa)	b (mm)	d (mm)	a (mm)	a/d	ρ (%)	ρ_h (%)	ρ_v (%)	P_{exp} (kN)	P_{exp}/P_{pred}		
										CSA-A23.3-14	ACI 318-14	Proposed Model
Tan et al. (1995), *Continue*...												
E-1.62-5.38	45.3	110	463	750	1.62	1.23	0.00	0.48	173	1.43	1.24	-
F-2.16-4.30	41.1	110	463	1000	2.16	1.23	0.00	0.48	150	2.36	1.57	-
G-2.70-5.38	42.8	110	463	1250	2.70	1.23	0.00	0.48	105	2.61	1.31	-
Tan et al. (1997a)												
I-1/0.75	99.4	110	443	375	0.85	2.58	0.00	0.00	1000	1.28	2.78	-
I-2N/0.75	86.8	110	443	375	0.85	2.58	0.00	2.86	1520	2.08	2.78	-
I-3/0.75	78.8	110	443	375	0.85	2.58	1.59	0.00	1120	1.61	1.96	-
I-4/0.75	92.3	110	443	375	0.85	2.58	1.59	0.00	1160	1.54	1.96	-
I-5/0.75	92.7	110	443	375	0.85	2.58	3.17	0.00	1550	2.04	2.78	-
I-6S/0.75	80.9	110	443	375	0.85	2.58	1.59	2.86	1550	2.17	2.70	-
II-1/1.00	88.2	110	443	500	1.13	2.58	0.00	0.00	510	0.69	1.28	-
II-2N/1.00	88.2	110	443	500	1.13	2.58	0.00	1.43	1040	1.41	1.69	-
II-3/1.00	80.5	110	443	500	1.13	2.58	1.59	0.00	780	1.11	1.15	-
II-4/1.00	89.4	110	443	500	1.13	2.58	1.59	0.00	660	0.88	0.93	-
II-5/1.00	89.4	110	443	500	1.13	2.58	3.17	0.00	940	1.27	1.32	-
II-6N/1.00	91.1	110	443	500	1.13	2.58	1.59	1.43	1340	1.79	2.00	-
III-1/1.50	88.2	110	443	750	1.69	2.58	0.00	0.00	370	0.72	1.64	-
III-2N/1.50	88.2	110	443	750	1.69	2.58	0.00	1.43	670	1.15	1.37	-
III-2S/1.50	88.2	110	443	750	1.69	2.58	0.00	1.43	800	1.19	1.43	-
III-3/1.50	80.5	110	443	750	1.69	2.58	1.59	0.00	400	0.78	0.83	-
III-4/1.50	89.4	110	443	750	1.69	2.58	1.59	0.00	380	0.69	0.68	-
III-5/1.50	89.4	110	443	750	1.69	2.58	3.17	0.00	530	0.88	0.68	-
III-6N/1.50	91.1	110	443	750	1.69	2.58	1.59	1.43	920	1.47	1.25	-
Tan et al. (1997b)												
1-2.00/0.75	71.2	110	448	375	0.84	2.00	0.00	0.48	1090	1.23	2.22	-
1-2.00/1.00	71.2	110	448	500	1.12	2.00	0.00	0.48	1000	1.64	2.17	-
1-2.00/1.50	72.1	110	448	750	1.67	2.00	0.00	0.48	500	1.69	1.39	-
2-2.58/0.25	69.9	110	443	125	0.28	2.58	0.00	0.48	1670	1.22	3.13	-
2-2.58/0.50	64.6	110	443	250	0.56	2.58	0.00	0.48	1480	1.16	2.22	-
2-2.58/0.75	64.6	110	443	375	0.85	2.58	0.00	0.48	1060	0.79	1.10	-
2-2.58/1.00	68.1	110	443	500	1.13	2.58	0.00	0.48	500	0.99	0.99	-
2-2.58/1.50	68.1	110	443	750	1.69	2.58	0.00	0.48	300	1.69	0.95	-
2-2.58/2.50	54.7	110	443	1250	2.82	2.58	0.00	0.48	310	1.02	2.86	-
3-4.08/0.25	69.9	110	420	125	0.30	4.08	0.00	0.48	1850	1.39	2.56	-
3-4.08/0.50	64.6	110	420	250	0.60	4.08	0.00	0.48	1440	1.49	2.17	-
3-4.08/0.75	64.6	110	420	375	0.89	4.08	0.00	0.48	1340	0.90	0.85	-
3-4.08/1.00	68.1	110	420	500	1.19	4.08	0.00	0.48	1040	2.27	1.32	-
3-4.08/2.00	69.9	110	420	1000	2.38	4.08	0.00	0.48	380	1.27	2.44	-
3-4.08/2.50	54.8	110	420	1250	2.98	4.08	0.00	0.48	270	1.37	2.08	-
4-5.80/0.75	71.2	110	398	375	0.94	5.80	0.00	0.48	1400	2.13	2.13	-
4-5.80/2.50	74.1	110	398	1250	3.14	5.80	0.00	0.48	530	1.01	2.17	-
1-500/0.50	49.1	140	444	250	0.56	2.60	0.00	0.00	850	0.92	2.17	-

Table A.1 - Evaluation steel-reinforced deep beam database.

Beam ID	f_c' (MPa)	b (mm)	d (mm)	a (mm)	a/d	ρ (%)	ρ_h (%)	ρ_v (%)	P_{exp} (kN)	P_{exp}/P_{pred}		
										CSA-A23.3-14	ACI 318-14	Proposed Model
Tan et al. (1997b), *Continue…*												
1-500/0.75	42.5	140	444	375	0.84	2.60	0.00	0.00	700	1.39	1.28	-
1-500/1.00	37.4	140	444	500	1.13	2.60	0.00	0.00	570	1.82	1.35	-
2-1000/0.50	31.2	140	884	500	0.56	2.60	0.06	0.06	875	1.01	2.08	-
2-1000/0.75	32.7	140	884	740	0.84	2.60	0.06	0.06	650	0.96	1.09	-
2-1000/1.00	30.8	140	884	1000	1.13	2.60	0.06	0.06	435	0.99	1.11	-
3-1400/0.50	32.8	140	1251	705	0.56	2.60	0.06	0.06	1175	1.20	1.72	-
3-1400/0.75	36.2	140	1251	1050	0.84	2.60	0.06	0.06	950	1.15	1.14	-
3-1400/1.00	35.3	140	1251	1420	1.13	2.60	0.06	0.06	800	1.43	1.02	-
4-1750/0.50	42.6	140	1559	880	0.56	2.60	0.06	0.06	1636	1.09	0.72	-
4-1750/0.75	40.4	140	1559	1320	0.84	2.60	0.06	0.06	1240	1.11	0.98	-
4-1750/1.00	44.8	140	1559	1760	1.13	2.60	0.06	0.06	1000	1.18	0.51	-
Shin et al. (1999)												
MHB1.5-0	52	125	215	323	1.50	3.77	0.00	0.00	112.9	1.11	1.00	-
MHB1.5-25	52	125	215	323	1.50	3.77	0.50	0.45	156.4	1.54	1.15	-
MHB1.5-50	52	125	215	323	1.50	3.77	0.50	0.91	208.0	2.05	1.54	-
MHB1.5-75	52	125	215	323	1.50	3.77	0.50	1.36	239.7	2.36	1.77	-
MHB1.5-100	52	125	215	323	1.50	3.77	0.50	1.81	257.5	2.53	1.90	-
MHB2.0-0	52	125	215	430	2.00	3.77	0.00	0.00	87.9	1.38	1.83	-
MHB2.0-25	52	125	215	430	2.00	3.77	0.50	0.32	110.7	1.74	1.92	-
MHB2.0-50	52	125	215	430	2.00	3.77	0.50	0.65	173.9	2.73	3.02	-
MHB2.0-75	52	125	215	430	2.00	3.77	0.50	0.97	185.4	2.91	3.22	-
MHB2.0-100	52	125	215	430	2.00	3.77	0.50	1.29	193.2	3.03	3.35	-
MHB2.5-0	52	125	215	538	2.50	3.77	0.00	0.00	142.2	1.14	1.34	-
MHB2.5-25	52	125	215	538	2.50	3.77	0.50	0.25	214.2	1.99	1.95	-
MHB2.5-50	52	125	215	538	2.50	3.77	0.50	0.47	246.2	2.80	2.74	-
MHB2.5-75	52	125	215	538	2.50	3.77	0.50	0.71	265.8	3.22	3.15	-
MHB2.5-100	52	125	215	538	2.50	3.77	0.50	0.94	280.3	3.32	3.24	-
HB1.5-0	73	125	215	323	1.50	3.77	0.00	0.00	99.4	1.06	0.93	-
HB1.5-25	73	125	215	323	1.50	3.77	0.50	0.45	142.7	1.60	1.17	-
HB1.5-50	73	125	215	323	1.50	3.77	0.50	0.91	195.9	1.84	1.34	-
HB1.5-75	73	125	215	323	1.50	3.77	0.50	1.36	230.1	1.98	1.45	-
HB1.5-100	73	125	215	323	1.50	3.77	0.50	1.81	242.1	2.09	1.53	-
HB2.0-0	73	125	215	430	2.00	3.77	0.00	0.00	80.4	1.18	1.91	-
HB2.0-25	73	125	215	430	2.00	3.77	0.50	0.32	115.6	1.69	2.28	-
HB2.0-50	73	125	215	430	2.00	3.77	0.50	0.65	148.9	2.32	3.14	-
HB2.0-75	73	125	215	430	2.00	3.77	0.50	0.97	166.9	2.73	3.68	-
HB2.0-100	73	125	215	430	2.00	3.77	0.50	1.29	183.8	2.87	3.88	-
HB2.5-0	73	125	215	538	2.50	3.77	0.00	0.00	112.9	1.45	1.73	-
HB2.5-25	73	125	215	538	2.50	3.77	0.50	0.25	156.4	2.09	2.07	-
HB2.5-50	73	125	215	538	2.50	3.77	0.50	0.47	208.0	2.69	2.67	-
HB2.5-75	73	125	215	538	2.50	3.77	0.50	0.71	239.7	3.01	2.99	-
HB2.5-100	73	125	215	538	2.50	3.77	0.50	0.94	257.5	3.32	3.30	-

Table A.1 - Evaluation steel-reinforced deep beam database.

Beam ID	f_c' (MPa)	b (mm)	d (mm)	a (mm)	a/d	ρ (%)	ρ_h (%)	ρ_v (%)	P_{exp} (kN)	P_{exp}/P_{pred}		
										CSA-A23.3-14	ACI 318-14	Proposed Model
Oh and Shin (2001)												
N4200	23.7	130	500	425	0.85	1.56	0.00	0.00	265.2	0.99	0.76	0.78
N42A2	23.7	130	500	425	0.85	1.56	0.43	0.12	284.1	1.06	0.62	0.84
N42B2	23.7	130	500	425	0.85	1.56	0.43	0.22	377.0	1.41	0.83	1.11
N42C2	23.7	130	500	425	0.85	1.56	0.43	0.34	357.5	1.34	0.79	1.06
H4100	49.1	130	500	250	0.50	1.56	0.00	0.00	642.2	0.88	1.03	0.87
H41A2(1)	49.1	130	500	250	0.50	1.56	0.43	0.12	713.1	0.98	0.92	0.97
H41B2	49.1	130	500	250	0.50	1.56	0.43	0.22	705.9	0.97	0.91	0.96
H41C2	49.1	130	500	250	0.50	1.56	0.43	0.34	708.5	0.97	0.92	0.96
H4200	49.1	130	500	425	0.85	1.56	0.00	0.00	401.1	0.85	0.56	0.85
H42A2(1)	49.1	130	500	425	0.85	1.56	0.43	0.21	488.2	1.03	0.52	1.04
H42B2(1)	49.1	130	500	425	0.85	1.56	0.43	0.22	456.3	0.97	0.48	0.97
H42C2(1)	49.1	130	500	425	0.85	1.56	0.43	0.34	420.6	0.89	0.45	0.89
H4300	49.1	130	500	625	1.25	1.56	0.00	0.00	337.4	1.24	0.42	1.02
H43A2(1)	49.1	130	500	625	1.25	1.56	0.43	0.12	347.1	1.28	0.43	1.05
H43B2	49.1	130	500	625	1.25	1.56	0.43	0.22	380.9	1.40	0.47	1.15
H43C2	49.1	130	500	625	1.25	1.56	0.43	0.34	402.4	1.48	0.50	1.22
H4500	49.1	130	500	1000	2.00	1.56	0.00	0.13	112.5	1.15	0.29	1.24
H45A2	49.1	130	500	1000	2.00	1.56	0.43	0.13	210.6	2.16	0.43	1.16
H45B2	49.1	130	500	1000	2.00	1.56	0.43	0.13	237.3	2.43	0.49	1.30
H45C2	49.1	130	500	1000	2.00	1.56	0.43	0.13	235.3	2.41	0.49	1.29
H41A0	50.7	120	500	250	0.50	1.29	0.00	0.13	347.4	1.05	1.17	0.84
H41A1	50.7	120	500	250	0.50	1.29	0.23	0.13	397.8	1.21	1.08	0.96
H41A2(2)	50.7	120	500	250	0.50	1.29	0.47	0.24	490.2	1.49	1.21	1.18
H41A3	50.7	120	500	250	0.50	1.29	0.94	0.37	454.8	1.38	1.12	1.10
H42A2(2)	50.7	120	500	425	0.85	1.29	0.47	0.13	392.4	1.85	0.85	1.48
H42B2(2)	50.7	120	500	425	0.85	1.29	0.47	0.13	360.6	1.70	0.78	1.36
H42C2(2)	50.7	120	500	425	0.85	1.29	0.47	0.13	373.8	1.76	0.81	1.41
H43A0	50.7	120	500	625	1.25	1.29	0.00	0.13	213.6	0.88	0.41	0.73
H43A1	50.7	120	500	625	1.25	1.29	0.23	0.13	260.4	1.08	0.40	0.89
H43A2(2)	50.7	120	500	625	1.25	1.29	0.47	0.13	276.6	1.15	0.43	0.95
H43A3	50.7	120	500	625	1.25	1.29	0.94	0.13	291.0	1.20	0.37	1.00
H45A2(2)	50.7	120	500	1000	2.00	1.29	0.46	0.13	165.0	1.88	0.43	1.01
U41A0	73.6	120	500	250	0.50	1.29	0.00	0.13	438.0	1.01	0.90	0.92
U41A1	73.6	120	500	250	0.50	1.29	0.23	0.13	541.8	1.25	0.92	1.14
U41A2	73.6	120	500	250	0.50	1.29	0.47	0.13	548.4	1.27	0.93	1.15
U41A3	73.6	120	500	250	0.50	1.29	0.94	0.13	546.6	1.26	0.93	1.15
U42A2	73.6	120	500	425	0.85	1.29	0.47	0.13	417.6	1.51	0.62	1.34
U42B2	73.6	120	500	425	0.85	1.29	0.47	0.24	410.4	1.48	0.61	1.32
U42C2	73.6	120	500	425	0.85	1.29	0.47	0.37	408.0	1.47	0.78	1.31
U43A0	73.6	120	500	625	1.25	1.29	0.00	0.13	291.0	0.94	0.31	0.90
U43A1	73.6	120	500	625	1.25	1.29	0.23	0.13	310.2	1.01	0.33	0.96
U43A2	73.6	120	500	625	1.25	1.29	0.47	0.13	338.4	1.10	0.36	1.05

Table A.1 - Evaluation steel-reinforced deep beam database.

Beam ID	f_c' (MPa)	b (mm)	d (mm)	a (mm)	a/d	ρ (%)	ρ_h (%)	ρ_v (%)	P_{exp} (kN)	P_{exp}/P_{pred}		
										CSA-A23.3-14	ACI 318-14	Proposed Model
Oh and Shin (2001), *Continue*...												
U43A3	73.6	120	500	625	1.25	1.29	0.94	0.13	333.0	1.08	0.35	1.04
U45A2	73.6	120	500	1000	2.00	1.29	0.47	0.13	213.6	1.88	0.38	1.16
N33A2	23.7	130	500	625	1.25	1.56	0.43	0.12	228.2	1.41	0.70	0.97
N43A2	23.7	130	500	625	1.25	1.56	0.43	0.12	254.8	1.58	0.78	1.09
N53A2	23.7	130	500	625	1.25	1.56	0.43	0.12	207.4	1.28	0.63	0.89
H31A2	49.1	130	500	250	0.50	1.56	0.43	0.12	745.6	1.02	0.87	0.80
H32A2	49.1	130	500	425	0.85	1.56	0.43	0.12	529.8	1.12	0.55	0.89
H33A2	49.1	130	500	625	1.25	1.56	0.43	0.12	377.7	1.39	0.56	1.14
H51A2	49.1	130	500	250	0.50	1.56	0.43	0.12	702.0	0.96	0.82	0.75
H52A2	49.1	130	500	425	0.85	1.56	0.43	0.12	567.5	1.20	0.59	0.95
H53A2	49.1	130	500	625	1.25	1.56	0.43	0.12	362.7	1.33	0.53	1.10
Aguilar et al. (2002)												
ACI-I	32	305	791	915	1.16	1.27	0.35	0.31	1357	1.36	1.41	1.06
STM-I	32	305	718	915	1.27	1.40	0.13	0.31	1134	1.29	1.33	1.12
STM-H	28	305	801	915	1.14	1.25	0.06	0.31	1286	1.43	1.58	1.00
STM-M	28	305	801	915	1.14	1.25	0.00	0.1	1277	1.42	1.56	1.00
Lertsrisakulart (2002)												
D200	38.4	150	200	200	1.00	1.91	0.00	0.00	214.2	1.05	1.02	-
D400	35.5	150	400	400	1.00	1.69	0.00	0.00	285.3	1.00	1.10	-
D600	40.8	150	600	600	1.00	1.76	0.00	0.00	424.5	1.00	1.13	-
Yang et al. (2003)												
L5-40	31.4	160	355	200	0.56	1.01	0.00	0.00	447	1.12	1.54	0.68
L5-60	31.4	160	555	300	0.54	0.97	0.00	0.00	535	1.17	1.82	0.64
L5-60R	31.4	160	555	300	0.54	0.97	0.00	0.00	479	1.05	1.63	0.92
L5-75	31.4	160	685	375	0.55	1.05	0.00	0.00	597	1.11	1.77	1.14
L5-100	31.4	160	935	500	0.53	0.90	0.00	0.00	582	1.04	1.72	1.17
UH5-40	78.5	160	955	200	0.56	1.01	0.00	0.00	733	0.95	1.08	1.14
UH5-60	78.5	160	555	300	0.54	0.97	0.00	0.00	823	0.90	1.20	0.88
UH-75	78.5	160	685	375	0.55	1.05	0.00	0.00	1010	0.93	1.28	1.04
UH5-100	78.5	160	935	500	0.53	0.90	0.00	0.00	1029	0.89	1.30	0.75
L10-40	31.4	160	355	400	1.13	1.01	0.00	0.00	192.1	0.99	0.90	0.85
L10-40R	31.4	160	355	400	1.13	1.01	0.00	0.00	311.6	1.61	1.45	0.91
L10-60	31.4	160	555	600	1.08	0.97	0.00	0.00	375.3	1.59	1.67	0.98
L10-75	31.4	160	685	750	1.09	1.05	0.00	0.00	271.5	0.93	0.99	0.98
L10-75R	31.4	160	685	750	1.09	1.05	0.00	0.00	330.3	1.14	1.20	1.00
L10-100	31.4	160	935	1000	1.07	0.90	0.00	0.00	543.9	1.72	1.94	0.92
UH10-40R	78.5	160	355	375	1.06	1.01	0.00	0.00	358.1	0.95	0.74	1.33
UH10-60	78.5	160	555	600	1.08	0.97	0.00	0.00	573.3	1.24	1.09	1.53
UH10-75	78.5	160	685	750	1.09	1.05	0.00	0.00	338.1	0.59	0.53	1.73
UH10-75R	78.5	160	685	750	1.09	1.05	0.00	0.00	360.6	0.63	0.56	0.94
UH10-100	78.5	160	935	1000	1.07	0.90	0.00	0.00	769.3	1.23	1.18	0.73
I-UL-8.5-0a	16.8	152	686	1029	1.50	1.88	0.00	0.69	984.8	2.47	2.75	1.00

Table A.1 - Evaluation steel-reinforced deep beam database.

Beam ID	f_c' (MPa)	b (mm)	d (mm)	a (mm)	a/d	ρ (%)	ρ_h (%)	ρ_v (%)	P_{exp} (kN)	P_{exp}/P_{pred}		
										CSA-A23.3-14	ACI 318-14	Proposed Model
Brown et al. (2006)												
I-UL-8.5-0b	18.2	152	686	1029	1.50	1.88	0.00	0.69	885.6	2.06	2.28	1.22
I-UL-0-0	22.3	152	686	1029	1.50	1.88	0.00	0.00	825.1	1.60	2.18	0.93
I-UL-0-8.5	18.2	152	686	1029	1.50	1.88	0.69	0.00	767.8	1.85	1.98	1.06
I-UL-17-17	18.3	152	686	1029	1.50	1.88	0.34	0.34	849.6	1.95	2.18	1.46
I-UL-17-0	18.3	152	686	1029	1.50	1.88	0.00	0.34	893.6	2.07	2.87	1.56
I-2C-8.5-0	22.1	152	686	1029	1.50	1.88	0.00	0.69	485.3	1.61	1.46	1.60
I-2C-0-0	22.1	152	686	1029	1.50	1.88	0.00	0.00	559.1	1.95	2.30	1.86
I-CL-8.5-0	17.8	152	686	1029	1.50	1.88	0.00	0.69	739.3	1.65	1.69	1.45
I-CL-0-0	16.3	152	686	1029	1.50	1.88	0.00	0.00	554.3	1.23	1.59	1.11
II-N-E-5.8-8	19.7	457	406	686	1.69	2.11	0.00	0.24	589.4	1.25	1.21	1.02
II-N-F-5.8-8	19.7	457	406	686	1.69	2.11	0.00	0.24	624.1	1.17	1.10	1.66
II-N-C-5.8-8	19.7	457	406	686	1.69	2.11	0.00	0.24	867.0	2.01	1.78	1.08
II-N-F-5.8-3	19.9	457	406	686	1.69	2.11	0.00	0.65	1006	1.70	1.76	1.14
II-N-C-4.6-8	19.9	457	406	686	1.69	2.11	0.00	0.24	1096	2.16	2.10	0.82
II-N-E-4.6-8	19.9	457	406	686	1.69	2.11	0.00	0.24	818.0	1.61	1.57	1.09
II-N-F-4.6-8	21.6	457	406	686	1.69	2.11	0.00	0.24	650.3	1.02	0.99	1.16
II-W-E-5.8-8	21.4	762	406	686	1.69	2.38	0.00	0.15	1636	3.27	3.08	1.16
II-W-E-4.5-8	24.6	762	406	686	1.69	2.38	0.00	0.15	1418	2.24	2.17	0.93
II-W-E-3-8	25.2	762	406	686	1.69	2.38	0.00	0.15	1035	1.37	1.37	0.90
Quintero-Febres et al. (2006)												
A1	22.0	150	370	525	1.42	2.79	0.1	0.28	251	1.47	1.98	1.08
A2	22.0	150	370	525	1.42	2.79	0.1	0.28	237	1.39	1.87	1.459
A3	22.0	150	370	525	1.42	2.79	0.00	0.00	221	1.30	1.74	1.012
A4	22.0	150	370	525	1.42	2.79	0.00	0.00	196	1.15	1.54	1.322
B1	32.4	150	375	334	0.89	2.04	0.1	0.23	456	1.27	1.72	1.102
B2	32.4	150	375	334	0.89	2.04	0.1	0.23	426	1.19	1.60	1.331
B3	32.4	150	375	304	0.81	2.04	0.00	0.00	468	1.30	1.76	1.007
B4	32.4	150	375	304	0.81	2.04	0.00	0.00	459	1.28	0.99	1.098
HA1	50.3	150	380	597	1.57	4.08	0.51	0.38	265	1.13	1.32	1.196
HA3	50.3	150	380	543	1.43	4.08	0.00	0.00	292	1.29	1.26	1.08
HB1	50.3	150	380	342	0.90	4.08	0.15	0.67	484	1.33	1.08	1.459
HB3	50.3	150	380	312	0.82	4.08	0.00	0.00	460	1.25	0.93	1.012
Zhang and Tan (2007b)												
1DB70bw	28.30	160	643	701	1.10	0.10	0.00	0.21	428	0.85	0.96	1.37
1DB100bw	28.70	231	904	1001	1.10	0.07	0.00	0.21	778	0.76	0.61	1.43
Birrcher et al. (2009)												
M-03-4-CCC	28.3	914	1016	1880	1.85	0.43	0.30	0.31	5021	1.12	0.76	1.14
M-09-4-CCC	28.3	914	1016	1880	1.85	0.43	0.30	0.86	6346	1.42	0.96	1.44
M-02-4-CCC	19.3	914	1016	1880	1.85	0.43	0.22	0.22	4904	1.54	1.08	1.27
M-02-4-CCC	20.7	914	1016	1880	1.85	0.43	0.30	0.31	4139	1.22	0.85	1.02
M-03-4-CCC	33.8	914	1016	1880	1.85	0.22	0.27	0.31	4877	1.04	0.62	1.05
I-03-2	36.1	533	978	1799	1.84	1.16	0.33	0.29	2533	0.84	0.61	1.07

Table A.1 - Evaluation steel-reinforced deep beam database.

Beam ID	f_c' (MPa)	b (mm)	d (mm)	a (mm)	a/d	ρ (%)	ρ_h (%)	ρ_v (%)	P_{exp} (kN)	P_{exp}/P_{pred}		
										CSA-A23.3-14	ACI 318-14	Proposed Model
Birrcher et al. (2009); *Continue*...												
I-03-4	36.7	533	978	1799	1.84	1.16	0.33	0.30	2925	0.95	0.70	1.22
I-02-2	27.2	533	978	1799	1.84	1.16	0.20	0.20	2019	0.87	0.65	0.93
I-02-4	28.7	533	978	1799	1.84	1.16	0.20	0.21	2350	0.97	0.72	1.06
II-03-CCC	22.7	533	980	1804	1.84	1.15	0.45	0.31	2223	1.31	0.98	1.46
II-03-CCC	24.0	533	980	1804	1.84	1.15	0.45	0.31	2124	1.19	0.89	1.56
II-03-CCT	30.4	533	980	1804	1.84	1.15	0.45	0.31	2828	1.26	0.93	1.60
II-03-CCT	29.0	533	980	1804	1.84	1.15	0.45	0.31	2658	1.42	1.05	1.86
II-02-CCT	21.5	533	980	1804	1.84	1.15	0.19	0.20	1786	1.28	0.95	1.45
II-02-CCC	21.6	533	980	1804	1.84	1.15	0.19	0.20	1490	1.06	0.79	1.11
II-02-CCC	31.9	533	980	1804	1.84	1.15	0.19	0.20	1464	0.63	0.46	1.02
II-02-CCT	32.7	533	980	1804	1.84	1.15	0.19	0.20	2525	1.05	0.77	1.66
III-1.85-02	28.3	533	980	1804	1.84	1.15	0.19	0.20	2171	1.19	0.88	1.08
III-1.85-025	28.3	533	980	1804	1.84	1.15	0.14	0.24	2294	0.96	0.72	1.14
III-1.85-03	34.4	533	980	1804	1.84	1.15	0.29	0.29	1835	0.64	0.47	0.82
III-1.85-01	34.5	533	980	1804	1.84	1.15	0.29	0.10	1213	0.42	0.31	1.09
III-1.85-03b	22.8	533	980	1804	1.84	1.15	0.18	0.31	2096	1.30	0.99	1.16
III-1.85-02b	22.8	533	980	1804	1.84	1.15	0.18	0.20	2081	1.29	0.98	1.16
III-1.2-02	28.3	533	980	1804	1.84	1.15	0.29	0.20	3767	1.90	1.43	0.93
III-1.2-03	29.1	533	980	1804	1.84	1.15	0.18	0.31	3690	1.81	1.36	0.90
III-2.5-02	31.9	533	980	1804	1.84	1.15	0.29	0.20	1327	0.60	0.45	1.24
III-2.5-03	34.7	533	980	1804	1.84	1.15	0.18	0.31	2296	0.95	0.71	1.03
IV-2175-1.85	34.0	533	1750	3238	1.85	1.29	0.29	0.20	3394	1.05	0.78	1.11
IV-2175-1.85	34.0	533	1750	3238	1.85	1.29	0.21	0.31	3749	1.16	0.87	1.22
IV-2175-2.5	34.5	533	1750	4375	2.50	1.29	0.21	0.21	2269	1.35	0.71	0.99
IV-2175-1.2	34.5	533	1750	2100	1.20	1.29	0.21	0.21	5441	0.76	0.82	1.37
IV-2123-1.85	28.7	533	495	916	1.85	2.32	0.30	0.30	1462	0.90	0.71	1.00
IV-2123-1.85	29.1	533	495	916	1.85	2.32	0.17	0.20	1544	0.94	0.73	1.05
IV-2123-2.5	31.5	533	495	1238	2.5	2.32	0.17	0.20	715	0.77	0.44	1.20
IV-2123-1.2	31.9	533	495	594	1.20	2.32	0.17	0.20	2633	0.68	0.71	0.68
Mihaylov et al. (2010)												
S0M	34.2	400	1094	1700	1.55	0.70	0.00	0.00	1420	1.15	1.47	0.81
S1M	33.0	400	1094	1700	1.55	0.70	0.00	0.10	1860	1.55	1.09	1.07
L0M	29.1	400	1094	2500	2.29	0.70	0.00	0.00	801	1.89	1.44	1.49
L1M	37.8	400	1094	2500	2.29	0.70	0.00	0.10	1295	2.52	1.15	2.25